NPS ARCHIVE
1960/V.2
DUNCAN, R.

GUIDANCE PARAMETERS AND CONSTRAINTS FOR CONTROLLED ATMOSPHERIC ENTRY

ROBERT C. DUNCAN

Library
U. S. Naval Postgraduate School
Monterey, California

GUIDANCE PARAMETERS AND CONSTRAINTS FOR CONTROLLED ATMOSPHERIC ENTRY

by

Robert C. Duncan, Lieutenant Commander, U.S. Navy

B.S. United States Naval Academy, 1945

B.S. United States Naval Postgraduate School, 1953

S.M. Massachusetts Institute of Technology, 1954

Volume II of II

Chapters 8 through 10
Appendix A through G

SUBMITTED IN PARTIAL FULFILLMENT OF THE

REQUIREMENTS FOR THE DEGREE OF

DOCTOR OF SCIENCE

at the

MASSACHUSETTS INSTITUTE OF TECHNOLOGY

1960

Library
U. S. Naval Postgraduate School
Monterey, California

OVERALL TABLE OF CONTENTS

Volume I:

Chapter 1 Introduction

Chapter 2 Conclusions and Recommendations for Further Study

Chapter 3 Three-Dimensional Kinematics of Entry

Chapter 4 Kinematics of Entry in Elliptical Parameters

Chapter 5 Forces Acting on the Entry Vehicle

Chapter 6 The Theory of Planar Motion

Chapter 7 Trajectory Constraints: Vehicular Heating and Human Acceleration Tolerances

Volume II:

Chapter 8 Separation of Trajectory into Keplerian, Intermediate, and Gas-Dynamic Phases; Boundary Conditions between Phases

Chapter 9 Approximate Analytical Solution of Guidance Parameters and Constraints for the Direct Entry Profile; Range Sensitivity to Errors in Control System Operation

Chapter 10 Approximate Analytical Solution of Guidance Parameters and Constraints for the Degenerate Orbital Entry Profile

Biographical Sketch

Appendix A Coordinate Frames Used in Entry Mission Analysis; Glossary of Symbols, Constants, and Definitions

Appendix B Physical Characteristics of Major Bodies of the Solar System

Appendix C Gravitational Mass Attraction and the Acceleration of Gravity

Appendix D Figure of the Planet and Definitions of Navigation Parameters

Appendix E The Atmosphere of the Planets and Their Natural Satellites

Appendix F Externally-Aided Adaptive Control of the Entry Vehicle

Appendix G Bibliography

Table of Contents: Volume II

Section	Title	Page
Chapter 8	Separation of Trajectory into Keplerian, Intermediate and Gas-Dynamic Phases; Boundary Conditions Between Phases	242
8.1	Definition of Trajectory Phases	242
8.2	Conservation of Energy and Angular Momentum	245
8.3	Relating the Flight Trajectory and the Conservation Parameter	248
8.4	Altitude Description of Boundaries Between Operational Phases of the Entry Trajectory	259
8.5	Description of Boundaries Between Operational Phases of the Entry Trajectory in Terms of Horizontal Component of Specific Forces	263
Chapter 9	Approximate Analytical Solution of Guidance Parameters and Constraints for the Direct Entry Profile; Range Sensitivity to Errors in Control System Operation	270
9.1	Introduction	270
9.2	The Conservation Parameter as a Switching Function	274
9.3	The Conservation Parameter as a Prediction Function	277
9.4	The Keplerian Phase	283
9.4.1	Description of the Transfer Ellipse in Terms of Geometric Quantities at the Trajectory Modification Point	286
9.4.2	Guidance Quantities in Terms of Geometric Quantities at the Trajectory Modification Point	288
9.4.3	Description of Transfer Ellipse in Terms of Velocity Impulse and Engine Gimbal Angle	290

Contents, cont.

Section	Title	Page
9.4.4	Guidance Quantities in Terms of Velocity Impulse and Engine Gimbal Angle	290
9.4.5	Optimum Engine Gimbal Angle	293
9.4.6	Range Sensitivity to Errors in Velocity and Inertial Flight Path Angle	297
9.4.7	Range Sensitivity to Errors in Velocity Impulse and Engine Gimbal Angle	297
9.5	The Intermediate Phase	298
9.6	The Gas-Dynamic Phase	303
9.6.1	Solution of the Ballistic Trajectory	313
9.6.2	Solution of the Glide Trajectory	317
9.6.3	Solution of the Skip Trajectory	322
9.6.4	Specific Forces Acting on the Entry Vehicle	330
9.6.5	Maximum Specific Force	331
9.6.6	Stagnation Point Temperature	333
9.6.7	Maximum Stagnation Point Temperature	334
9.7	Summary	336
9.8	Derivation Summaries	338
	9.1: Solution of Keplerian Phase of Trajectory in Terms of Geometric Quantities at Trajectory Modification Point	339
	9.2: Solution of the Ballistic Trajectory	345
	9.3: Solution of the Glide Trajectory	347
	9.4: Solution of the Skip Trajectory	350

Contents, cont.

Section	Title	Page
Chapter 10	Approximate Analytical Solution of Guidance Parameters and Constraints for the Degenerate Orbital Entry Profile	354
10.1	Introduction	354
10.2	The Altitude Differential Equation	356
10.3	Circular Orbital Entry	360
10.4	The Degenerate Elliptical Entry Trajectory	379
10.5	Summary	393
10.6	Derivation Summary 10.1: Expansion of $e^{a \cos x}$ in Terms of Modified Bessel Function of the First Kind	396
	Biographical Sketch	398
Appendix A	Coordinate Frames Used in Entry Trajectory Analysis; Glossary of Symbols, Constants, and Definitions	399
A.1	Coordinate Frames	399
A.2	The Two Dimensional Trajectory	415
A.3	The Instantaneous Ellipse	415
A.4	Glossary of Symbols	420
	1. Mathematical Symbols	420
	2. Subscripts	421
	3. Symbols	421
	(a) English Letters	422
	(b) Multiple letter symbols	433
	(c) Greek symbols	434

Contents, cont.

Section	Title	Page
A.5	Summary of Physical Constants of the Planets and Atmospheres	438
Appendix B	Physical Characteristics of Major Bodies of the Solar System	440
Appendix C	Gravitational Mass Attraction and the Acceleration of Gravity	449
C.1	Gravitation	449
C.2	Gravitational Field of Oblate Spheroidal Planets	451
C.3	Gravity	454
Appendix D	Figure of the Planet and Definition of Navigational Parameters	457
D.1	Figure of the Planet	457
D.2	Navigational Parameters	458
D.3	Comparison of Geocentric Latitude and Geographic Latitude	462
D.4	Radius of Spheroidal Planets as Function of Latitude	464
D.5	Position Reference for First-Time Entry into the Atmospheres of Strange Planets	465
Appendix E	The Atmosphere of the Planets and Their Natural Satellites	468
E.1	Composition of Atmospheres of the Planets and Their Natural Satellites	468
E.2	Models of the Atmosphere	474
E.3	The Venusian Model Atmosphere	476

Contents, cont.

Section	Title	Page
E.4	The Martian Model Atmosphere	478
E.5	Model Atmosphere for the Giant Planets and Titan	481
E.6	Model Atmosphere for Earth	483
E.7	Gas-Dynamic Comparison of the Exponential Model Atmospheres of Venus, Earth, and Mars	489
Appendix F	Externally-Aided Self Adaptive Control of the Entry Vehicle	492
Appendix G	Bibliography	496

List of Illustrations: Volume II

Figure	Title	Page
8.1	Phases of the Entry Trajectory and Definition of Boundary Conditions	244
8.2	Kinetic-Potential Energy Transfer Rate as Function of Ratio of Percentage Change in Radial Distance of the Entry Vehicle from the Planet Center to the Percentage Change in Horizontal Velocity	249
8.3	Flight Regimes of Entry Trajectory	252
8.4	Behavior of ξ - Parameter During Braking Pass	255
8.5	Behavior of ξ - Parameter During the Direct Entry Profile	256
8.6	Flight Regimes of Entry Trajectory as Function of Conservation Parameter	258
8.7	Behavior of ξ - Parameter as a Function of Altitude at Various Flight Path Angles	262
8.8	Phase Boundaries of Intermediate Phase for Various Drag Parameters	264
8.9	Horizontal Specific Force vs. Altitude	267
8.10	Level of Horizontal Specific Force at Boundaries Between Operational Phases as a Function of Flight Path Angle	269
9.1	The Degenerate Orbit of a Vehicle About a Planet Which Possesses an Atmosphere	271
9.2	Altitude, Total Energy, and Conservation Parameter vs. Time for a Typical Degenerate Orbit	279
9.3	Geometry of the Transfer Ellipse; Definitions of Quantities and Geometric Identities	287
9.4	Geometric Relations Between Flight Path Angle and Inertial Flight Path Angle	292
9.5	Vacuum Ground Range vs. Engine Deflection Angle	294

Illustrations, cont.

Figure	Title	Page
9.6	Velocity Impulse vs. Engine Deflection Angle for Vacuum Trajectory of Fixed Ground Range	295
9.7	Regions Where Approximate Solutions of This Thesis are Accurate	306
9.8	Comparison of Approximate "Ballistic" Solution to Machine Computed Numerical Solutions	310
9.9	Comparison of Approximate Glide Solution to Machine Computed Numerical Solutions	311
9.10	Comparison of Approximate Skip Solution to Machine Computed Numerical Solutions	312
10.1	Comparison of Analytical Solution to Machine-Computed Numerical Solution for Zero-Lift Vehicle Initially in Circular Orbit at 120 miles Altitude Above Earth	366
10.2	Comparison of Analytical Solution to Machine-Computed Numerical Solution for 10 Orbits of Low-Drag Zero-Lift Vehicle Initially in Circular Orbit at 120 miles Altitude above Earth	368
10.3	Comparison of Analytical Solution to Machine-Computed Numerical Solution for High Drag Zero-Lift Vehicle Initially in Circular Orbit at 120 miles Altitude Above the Earth	369
10.4	Comparison of Analytical Solution to Machine-Computed Numerical Solution for 8 Orbits of High-Drag Zero-Lift Vehicle Initially in Circular Orbit at 120 miles Altitude above Earth	371
10.5	Comparison of Analytical Solution to Machine-Computed Numerical Solution for Zero-Lift Vehicle Initially in Circular Orbit at 80 miles Altitude Above Earth	373
10.6	Comparison of One-Step and Two-Step Analytical Solutions to Machine-Computed Numerical Solution For Zero-Lift Vehicle Initially in Circular Orbit at 80 miles Altitude Above Earth	374

Illustrations, cont.

Figure	Title	Page
10.7	Comparison of Analytical Radial Velocity Solution to Machine-Computed Numerical Solution for Zero-Lift Vehicle Initially in Circular Orbit at 80 miles Altitude Above Earth	377
10.8	Minimum Earth Altitude for Which Elliptical Solution is Accurate in the Case of Lifting Entry	382
10.9	Values of Coefficients in Elliptical Trajectory Solution for Small A_4	386
10.10	Comparison of Perigeal and Apogeal Altitudes of Analytical Solution with Those Determined Numerically with IBM-704. Lifting Vehicle Launched with Initial Velocity 3% Greater than Circular Orbital Velocity	389
A.1	Coordinate Frames Useful in Analysis of Entry Trajectory	402
A.2	Coordinates of Trajectory	405
A.3	"Wings Level" and "Vehicle" Coordinate Triad	409
A.4	Engine Gimbal Angles	413
A.5	The Two-Dimensional Trajectory	416
A.6	The Instantaneous Ellipse	419
C.1	Gravitational Field of Oblate Spheroidal Planet	452
C.2	Relations of Gravitation and Gravity	456
D.1	The Reference Ellipsoid	462
E.1	Comparison of Recent Measurements of Atmospheric Density with ARDC Model Atmosphere	485
E.2	Comparison of Exponential Model with ARDC Model of Earth Atmosphere	486

Illustrations, cont.

Figure	Table	Page
E.3	Dimensionless Exponential Parameter k for ARDC Model of Earth Atmosphere	488
E.4	Isothermal Atmospheric Models for Terrestrial Planets	490
F.1	Functional Diagram of Normal Acceleration Flight Control System Which Adapts to the Operating Environment	493

List of Tables: Volume II

Number	Title	Page
8.1	Conversion Quantities for Use in Equation (8-23)	260
8.2	Conversion Quantities for Use in Equation (8-27)	265
A.1	Angular Relations Among Coordinate Systems Given in Fig. A.2	407
A.2	Approximate Values of Heating and Acceleration Constants for Terrestrial Planets	434
A.3	Summary of Planetary Atmospheric and Physical Data	438
B.1	Summary of Physical Data on Principle Bodies of Solar System	442
E.1	Composition of the Atmospheres of the Planets and Their Major Natural Satellites	472
E.2	Model Atmosphere for Giant Planets and Titan	482
E.3	Comparison of ARDC Model Atmosphere (1956) with Exponential Approximation	491

Chapter 8

SEPARATION OF TRAJECTORY INTO KEPLERIAN, INTERMEDIATE, AND GAS-DYNAMIC PHASES; BOUNDARY CONDITIONS BETWEEN PHASES

8.1 Definition of Trajectory Phases

The function of a guidance system in a vehicle entering the atmosphere of a planet is complicated by the radically different operational environment it encounters during the course of entry. For example, the density of the atmosphere changes from an insignificantly small quantity at orbital altitudes to the dominating factor affecting the shape of the trajectory at low altitudes.

It is convenient to consider the entry trajectory as made up of three separate phases:

(1) Keplerian Phase (Free-Fall Phase):

That segment of the trajectory, at high altitudes, where gas-dynamic forces are insignificantly small ($\rho \cong 0$).

(2) Intermediate Phase:

That segment of the trajectory where accelerations due to gas-dynamic terms are of comparable magnitude with other terms in the dynamical equations of motion.

(3) Gas-Dynamic Phase:

That segment of the trajectory where gas-dynamic accelerations

are the predominant terms affecting the shape of the trajectory.

Figure 8.1 shows the various phases of the entry trajectory and gives definitions of boundaries between phases.

In the Intermediate Phase, either a pure Keplerian description of the trajectory or the gas-dynamic simplifications* in the equations of motion are not warranted. Chapman[15] considers the entry trajectory as made up of two phases only** which are fitted together by matching boundary conditions. He defines the onset of the Gas-Dynamic Phase as that point at which drag has reduced the vehicle velocity by about 0.01 of the initial velocity. It is shown in this chapter that the Intermediate Phase may span an operating band of sufficient width that three, rather than two, separate segments of the trajectory should be considered in a piecewise analysis.

The investigation described in this chapter is unique in that three separate operating regions are suggested for guidance analysis; the boundaries between these operational phases are defined on the basis of the rate at which angular momentum and energy are being transferred from the vehicle to the planetary atmosphere. For this purpose, a Conservation Parameter is defined which is related directly to the rate of transfer of energy and angular momentum. The Conservation Parameter may be determined in flight from measurements of specific force levels and flight path angle. Quantitative estimates are given for the specific force level and altitude at the phase boundaries between the three operating regimes for vehicles with various lift and

- - - - - - - - - - - - - - - - -

* See Chapter 9

** Keplerian and Gas-Dynamic

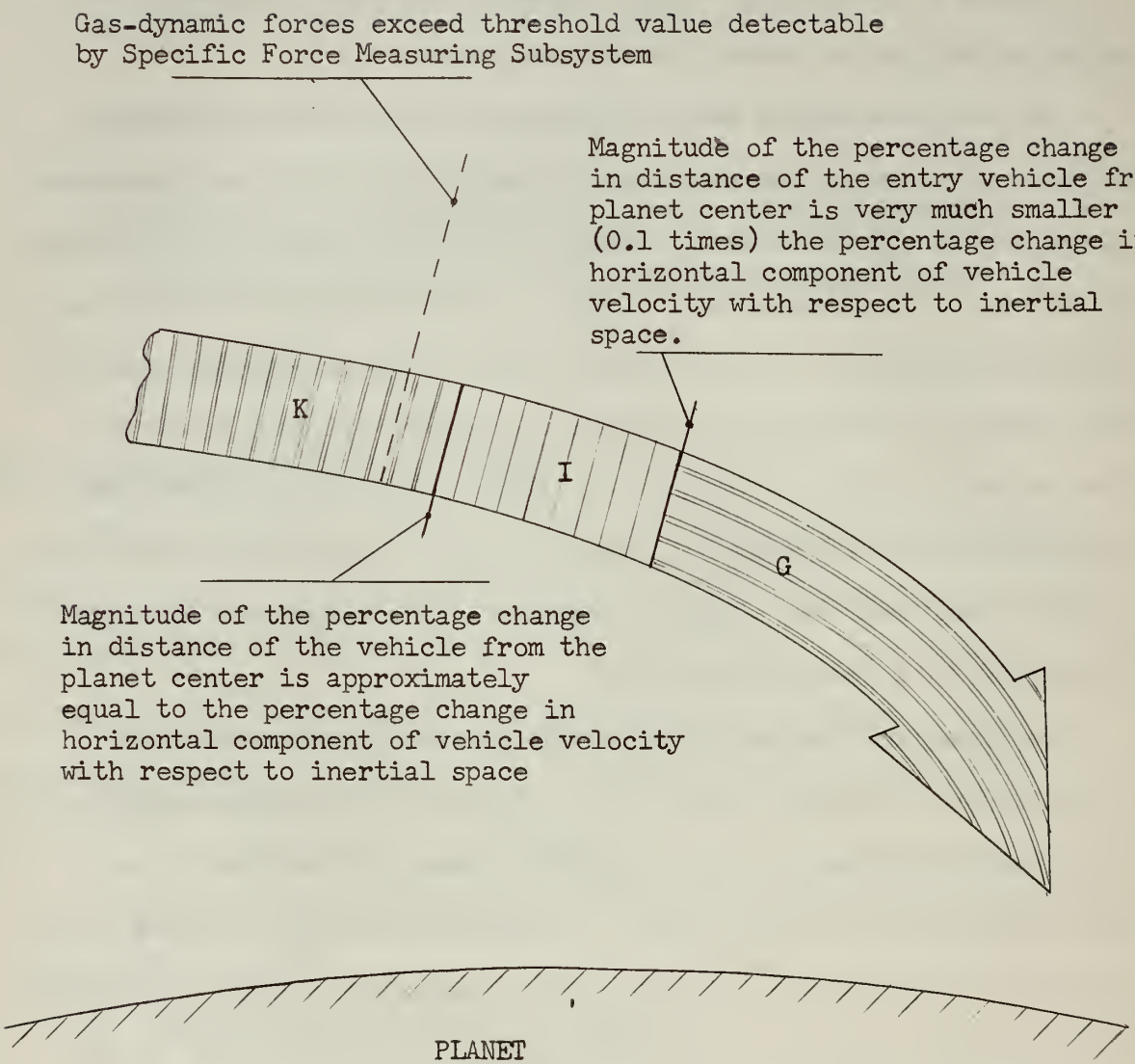

Key

K: Keplerian Phase
I: Intermediate Phase
G. Gas-Dynamic Phase

Fig. 8.1 : Phases of the Entry Trajectory and Definition of Boundary Conditions

drag characteristics.

The Keplerian Phase and the Gas-Dynamic Phase have been examined extensively in the current literature. The Intermediate Phase, on the other hand, has been largely ignored in trajectory studies. From the guidance standpoint, this is a very important phase, particularly in the degenerate orbital entry profile where perturbations in the Intermediate Phase in the vicinity of perigee are the mechanism by which eventual entry is induced. The Intermediate Phase is also important in the direct entry profile; this transition from Keplerian motion to Gas-Dynamic flight spans an altitude band of the order of 20 miles in the case of entry into the Earth's atmosphere*. The distance flown while in the Intermediate Phase may be a significant portion of the total vehicular range.

8.2 Conservation of Energy and Angular Momentum

Angular momentum was defined in equation (4-1) as:

$$P = RV_{I\phi} \qquad (4\text{-}1)$$

The time rate of change of angular momentum is therefore:

$$\dot{P} = \dot{R}V_{I\phi} + R\dot{V}_{I\phi} \qquad (8\text{-}1)$$

Defining the following auxiliary parameter:

$$\xi = -\frac{\dot{R}/R}{V_{I\phi}/V_{I\phi}} \qquad (8\text{-}2)$$

- - - - - - - - - - - - - - - -

* Assuming constant flight path angle and constant drag coefficient. If the drag coefficient is reduced by a factor of $\frac{1}{2}$ during the course of this phase, such as might occur if the flow regime changes from free molecular to continuum, the altitude band of this phase increases to approximately 24 miles.

With equation (8-2), equation (8-1) is written:

$$\dot{P} = -\frac{(1-\xi)\dot{}}{\xi} R V_{I\phi} \qquad (8\text{-}3)$$

Using the non-dimensionalizing procedure described in Chapter 6, equation (8-3) is written in dimensionless form as follows:

$$p' = -\frac{(1-\xi)}{\xi} r' v_{I\phi} \qquad (8\text{-}4)$$

The Conservation Parameter was defined as follows:

$$(\text{Conservation Parameter}) \equiv \left| \frac{1-\xi}{\xi} \right| \qquad (8\text{-}5)$$

The name Conservation Parameter was chosen because of the close relation of this quantity to conservation of energy and angular momentum.

The magnitude of the rate of transfer of angular momentum from the vehicle to the atmosphere is the product of the Conservation Parameter, the rate of change of altitude, and the horizontal component of velocity with respect to inertially fixed coordinates. During the Intermediate Phase, the change of velocity is small, hence the $v_{I\phi}$ term in equation (8-4) is nearly constant in this phase.

Total energy per unit mass was defined in equation (4-10) as:

$$\frac{\mathcal{E}_{tot}}{M} = \frac{-\gamma_g M_o}{R} + \frac{\bar{V}_I \cdot \bar{V}_I}{2} \qquad (4\text{-}10)$$

In dimensionless form, this was written in equation (6-54) as:

$$E_{(tot)} = \frac{v_I^2}{2} - \frac{1}{r} \qquad (6\text{-}54)$$

Equation (6-55) showed that the rate of change of total energy may be expressed as:

$$E'_{(kin)} + E'_{(pot)} = \bar{f} \cdot \bar{v}_I = r' f_r + v_{I\phi} f_\phi \qquad (8\text{-}6)$$

where f_r and f_ϕ are the radial and horizontal components of external specific forces in mean surface g's of the planet.

Differentiating equation (6-54), substituting into equation (8-6), and rearranging gives:

$$1 + \frac{E'_{(kin)}}{E'_{(pot)}} = r^2 \left[fr + \frac{v_{I\phi}}{r'} f\phi \right] \qquad (8\text{-}7)$$

It was shown in Chapter 6 that for a spherical planet:

$$F_\phi = \dot{V}_{I\phi} + \frac{\dot{R}}{R} V_{I\phi} \qquad (8\text{-}8)$$

Equation (8-8) is written in dimensionless form as:

$$f_\phi = (1 - \xi)\, v'_{I\phi} \qquad (8\text{-}9)$$

Therefore, equation (8-7) may be written:

$$1 + \frac{E'_{(kin)}}{E'_{(pot)}} = r^2 \left[fr - \left(\frac{1-\xi}{\xi}\right) \frac{v^2_{I\phi}}{r} \right] \qquad (8\text{-}10)$$

Equation (8-10) shows that in a Keplerian trajectory ($fr = 0$, $\xi = +1.0$) :

$$E'_{(kin)} = - E'_{(pot)} \qquad (8\text{-}11)$$

This corresponds to a continuous trade-off of kinetic and potential energy throughout the trajectory; total energy remains constant. For small flight path angles, the radial component of external specific force is approximately equal to n_L and the horizontal component is

approximately equal to $-n_D$. The predominant term in the bracket on the right-hand-side of equation (8-7) is $\frac{v_{I\phi}}{r'} f\phi$ because r' is generally very much smaller than $v_{I\phi}$ until near the terminal phase of the mission. Therefore, in the vicinity of atmospheric perturbations where velocities are generally high and flight path angles are relatively small, equation (8-10) reduces to the following approximate form:

$$1 + \frac{E'(kin)}{E'(pot)} = - \left(\frac{1-\xi}{\xi}\right) v_{I\phi}^2 r \qquad (8\text{-}12)$$

Equation (8-12) is plotted in Fig. 8.2. The Keplerian Phase of the trajectory corresponds to ξ in the vicinity of +1 while the Gas-Dynamic Phase corresponds to ξ in the vicinity of zero. All other values of ξ correspond to flight in the Intermediate Phase. In the Keplerian Phase, the rate of change of kinetic energy is equal to the negative of the rate of change of potential energy. In the Gas-Dynamic Phase, the magnitude of kinetic energy transfer rate is very much greater than the magnitude of the potential energy transfer rate.

8.3 Relating the Flight Trajectory and the Conservation Parameter

Gas-Dynamic forces become significant, from the guidance standpoint, when they are of sufficient magnitude to be detectable by accelerometers carried within the vehicle. The trajectory is described by a pure Keplerian transfer ellipse as long as the angular momentum of the entry trajectory is conserved. Under these conditions, $F_\phi = 0$ in equation (8-8); therefore:

$$\frac{\dot{V}_{I\phi}}{V_{I\phi}} = - \frac{\dot{R}}{R} \qquad (8\text{-}13)$$

or

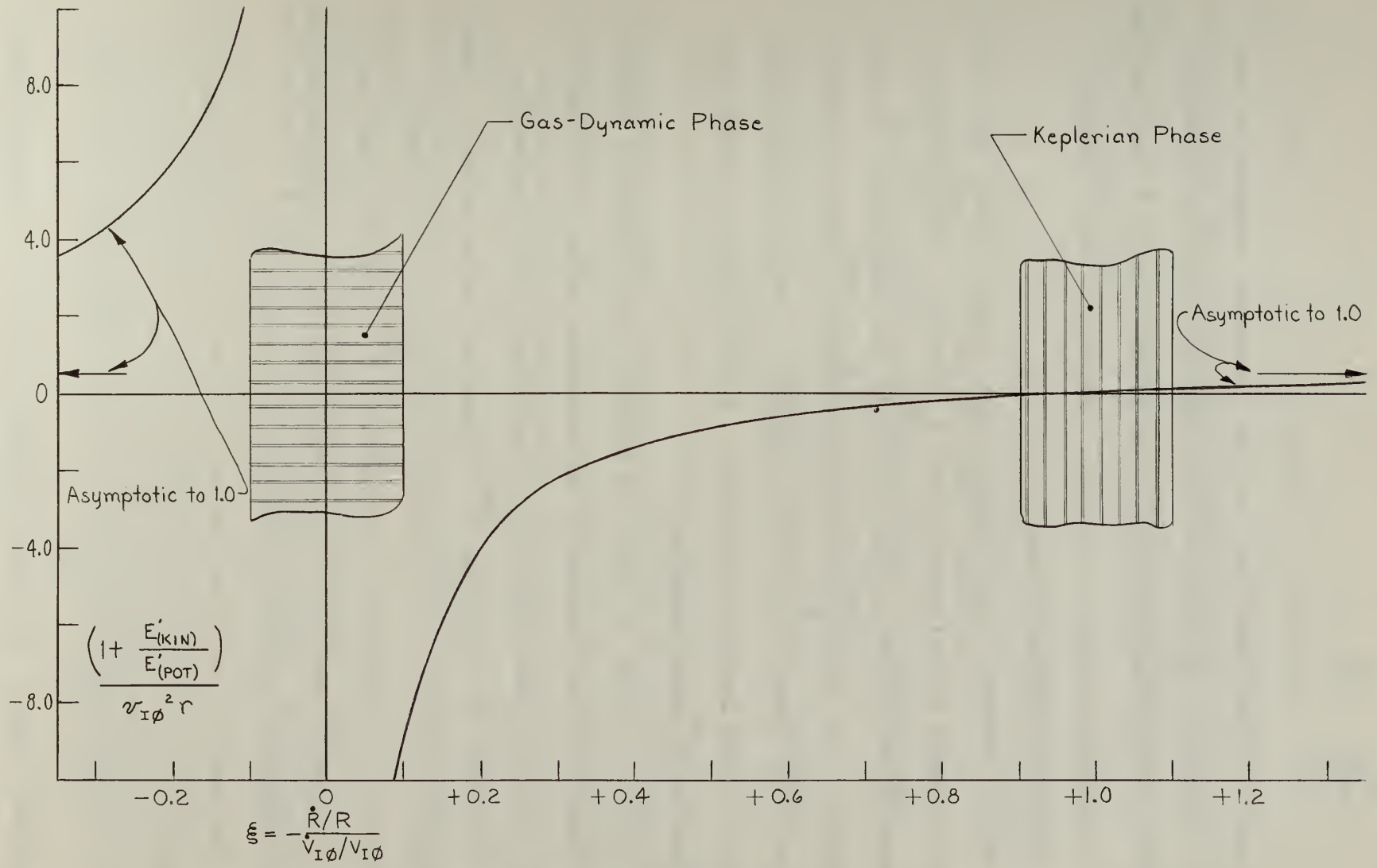

Fig. 8.2: Kinetic-Potential Energy Transfer Rate as Function of Ratio of Percentage Change in Radial Distance of the Entry Vehicle from the Planet Center to the Percentage Change in Horizontal Velocity.

$$\frac{dV_{I\phi}}{V_{I\phi}} = - \frac{dR}{R} \qquad (8\text{-}14)$$

Equation (8-14) shows that in order for angular momentum of the entry trajectory to be conserved, the percentage change in distance of the entry vehicle from the center of the planet is equal to the negative of the percentage change in horizontal component of vehicle velocity with respect to inertial space.

Angular momentum is <u>not</u> conserved when external forces (e.g., lift, drag, and thrust forces) exist in the $\bar{l}_\phi$ direction. The auxiliary parameter ξ was defined in equation (8-2). The magnitude of ξ is an expression of the ratio of the percentage change in radial distance to the percentage change in horizontal component of vehicle velocity with respect to fixed inertial coordinates. ξ must be equal to unity for conservation of angular momentum.

During the course of entry, the magnitude of the ratio of percentage change in radial distance to the percentage change in horizontal velocity will decrease toward zero as gas-dynamic forces become predominant factors in specifying the ultimate path of the vehicle. Hence, the magnitude of ξ is an indication of the degree to which angular momentum of the trajectory is conserved; as ξ becomes very much smaller than 1.0, angular momentum is transferred rapidly to the gaseous envelope of the atmosphere through the mechanism of lift and drag.

From equation (8-9), the horizontal component of external specific force is:

$$f_\phi = - \left(\frac{1-\xi}{\xi}\right) \frac{r'}{r} v_{I\phi} \qquad (8\text{-}15)$$

In powerless flight, f_ϕ results entirely from lift and drag gas-dynamic

forces:

$$f_{\phi} = -(n_D \cos\gamma + n_L \sin\gamma) = -n_D \cos\gamma\,(1 + (L/D)\tan\gamma) \qquad (8\text{-}16)$$

For small flight path angles, f_{ϕ} is always negative*. With the left side of equation (8-15) negative, the following conditions are required of the right hand side:

If $\dot{V}_{I\phi} < 0$: ξ must be less than +1.0 or must be negative.

If $\dot{V}_{I\phi} > 0$: ξ must be greater than +1.0.

If $\dot{R} < 0$ (i.e., descending flight): ξ must be greater than +1.0 or it must be negative.

If $\dot{R} > 0$ (i.e., ascending flight): ξ must lie between 0 and +1.0.

Fig. 8.3 shows the resulting flight regimes for a vehicle entering the planetary atmosphere. Boundaries separating the various phases of the trajectory are shown on Fig. 8.3 in terms of the auxiliary parameter ξ. It is noted that a true Keplerian description of the trajectory applies only for $\xi = +1.0$; it was assumed in this analysis that the Keplerian description of the trajectory is adequate for small departures of ξ from 1.0 (i.e., $0.9 < \xi < 1.1$).

Fig. 8.3 can best be visualized as a cylindrical graph; i.e., the points at $\xi = \pm\infty$ should be connected together. The Keplerian

- - - - - - - - - - - - - - - - -

* For descending flight (i.e., γ negative), it is seen from equation (8-16) that $f\phi$ is positive only when $|(L/D)\tan\gamma| > 1.0$, a condition which could arise only for relatively large negative flight path angles with a vehicle having a relatively high lift-drag ratio.

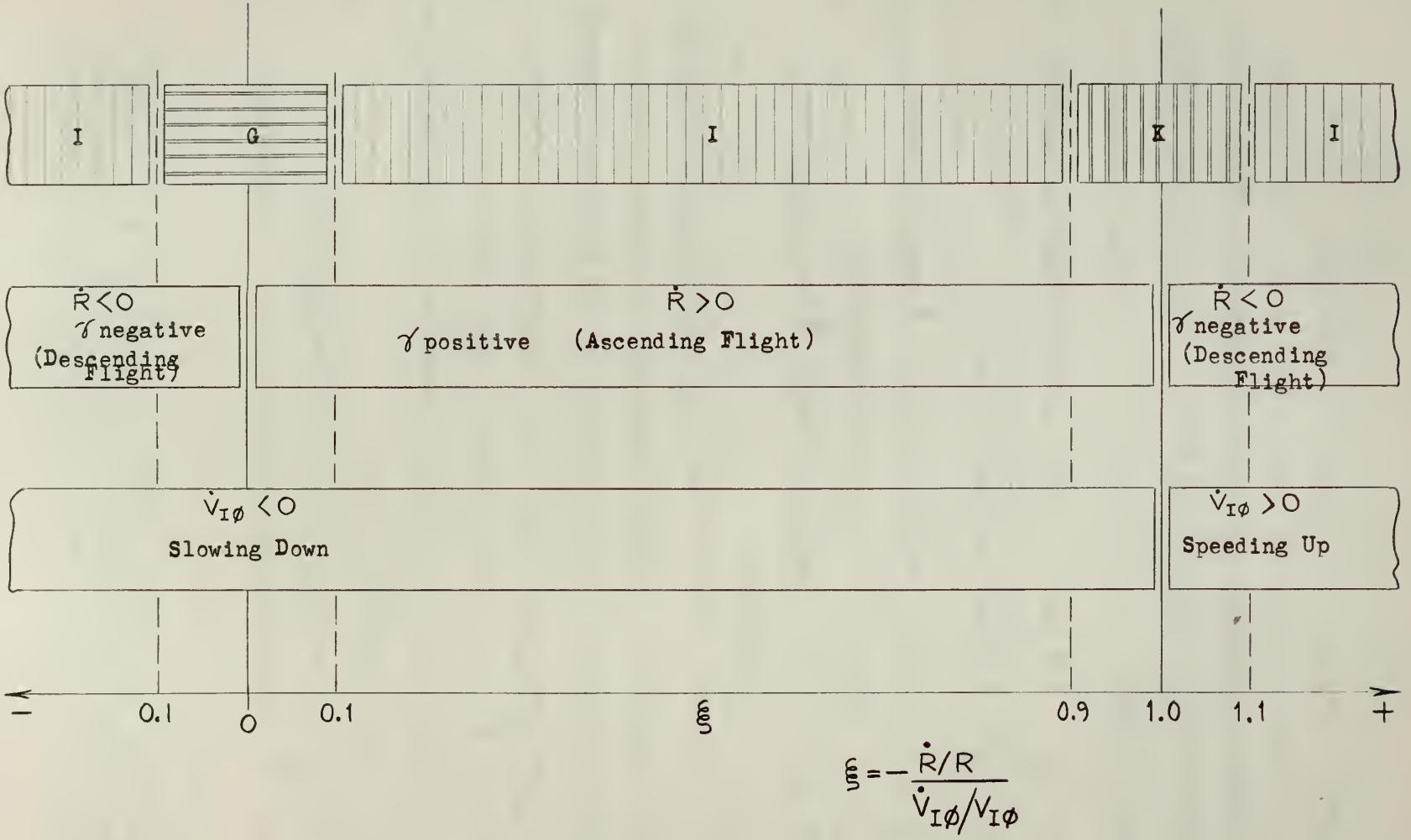

Fig. 8.3: Flight Regimes of Entry Trajectory

Key
K: Keplerian Phase
I: Intermediate Phase
G: Gas-Dynamic Phase

Phase is a small region in the neighborhood of $\xi = +1.0$. The region within $\pm$ 0.1 of $\xi = 1.0$ is the region in which the gas-dynamic terms in the equations of motion are negligibly small in comparison to the other terms; i.e., the terms involving n_L and n_D in equations (6-47) and (6-48) are zero for $\xi = 1.0$ and are negligible for $0.9 < \xi < 1.1$. The Gas-Dynamic Phase, on the other hand, is a small region in the vicinity of $\xi = 0$. In the band $-0.1 < \xi < +0.1$, the $\frac{v_r v_\phi}{r}$ term in equation (6-48) is less than 0.1 of the lift and drag terms and can reasonably be ignored. The Intermediate Phase spans all other values of ξ not included in the Gas-Dynamic Phase and the Keplerian Phase. In the Intermediate Phase, all terms in the equations of motion must be retained for a reasonably accurate guidance analysis of entry.

The fact that the parameter ξ has a sharp behavior during the course of an entry mission can be inferred from Fig. 8.3. For this purpose, the $\dot{R}$ and $\dot{V}_{I\phi}$ bands shown in this figure are instructive. ξ lies between zero and 1.0 for climbing flight; i.e., γ is positive in this region. For ξ negative and for $\xi > +1.0$, the vehicle is in descending flight (γ = negative). The vehicle is always slowing down ($\dot{V}_{I\phi} < 0$) in ascending flight; if it is slowing down at the same time it is descending, then ξ must be negative. The speed of the vehicle increases only in descending flight and only when $\xi > 1.0$. At these points where $\dot{V}_{I\phi} = 0$, ξ is $\pm\infty$. The behavior is sharp because ξ moves from infinity to zero during the time interval between the instant that $\dot{V}_{I\phi} = 0$ and $\dot{R} = 0$. In elliptical flight with small drag forces, for example, these two points occur very close to each other in the vicinity of perigee and apogee. They would occur simultaneously in

pure vacuum flight. In the vicinity of perigee when small drag forces exist, $\dot{V}_{I\phi}$ goes to zero shortly <u>before</u> $\dot{R}$ goes to zero. In the vicinity of apogee if some drag exists, $\dot{V}_{I\phi}$ goes to zero a very short time <u>after</u> $\dot{R} = 0$.

To illustrate the behavior of ξ as a consequence of the foregoing conditions, it is instructive to consider a couple of simple examples. Fig. 8.4 shows a typical braking pass in the planetary atmosphere such as occurs in the vicinity of perigee during the unstable orbital profile. When the vehicle is approaching the planet at a very high altitude, gas-dynamic forces are negligible and ξ is near 1.0. In this, the Keplerian region, the vehicle is descending ($\dot{R} < 0$) and velocity is increasing ($\dot{V}_{I\phi} > 0$) due to kinetic-potential energy trade-off. As drag forces increase, ξ increases to 1.1 when the Keplerian-Intermediate Phase boundary is crossed; velocity is still increasing due to energy trade-off, but the rate of increase decreases as drag forces become more pronounced. Ultimately in the Intermediate Phase, the effects of drag and the effects of energy trade-off cancel; at this point $\dot{V}_{I\phi} = 0$ and ξ passes from $+\infty$ to $-\infty$. At some later time perigee is crossed ($\dot{R} = 0$); ξ has increased rapidly from $-\infty$ to its value of zero at perigeal passage. As the vehicle now ascends through the outer reaches of the atmosphere, $\dot{R}$ is positive and $\dot{V}_{I\phi}$ is negative; here ξ continues to increase as atmospheric drag forces become less significant until at about $\xi = 0.9$, the vehicle is again effectively in Keplerian flight. During this braking pass, a pulse of energy and a pulse of angular momentum are transferred to the planetary atmosphere.

Fig. 8.5 shows a gliding direct entry profile. Unless skipping

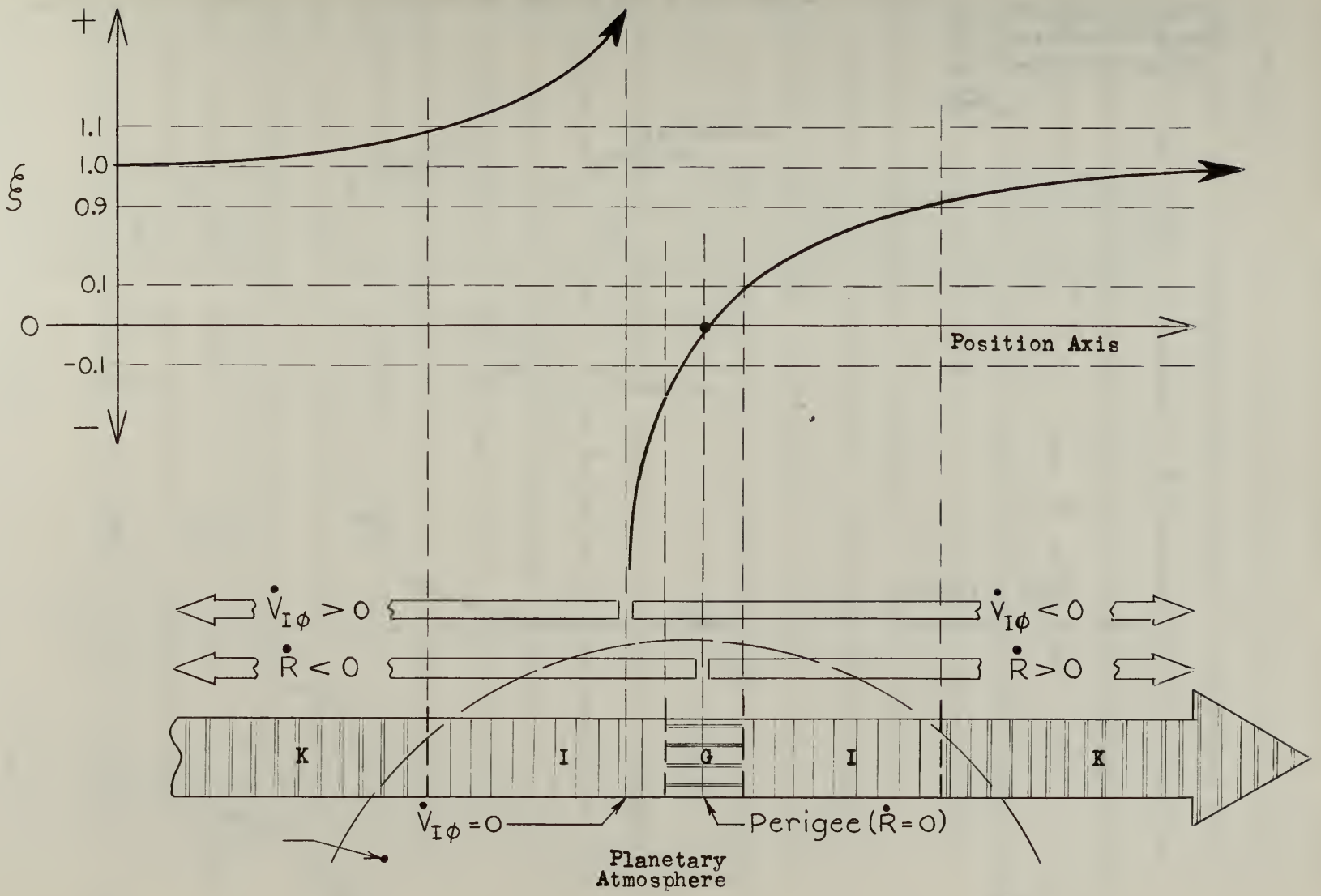

Fig. 8.4: Behavior of ξ-Parameter During a Braking Pass

Key

K: Keplerian Phase
I: Intermediate Phase
G: Gas-Dynamic Phase

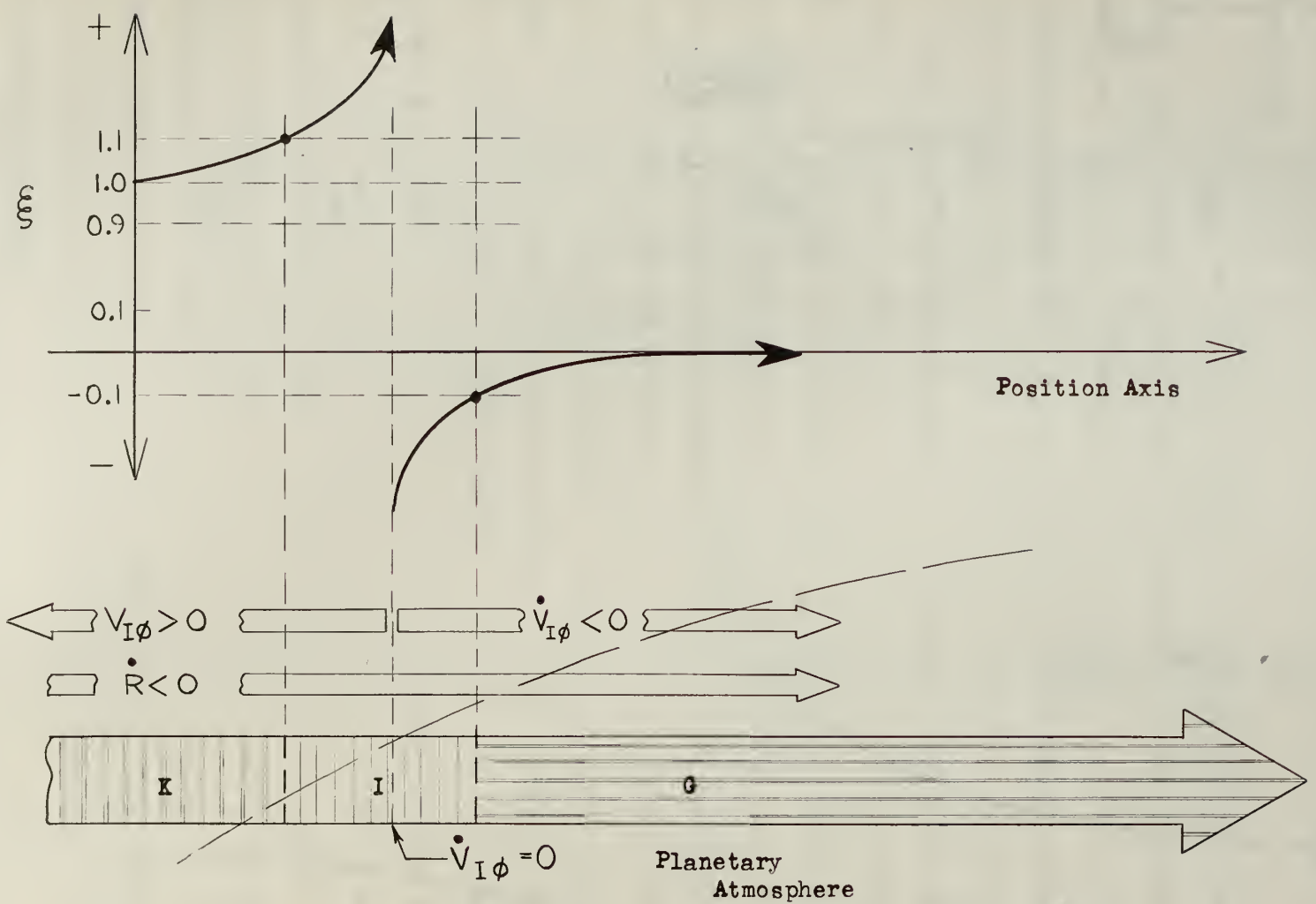

Key

K: Keplerian Phase
I: Intermediate Phase
G: Gas-Dynamic Phase

Fig. 8.5: Behavior of ξ-Parameter During the Direct Entry Profile

motion is induced by the planetary atmosphere*, the radius is always decreasing; i.e., $\dot{R} < 0$. During the Keplerian portion of flight and during part of the Intermediate Phase, velocity is increasing due to kinetic-potential energy trade-off. ξ increases from its characteristic value of 1.0 in Keplerian flight to $+\infty$ as drag forces increase. When drag forces reduce $\dot{V}_{I\phi}$ to zero, ξ moves from + to - at infinity. ξ increases from $-\infty$ toward zero as gas-dynamic drag builds up with altitude loss; when $\xi \cong -0.1$, the vehicle enters the Gas-Dynamic phase and remains in this phase of flight thereafter.

Equations (8-4), (8-12) and (8-15) expressed rate of change of angular momentum, energy, and horizontal force level as functions of ξ. In all cases, ξ appears in the combination $(\frac{1-\xi}{\xi})$. The magnitude of this combination was defined in this thesis as the Conservation Parameter; this is a convenient quantity for defining the boundary conditions between phases. At the Keplerian-Intermediate Phase boundary, the Conservation Parameter is approximately equal to 0.1; and at the Intermediate-Gas-Dynamic phase boundary, the Conservation Parameter is approximately equal to 10. The information of Fig. 8.3 is shown on Fig. 8.6 as a function of $(\frac{1-\xi}{\xi})$. From this figure it is seen that the vehicle is in ascending flight when $(\frac{1-\xi}{\xi})$ is positive and in descending flight when this quantity is negative. $\dot{V}_{I\phi}$ is negative in all regimes except $-1.0 < (\frac{1-\xi}{\xi}) < 0$; i.e., the horizontal velocity of the vehicle can increase only in the Keplerian Phase and during a portion of the Intermediate Phase.

- - - - - - - - - - - - - - - - -

* See Chapter 9 for a discussion of skipping flight.

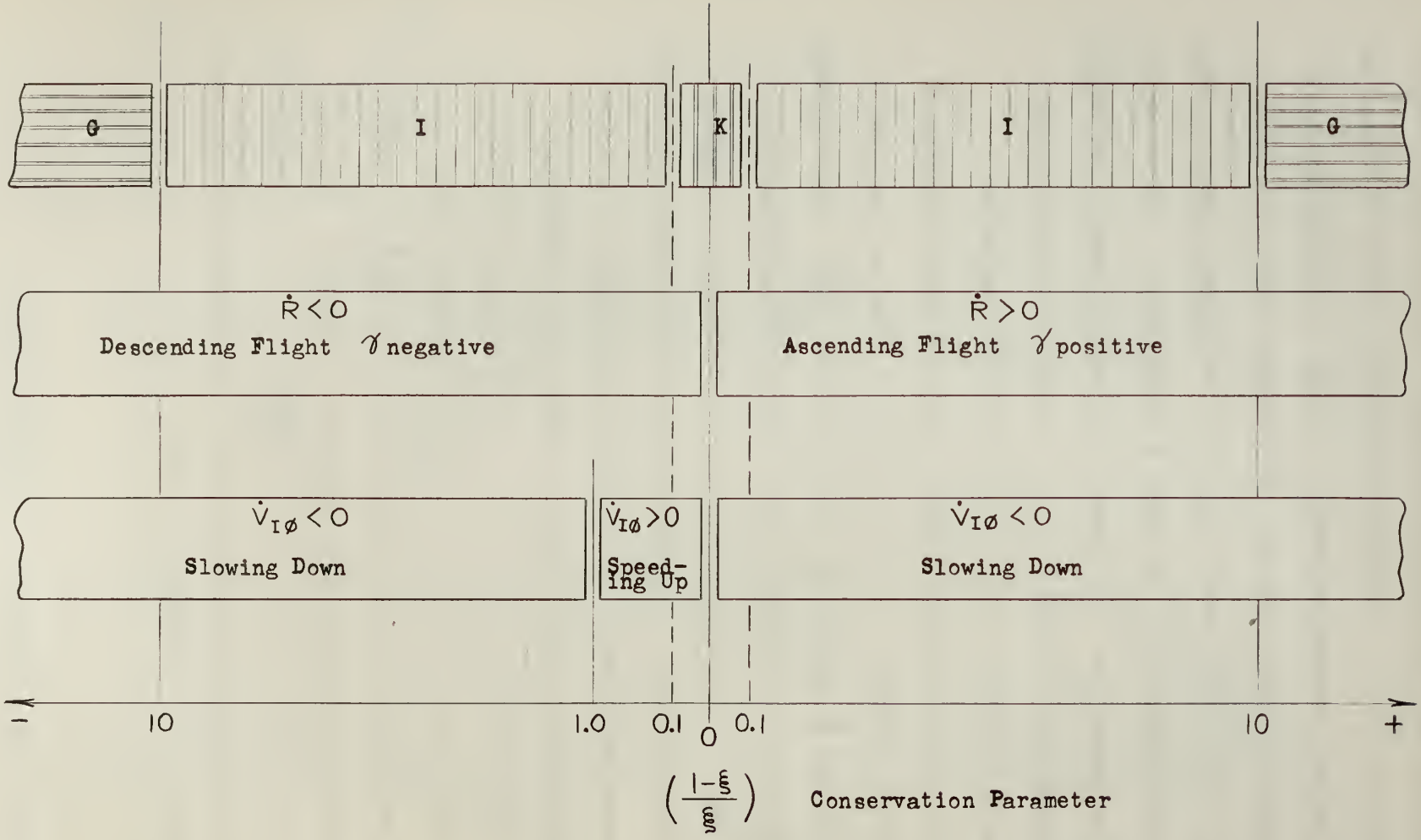

Fig. 8.6: Flight Regimes of Entry Trajectory as a Function of the Conservation Parameter

8.4 Altitude Description of Boundaries Between Operational Phases of the Entry Trajectory

The horizontal component of specific force was written as a function of the Conservation Parameter in equation (8-15) and as a function of lift and drag forces in equation (8-16). Eliminating f_ϕ from these two equations gives:

$$n_D \cos\gamma + n_L \sin\gamma = \left(\frac{1-\xi}{\xi}\right) \frac{r'}{r} v_{I\phi} \tag{8-17}$$

The following relations were given in Chapter 6 for the dimensionless quantities required in Equation (8-17) (assuming the exponential atmospheric model and no atmospheric winds):

$$n_D = \left(\frac{C_D S}{M}\right) \frac{\rho_{(SL)}}{2} R_{(m)o} v^2 e^{-kh} \tag{8-18}$$

$$n_L = n_D (L/D) \tag{8-19}$$

$$r' = v \sin\gamma \tag{8-20}$$

$$v_{I\phi} = v \cos\gamma + r\Omega \cos\psi \tag{8-21}$$

Substituting equations (8-18) through (8-21) into equation (8-17) gives:

$$\frac{R_{(m)o}\, \rho_{(SL)}}{2} \frac{S}{M} e^{-kh} \left[\frac{C_D}{\sin\gamma} + \frac{C_L}{\cos\gamma}\right] = \left(\frac{1-\xi}{\xi}\right)\left(\frac{1}{r} + \frac{\Omega\cos\psi}{v\cos\gamma}\right) \tag{8-22}$$

This is written in logarithmic form as follows:

$$K_{EO} h + C_e + 2.59 \times 10^{-3} \log\left[\frac{1}{r} + \frac{\Omega\cos\psi}{v\cos\gamma}\right]$$

$$= 2.59 \times 10^{-3} \left\{ \log\left(\frac{5.64 \times 10^4}{M/S}\right) + \log\left[\left(\frac{C_D}{\sin\gamma} + \frac{C_L}{\cos\gamma}\right)\left(\frac{\xi}{2(1-\xi)}\right)\right]\right\} \tag{8-23}$$

where

$$C_e \equiv - \frac{1}{k_E \log e} \log \left(\frac{\rho_{(\overline{SL})}}{\rho_{(\overline{SL})_E}} \frac{R_{(m)o}}{R_{(m)E}} \right) \qquad (8\text{-}24)$$

The following table gives values of quantities on the left side of equation (8-23):

Table 8.1: Conversion Quantities for use in Equation (8-23)

	Venus	Earth	Mars
K_{EO}	1.14	1.0	0.207
C_e	-2.77×10^{-3}	0	3.87×10^{-3}
Ω	2.69×10^{-4}	5.87×10^{-2}	6.75×10^{-2}

The left side of equation (8-23) expresses dimensionless altitude directly for the Earth (for $v > 0.1$). It is plotted as "altitude function" on subsequent graphs. At very low velocities, the term on the left side of this equation involving planetary rotation becomes significant. For example:

If: $v \cos\gamma = 0.01$

$\psi = 0°$ (equatorial trajectory)

$1/r \cong 1.0$

$$2.59 \times 10^{-3} \log \left(\frac{1}{r} + \frac{\Omega \cos\psi}{v \cos\gamma}\right) \cong 2.16 \times 10^{-3}$$

$$\cong 8.7 \text{ miles (Earth)}$$

At velocities actually existing in the altitude range for which equation

(8-23) is useful (i.e., in specifying boundaries of the Intermediate Phase), the third term on the left side is negligible.

In order to illustrate the behavior of equation (8-23), the vehicle with $(L/D)_{max} = 2.0$ listed in Table 5.1 was plotted on Fig. 8.7. Mass characteristics chosen for this graph was $M/S = 1.0$ slugs/ft^2. The effect on the location of the resulting curves for other M/S is indicated in the figure. Four separate flight path angles were selected; these ranged in value from $\gamma = \pm 0.01°$ to $\pm 10°$. The effects of varying the angle of attack from zero to the value corresponding to $(L/D)_{max}$ is shown for each flight path angle.

The curves of Fig. 8.7 were plotted for constant flight path angles. In general, the trajectory of the lifting entry vehicle will be characterized by a changing flight path angle as it passes through the Intermediate Phase, hence the true altitude band in this phase may be greater or less than that indicated by a constant γ curve. For example, if the vehicle has a flight path angle of -10° at an altitude of 15×10^{-3} on Fig. 8.7, it corresponds to a near Keplerian trajectory (abscissa near 1.0). If the magnitude of the flight path angle rapidly decreases to -0.01°, as in the early phase of a skip, the trajectory (at the same altitude) may be described as in the Gas-Dynamic Phase (abscissa less than 0.1). These figures show that for a given flight path angle, angular momentum is essentially conserved down to an altitude that is strongly dependent on the characteristics of the vehicle and on the flight path angle. Once the vehicle has descended to this altitude, angular momentum rapidly is transferred to the atmosphere. The altitude range over which the abscissa of Fig. 8.7 moves from approximately 1.0 to approximately 0.1 is called herein the

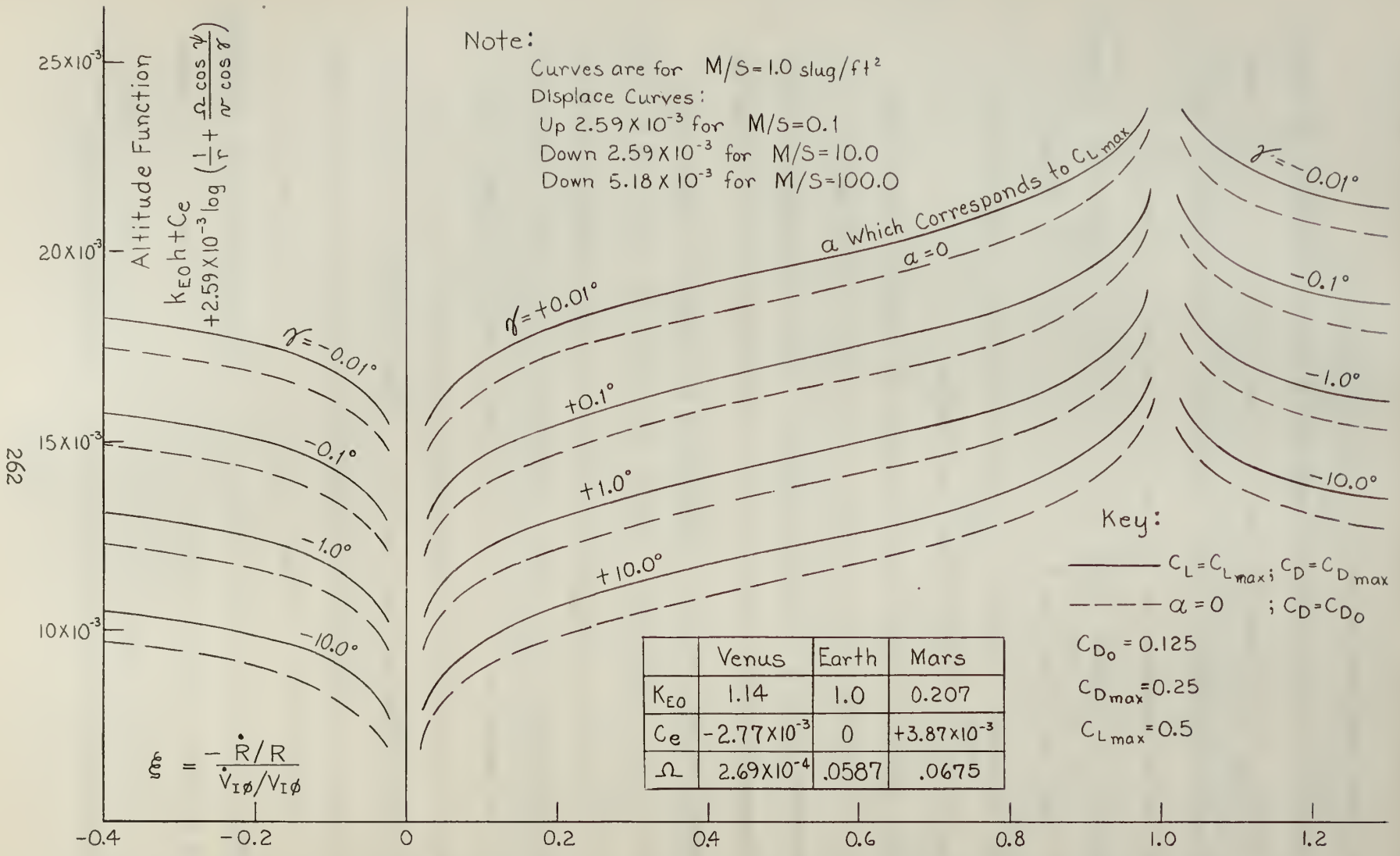

	Venus	Earth	Mars
K_{EO}	1.14	1.0	0.207
C_e	-2.77×10^{-3}	0	$+3.87 \times 10^{-3}$
Ω	2.69×10^{-4}	.0587	.0675

Fig. 8.7: Behavior of ξ-Parameter as a Function of Altitude at Various Flight Path Angles for $(L/D)_{max} = 2.0$

Note: Angular Momentum is Conserved at abscissa = 1.0

Intermediate Phase. Below this altitude, the trajectory is described as in the Gas-Dynamic Phase.

At flight path angles with magnitudes less than 10°, the upper and lower altitude bounds of the Intermediate Phase is a very weak function of lift coefficient. This weak dependence arises from the fact that (at γ small) the horizontal component of external specific force is made up almost entirely of gas-dynamic drag. This weak dependence on lift was verified by plotting curves similar to Eq. 8.7 for many classes of vehicles with and without the lift term included. The lift term generally caused such slight displacement of the phase boundaries as to be virtu ally unperceptible. Lift terms become significant only with large lift-drag ratios at flight path angles greater than five to ten degrees.

With the weak dependence of the locus of the Intermediate Phase boundaries on lift having been established, Fig. 8.8 was plotted to show the phase boundaries for various drag parameters.

The curves of Fig. 8.8 show the Keplerian-Intermediate phase boundary and the Intermediate-Gas-dynamic phase boundary for four separate flight path angles, $\gamma = \pm$ 0.01°, 0.1°, 1°, and 10°. The altitude band spanned by the Intermediate Phase at a given drag parameter and a given flight path angle is approximately 25 miles for Venus, 20 miles for Earth, and 10 miles for Mars.

8.5 Description of Boundaries Between Operational Phases of the Entry Trajectory in Terms of the Horizontal ($\bar{1}_\phi$) Component of Specific Force

The horizontal component of the specific forces measured by an accelerometer oriented in the $\bar{1}_\phi$ direction was given in equation (8-16).

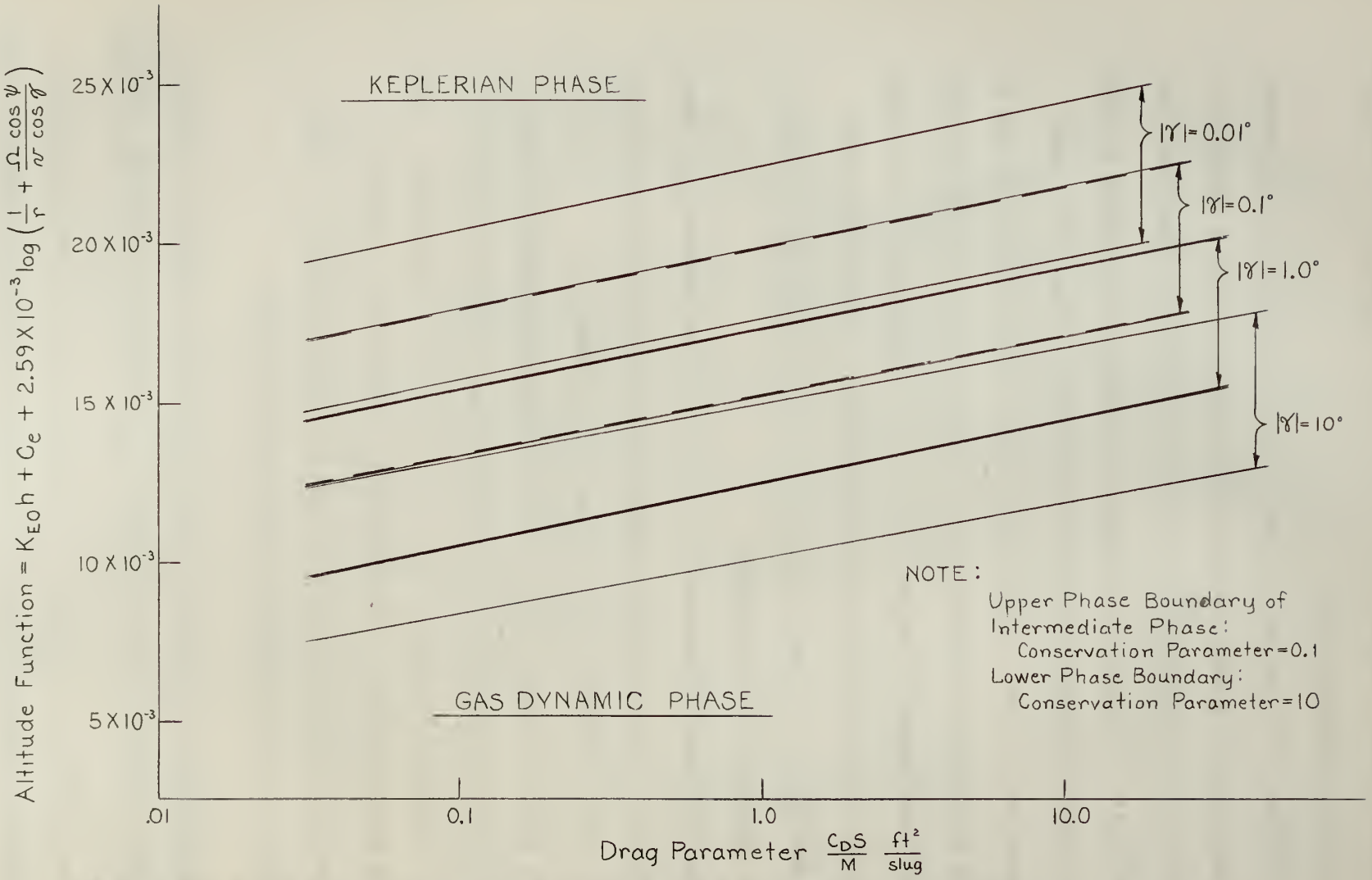

Fig. 8.8: Phase Boundaries of Intermediate Phase for Various Drag Parameters

Using equations (8-18) and (8-19) this is written:

$$f_\phi = -\left(\frac{C_D S}{M}\right)\frac{\rho_{(\overline{SL})}}{2} R_{(m)o}\, v^2\, e^{-kh}\left(1 + \frac{L}{D}\tan\gamma\right)\cos\gamma \qquad (8\text{-}25)$$

In order to express f_ϕ in Earth g's, the following is used:

$$f_{E\phi} = \frac{G_{(m)o}}{G_{(m)E}} f_\phi \quad \text{Earth g's} \qquad (8\text{-}26)$$

Using equation (8-26), equation (8-25) is written in logarithmic form as follows:

$$K_{EO}h + C_e + C_g = 2.59 \times 10^{-3}\left[\log\left(1 + \frac{L}{D}\tan\gamma\right) + \log\left(\frac{5.64 \times 10^4}{M/S}\right) + \log C_D \cos\gamma - \log\left(\frac{-2 f_{E\phi}}{v^2}\right)\right] \qquad (8\text{-}27)$$

where C_e is given by equation (8-24) and:

$$C_g \equiv \frac{1}{k_E \log e}\log\left(\frac{G_{(m)o}}{G_{(m)E}}\right) \qquad (8\text{-}28)$$

The following table lists values of quantities given on the left side of equation (8-27).

Table 8.2: Conversion Quantities for use in Equation (8-27)

	Venus	Earth	Mars
K_{EO}	1.14	1.0	0.207
C_e	-2.77×10^{-3}	0	3.87×10^{-3}
C_g	0.0342×10^{-3}	0	0.713×10^{-3}

It is noted that the left side of equation (8-27) expresses dimensionless altitude directly, in the case of the planet Earth.

Equation (8-27) is plotted on Fig. 8.9 for the classes of vehicles listed in Table 5.1 with $M/S = 1.0$ slug/ft^2 and for a zero-lift vehicle with $C_D S/M = 20$. For small flight path angles and moderate lift-drag ratios, the curves are essentially independent of γ. The curves are drawn for values of C_D and C_L at $(L/D)_{max}$ for the lifting vehicles.

Equation (8-15) may be written as follows:

$$f_\phi = - \left(\frac{1-\xi}{\xi}\right) v^2 \sin\gamma \cos\gamma \left[\frac{1}{r} + \frac{\Omega \cos\psi}{v \cos\gamma}\right] \qquad (8\text{-}29)$$

At the altitudes and velocities which are important at the boundaries of the Intermediate Phase, the quantity in square brackets in equation (8-29) is approximately equal to 1.0. Therefore:

$$f_\phi \cong - \left(\frac{1-\xi}{\xi}\right) v^2 \sin\gamma \cos\gamma \cong - \left(\frac{1-\xi}{\xi}\right) v^2 \gamma \qquad (8\text{-}30)$$

Equation (8-29), and its simplified version (8-30), show the interesting result that transition from Keplerian flight through the Intermediate Phase to Gas-Dynamic flight is independent of the surface loading and lift-drag characteristics of the vehicle. The magnitude of the horizontal component of specific force in transition depends only on velocity and flight path angle. Hence, if flight path angle, velocity, and horizontal specific force are measured or computed by the guidance system, then the magnitude of the Conservation Parameter can be specified; this is an index of the degree to which angular momentum is being conserved and is indicative of whether the vehicle is in the Keplerian, Intermediate, or Gas-Dynamic Phases of the trajectory.

Equation (8-30) is plotted in Fig. 8.10 to show the boundaries between the various operational regimes as a function of the horizontal specific force measured by the accelerometers of the vehicle. This

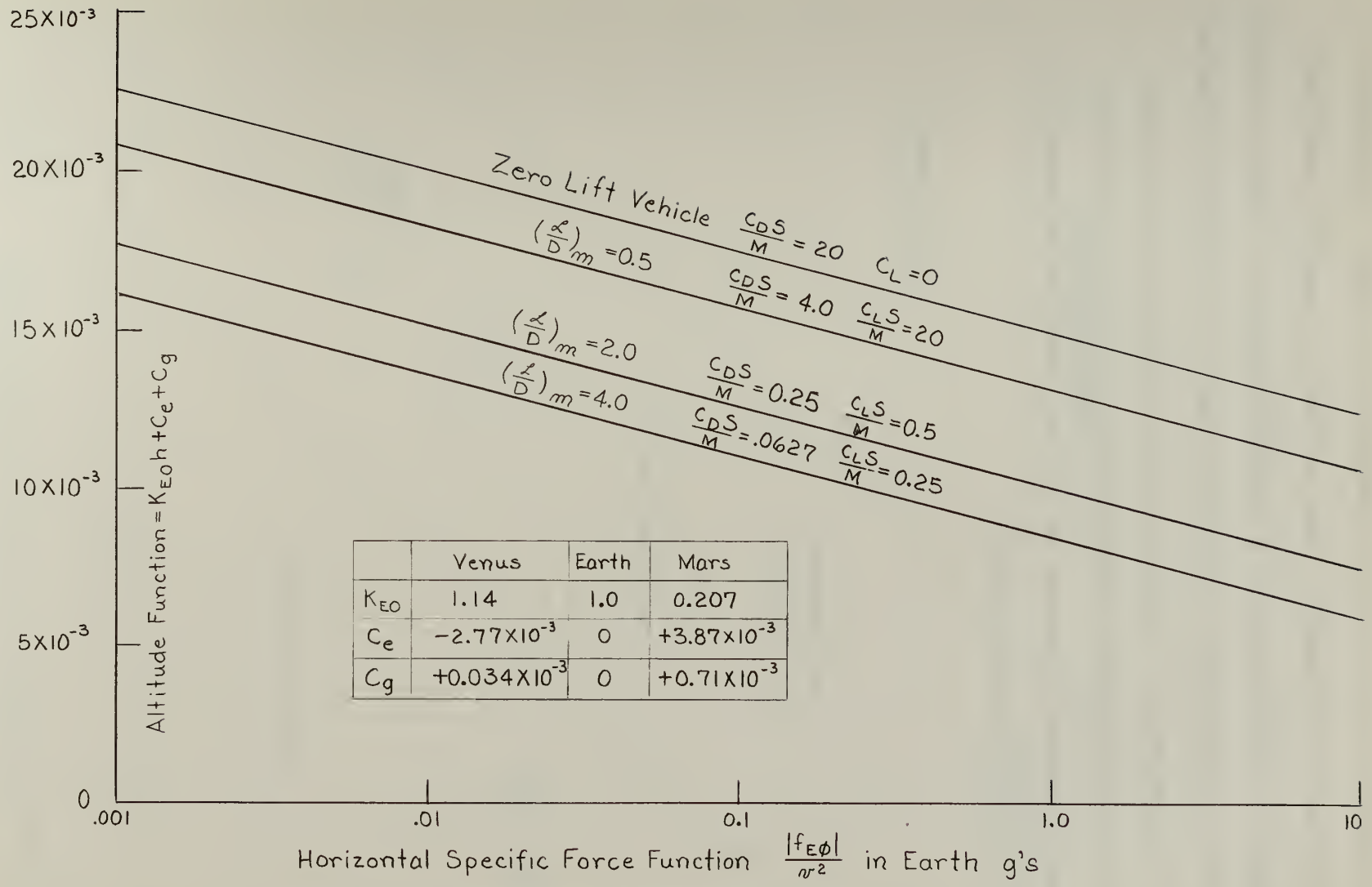

	Venus	Earth	Mars
K_{EO}	1.14	1.0	0.207
C_e	-2.77×10^{-3}	0	$+3.87\times10^{-3}$
C_g	$+0.034\times10^{-3}$	0	$+0.71\times10^{-3}$

Fig. 8.9: Horizontal Specific Force vs Altitude

figure shows that the force level changes by two orders of magnitude in traversing the Intermediate Phase and that the specific force level at transition between phases is a sensitive function of flight path angle.

The horizontal specific force level cannot give accurate information on the relative rate of transfer of angular momentum from the vehicle to the planetary atmosphere without accurate specification of flight path angle, which is tantamount to requiring precision measurements of vertical velocity (altitude rate).

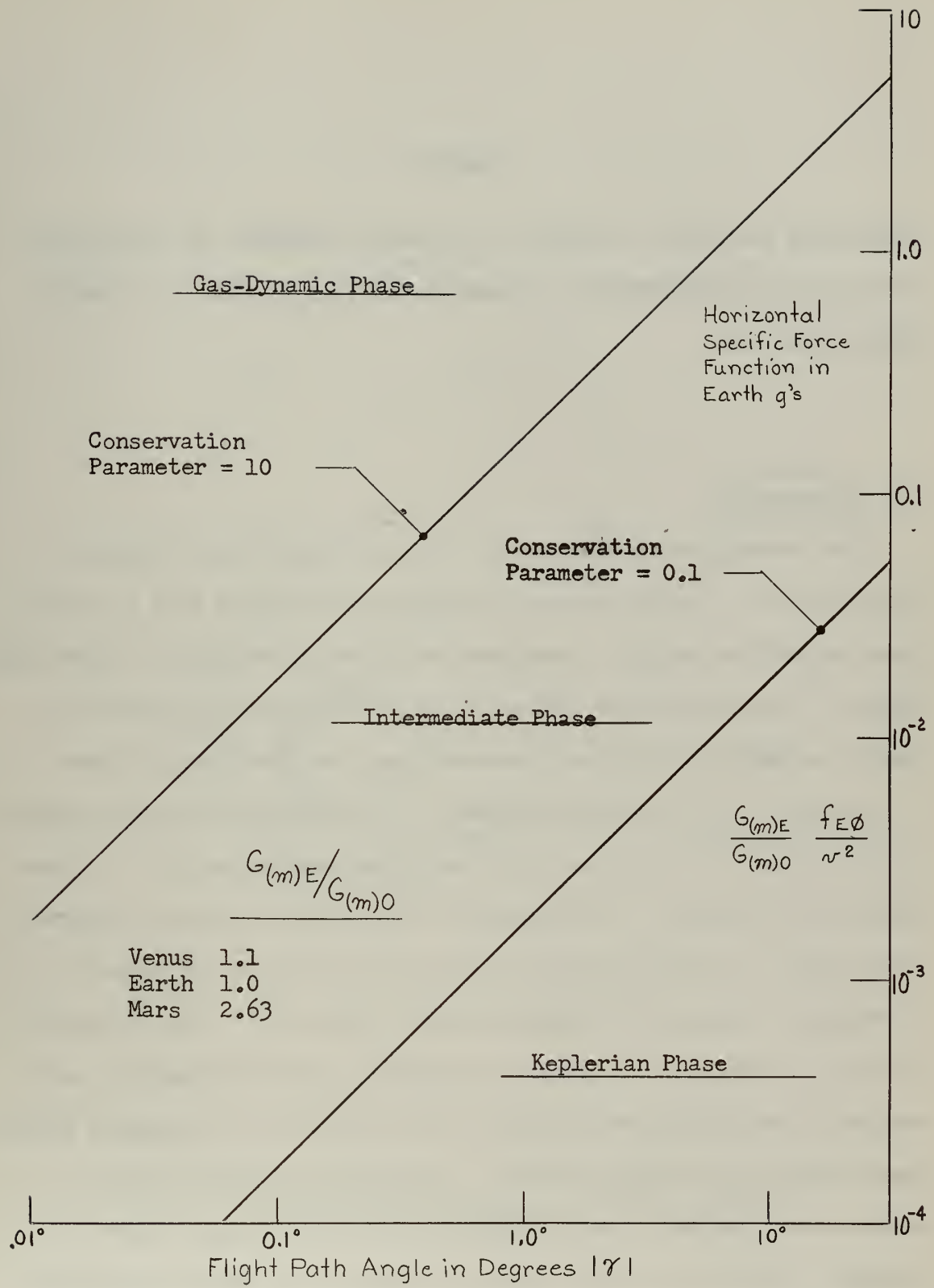

Fig. 8.10 : Level of Horizontal Specific Force at Boundaries Between Operational Phases as a Function of Flight Path Angle.

Chapter 9

APPROXIMATE ANALYTICAL SOLUTION OF GUIDANCE PARAMETERS AND CONSTRAINTS FOR THE DIRECT ENTRY PROFILE; RANGE SENSITIVITY TO ERRORS IN CONTROL SYSTEM OPERATION

9.1 Introduction

The investigation described in Chapter 8 demonstrated that the trajectory of a vehicle entering a planetary atmosphere from an initial point beyond the sensible atmosphere traverses three distinct operational regimes; these regimes are called in this thesis, for convenience in identification, the Keplerian, Intermediate, and Gas-Dynamic Phases.

Studies of entry vehicle dynamics in the past have largely ignored the existence of the Intermediate Phase as a separate entity. In some trajectories, however, the Intermediate Phase may be the most important single phase in specifying the ultimate destination of the vehicle. As an example, consider the degenerate orbit of Fig. 9.1. The trajectory of Fig. 9.1 consists of a series of "braking passes" through the outer reaches of the atmosphere; energy is transferred to the planetary atmosphere during each perigeal passage. During most of each orbit, the vehicle obeys Kepler's laws of planetary motion to a high degree of accuracy. However, in the vicinity of perigee, the vehicle enters the Intermediate Phase of operation momentarily and returns again to the

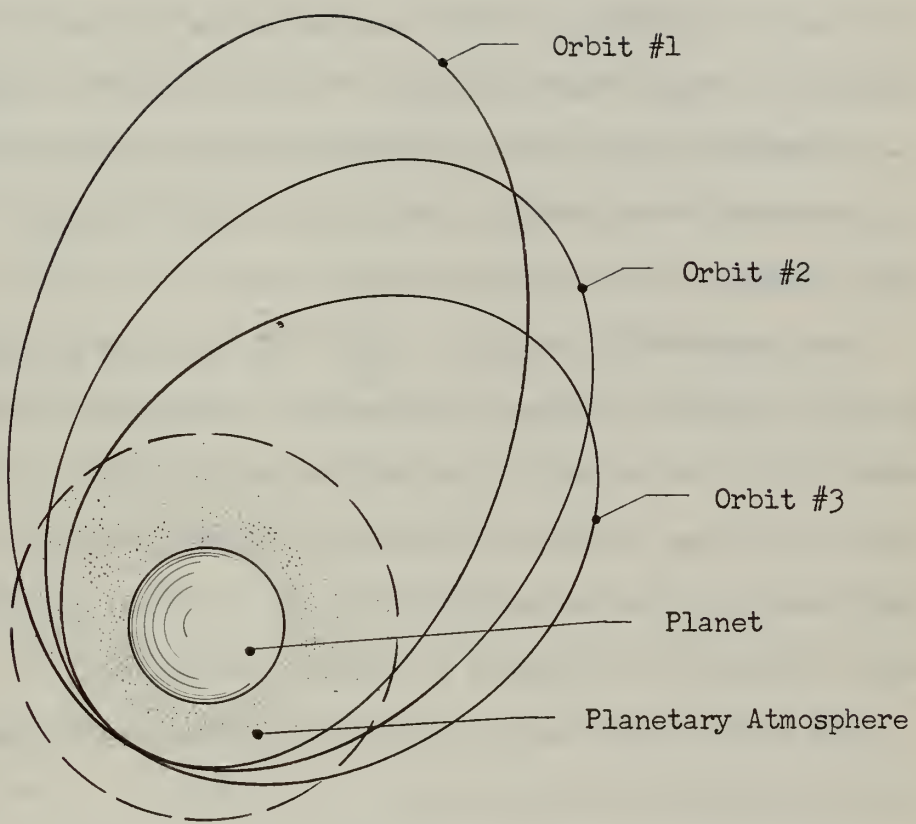

Fig. 9.1: The Degenerate Orbit of a Vehicle About a Planet Which Possesses an Atmosphere

Keplerian Phase. As a result of the impulses in the Intermediate Phase each successive apogee occurs at a lower altitude and eventual entry is assured. If the pilot desires to control the number of orbits remaining, he may change the drag characteristics of the vehicle during these impulses in the Intermediate Phase to bring about increased or decreased total energy transfer per orbit, and therefore shorten or lengthen, as desired, the flight time remaining. The fact that the vehicle enters the Intermediate Phase during trajectories such as sketched in Fig. 9.1 makes eventual entry possible without the use of external thrust; otherwise, the flight would continue indefinitely.

The Conservation Parameter $\left|\frac{1-\xi}{\xi}\right|$ was selected as convenient for defining boundaries between the Keplerian, Intermediate, and Gas-Dynamic Phases of the trajectory. ξ was defined as the negative of the ratio of percentage change in radial distance of the entry vehicle from the planet center to the percentage change in horizontal component of vehicle velocity with respect to inertial coordinates.

The phases of the entry trajectory were defined in Chapter 8 in terms of the Conservation Parameter as follows:

(1) Keplerian Phase:

A true Keplerian trajectory exists when $\xi = 1.0$. The trajectory is near-Keplerian when

$$\left|\frac{1-\xi}{\xi}\right| < 0.1$$

(2) Intermediate Phase:

$$10 > \left|\frac{1-\xi}{\xi}\right| > 0.1$$

(3) Gas-Dynamic Phase:

$$\left|\frac{1-\xi}{\xi}\right| > 10$$

The phase boundary between the Keplerian and Intermediate Phases was defined as $\left|\frac{1-\xi}{\xi}\right| = 0.1$; and between the Intermediate and Gas-Dynamic Phases as $\left|\frac{1-\xi}{\xi}\right| = 10.0$. It is noted that the Conservation Parameter changes by two orders of magnitude in spanning the Intermediate Phase.

Methods of altering the trajectory of the entry vehicle in accordance with guidance commands may be vastly different in each operational regime. In a pure Keplerian orbit, perturbations may be introduced by the use of rocket or ion thrust or by means of external pressure techniques, such as through streaming a solar radiation sail. Thrust forces may be used equally well in the Intermediate and Gas-Dynamic Phases. Varying the lift and drag coefficients*, however, has no effect on the Keplerian trajectory but may have a striking influence on the trajectory in the Intermediate and Gas-Dynamic operational phases.

The investigation described in subsequent sections of this chapter considers each phase of the entry trajectory separately. Solutions obtained are continuous or piecewise-continuous within each phase; the Conservation Parameter serves as a unifying quantity for matching solutions at boundaries and for relating the solution of one phase to the solutions of other phases. The accuracy of approximations made in each

- - - - - - - - - - - - - - - -

* Lift and drag coefficients may be controlled by changing the angle of attack or by introducing auxiliary high-lift or high-drag devices. Since lift and drag coefficients are coupled through angle of attack, auxiliary devices must be used if independent lift and/or drag control is necessary. It is important to note that the coupling of lift and drag with angle of attack is different depending on which side of the lift curve the vehicle is operating. For example, the vehicle may be flown in the "high drag configuration"; i.e., angle of attack near 90°. Decreasing the angle of attack reduces drag and increases lift in this configuration. In the "low drag configuration" (small angles of attack), however, reduction in angle of attack causes both lift and drag to decrease.

phase are discussed, and the accuracy of the solutions derived are compared to numerical solutions obtained from the non-linear equations of motion. Limitations of the approximate solutions were established as a result of this comparison.

The feasibility of using the Conservation Parameter as a switching function for the guidance system and as a prediction function for range control in degenerate orbits is discussed. In-flight computation of the Conservation Parameter from navigational data is shown to be possible.

The solutions of this chapter are oriented toward the determination of guidance quantities. It may be noted that guidance considerations of this chapter are relatively unsophisticated, however, consisting primarily of determination of range capabilities and sensitivity in range to control system errors. The hazards of exceeding tolerable acceleration and temperature levels are considered.

9.2 The Conservation Parameter as a Switching Function:

Considerable simplification is possible in the design of the guidance system if:

(1) Computations are based on simplified* equations of motion.

(2) An adequate means is available to shift from one simplified guidance mode to another as phase boundaries are crossed. The switching parameter should be based on in-flight measurements and/or computations.

At any given time as the entry vehicle passes through the planetary atmosphere, the dominant terms in the equations of motion depend upon

- - - - - - - - - - - - - - - - -

* Provided reasonable accuracy is not sacrificed in the process of simplifying the equations.

the phase of the trajectory in which the vehicle is operating. The parameter $\left|\frac{1-\xi}{\xi}\right|$ may be a convenient switching function to shift the guidance computer from one set of simplified equations (Keplerian Phase), through the region in which few simplifications in the dynamical equations of motion are permitted (Intermediate Phase), into the region where another set of simplified equations provide an adequate description of the trajectory (Gas-Dynamic Phase).

It was shown in Chapter 8 that:

$$f_{E\phi} \cong - \frac{G(m)o}{G(m)o} \frac{(1-\xi)}{\xi} \frac{v^2}{r} \sin\gamma\cos\gamma \qquad (9\text{-}1)$$

where $f_{E\phi}$ = tangential component of specific force (in Earth G's) measured by accelerometers carried by the vehicle.

v = velocity of the vehicle with respect to coordinates rotating with the planet (non-dimensionalized with respect to circular satellite velocity at the surface of the planet).

γ = flight path angle; angle between the local horizon and v -- positive for climbing flight.

r = distance from center of planet to vehicle, non-dimensionalized with respect to mean planetary radius.

$\frac{G_{(m)o}}{G_{(m)E}}$ = ratio of mean gravitational acceleration at the surface of the planet 0 to that at the surface of the Earth.

Equation (9-1) shows that if flight path angle, velocity, altitude and tangential specific force are measured or computed by the guidance system, it is an easy matter for the system to determine $(\frac{1-\xi}{\xi})$, which is a measure of the degree to which energy and angular momentum are being conserved and is indicative of whether the vehicle is in the Keplerian, Intermediate, or Gas-Dynamic Phases of the trajectory. Equation (9-1) is significant because it demonstrates that the specific force level at

transition between phases is independent of the lift-drag characteristics of the vehicle, the frontal loading of the vehicle (M/S), and the atmospheric density variation with altitude.

The variation of atmospheric density with altitude is not known or measurable in advance to a high degree of accuracy, particularly for the first-time entry into the atmosphere of a strange planet. Atmospheric density may vary more than two to one between day and night, may vary significantly with latitude, and may change considerably with the seasons of the year. The specification of the aerodynamic properties of the vehicle may also be subject to error. Determination of aerodynamic characteristics at near-orbital velocities is presently not experimentally feasible; these properties are generally specified on a theoretical rather than an experimental basis.

Equation (9-1) has serious disadvantages as a suitable means for computing $(\frac{1-\S}{\S})$. The direction of the horizon must be known in order to measure the horizontal component of specific force. An extremely troublesome factor is $\sin\gamma$, which is small for small flight path angles. If γ is measured as 0.1°, but is actually 1°, then the computed value of $(\frac{1-\S}{\S})$ is off by a factor of ten. Strong dependence on flight path angle is the most serious handicap on the practical use of equation (9-1).

A method for computing the Conservation Parameter that is independent of the sine of flight path angle was derived in Chapter 8 by relating it to Energy transfer rates:

$$\frac{E'_{(kin)}}{E'_{(pot)}} \cong -\frac{(1-\S)}{\S} v_{I\phi}^{2r} - 1 \qquad (9\text{-}2)$$

In equation (9-2):

$E_{(kin)}$ = dimensionless kinetic energy per unit mass = $\frac{v_I^2}{2}$

v_I = dimensionless velocity of the vehicle with respect to inertial coordinates.

$E_{(pot)}$ = dimensionless potential energy per unit mass = $-\frac{GR}{(G_{(m)o} R_{(m)o})}$ (zero level at infinity).

R = radius from center of planet to vehicle

G = local gravitational acceleration at vehicle.

The prime denotes differentiation with respect to dimensionless time τ.

Equation (9-2) has all the advantages of equation (9-1), independence of atmospheric density and vehicle aerodynamic characteristics, plus the additional strong advantage of being essentially independent of flight path angle. The energy quantities in equation (9-2) depend on velocity, altitude, and gravitation; these quantities may be measured or computed by the navigation system from data obtained either within the vehicle or from external tracking stations.*

9.3 The Conservation Parameter as a Prediction Function

One of the problems encountered in the guidance of vehicles undergoing braking passes through the atmosphere is control of the point at which final entry is to be initiated. A vehicle entering the atmosphere of a strange planet from an interplanetary transfer ellipse may make many braking passes through the atmosphere prior to final entry. A

---

* For first-time entry into a planetary atmosphere, a parent satellite from which the entry vehicle is launched appears to be the best external source of navigational information in the absence of ground-based tracking stations. If there is no parent satellite, then a navigational satellite may be left in the original orbit prior to initiating entry.

similar trajectory may result if the vehicle is launched from the surface of a planet for the purpose of orbiting a few turns and re-entering. The latter trajectory pattern is planned for the Mercury "man in space" program scheduled for operational firings in the early 1960's.

The most significant characteristic of the degenerate elliptical orbit is that the perigeal altitude remains essentially constant* while the apogeal altitude drops after each pass through the atmosphere. The vehicle transfers energy to the planetary atmosphere in the vicinity of perigee during each pass until the total energy level is reduced to a point where further orbits may not persist.

General characteristics of the time-varying nature of altitude, total energy, and the Conservation Parameter are shown in Fig. 9.2. This figure does not represent quantitatively any particular trajectory, but it does contain all the features of a typical trajectory. During most of each orbit, the vehicle obeys Kepler's laws of planetary motion to a high degree of accuracy. A near pulse of energy is transferred to the surrounding atmosphere as perigee is approached. Here, the vehicle enters the Intermediate Phase momentarily, then returns to the Keplerian Phase.

After each perigeal passage, the total energy level remains essentially constant for most of the following orbit at a lower level than that of the preceding orbit. The elliptical orbit consequently undergoes a "circularization" process. The apogee of the elliptical orbit is slowly reduced by drag, primarily exerted near perigee, eventually to become a circle. Thereafter, the circle decays spirally as the vehicle

- - - - - - - - - - - - - - - - - -

* See Chapter 10 for a discussion of perigeal altitude decay rates.

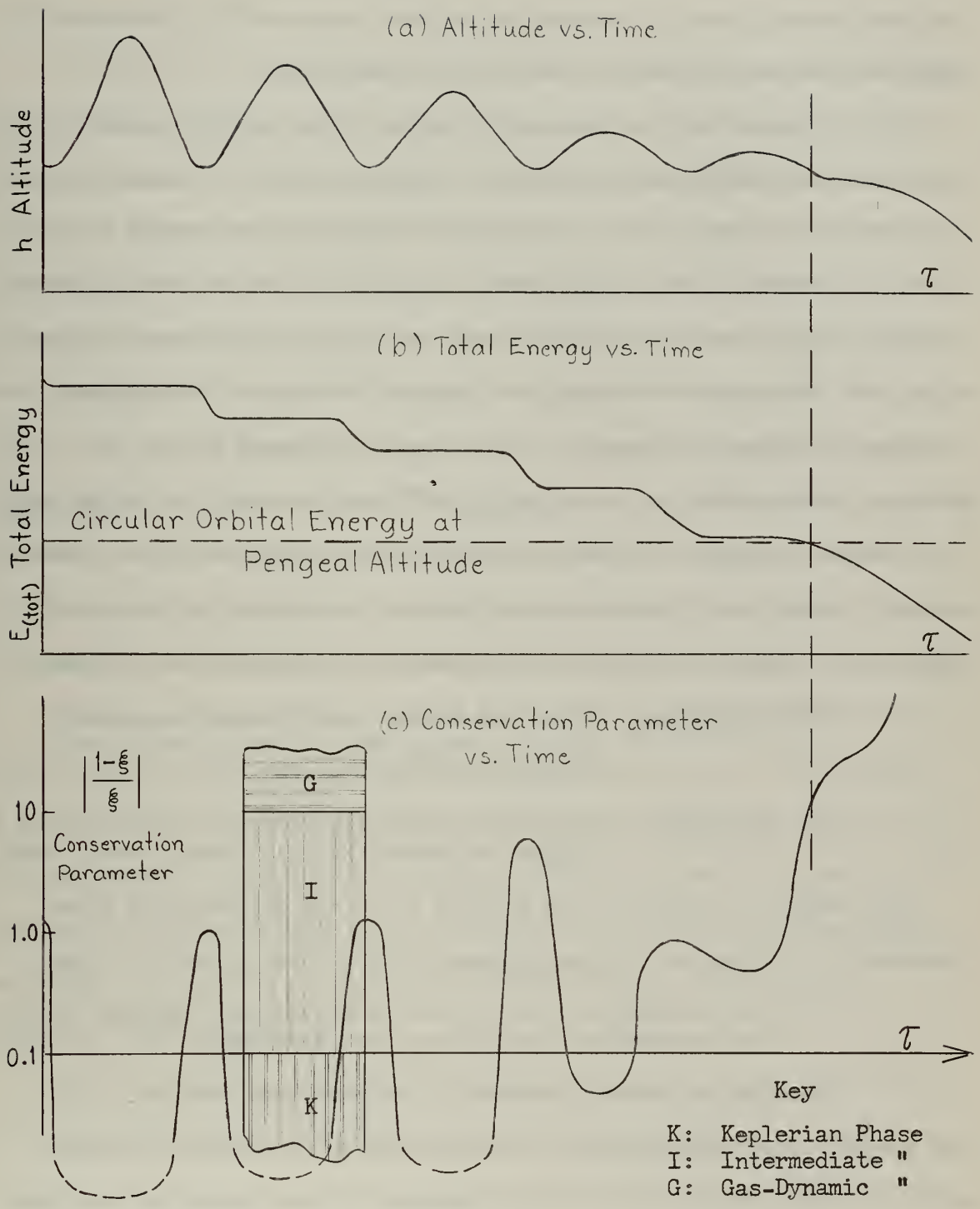

Fig. 9.2 : Altitude, Total Energy, and Conservation Parameter vs Time for a Typical Degenerate Orbit.

glides through the Gas-Dynamic Phase of flight to a landing. When the total energy level is reduced below that required for a circular orbit at perigeal altitude, final entry is inevitable.

It is interesting to examine the nature of the energy transfer. Since each succeeding perigee occurs at approximately the same altitude, the potential energy is nearly constant. Therefore, the energy transferred at perigee is basically kinetic energy. At the following apogee, however, kinetic energy is greater than it was at the preceding apogee since the velocity of the vehicle at apogee increases as the apogeal altitude is reduced. Therefore, the energy transferred during the perigeal passage results in an <u>increase</u> in kinetic energy and a <u>decrease</u> in potential energy at the following apogee when compared to the preceding apogee. During the circularization process, the changes in levels of energy when viewed at perigee and apogee may be summarized as follows:

(1) <u>At perigee</u>: Potential energy level remains constant; kinetic energy level decreases with each impulsive energy transfer.

(2) <u>At apogee</u>: Potential energy level drops as altitude of apogee decreases; kinetic energy level rises.

The length of time that the vehicle is in the Intermediate Phase increases in successive perigeal passes; this is due to the fact that:

(1) The velocity of the vehicle is slower near perigee during each succeeding pass (less kinetic energy).

(2) The trajectory continually becomes more shallow.

The energy transferred per orbit becomes greater as the orbit becomes more circular. The width* of the Intermediate Phase pulses on the graph

- - - - - - - - - - - - - - - - -

* More precisely, the area enclosed by the pulses. Practically all of the energy is transferred in the vicinity of perigee.

of Conservation Parameter vs. Time is an indication of the total energy transferred per orbit.

If the total energy level at the first perigeal passage is computed, the amount of energy in excess of circular orbital energy (corresponding to the perigeal altitude) is easily determined. The magnitude of the impulse of energy transferred during the next orbit (i.e., during next perigeal passage) shows the rate of energy decay. Energy decays as a series of successively larger steps (see Fig. 9.2-b). For given vehicle drag characteristics, and for a particular initial energy level, the measurement of the magnitude of one energy step uniquely specifies all future steps (for constant altitude at perigee and constant drag characteristics). Therefore, the number of orbits remaining until the energy level has decayed to the circular orbital level may be predicted from measurements and computations during the first complete orbit.

Energy decay per orbital period may serve as a useful method for predicting how many orbits remain before final entry; i.e., the number of orbits until the onset of the Gas-Dynamic Phase of flight. With the relation between energy transfer rates and the Conservation Parameter of equation (9-2), the time-varying characteristics of the parameter $(\frac{1-\xi}{\xi})$ may serve equally well as a prediction function for determining the number of orbits remaining.

Control of the number of orbits remaining may be implemented either by the use of thrust or by changing the drag characteristics of the vehicle. If no control action is taken by the pilot, the width of the Intermediate Phase pulses observed during successive orbits is an indication of how long the flight will last. The flight may be extended or shortened only through suitable control action within the limits of

thrust or drag modulation available.

A framework therefore has been established for the utilization of the Conservation Parameter for prediction and control of degenerate orbits based on its relation to energy transfer rates (Eq. 9-2) and predicated on the fact that knowledge of the energy decay per period and the initial energy level uniquely specifies the number of orbits remaining. Control of the number of orbits remaining is vested either in the engines of the vehicle or in the pilot's facility to vary the magnitude of the energy transferred during each braking pass by means of drag adjustments.

The range capability of the vehicle in the Gas-Dynamic Phase is small compared to the total range of the orbital phase. If the pilot changes the number of orbits remaining by one, through suitable control action, he has changed the total range of the vehicle more than the distance normally traversed throughout the entire Gas-Dynamic Phase. Range corrections in the Gas-Dynamic Phase may be adjudged vernier corrections when compared to range corrections in terms of changing the number of orbits.

The function of the guidance system in a vehicle which is undergoing the circularization process such as sketched in Fig. 9.1 may be summarized as follows:

(1) To determine in advance a suitable geographic point for entry; i.e., the point for initiating the Gas-Dynamic Phase of flight.

(2) To adjust the orbital characteristics of the vehicle in order to hit this entry point.

(3) To make range corrections in the Gas-Dynamic Phase to correct for position errors in the initial entry point and to correct for range errors which may arise as a

result of perturbations from the nominal trajectory in the Gas-Dynamic Phase.

The geographic location of the entry point is determined by solving the trajectory backwards from the geographic location of the predetermined landing site. The maximum and minimum range capabilities of the vehicle in the Gas-Dynamic Phase may be determined from the approximate range expressions derived in section 9.6. The entry point is selected as a mean position between the limits imposed by backing off from the landing point the maximum and minimum ranges obtainable. If the actual entry point lies within the corridor thus prescribed, adequate control is available to the pilot to prevent overshooting or undershooting his destination.

9.4 The Keplerian Phase

Any method for guiding the entry vehicle to a selected geographical point on the surface of the planet must necessarily involve a perturbation of its original orbit. Because of the tremendous energy possessed by the vehicle in orbit, it is difficult to perturb the orbit greatly without investing a large portion of the total mass of the vehicle in rocket fuel.

The vacuum phase of the trajectory that follows the initiation of entry from a satellite orbit beyond the sensible atmosphere is a part of the general problem of transfer between orbits that has received considerable attention in the literature. The special nature of the entry problem, however, requires solutions that are not available in general treatises on the subject of transfers between orbits.

Excellent examples of published papers concerning investigations of transfer maneuvers between orbits are the works of Hohmann[48], Lawden[49],

and Battin[50]. Hohmann and Lawden have shown that the optimum transfer maneuver between elliptical orbits involves the application of impulsive forces at departure from one orbit and at arrival in the other orbit. Battin has shown that several important features of the transfer problem are basically three-dimensional in nature and that two-dimensional models are inadequate. Very little has been published concerning guidance requirements for the special problem of transfer from a satellite orbit to a particular landing point on the surface of the planet.

The development carried out herein is unique in that the transfer ellipse is solved in terms of geometric quantities at the trajectory modification point*. These quantities are:

(1) Inertial flight path angle (see Figs. 9.3 and 9.4)

(2) Altitude

(3) Velocity

The solution is valid for entry from either circular or elliptical orbits.

In addition to the general solutions described above, special solutions were obtained for entry from circular orbits in terms of:

(1) Velocity Impulse

(2) Engine Gimbal Angle

(3) Circular Orbital Velocity.

It should be noted that the relation between $\left\{\begin{array}{l}\text{inertial flight}\\ \text{path angle, altitude, and velocity}\end{array}\right\}$ at the trajectory modification point and $\left\{\begin{array}{l}\text{velocity impulse, engine gimbal angle, and orbital velocity}\end{array}\right\}$ are uniquely defined only if the entry vehicle is launched from a

---

* The trajectory modification point is that point in the original orbit at which entry is initiated through generation of thrust forces, see Fig. 9.3.

circular orbit. For transfer from an elliptical orbit, the relation between these two sets of quantities depends on the particular point in the original elliptical orbit where perturbations are introduced. The first set of quantities are more useful for generalized study of transfer from elliptical orbits, the second set for specialized study of transfer from circular orbits.

Results are presented in dimensionless form for general application to any planet. A generalized range expression is developed in terms of the foregoing quantities, and range sensitivity to errors in these quantities is discussed.

Various methods are available for perturbing the satellite orbit to bring about controlled entry:

(1) Impulsive application of forces at departure point by means of chemical rockets or other high thrust propulsive systems.

(2) Continuous application of low thrust (e.g., ion rockets).

(3) Multiple impulses at intermediate* thrust levels.

(4) Drag modulation, if portions of the orbit pass through the planetary atmosphere.

The analysis of this section is restricted to the first method. The analysis is simplified to the two-dimensional trajectory near a spherical planet.

The Keplerian Phase of the trajectory was defined previously as that portion of the trajectory where $\left|\frac{1-\xi}{\xi}\right| < 0.1$. The equations of motion developed in Section 6.4 may be written for the Keplerian Phase as:

$$X'_N = \frac{v_\phi}{r} \qquad (9\text{-}3)$$

- - - - - - - - - - - - - - - - -

* Thrust levels between those obtainable with chemical rockets and with continuous ion propulsion.

$$h' = r' = v_r = v_{Ir} \tag{9-4}$$

$$v'_r = \frac{v_{I\phi}^2}{r} - \frac{1}{r^2} \tag{9-5}$$

$$v_{\phi}' = \frac{v_r}{r} (v_{\phi} - 2 v_{I\phi}) \tag{9-6}$$

Fig. 9.3 describes the geometry of the entry trajectory. Quantities at the trajectory modification point are denoted by the subscript "m". The transfer ellipse is solved in Derivation Summary (9-1). A brief summary of the solutions obtained are tabulated in sections 9.4.1, 9.4.2, 9.4.3, and 9.4.4 following.

9.4.1 Description of the Entry Transfer Ellipse in Terms of Geometric Quantities at the Trajectory Modification Point (Applicable to Entry from Elliptical and Circular Orbits).

a) Eccentricity:

$$\mathcal{E} = \left[1 - v_{Im}^2 r_m \cos^2 \gamma_{Im} (2 - v_{Im}^2 r_m)\right]^{\frac{1}{2}} \tag{9-7}$$

b) Dimensionless semi-major axis:

$$a_N = \frac{r_m}{\left[2 - v_{Im}^2 r_m\right]} \tag{9-8}$$

c) Dimensionless semi-minor axis:

$$b_N = a_N \sqrt{1 - \mathcal{E}^2} \tag{9-9}$$

d) Dimensionless latus rectum:

$$l_N = a_N (1 - \mathcal{E}^2) \tag{9-10}$$

e) Dimensionless area of ellipse:

$$\text{Area} = \pi a_N b_N \tag{9-11}$$

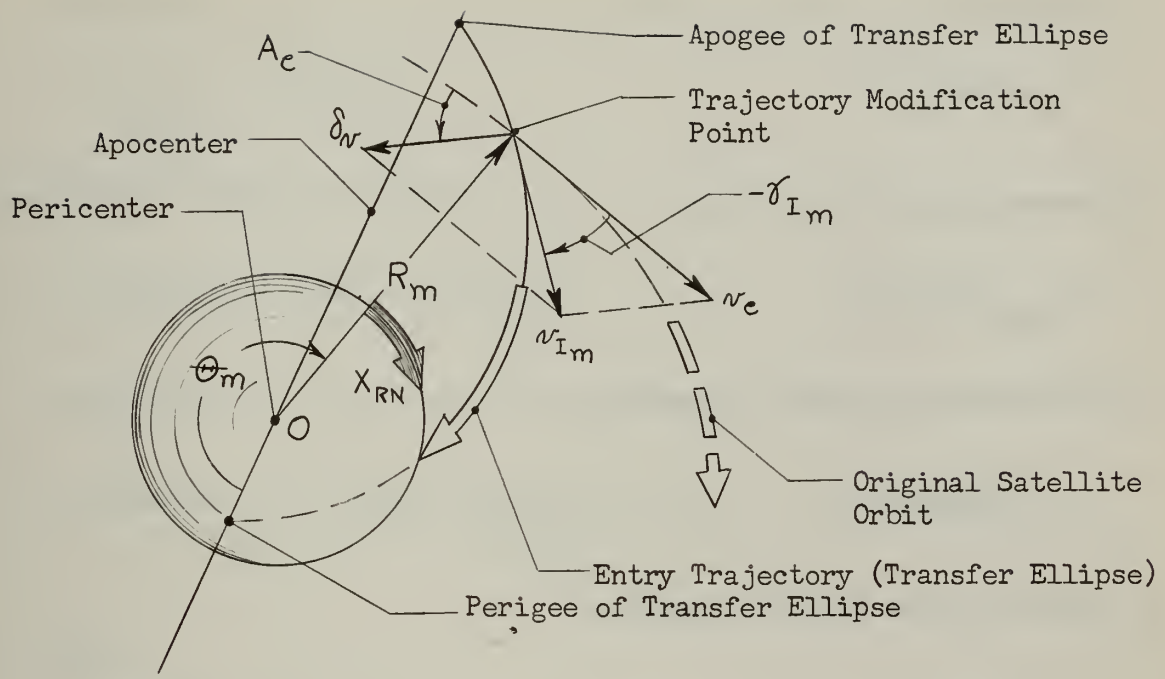

v_c = dimensionless circular orbital velocity prior to modification

δ_v = dimensionless velocity impulse imparted

θ_m = true anamoly of trajectory modification point

v_{I_m} = dimensionless velocity of vehicle with respect to inertial coordinates immediately after modification

γ_{I_m} = inertial flight path angle immediately after modification

A_e = engine deflection angle

X_N = dimensionless distance traversed from modification point.

ANGULAR RELATIONS

$$(9.3\text{-}1) \quad \sin(-\gamma_{Im}) = (\delta v)\sin A_e / v_{Im}$$

$$(9.3\text{-}2) \quad \cos(-\gamma_{Im}) = \left[v_c - (\delta v)\cos A_e \right] / v_{Im}$$

$$(9.3\text{-}3) \quad \tan(-\gamma_{Im}) = (\delta v)\sin A_e / \left[v_c - (\delta v)\cos A_e \right]$$

VELOCITY RELATIONS

$$(9.3\text{-}4) \quad v_{Im} = \left[(\delta v)^2 + v_c^2 - 2(\delta v) v_c \cos A_e \right]^{1/2}$$

$$(9.3\text{-}5) \quad v_c = \sqrt{\frac{GR}{G_{(m)o} R_{(m)o}}} = \sqrt{\frac{1}{r_m}}$$

Fig. 9.3: Geometry of the Transfer Ellipse; Definitions of Quantities and Geometric Identities.

f) Dimensionless period of orbit:

$$T_N = 2\pi a_N^{3/2} \tag{9-12}$$

g) Dimensionless total energy:

$$E_{(tot)} = -1/2a_N \tag{9-13}$$

h) Dimensionless angular momentum:

$$p = r_m v_{Im} \cos \gamma_{Im} \tag{9-14}$$

i) Dimensionless radius at perigee:

$$r_\pi = a_N(1-\varepsilon) \tag{9-15}$$

j) Dimensionless velocity at perigee:

$$v_{I_\pi} = \sqrt{\frac{1+\varepsilon}{r_\pi}} \tag{9-16}$$

k) Dimensionless radius at apogee:

$$r_a = a_N(1+\varepsilon) \tag{9-17}$$

l) Dimensionless velocity at apogee:

$$v_{I_a} = \sqrt{\frac{1-\varepsilon}{r_a}} \tag{9-18}$$

9.4.2 Guidance Quantities in Terms of Geometric Quantities at the Trajectory Modification Point (Applicable to Entry from Elliptical and Circular Orbits)

a) Time of flight ($\tau_m = 0$)

$$\tau = \frac{p^3}{(1-\varepsilon^2)} \left\{ \frac{-\varepsilon \sin \theta}{1+\varepsilon \cos \theta} + \frac{2}{\sqrt{1-\varepsilon^2}} \tan^{-1} \left(\frac{(1-\varepsilon)\tan \theta/2}{\sqrt{1-\varepsilon^2}} \right) \right\}_{\theta_m}^{\theta} \tag{9-19}$$

b) Dimensionless velocity:

$$v_I = \left[\frac{2}{r} - \frac{(2 - v_{Im}^2 r_m)}{r_m} \right]^{\frac{1}{2}} \tag{9-20}$$

c) Inertial flight path angle:

$$\gamma_I = \arccos \left[\frac{r_m}{r} \frac{v_{Im}}{v} \cos \gamma_{Im} \right] \tag{9-21}$$

Using equation (9-20), this may be written:

$$\gamma_I = \arccos \left\{ \frac{\frac{r_m}{r} v_{Im} \cos \gamma_{Im}}{\left[2/r - \frac{(2 - v_{Im}^2 r_m)}{r_m} \right]^{\frac{1}{2}}} \right\} \tag{9-22}$$

d) Range:

$$X_N = \theta - \theta_m \tag{9-23}$$

where

$$\cos \theta = (1/\varepsilon) \left(\frac{p^2}{r} - 1 \right) \tag{9-24}$$

$$\cos \theta_m = (1/\varepsilon) \left(\frac{p^2}{r_m} - 1 \right) \tag{9-25}$$

Range may be expressed in closed form as:

$$\cos X_N = \frac{\{\ \}}{\varepsilon^2 r\, r_m} \tag{9-26}$$

where:

$$\{\ \} = \left\{ (p^2 - r)(p^2 - r_m) + \left[\varepsilon^2 r^2 - (p^2 - r)^2 \right]^{\frac{1}{2}} \left[\varepsilon^2 r_m^2 - (p^2 - r_m)^2 \right]^{\frac{1}{2}} \right\} \tag{9-27}$$

9.4.3: Description of Transfer Ellipse in Terms of Velocity Impulse and Engine Gimbal Angle. Applicable to Entry from Circular Orbits Only.

The variables used in the following equations are defined in Fig. 9.3. Equations (9.3-1) through (9.3-5) given in Fig. 9.3 give various relations for vehicle velocity and inertial flight path angle at the trajectory modification point in terms of velocity impulse and engine gimbal angle.

The following quantity is defined:

$$\delta v_c \equiv \frac{\delta V}{V_c} \equiv$$ velocity impulse non-dimensionalized with respect to circular orbital velocity at the trajectory modification point. (9-28)

a) Eccentricity:

$$\epsilon = \left\{ 1 - (1 - \delta v_c \cos A_e)^2 \left[1 - \delta v_c \left(\delta v_c - 2 \cos A_e \right) \right] \right\}^{\frac{1}{2}} \qquad (9\text{-}29)$$

b) Dimensionless semi-major axis:

$$a_N = \frac{1}{v_c^2 \left[1 - \delta v_c \left(\delta v_c - 2 \cos A_e \right) \right]} \qquad (9\text{-}30)$$

All other quantities listed in Section 9.4.1 are the same except the following:

h) Dimensionless angular momentum:

$$p = \frac{(1 - \delta v_c \cos A_e)}{v_c} \qquad (9\text{-}31)$$

9.4.4: Guidance Quantities in Terms of Velocity Impulse and Engine Gimbal Angle. Aplicable to Entry from Circular Orbits Only.

a) Time of Flight:

Same as Equation (9-19)

b) Dimensionless Velocity:

$$v_I = \left\{ \frac{2}{r} - v_c^2 \left[1 - \delta v_c \left(\delta v_c - 2 \cos A_e \right) \right] \right\}^{\frac{1}{2}} \qquad (9\text{-}32)$$

c) Flight Path Angle:

$$\gamma_I = \arccos \left\{ \frac{(1 - \delta v_c \cos A_e)}{v_c \, v_I \, r} \right\} \qquad (9\text{-}33)$$

or

$$\gamma_I = \arccos \left\{ \frac{(1 - \delta v_c \cos A_e)}{\left[2v_c^2 r - v_c^4 r^2 \left(1 - \delta v_c \left[\delta v_c - 2 \cos A_e \right] \right) \right]^{\frac{1}{2}}} \right\} \qquad (9\text{-}34)$$

d) Range:

Equations (9-23) through (9-25) apply. An alternate expression for range is:

$$\cos X_N = \frac{v_c^2}{\mathcal{E}^2 r} \{ \} \qquad (9\text{-}35)$$

where:

$$\{ \} = \left\{ (p^2 - r)\left(p^2 - \frac{1}{v_c^2}\right) + \left[\mathcal{E}^2 r^2 - (p^2 - r)^2 \right]^{\frac{1}{2}} \left[\frac{\mathcal{E}^2}{v_c^4} - \left(p^2 - \frac{1}{v_c^2}\right)^2 \right]^{\frac{1}{2}} \right\}$$

Fig. 9.4 shows the geometric relation between flight path angle, γ, and inertial flight path angle, γ_I. Equations (9.4-1) through (9.4-8) given as part of this figure are useful for relating velocities and angles. The solutions for the Intermediate and Gas Dynamic Phases given in later sections of this chapter are generally written in terms of γ because this angle is more convenient when drag and lift terms are important (since these quantities involve velocities with respect to the atmosphere of the planet). Fig. 9.4 and the equations listed therein enable conversion of angles at phase boundaries such that the most

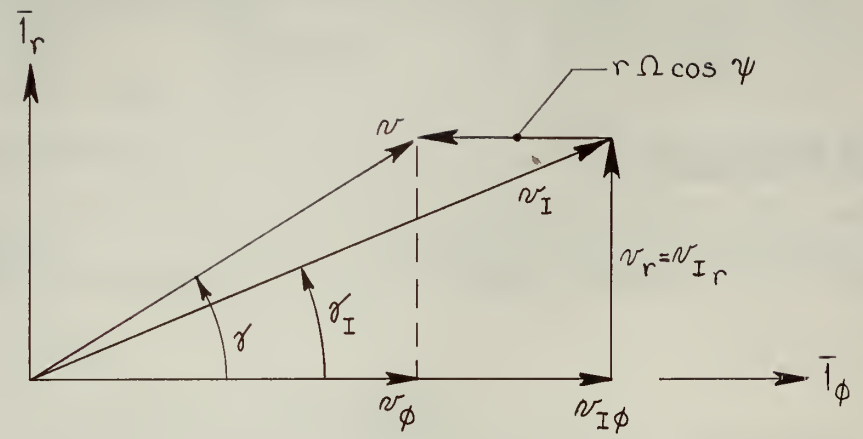

$$v_{I\phi} = v_I \cos\gamma_I = v\cos\gamma + r\Omega\cos\psi \tag{9.4-1}$$

$$r' = h' = v_I \sin\gamma_I = v\sin\gamma \tag{9.4-2}$$

$$p = r v_I \cos\gamma_I \tag{9.4-3}$$

$$\sin\gamma = \frac{v_I}{v}\sin\gamma_I \tag{9.4-4}$$

$$v^2 = v_I^2 - 2v_I\cos\gamma_I r\Omega\cos\psi + r^2\Omega^2\cos^2\psi \tag{9.4-5}$$

$$v_I^2 = v^2 + 2v\cos\gamma r\Omega\cos\psi + r^2\Omega^2\cos^2\psi \tag{9.4-6}$$

$$\cos\gamma = \frac{v_I\cos\gamma_I - r\Omega\cos\psi}{v} \tag{9.4-7}$$

$$\cos\gamma_I = \frac{v\cos\gamma + r\Omega\cos\psi}{v_I} \tag{9.4-8}$$

Fig. 9.4: Geometric Relations Between Flight Path Angle and Inertial Flight Path Angle.

convenient definition of flight path angle may be used in the analytical study of each phase.

9.4.5: Optimum Engine Gimbal Angle:

A thorough graphical representation of equations (9-7) through (9-35) was not undertaken in this thesis. An example of a solution to the circular orbital equations (given in subsections 9.4.3 and 9.4.4) in order to determine optimum engine gimbal angle is presented graphically in Figures 9.5 and 9.6. The circular orbital altitude was chosen as $h_m = .07575$, corresponding to an altitude of 300 miles above the Earth. The final altitude was selected to be $h_f = 0$, corresponding to impact with the planet. No atmospheric effects were considered.

The following velocity impulses were chosen:

$$\delta_v = 0.0385;\ 0.0772;\ 0.1156;\ \text{and } 0.1542$$

These correspond to velocity impulses of 1000, 2000, 3000, and 4000 ft/sec, respectively, for the planet Earth.

Figs. 9.5 and 9.6 show that there is one value of engine deflection angle for which range is minimized with a given magnitude of velocity impulse.* At this engine deflection angle, any errors in alignment of the engine gimbals result in minimum range error. For example, if $\delta_v = .0385$, the optimum engine angle is $A_e = +34°$; if $\delta_v = .1542$, optimum engine angle is $A_e = +60°$.

It is interesting to note in Fig. 9.5 that at velocity impulses of large magnitudes, range is relatively insensitive to errors in engine gimbal angle from the optimum angle. The range sensitivity to errors in

- - - - - - - - - - - - - - - - - -

* Labeled "Optimum Engine Deflection Angle" on the graphs.

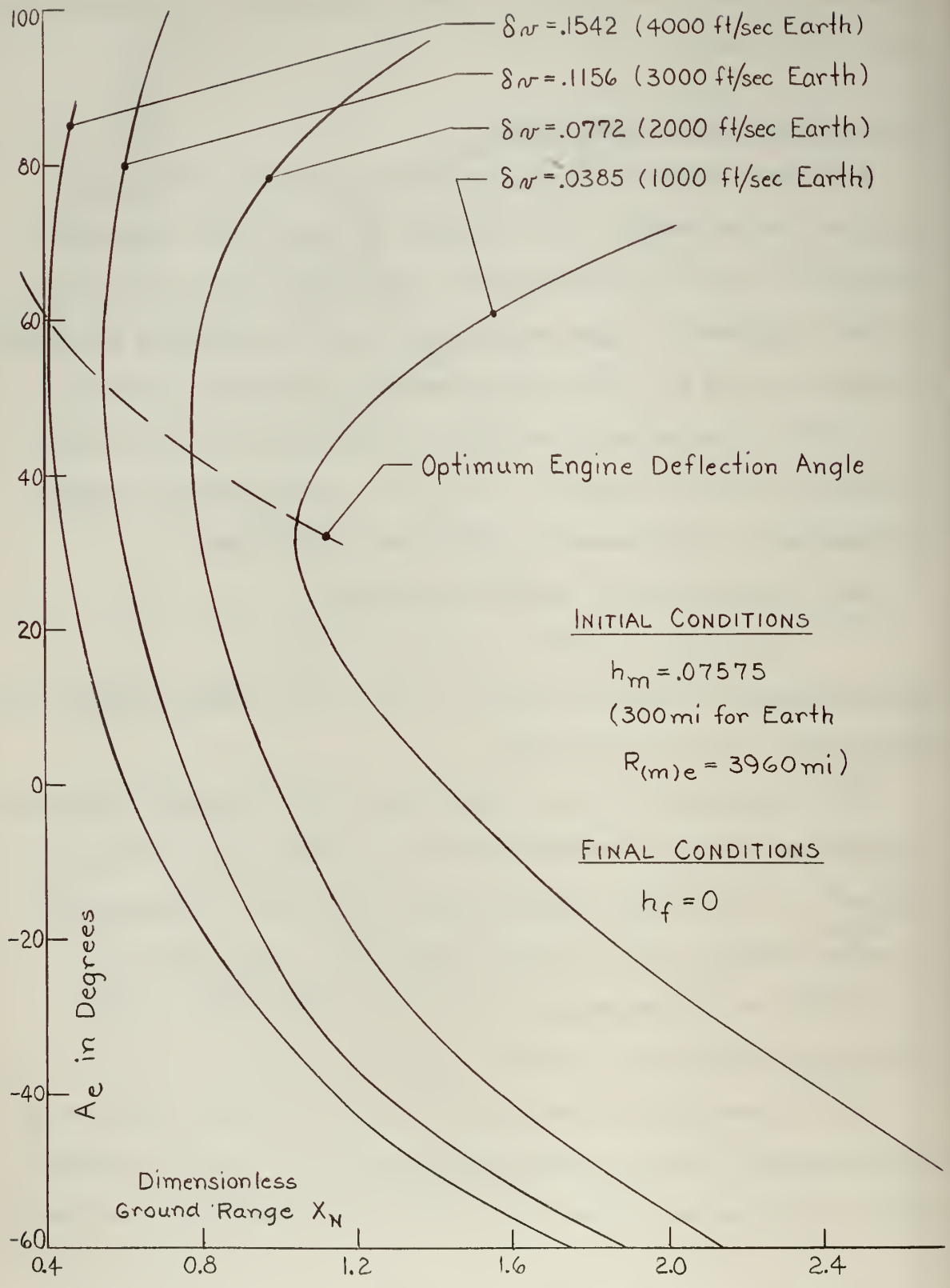

Fig. 9.5 : Vacuum Ground Range vs Engine Deflection Angle.

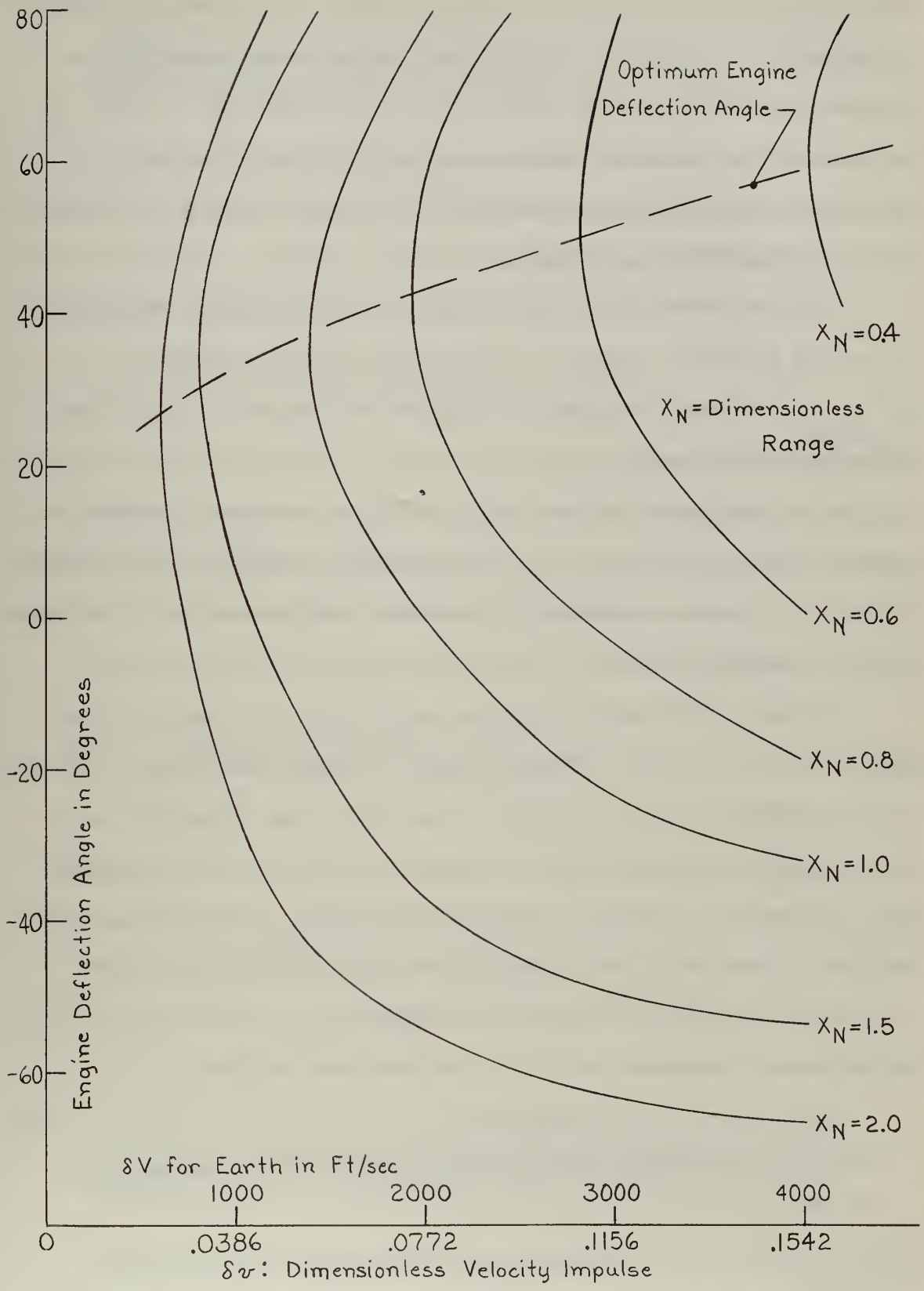

Fig. 9.6 : Velocity Impulse vs Engine Deflection Angle for Vacuum Trajectories of Fixed Ground Range

engine gimbal angle increases as the magnitude of the velocity impulse is reduced.* It might be concluded that large thrust capability for extended periods (i.e., big engines with large quantities of fuel) is the cure-all for improving impact accuracy of the entry vehicle. A compromise is generally dictated in fuel and engine weight allowances, however, by payload requirements.

It may be observed that with a given velocity impulse and range, the engine deflection angle is a two-valued function (except at $A_{e_{optimum}}$). A given range may be obtained with either of two values of engine deflection angle.

It is significant to note in Fig. 9.5 that the range interval between curves decreases as δ_v is increased.** Therefore, the magnitude of reduction in range decreases for a given step increase in δ_v at high impulsive velocity levels.

Graphical determination of range sensitivity to errors in either engine deflection angle or velocity impulse exemplified by Figs. 9.5 and 9.6 is cumbersome and inefficient. A particular set of initial conditions must be assumed; then the trajectory must be solved repeatedly using systematically chosen values of engine gimbal angle and velocity impulse. A more effective analytical method of obtaining the same information was derived in Derivation Summary 9.1. The results of this derivation are discussed briefly in the next two sections.

- - - - - - - - - - - - - - - - -

* That is, the curves are more pointed in the vicinity of $A_{e_{optimum}}$ for small δ_v.

** On fig. 9.5, the curves are more closely spaced at high values of δ_v.

9.4.6: Analytical Determination of Range Sensitivity to Errors in Operation of Propulsive System: Range Sensitivity to Errors in Velocity and Inertial Flight Path Angle (Applicable to Entry from Elliptical and Circular Reconnaissance Orbits).

A single equation relating altitude h, altitude at which entry is initiated h_m, velocity and inertial flight path angle at the trajectory modification point, and range was derived in Derivation Summary 9.1 as follows (note: r = 1 + h):

$$\frac{r_m^2}{r} v_{I_m}^2 \cos^2 \gamma_{I_m} - 1 = r_m v_{I_m}^2 \cos^2 \gamma_{I_m} \cos(X_N + \gamma_{I_m}) - \cos X_N \qquad (9\text{-}36)$$

This equation was written in other forms in equations (28) and (29) of Derivation Summary 9.1. Implicit partial differentiation of equation (9-36) yields equations which may be used to evaluate range sensitivity to errors in either altitude, velocity, or flight path angle.

Equation (9-37) gives range sensitivity to variations in:

$$\frac{\partial X_N}{\partial v_{I_m}} = \frac{2 r_m v_{I_m} \cos^2 \gamma_{I_m} \left[\frac{r_m}{r} - \cos(X_N + \gamma_{I_m})\right]}{\left[\sin X_N - r_m v_{I_m}^2 \cos^2 \gamma_{I_m} \sin(X_N + \gamma_{I_m})\right]} \qquad (9\text{-}37)$$

Equation (9-38) gives range sensitivity to variations in γ_{I_m}:

$$\frac{\partial X_N}{\partial \gamma_{I_m}} = \frac{v_{I_m}^2 r_m \cos \gamma_{I_m} \left\{2 \sin \gamma_{I_m} \left[\cos(X_N + \gamma_{I_m}) - \frac{r_m}{r}\right] + \cos \gamma_{I_m} \sin(X_N + \gamma_{I_m})\right\}}{\left[\sin X_N - r_m v_{I_m}^2 \cos^2 \gamma_{I_m} \sin(X_N + \gamma_{I_m})\right]} \qquad (9\text{-}38)$$

9.4.7: Analytical Determination of Range Sensitivity to Errors in Operation of Propulsive System; Range Sensitivity to Errors in Velocity Impulse and Engine Gimbal Angle (Applicable to Entry from Circular Reconnaissance Orbits Only).

A single equation relating altitude, altitude of the circular orbit, velocity impulse, engine gimbal angle, and range was derived in the

following forms by the methods of Derivation Summary 9.1.

$$(\delta v_c)^2 \cos^2 A_e \left[\frac{r_m}{r} - \cos X_N + \sin X_N \tan A_e\right] - \delta v_c \cos A_e \left[2\left(\frac{r_m}{r} - \cos X_N\right) + \sin X_N \tan A_e\right] + \frac{r_m}{r} - 1 = 0 \tag{9-39}$$

or

$$\delta v_c = \left\{\left[2\left(\frac{r_m}{r} - \cos X_N\right) + \sin X_N \tan A_e\right] - \left[\sin^2 X_N \tan^2 A_e + 4(1 - \cos X_N)\left(\frac{r_m}{r} - \cos X_N + \tan A_e \sin X_N\right)\right]^{1/2}\right\} \Big/ 2 \cos A_e \left(\frac{r_m}{r} - \cos X_N + \sin X_N \tan A_e\right) \tag{9-40}$$

Range sensitivity to retro-rocket system operation was determined by implicity differentiation of equations (9-39) or (9-40):

$$\frac{\partial X_N}{\partial A_e} = \frac{(\delta v_c)\left[\sin A_e (\cos X_N - \frac{r_m}{r} - \sin X_N \tan A_e) + \frac{\sin X_N}{\cos A_e}\right] - \frac{1}{\cos^2 A_e}\left[\sin X_N - \frac{\sin A_e}{\delta v_c}\left(\frac{r_m}{r} - 1\right)\right]}{-\delta v_c \sin(X_N + A_e) + 2 \sin X_N + \cos X_N \tan A_e} \tag{9-41}$$

$$\frac{\partial X_N}{\partial(\delta v_c)} = \frac{2 \cos A_e \left(\frac{r_m}{r} - \cos X_N + \sin X_N \tan A_e\right) - \frac{1}{\delta v_c}\left[2\left(\frac{r_m}{r} - \cos X_N\right) + \sin X_N \tan A_e\right]}{(2 \sin X_N + \cos X_N \tan A_e) - \delta v_c \sin(X_N + A_e)} \tag{9-42}$$

With the aid of equations (9-36) through (9-42), a description of range sensitivity to errors in retro-rocket system operation is available for analysis of entry into any planetary atmosphere from elliptical or circular reconnaissance orbits.

9.5: The Intermediate Phase

The Intermediate Phase presents the most complex computing phase for the guidance system. In this phase accelerations due to gas-dynamic

terms are of comparable magnitude with other terms in the dynamical equations of motion. Some of the simplifying assumptions made by most authors* analyzing entry trajectories are not permissible in the Intermediate Phase. A partial list of typical assumptions and their accuracy with respect to the Intermediate Phase are summarized below:

(1) Lift and Drag coefficients are independent of Mach Number and Reynolds Number. This assumption is generally accurate at the high Mach numbers of the Intermediate Phase.

(2) Gravitational acceleration is constant. This is clearly a poor assumption in the Keplerian Phase, and a questionable assumption in the Intermediate Phase. For example, the gravitational acceleration of the Earth decreases about 1% for each 20 miles increase in altitude. It was shown in Chapter 8 that, for constant γ, the Intermediate Phase spans an altitude band of 20 miles for the Earth's atmosphere. If a value of gravitation acceleration is used that corresponds to the average altitude of the Intermediate Phase, then variations of gravitational acceleration of less than 1% from this local average value may be expected in the Intermediate Phase.

(3) An isothermal atmosphere is assumed; therefore, atmospheric density decays exponentially with altitude. This assumption is reasonably accurate for Earth below altitudes of 80 miles (see Fig. E.2); the accuracy of this assumption for other planets cannot be predicted at this time. It was shown in

- - - - - - - - - - - - - - - -

* See, for example, Chapman[15], Eggers, Allen and Neice[31], and Allen and Eggers[51].

Chapter 8 that the onset of the Intermediate Phase may be higher than 80 miles. In general, the altitude of the Keplerian-Intermediate Phase boundary increases as:

(1) Drag coefficient is increased;

(2) Surface loading (M/S) is decreased;

(3) The magnitude of flight path angle is decreased.

Since the altitude of the Intermediate Phase may be above the region where the exponential approximation of the atmosphere is accurate, either a power approximation or a variable decay parameter k may be more accurate representation for analytical studies of this Phase.

(4) Planetary rotation is neglected; therefore, Coriolis forces are not included in the equations of motion (even though these equations are written in a coordinate system that rotates with respect to inertial space). This assumption is reasonably accurate in the Intermediate and Gas-Dynamic Phases for terrestrial planets.

(5) $(1 + L/D \tan\gamma) \simeq 1.0$. This assumption is accurate in all phases for moderate lift-drag ratios and normal flight path angles (except in steep terminal phases near the end of the Gas-Dynamic Phase).

(6) Quantities in the equations of motion involving* $\frac{v_r v_\phi}{r}$ are neglected. This is equivalent to assuming $\left|\frac{1-\xi}{\xi}\right| > 10$ (i.e., $|\xi| \ll 1.0$). It was shown in Chapter 8 that this assumption is accurate only in the Gas-Dynamic Phase. This

- - - - - - - - - - - - - - - - -

* Or terms equivalent to this quantity.

assumption cannot be made in the Intermediate and Keplerian Phases. Solutions to the simplified equations of motion in the Keplerian and Gas-Dynamic Phases are discussed in other sections of this chapter. Few simplifying approximations are warranted in the Intermediate Phase, however, and closed form solutions were not obtained for this phase.

In powerless flight*, the two-dimensional equations of motion may be written in terms of velocity, altitude, and the Conservation Parameter as follows:

$$X'_N = \frac{v_\phi}{r} \tag{9-43}$$

$$h' = r' = v_r \tag{9-44}$$

$$v_r' = \frac{v_{I\phi}^2}{r} - \frac{1}{r^2} - \frac{v_r^2 v_{I\phi}}{v_\phi r}\left(\frac{1-\xi}{\xi}\right)\frac{\left(1-(L/D)\frac{v_\phi}{v_r}\right)}{\left(1+(L/D)\frac{v_r}{v_\phi}\right)} \tag{9-45}$$

$$v_\phi' = \frac{v_r}{r}\left[v_\phi - \frac{(1+\xi)}{\xi} v_{I\phi}\right] \tag{9-46}$$

where

$$v_{I\phi} = v_\phi + r\Omega\cos\psi \tag{9-47}$$

Equation (9-45) may be simplified slightly by assumption (5) discussed previously:

$$\left(1 + {}^{L}/_{D}\,\frac{v_r}{v_\phi}\right) = \left(1 + {}^{L}/_{D}\tan\gamma\right) \cong 1.0$$

The Intermediate Phase may be traversed impulsively by using certain

- - - - - - - - - - - - - - - -

* Thrust terms are zero in powerless flight, i.e., $\Upsilon_N = 0$.

trajectory control techniques at the onset of this phase; i.e., at the point where $\left|\frac{1-\xi}{\xi}\right| = 0.1$. Examples of such techniques are:

(1) Application of thrust:

When the phase boundary between the Keplerian and Intermediate Phases is approached, the Conservation Parameter rises from near zero to 0.1. At the point where this parameter reaches 0.1, impulsive retro-thrust may be applied in such a manner as to cause $\left|\frac{1-\xi}{\xi}\right|$ to step to 10 or greater, corresponding to flight in the Gas-Dynamic Regime.

(2) Use of Auxiliary High-Drag Device*

Fig. 8.8 showed upper and lower phase boundaries of the Intermediate Phase as a function of drag coefficient. It may be observed from this figure that a step change in drag coefficient of approximately two orders of magnitude is required to move the operating phase of the vehicle from the Keplerian-Intermediate Phase boundary to the Intermediate-Gas-Dynamic Phase boundary (with constant altitude). This step drag increase may be obtained at the onset of the Intermediate Phase, for example, by streaming a drogue chute or umbrella. If the horizontal component of external specific force steps two orders of magnitude as the drag device is extended, then the Intermediate Phase is traversed during the step drag increase.

Certain lift-drag programs** may be performed in the Intermediate

- - - - - - - - - - - - - - - - -

* Such as a drogue chute or umbrella.

** Programmed lift and drag, such as discussed in this section, are not easily realized in practice.

Phase to induce a particular trajectory pattern. One example of such a lift-drag program is that of holding constant flight path angle throughout the Intermediate Phase.

The required lift program to hold constant flight path angle, γ, may be determined by setting $\gamma' = 0$ in equation (6-41). The drag program is determined by integrating $\frac{dv}{dh}$ from equations (6-40) and (6-43) with γ constant. It may be seen that the flight path angle remains constant if lift and drag are programmed as follows:

$$L/D = \frac{\cot\gamma\,(1 - v^2)\left(1 - \frac{e^{-khi}}{e^{-kh}}\right)}{kv^2 \ln\left(\frac{v}{v_i}\right)} \qquad (9\text{-}48)$$

$$C_L = \frac{\cos\gamma\,(1 - v^2)}{\left(\frac{\rho(\overline{SL})R(m)o}{2M/S}\right)v^2 e^{-kh}} \qquad (9\text{-}49)$$

$$C_D = \frac{k \sin\gamma \ln\frac{v}{v_i}}{\left(\frac{\rho(\overline{SL})R(m)o}{2M/S}\right)(e^{-kh} - e^{-khi})} \qquad (9\text{-}50)$$

It is noted that the exponential atmospheric model was assumed and that terms involving planetary rotation were dropped because they are higher order effects in comparison to the quantities retained.

By switching to the above lift-drag program as $\left|\frac{1-\zeta}{\zeta}\right|$ rises to 0.1 and maintaining it until $\left|\frac{1-\zeta}{\zeta}\right| = 10$, the Intermediate Phase is traversed at constant flight path angle. Closed form expressions for range and other quantities developed in section 9.6 for the "Ballistic Trajectory" apply in the Intermediate Phase if this lift-drag program is maintained.

9.6 The Gas-Dynamic Phase:

The final portion of any entry mission to the surface of a planet through its atmosphere necessarily involves flight in the Gas-Dynamic

Phase. The analysis of motion of vehicles in this operational regime has been a substantial percentage of man's total scientific effort during the past half-century and resulted in the evolution of an entirely new branch of science and engineering, viz. "aeronautics". With each advance in propulsive system design, the increased velocity and altitude capabilities of the vehicle has brought on problems of increasing complexity.

The German V-2 program was the first substantial step up the ladder toward flight beyond the sensible atmosphere at hypervelocities. This beginning has been greatly extended in the IRBM and ICBM programs in the United States and the Soviet Union.

The character of the atmospheric phase of flight at near orbital velocities is, in many ways, far removed from that of flight at sonic or subsonic velocities. The vehicle possesses tremendous energy and angular momentum at near-orbital velocities. Most of this energy must be transferred to the atmospheric envelope surrounding the planet prior to initiating a safe landing. Two of the primary dangers encountered during the process of transferring this energy are manifested as heating of the vehicle and deceleration of the vehicle and its occupants. It was not until the feasibility of space activities was clearly demonstrated in the post World War II period that analytical investigation of hypersonic flight was carried out on a scale more extensive than the occasional publication of a paper touching the subject*. Since 1955, the interest in this problem has grown rapidly, as evidenced by the steadily increasing frequency of published work. Among the papers

- - - - - - - - - - - - - - - - - -

* One of the earliest papers of significance is that of Sanger[52], published in 1933.

published in recent years, some of the best are the works of Sanger and Bredt[53] (1944); Eggers, Allen, and Neice[31] (1957); Allen and Eggers[51] (1957); Allen[54] (1957); and Chapman[15] (1958). Chapman considers atmospheric entry into not only Earth but also other planets of the solar system; the other authors cited above restrict their analysis to the Earth system. Much of the results presented in the following pages are based on conclusions of the foregoing papers. The results that follow, however, go beyond the scope of the above treatises to the derivation of guidance quantities in terms of certain independent variables (such as time and atmospheric density ratio) not previously considered.

Three basic trajectory patterns are possible in the Gas-Dynamic Phase. The trajectory profile which is traced out on entry depends strongly on the initial flight conditions and on the lift-drag characteristics of the vehicle. These trajectories are classified as follows:

(1) Ballistic trajectory: Non-lifting vehicle with large initial flight path angle.

(2) Glide trajectory: Lifting vehicle with zero initial flight path angle.

(3) Skip trajectory: Lifting vehicle with finite initial flight path angle.

Approximate analytical solutions were derived in this thesis for each of these classes of trajectories. Fig. 9.7 shows the regions in which these approximate analytical solutions are an accurate representation of the trajectory when compared to numerical solutions obtained from the non-linear dynamical equations of motion.

Chapman[15] discussed trajectories in the Gas-Dynamic Phase by transforming the equations of motion to a single, ordinary, non-linear differential equation of second order. A transformation similar to

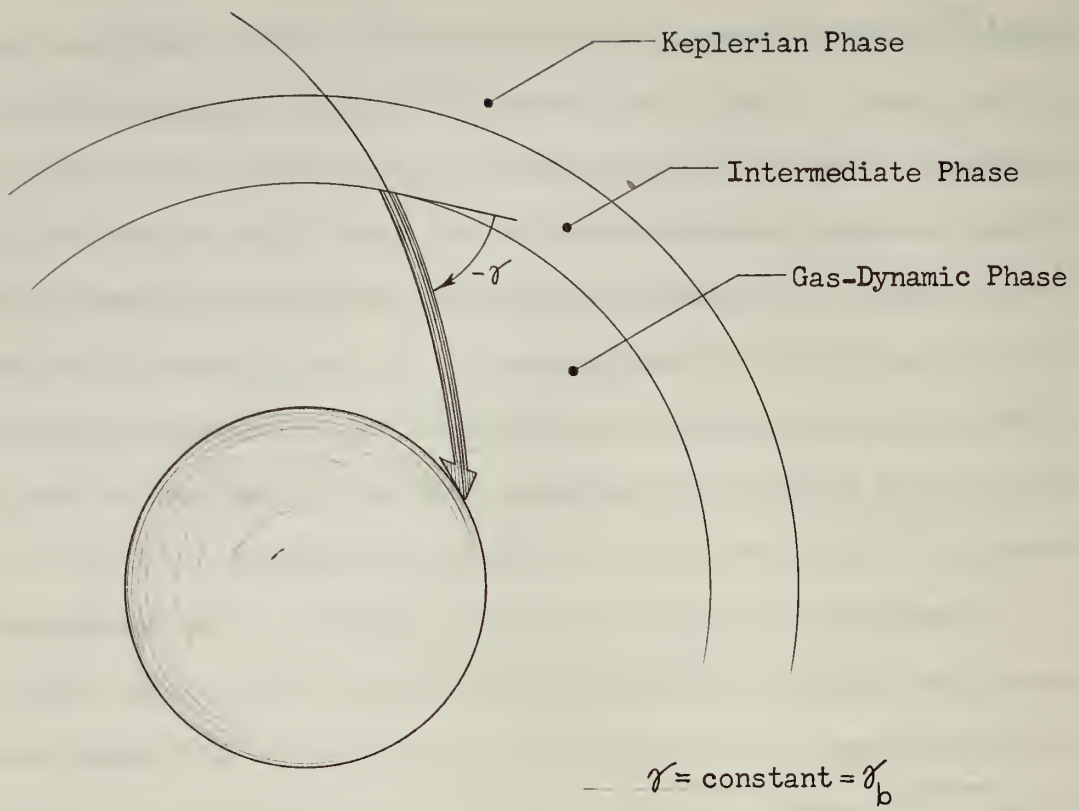

Initial Conditions: Zero lift vehicle with steep flight path ; or programmed lift-drag to maintain constant flight path angle.

Limitations of Approximate Solution:

Approximate solution is accurate

(1) Throughout the velocity spectrum for $k^{1/2}\gamma \gg 2.5$ (this corresponds to entry at $|\gamma| \geq 5°$ for Earth).

(2) For flight path angles less than listed in (1) above, approximate solution is accurate down to v equal to about 0.8.

(a) BALLISTIC TRAJECTORY

Fig. 9.7: Regions Where Approximate Solutions of This Thesis are Accurate.

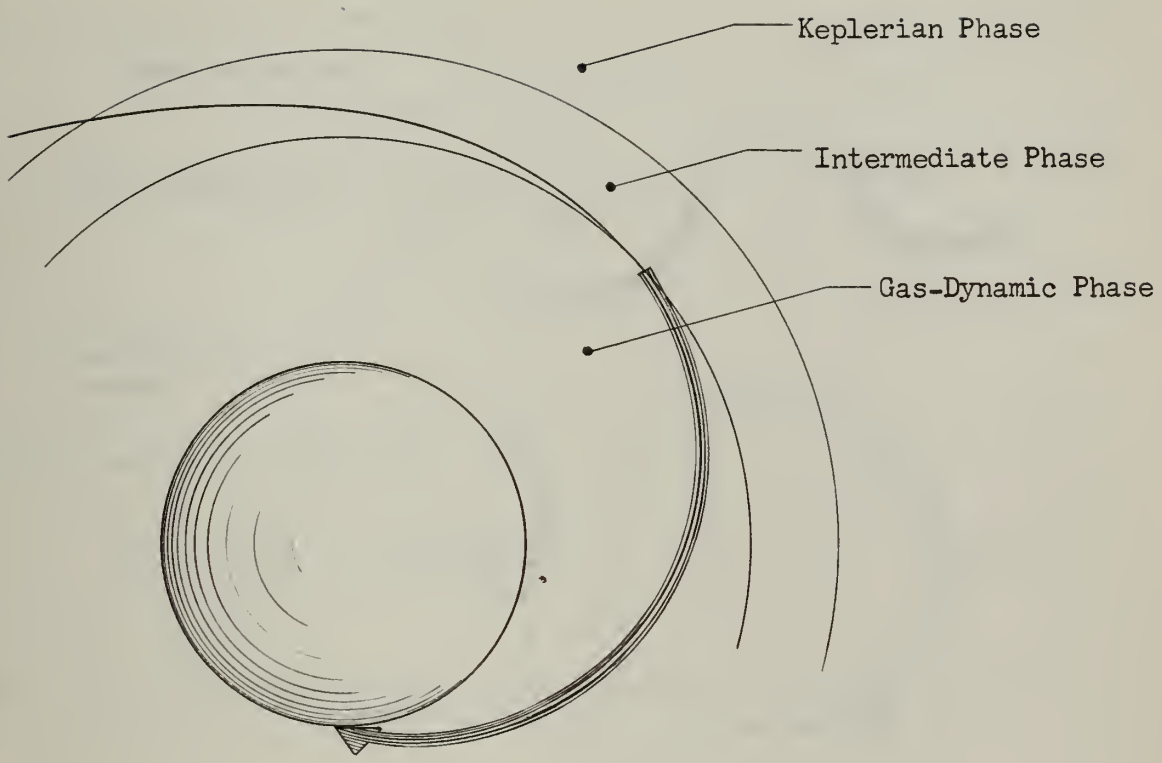

Initial Conditions: Lifting vehicle with zero initial flight path angle.

Limitations of Approximate Solution:

Approximate solution is accurate:

(1) For $v > 0.2$ if vehicle characteristics are:
$k^{1/2} L/D \geq 30$ (i.e., $(L/D)_{Earth} \geq 1.0$)

(2) For $v > 0.5$ if vehicle characteristics are:
$30 > k^{1/2} L/D \geq 15$ (i.e., $1.0 > (L/D)_{Earth} \geq 0.5$)

(3) For $v > 0.7$ if vehicle characteristics are:
$15 > k^{1/2} L/D \geq 7.5$ (i.e., $0.5 > (L/D)_{Earth} \geq 0.25$)

(b) GLIDE TRAJECTORY

Fig. 9.7: Regions where approximate solutions of this thesis are accurate.

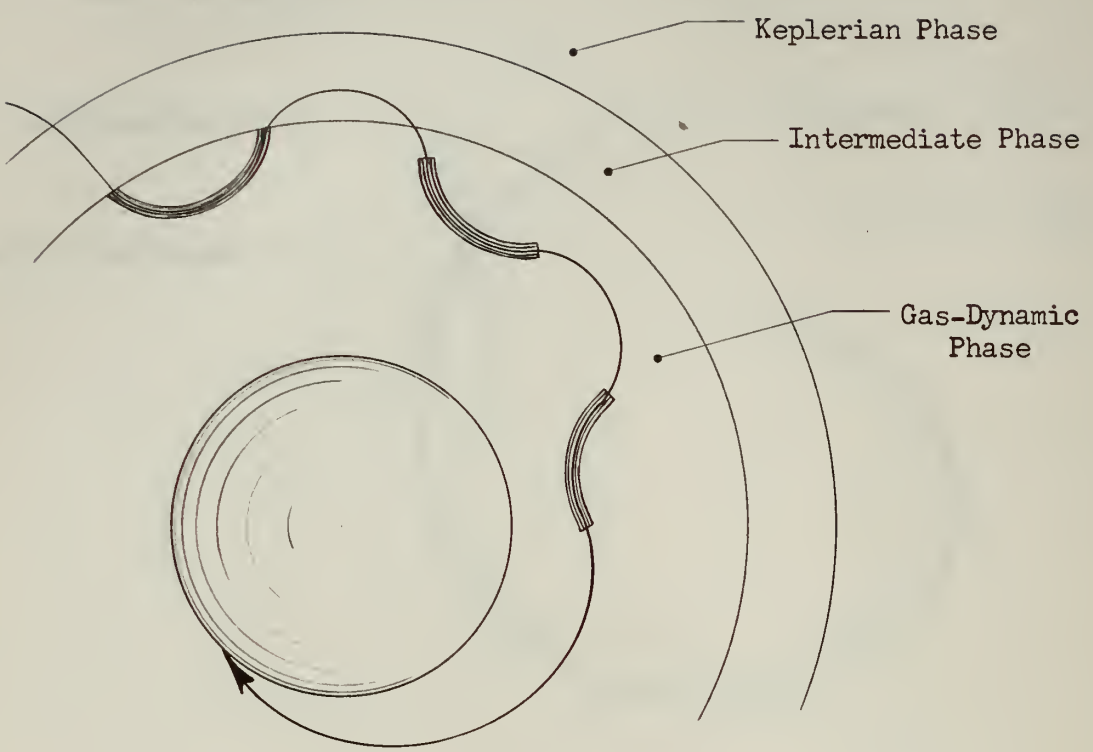

Initial Conditions: Lifting vehicle with finite initial flight path angle.

Limitations of approximate solution:

Approximate solution is accurate if $2\,k\,|\gamma_i\,L/D| \gg 1.0$

(i.e., $|\gamma_i\,L/D|_{Earth} \gg 5.6 \times 10^{-4}$)

Approximate solution can be applied only to a single skip. Subsequent skips may be analyzed by considering each skip individually with a new set of initial conditions.

(c) SKIP TRAJECTORY

Fig. 9.7: Regions where approximate solutions of this thesis are accurate.

Chapman's Z-transformation may be applied to equations (9-45) and (9-46) with the following assumptions:

$$1 + (L/D)\tan\gamma \cong 1.0$$

$$v_{I\phi} \cong v_\phi$$

$$\xi \ll 1.0$$

$$r \cong 1.0$$

The equivalent Z-transformation is:

$$Z \equiv \frac{v_r v_\phi}{\xi k^{\frac{1}{2}} v} \equiv \frac{v \cos\gamma \sin\gamma}{k^{\frac{1}{2}} \xi} \qquad (9\text{-}51)$$

The single equation derived by performing this transformation is:

$$\underbrace{\nu_\phi \frac{d^2 Z}{d\nu_\phi^2}}_{\text{Vertical Acceleration}} - \underbrace{\left\{\frac{dZ}{d\nu_\phi} - \frac{Z}{\nu_\phi}\right\}}_{\text{Vertical Component of drag}} = \underbrace{(1-\nu_\phi^2)\frac{\cos^4\gamma}{Z\nu_\phi}}_{\text{Gravity minus Centrifugal Force}} - \underbrace{k^{\frac{1}{2}}\frac{L}{D}\cos^3\gamma}_{\text{Lift Force}} \qquad (9\text{-}52)$$

Alternate forms of expressing the Z-function are as follows:

$$Z = \frac{n_D \cos\gamma}{k^{\frac{1}{2}} v} = -\frac{f_\phi}{k^{\frac{1}{2}} v} \qquad (9\text{-}53)$$

Chapman's numerical solutions are compared to the approximate solutions of the dynamical equations of motion derived in this thesis in Figs. 9.8, 9.9, and 9.10 for the ballistic, glide, and skip trajectories respectively. The abscissa on each of these graphs is the horizontal component of dimensionless velocity with respect to the atmosphere; The ordinate is the horizontal component of specific force

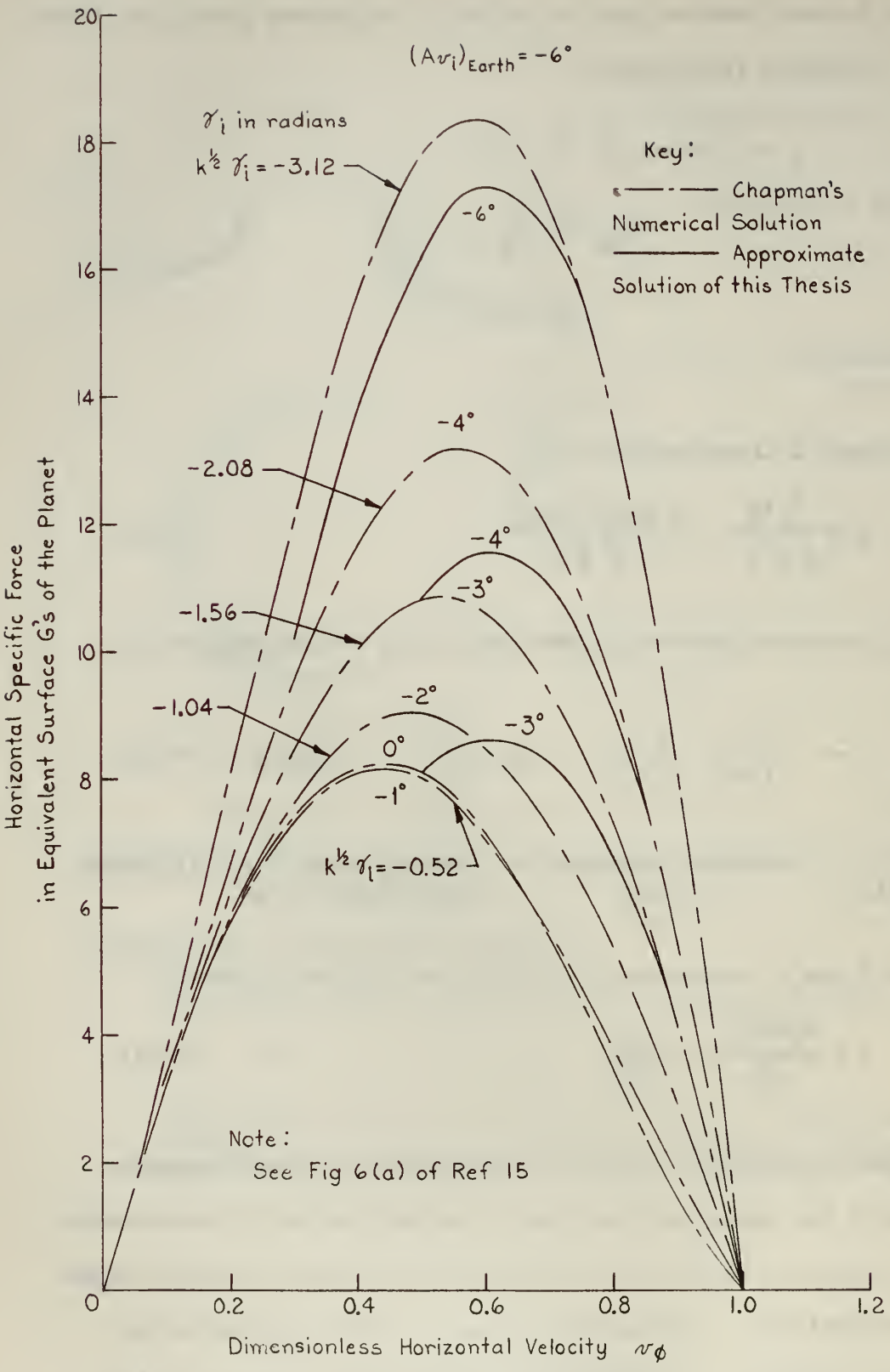

Fig. 9.8 : Comparison of Approximate "Ballistic" Solution to Machine Computed Numerical Solutions.

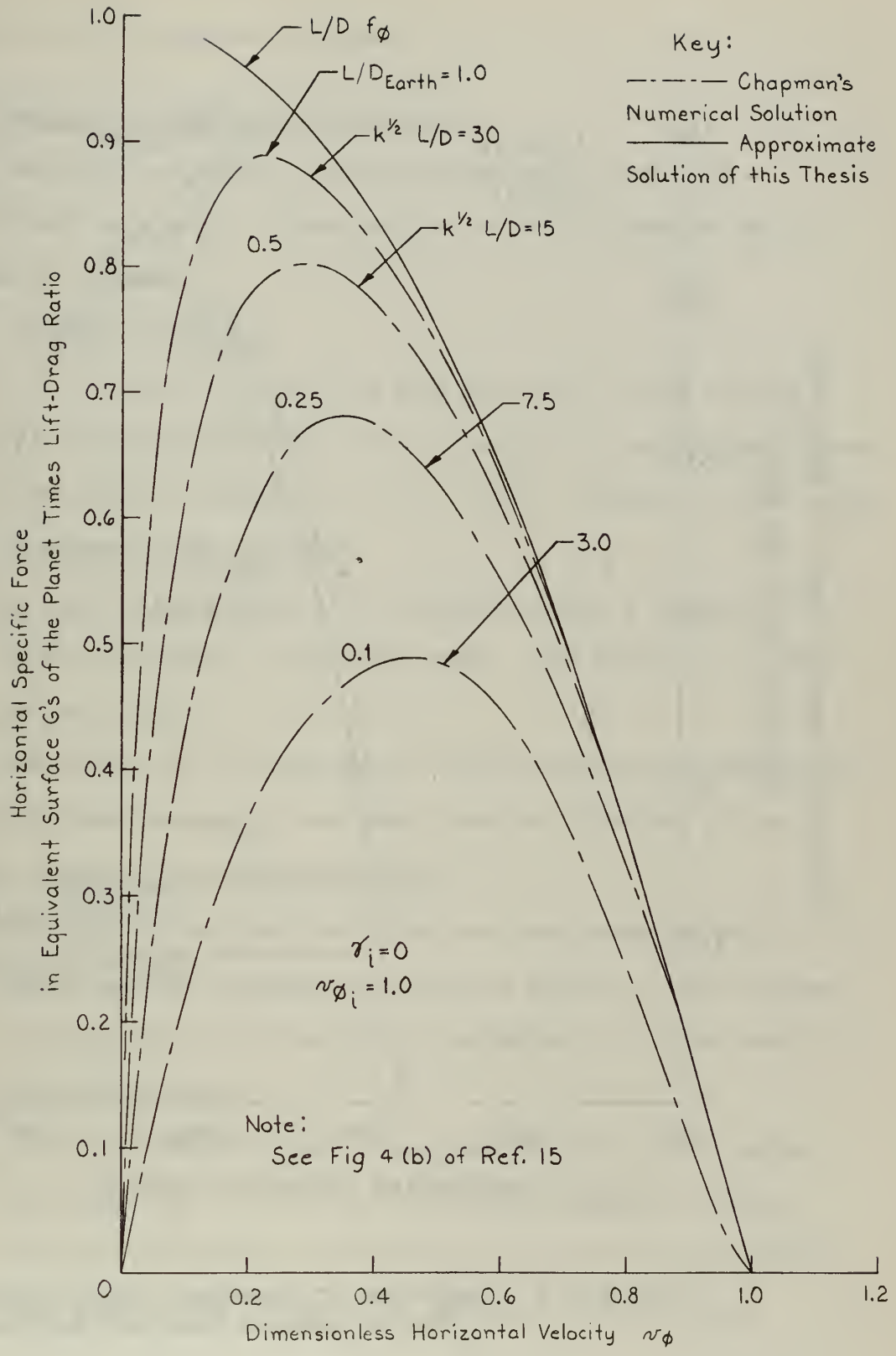

Fig. 9.9 : Comparison of Approximate "Glide" Solution to Machine Computed Numerical Solutions.

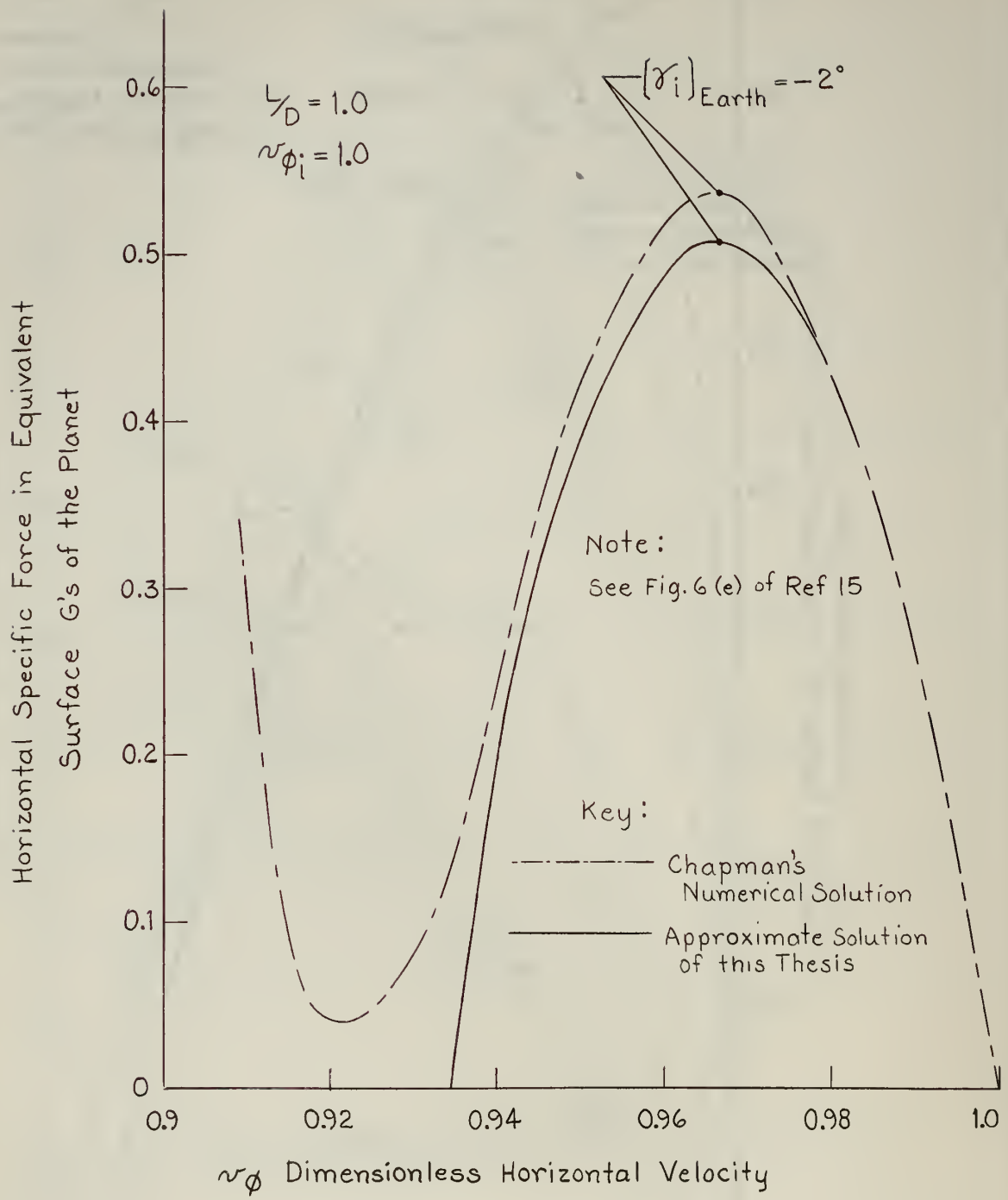

Fig. 9.10 : Comparison of Approximate "Skip" Solution to Machine Computed Numerical Solutions.

in surface g's of the planet concerned.*

9.6.1 Solution of the Ballistic Trajectory

The ballistic trajectory is characterized geometrically by a constant flight path angle. Prerequisites for this trajectory may be summarized as follows:

(1) Zero-Lift Vehicles:

If entry is made along such a steep path that the sum of vertical components of lift, gravity, and centrifugal forces are small in comparison to the vertical component of drag force.

(2) Programmed Lift and Drag:

If lift and drag are programmed in such a manner as to maintain constant flight path angle. (See equations (9-48) through (9-50).

The limitations of the approximate solution developed in Derivation Summary (9-2) when compared to more exact computer solutions of the non-linear system of equations are briefly:

(1) The solution derived here is an excellent approximation for $\left|\sqrt{k}\,\gamma\right| \geq 2.5$ throughout the velocity spectrum. This corresponds to entry into the Earth's atmosphere at angles equal to or greater than 5°.

(2) The approximate solution is accurate for flight path angles less than $\left|\sqrt{k}\,\gamma\right| = 2.5$ over the limited velocity spectrum $v > 0.8$. Therefore, the solution is accurate for all flight path angles down to velocities corresponding to maximum

- - - - - - - - - - - - - - - - -

* Ordinate is (L/D) times horizontal specific force in Fig. 9.9 for glide vehicle.

stagnation point temperature.*

Comparison of the approximate solution derived herein to numerical solutions computed by Chapman[15] is presented graphically in Fig. 9.8. The derivation carried out in Derivation Summary (9-2) and summarized below is based on the same approximations made by Chapman in deriving his Z_I solution and by Eggers, Allen, and Neice[31] for their "Ballistic Trajectory". The solutions of this thesis, however, extend the work of the cited papers to include guidance quantities expressed with either density ratio, range, velocity, or time as the independent variable.

(1) Density ratio σ as independent variable: $\left(\sigma \equiv \frac{\rho}{\rho_{(\bar{SL})}} \cong e^{-kh}\right)$

(a) Altitude: $h(\sigma) = -(1/k)\ln\sigma$ (9-54)

(b) Velocity:** $v(\sigma) = v_i e^{\left[\frac{UC_D}{k \sin\gamma_b}(\sigma-\sigma_i)\right]}$ (9-55)

(c) Range:

$$X_N(\sigma) = X_{Ni} + \cot\gamma_b \ln\left[\frac{(1-(1/k)\ln\sigma)}{(1-(1/k)\ln\sigma_i)}\right] \cong X_{Ni} \frac{-\cot\gamma_b \ln\sigma/\sigma_i}{k} \quad (9\text{-}56)$$

(2) Altitude as independent variable:

(a) Density ratio: $\sigma(h) = e^{-kh}$ (9-57)

- - - - - - - - - - - - - - - - -

* Maximum stagnation point temperature occurs when $v = 0.846\, v_i$ (See Derivation Summary 9-2).

** For convenience in writing this and all subsequent equations, the following quantity is defined:

$$U = \frac{\rho(\bar{SL})R_{(m)}O^S}{2M}$$

(b) Velocity:

$$v(h) = v_i e^{\frac{UC_D}{k \sin \gamma_b}(e^{-kh} - e^{-kh_i})} \tag{9-58}$$

(c) Range:

$$X_N(h) = X_{Ni} + \cot \gamma_b \ln \left[\frac{(1+h)}{(1+h_i)}\right] \cong X_{Ni} + (h-h_i) \cot \gamma_b \tag{9-59}$$

(3) Velocity as independent variable:

(a) Density ratio:

$$\sigma(v) = \frac{k \sin \gamma_b}{UC_D} \ln \frac{v}{v_i} + \sigma_i \tag{9-60}$$

(b) Altitude:

$$h(v) = -\frac{1}{k} \ln \left(\frac{k \sin \gamma_b}{UC_D} \ln \frac{v}{v_i} + e^{-kh_i} \right) \tag{9-61}$$

(c) Range:

$$X_N(v) = X_{Ni} + \cot \gamma_b \ln \left[\frac{1 - \frac{1}{k} \ln \left(\frac{k \sin \gamma_b}{UC_D} \ln \frac{v}{v_i} + \sigma_i \right)}{(1+h_i)} \right] \tag{9-62}$$

$$X_N(v) \cong X_{Ni} - \cot \gamma_b \left[\frac{1}{k} \ln \left(\frac{k \sin \gamma_b}{UC_D} \ln \frac{v}{v_i} + \sigma_i \right) + h_i \right] \tag{9-63}$$

(4) Dimensionless time τ as independent variable:

Note: Solution is valid if $\left| \frac{UC_D \sigma}{k \sin \gamma_b} \right| < 1.0$

(a) Density ratio:

$$-k v_i \sin \gamma_b \left(e^{\frac{-UC_D \sigma_i}{k \sin \gamma_b}} \right) (\tau - \tau_i) = \ln \left| \frac{\sigma}{\sigma_i} \right| + \sum_{n=1}^{\infty} \left(\frac{-UC_D}{k \sin \gamma_b} \right)^n \frac{(\sigma^n - \sigma_i^n)}{n \cdot n!} \tag{9-64}$$

(b) Altitude:

$$-(\tau-\tau_i)k v_i \sin\gamma_b\, e^{\frac{-UC_D}{k\sin\gamma_b}} e^{-kh_i} = k(h_i-h) + \sum_{n=1}^{\infty}\left(\frac{-UC_D}{k\sin\gamma_b}\right)^n \frac{(e^{-nkh}-e^{-nkh_i})}{n\cdot n!} \tag{9-65}$$

(c) Velocity:

$$-(\tau-\tau_i)k v_i \sin\gamma_b\, e^{\frac{-UC_D\sigma_i}{k\sin\gamma_b}} = \ln\left|\frac{k\sin\gamma_b}{UC_D\sigma_i}\ln\frac{v}{v_i}+1\right| + \sum_{n=1}^{n=\infty}\frac{(-\ln\frac{v}{v_i})^n}{n\cdot n!} \tag{9-66}$$

(d) Range:

$$-(\tau-\tau)k v_i \sin\gamma_b\, e^{\frac{-UC_D\sigma_i}{k\sin\gamma_b}} = \tag{9-67}$$

$$-k(X_N-X_{N_i})\tan\gamma_b + \sum_{n=1}^{n=\infty}\frac{\left(\frac{-UC_D\sigma_i}{k\sin\gamma_b}\right)^n\left[e^{-nk\tan\gamma_b(X_{\bar{N}}-X_{N_i})}-1\right]}{n\cdot n!}$$

(5) Range X_N as independent variable:

(a) Density ratio:

$$\sigma(X_N) = \sigma_i e^{-k(X_N - X_i)\tan\gamma_b} \tag{9-68}$$

(b) Altitude:

$$h(X_N) = (1 + h_i)e^{(X_N - X_{Ni})\tan\gamma_b} - 1 \tag{9-69}$$

(c) Velocity:

$$v(X_N) = v_i\, e^{\frac{UC_D}{k\sin\gamma_b}\left\{-\sigma_i + e^{k\left[1-(1+h_i)e^{k\tan\gamma_b(X_{\bar{N}}-X_{N_i})}\right]}\right\}} \tag{9-70}$$

$$v(X_N) \cong v_i\, e^{\frac{UC_D}{k\sin\gamma_b}\left\{e^{-k\left[\tan\gamma_b(X_N-X_{N_i})+h_i\right]}-\sigma_i\right\}} \tag{9-70a}$$

As a typical example of a ballistic trajectory solution, consider a vehicle entering the Earth's atmosphere with:

$$h_i = 80 \text{ miles}$$

$$\gamma_b = -6^\circ$$

$$X_{Ni} = 0$$

The solution for total range from Equation (9-59) is:

$$X_N = 0.192 \cong 760 \text{ statute miles}$$

From Fig. 9.6, it may be seen that the vehicle would experience about 18 g's maximum specific force at $v \cong 0.6$. The velocity spectrum and time of flight depend on the drag and density characteristics of the vehicle.

9.6.2 Solution of The Glide Trajectory

The glide trajectory is characterized geometrically by a monotonically increasing negative flight path angle. The flight path angle initially starts at zero and remains small throughout most of the trajectory. The flight path angle increases to appreciable magnitudes in the terminal phases of the trajectory after velocity has decayed to subsonic values. The gliding trajectory occurs when the flight path angle is shallow enough and velocity is small enough that vertical accelerations and the vertical component of drag force are negligible in comparison to other terms in the dynamical equations of motion. In equilibrium gliding flight, there is a balance of lift, gravity, and centrifugal forces.

The limitations of the approximate solution presented here when compared to more exact computer solutions of the complete system of equations are summarized below:

(1) The approximate solution derived here is accurate for $\sqrt{k}\, L/D \geq 30$ for dimensionless velocities greater than 0.2. For the planet Earth, this corresponds to (L/D) equal to or greater than 1.0 and velocities greater than 5200 ft/sec. (Mach $\geq$ 4.5). The assumption that lift and drag coefficients are independent of Mach number is generally accurate over this velocity spectrum only*.

(2) The approximate solution is accurate over the velocity spectrum $v > 0.5$ for $\sqrt{k}\, L/D = 15$. This corresponds to $(L/D)_{Earth} = 0.5$.

(3) The approximate solution is accurate for $v > 0.7$ for $\sqrt{k}\, L/D = 7.5$. This corresponds to $(L/D)_{Earth} = 0.25$.

Comparison of the approximate solution derived herein to numerical solutions computed by Chapman is presented graphically in Fig. 9.9.

The derivation carried out in Derivation Summary 9.3 and summarized below is based on approximations originally made by Sanger[52]. These approximations were also used by Eggers, Allen, and Neice[31] in discussing the "glide trajectory", and by Chapman[15] in deriving his

- - - - - - - - - - - - - - - - -

* The worth of generalized numerical solutions of entry trajectories for velocities less than Mach 5.0 may be questioned since Mach Number variations of lift and drag coefficients become significant at these lower velocities. The variation of C_L and C_D with Mach Number for Mach less than 5.0 is difficult to generalize because of the strong dependence on design characteristics of the vehicle. Most authors assume lift and drag coefficients are independent of Mach Number effects throughout the entire velocity spectrum. Exceptions, of course, are studies of a particular vehicle configuration using C_L and C_D data from experimental tests.

Z_{II} solution. The derivation summarized here, however, extends the solutions of the above authors to expressing guidance quantities in terms of independent variables such as dimensionless time, density ratio, etc.

(1) Density ratio σ as independent variable:

(a) Altitude:

Equation (9-54)

(b) Velocity:

$$v_{\phi}(\sigma) = \frac{1}{(1+UC_D \frac{L}{D}\sigma)^{\frac{1}{2}}} \qquad (9\text{-}71)$$

(c) Flight path angle:

$$\tan\gamma = \frac{-2\ (1+UC_D (L/D)\sigma\ )}{k(L/D)} \qquad (9\text{-}72)$$

(d) Range:

$$X_N(\sigma)=X_{N_i}+\frac{L}{2D}\left(\ln\frac{\sigma}{\sigma_i}-\ln\left|\frac{1+UC_D\frac{L}{D}\sigma}{1+UC_D\frac{L}{D}\sigma_i}\right|\right) \qquad (9\text{-}73)$$

(2) Altitude h as independent variable:

(a) Density ratio:

Equation (9-57)

(b) Velocity:

$$v_{\phi}(h) = \frac{1}{(1+UC_{DD}\frac{L}{D}e^{-kh})^{\frac{1}{2}}} \qquad (9\text{-}74)$$

(c) Flight Path Angle:

$$\tan\gamma = \frac{-2\ (1+UC_{DD}\frac{L}{D}e^{-kh})}{k\frac{L}{D}} \qquad (9\text{-}75)$$

(d) Range:

$$X_N(h)=X_i+\frac{k}{2}\frac{L}{D}\left[(h_i-h)-\frac{1}{k}\ln\left|\frac{1+UC_D\frac{L}{D}e^{-kh}}{1+UC_D\frac{L}{D}e^{-kh_i}}\right|\right] \tag{9-76}$$

(3) Flight Path Angle as independent variable:

(a) Density ratio:

$$\sigma(\gamma)=-\frac{k\gamma}{2UC_D}-\frac{1}{UC_D\frac{L}{D}} \tag{9-77}$$

(b) Altitude:

$$h(\gamma)=-\frac{1}{k}\ln\left[\frac{-(k\gamma\frac{L}{D}+2)}{2UC_D\frac{L}{D}}\right] \tag{9-78}$$

(c) Velocity:

$$v_\phi(\gamma)=\left[\frac{-2}{k(\frac{L}{D})\tan\gamma}\right]^{1/2} \tag{9-79}$$

(d) Range:

$$X_N(\gamma)=X_{N_i}+\frac{1}{2}\frac{L}{D}\ln\left[1+\frac{2}{k\frac{L}{D}\tan\gamma\,(1-v_{\phi_i}^2)}\right] \tag{9-80}$$

(4) Velocity (v_ϕ) as independent variable:

(a) Density ratio:

$$\sigma(v_\phi)=\frac{(1-v_\phi^2)}{UC_D\frac{L}{D}v_\phi^2} \tag{9-81}$$

(b) Altitude:

$$h(v_\phi)=-\frac{1}{k}\ln\left[\frac{(1-v_\phi^2)}{UC_D\frac{L}{D}v_\phi^2}\right] \tag{9-82}$$

(c) Flight Path Angle:

$$\gamma(v_\phi) = \tan^{-1}\left[\frac{-2}{k\left(\frac{L}{D}\right) v_\phi^{\,2}}\right] \tag{9-83}$$

(d) Range:

$$X_N(v_\phi) = X_{N_i} + \frac{1}{2}\,\frac{L}{D}\,\ln\left[\frac{(1-v_\phi^{\,2})}{(1-v_{\phi_i}^{\,2})}\right] \tag{9-84}$$

(5) Dimensionless time as independent variable: $\tau_i = 0$

(a) Density ratio:

$$\sigma(\tau) = \frac{1}{UC_D\,\frac{L}{D}}\left\{\frac{1-\left[\dfrac{(1+v_{\phi_i}) - (1-v_{\phi_i})\,e^{\frac{2\tau}{L/D}}}{(1+v_{\phi_i}) + (1-v_{\phi_i})\,e^{\frac{2\tau}{L/D}}}\right]^2}{\left[\dfrac{(1+v_{\phi_i}) - (1-v_{\phi_i})\,e^{\frac{2\tau}{L/D}}}{(1+v_{\phi_i}) + (1-v_{\phi_i})\,e^{\frac{2\tau}{L/D}}}\right]^2}\right\} \tag{9-85}$$

(b) Altitude:

$$h(\tau) = -\frac{1}{k}\ln\left[\sigma(\tau)\right] \tag{9-86}$$

(c) Velocity:

$$v_\phi(\tau) = \frac{1-\dfrac{(1-v_{\phi_i})}{(1+v_{\phi_i})}\,e^{\frac{2\tau}{L/D}}}{1+\dfrac{(1-v_{\phi_i})}{(1+v_{\phi_i})}\,e^{\frac{2\tau}{L/D}}} \tag{9-87}$$

(d) Flight Path Angle:

$$\tan\gamma = \frac{-2}{k\frac{L}{D}}\left[\frac{(1+v_{\phi_i}) + (1-v_{\phi_i})\,e^{\frac{2\tau}{L/D}}}{(1+v_{\phi_i}) - (1-v_{\phi_i})\,e^{\frac{2\tau}{L/D}}}\right]^2 \tag{9-88}$$

(e) Range:

$$X_N(\tau) = X_{N_i} + \frac{1}{2}\frac{L}{D}\ln\left\{\frac{\left(1-\left[\frac{(1+v_{\phi_i})-(1-v_{\phi_i})e^{\frac{2\tau}{L/D}}}{(1+v_{\phi_i})+(1-v_{\phi_i})e^{\frac{2\tau}{L/D}}}\right]^2\right)}{(1-v_{\phi_i}^2)}\right\} \tag{9-89}$$

(6) Range as independent variable:

(a) Density ratio:

$$\sigma(X_N) = \left\{\frac{(1-v_{\phi_i}^2)\,e^{\frac{2}{L/D}(X_N - X_{N_i})}}{UC_D\frac{L}{D}\left[1-(1-v_{\phi_i}^2)e^{\frac{2}{L/D}(X_N-X_{N_i})}\right]}\right\} \tag{9-90}$$

(b) Altitude:

$$h(X_N) = -\frac{1}{k}\ln\left[\sigma(X_N)\right] \tag{9-91}$$

(c) Velocity:

$$v_\phi(X_N) = \left[1-(1-v_{\phi_i}^2)e^{\frac{2}{L/D}(X_N-X_{N_i})}\right]^{1/2} \tag{9-92}$$

(d) Flight path angle:

$$\tan\gamma = -\frac{2}{k\frac{L}{D}\left[1-(1-v_{\phi_i}^2)e^{\frac{2}{L/D}(X_N-X_{N_i})}\right]} \tag{9-93}$$

9.6.3 Solution of The Skipping Trajectory

The glide solution discussed in section 9.6.2 is valid only when a lifting vehicle enters the atmosphere under very special initial conditions, viz. zero initial flight path angle at sub-orbital velocities. The glide solution does not apply to trajectories with non-zero initial

flight path angles because a finite initial vertical velocity induces a trajectory in which the vertical acceleration term in the equations of motion is not small compared to lift force.

A skipping trajectory is the consequence of a lifting vehicle penetrating the atmosphere at high velocity with a finite initial flight path angle. The magnitude of the skip in terms of the spectrum of altitude, velocity, and specific force spanned during the skip is primarily a function of the initial conditions. A number of skips in the Gas-Dynamic Phase may be anticipated; the number of skips and the severity of the skips depend strongly on the initial conditions and the lift-drag characteristics of the vehicle.

The derivation of an approximate analytical solution of the Skip Trajectory is carried out in Derivation Summary (9.4). This derivation is based on the following assumptions:

(1) The difference between the components of gravitation and centrifugal force in the lift direction is negligible when compared to lift force.

(2) Coreolis force is negligible when compared to lift force.

(3) The difference between the components of gravitation and centrifugal forces in the drag direction is negligible when compared to drag force.

(4) $\sin\gamma \cong \gamma$; $\cos\gamma \cong 1 - \frac{\gamma^2}{2}$

The approximate solution of this thesis is applicable only for flight in the Gas-Dynamic Phase and may be applied only to one skip with a given set of initial conditions. Subsequent skips may be analyzed by considering each skip individually with a new set of initial conditions.

Fig. 9.7 shows the regions in which the approximate skip solution is applicable. The approximate solution is accurate for lift-drag ratios and initial flight path angles that satisfy the following:

$$2k\left|\gamma\frac{L}{D}\right| \gg 1.0$$

A comparison of the accuracy of the approximate solution of this thesis to a numerical solution for the first skip of a vehicle entering the Earth's atmosphere is presented graphically in Fig. 9.10. Initial conditions for this trajectory were:

$$L/D = 1.0$$

Planet : Earth

$$\gamma_i = -2°$$

$$v_{\phi i} = 1.0$$

Note: $2k\left|\gamma\frac{L}{D}\right| \cong 62$

The fact that analytical approximate solutions to the skipping trajectory must be performed in a series of individual piece-wise continuous solutions with proper matching of end conditions for each skip may appear to relegate such a solution to the "academically interesting but impractical" category. This is not entirely true. In general, a skipping trajectory for the manned entry vehicle is undesirable because of a number of aerodynamic and thermodynamic reasons.*

- - - - - - - - - - - - - - - - -

* One of the disadvantages of the skip vehicle is the relatively high lateral loads that the vehicle would be required to withstand during a skip. These loads, coupled with high thermal stresses due to high convective heating rates, would require the vehicle structure to be stronger and heavier than that of a comparable glide vehicle.

Eggers[31] concludes that skip vehicles with L/D = 4.0 and 6.0 cannot radiate heat at rates comparable to the maximum convective

There may be guidance advantages, however, to inducing a partial skip early in the Gas-Dynamic Phase in order to reduce a large flight path angle** to zero, or near zero, then "turn off" lift to maintain either a constant altitude or slowly descending flight path in order that an appreciable percentage of the total energy be transferred at high altitudes where heating and deceleration loads are less severe. The skipping solution derived in Derivation Summary (9.4) and summarized below may be used to analyze this partial skip with a reasonably high degree of accuracy.

(1) Density ratio σ as independent variable

(a) Altitude:

Equation (9-54)

(b) Velocity

$$v(\sigma) = v_i \, e^{\left\{ \frac{\gamma_i}{L/D} - \left[\left(\frac{\gamma_i}{L/D} \right)^2 - \frac{2UC_D}{k(L/D)} (\sigma - \sigma_i) \right]^{1/2} \right\}} \qquad (9\text{-}94)$$

- - - - - - - - - - - - - - - - -

heating rate. The skip vehicle with lift-drag ratios in the neighborhood of 2.0 absorbs less heat than vehicles developing higher lift-drag ratios; the former vehicle, however, still absorbs more heat than a glide vehicle or a comparable high-pressure-drag ballistic vehicle.

** In order to control accurately the geographic position at which the vehicle enters the Intermediate Phase, it is desired that the Keplerian transfer ellipse intersect the atmosphere at as large an angle as possible. This may be visualized on the physical grounds that if the flight path is nearly horizontal, the slightest error in altitude or a perturbation in the density of the upper atmosphere may cause a large position error at the penetration point.

It was shown in Chapter 8 that the effective altitude of the sensible atmosphere decreases for steep flight paths; therefore, a bonus advantage of entering with a large flight path angle is that the exponential atmospheric approximation is a more accurate representation of actual conditions.

(c) Flight Path Angle:

$$\gamma(\sigma)=\pm\left[(\sigma_i-\sigma)\ \frac{2UC_D\ L/D}{k}+\gamma_i^{\,2}\right]^{1/2} \tag{9-95}$$

(d) Range:

$$X_N(\sigma)=X_{N_i}\pm\frac{1}{k\Theta}\left\{\ln\left[\frac{(\gamma-\Theta)(\gamma_i+\Theta)}{(\gamma+\Theta)(\gamma_i-\Theta)}\right]\right\} \tag{9-96}$$

where $\gamma(\sigma)$ is given by equation (9-95) and the following quantity is defined:

$$\Theta=\left(\gamma_i^{\,2}+\frac{2UC_D\frac{L}{D}\sigma_i}{k}\right)^{\frac{1}{2}} \tag{9-97}$$

(2) Altitude h as independent variable

(a) Density ratio:

Equation (9-57)

(b) Velocity:

$$v(h)=v_i\,e^{\left\{\frac{\gamma_i}{L/D}-\left[\left(\frac{\gamma_i}{L/D}\right)^2-\frac{2UC_D}{k\frac{L}{D}}\left(e^{-kh}-e^{-kh_i}\right)\right]^{1/2}\right\}} \tag{9-98}$$

(c) Flight Path Angle:

$$\gamma(h)=\pm\left[\gamma_i^{\,2}-\left(e^{-kh}-e^{-kh_i}\right)\ \frac{2UC_D\frac{L}{D}}{k}\right]^{\frac{1}{2}} \tag{9-99}$$

(d) Range:

Same as equation (9-96) with equation (9-99) for γ

and equation (9-97) for Ⓗ .

(3) Flight Path Angle as independent variable

(a) Density ratio:

$$\sigma(\gamma)=\sigma_i+\frac{k}{2UC_D\frac{L}{D}}\left(\gamma_i^2-\gamma^2\right) \tag{9-100}$$

(b) Altitude:

$$h(\gamma) = -\frac{1}{k}\ln\left[\sigma(\gamma)\right] \tag{9-101}$$

(c) Velocity:

$$v(\gamma) = v_i e^{\frac{\gamma_i-\gamma}{L/D}} \tag{9-102}$$

(d) Range:

Same as equation (9-96).

(4) Velocity v as independent variable

(a) Density ratio:

$$\sigma(v)=\sigma_i+\frac{k\ln\left(\frac{v}{v_i}\right)}{2UC_D}\left(2\gamma_i-\frac{L}{D}\ln\frac{v}{v_i}\right) \tag{9-103}$$

(b) Altitude:

$$h(v) = -\frac{1}{k}\ln\left[\sigma(v)\right] \tag{9-104}$$

(c) Flight Path Angle:

$$\gamma(v)=\gamma_i-\frac{L}{D}\ln\frac{v}{v_i} \tag{9-105}$$

9.6.4 Specific Forces Acting on the Entry Vehicle:

The specific force in Earth g's measured by accelerometers carried by the entry vehicle is:

$$f_E = \frac{G_{(m)o}}{G_{(m)E}} U v^2 C_D \sigma \left[1 + (L/D)^2\right]^{\frac{1}{2}} \qquad (9\text{-}116)$$

Specific force may be written as a function of any one of the independent variables given in equations (9-54) through (9-115) by substituting the appropriate expressions for v and σ as functions of the single independent variable selected. As an example, the specific force may be written as a function of velocity by substituting $\sigma(v)$ as follows:

(1) Ballistic Trajectory ($L = 0$; γ = constant = γ_b) :

$$f(v)_E = \frac{G_{(m)o}}{G_{(m)E}} U v^2 C_D \left[\sigma_i + \frac{k \sin \gamma_b}{U C_D} \ln \frac{v}{v_i}\right] \qquad (9\text{-}117)$$

(2) Glide Trajectory:

$$f(v_\phi)_E = \frac{G_{(m)o}}{G_{(m)E}} \frac{(1-v_\phi^2)}{(L/D)} \left[1 + (L/D)^2\right]^{\frac{1}{2}} \qquad (9\text{-}118)$$

(3) Skip Trajectory:

$$f(v)_E = \frac{G_{(m)o}}{G_{(m)_E}} v^2 \left[1+\left(\frac{L}{D}\right)^2\right]^{\frac{1}{2}} \left[\sigma_i U C_D + \frac{k}{2} \ln \frac{v}{v_i} \left(2\gamma_i - \frac{L}{D} \ln \frac{v}{v_i}\right)\right] \qquad (9\text{-}119)$$

Since $\sigma_i \ll \sigma$ during most of the ballistic trajectory, Equation (9-117) shows that the total specific force is essentially independent of vehicle drag characteristics, vehicle mass to area ratio, and planetary surface satellite dynamic pressure. It is a function primarily of the exponential decay characteristics of the planetary atmosphere, velocity, and flight path angle.

It is interesting to note that the total specific force for the glide trajectory, on the other hand, is independent of the decay characteristics of the planetary atmosphere. Specific force decreases as (L/D) is increased for the glide vehicle.

The approximation $\sigma_i \ll \sigma$ cannot generally be made in the case of the skipping vehicle since altitude may not change by orders of magnitude during any one skip. At the bottom of the skip, however, this approximation is reasonably accurate; hence, the specific force experienced at the bottom of the skip is independent of C_D, vehicle frontal loading, and surface atmospheric density. It is a strong function of the planetary atmospheric decay characteristics, velocity, and flight path angle at the beginning of the skip.

9.6.5 Maximum Specific Force

It may be seen from equation (9-116) that the specific force is a maximum when:

$$\frac{d(v^2\sigma)}{d\tau} = 0 \qquad (9\text{-}120)$$

Therefore, specific force is a maximum when:

$$v' = \frac{kv^2}{2} \sin\gamma \qquad (9\text{-}121)$$

Using equation (3) of Derivation Summary 9.2, it is seen that maximum specific force of the ballistic vehicle occurs when:

$$v \cong 0.607\, v_i \qquad (9\text{-}122)$$

The magnitude of the maximum specific force for the 760 mile ballistic vehicle discussed in section 9.6.1 is readily determined by substituting equation (9-122) into equation (9-117) (assuming $v_i = 1.0$). A maximum

force of 17.3 g's at v = 0.607 was computed in this manner; this result compares well with a value of 18.3 g's at v = 0.59 determined from numerical solution of the non-linear equations of motion.

Solving equation (9-121) for the glide vehicle results in maximum specific force at v = 0. This result could have been predicted by noting on Fig. 9.9 that the approximate solution of this thesis has its maximum ordinate value when the abscissa equals zero. Numerical calculations, on the other hand, show that:

(1) For $\sqrt{k}\ L/D = 30$, v_ϕ at $f_{max} \cong 0.23$ (Corresponds to $(L/D)_{Earth} \cong 1.0$)

(2) For $\sqrt{k}\ L/D = 15$, v_ϕ at $f_{max} \cong 0.29$ (Corresponds to $(L/D)_{Earth} \cong 0.5$)

(3) For $\sqrt{k}\ L/D = 7.5$, v_ϕ at $f_{max} \cong 0.35$ (Corresponds to $(L/D)_{Earth} \cong 0.25$)

(4) For $\sqrt{k}\ L/D = 3.0$, v_ϕ at $f_{max} \cong 0.45$ (Corresponds to $(L/D)_{Earth} \cong 0.1$)

In general, the velocity at maximum specific force for glide vehicles in excess of $(L/D)_{Earth} = 1.0$ occurs at velocities less than 0.2.

It was shown in Derivation Summary (9.4) that flight path angle is a convenient parameter for determining the point of maximum specific force for the skip vehicle.

$$(\gamma)_{f_{max}} = \frac{L}{2D}\left[1-\sqrt{1+\left(\frac{2D}{L}\right)^2\left(\gamma_i^2+\frac{2UC_D\frac{L}{D}}{k}\sigma_i\right)}\right] \cong \frac{L}{2D}\left[1-\sqrt{1+\left(\frac{\gamma_i}{L/2D}\right)^2}\right] \qquad (9\text{-}123)$$

For small initial flight path angles and large lift-drag ratios, the maximum specific force occurs when $\gamma \cong 0$. The velocity at maximum

specific force for the skip vehicle is:

$$(n)_{f_{max}} = n_i \, e^{\left\{ \frac{\gamma_i}{L/D} - \frac{1}{2}\left[1 - \sqrt{1 + \left(\frac{\gamma_i}{L/2D} \right)^2} \right] \right\}} \qquad (9\text{-}124)$$

9.6.6 Stagnation Point Temperature

The stagnation point temperature was written in equation (7-21) as follows:

$$T_S = 1.392 \times 10^4 (HF)_{EO}^{\frac{1}{4}} (VF)^{\frac{1}{4}} (v^6 \sigma)^{\frac{1}{8}} \quad ^\circ\text{Rankine} \qquad (9\text{-}125)$$

where $(HF)_{EO}$ is a "heating function ratio" of the atmosphere of planet 0 with respect to that of the Earth, and (VF) is a vehicle function depending on the emissivity of the skin structure and on the radius of curvature in the vicinity of the stagnation point.

Stagnation point temperature may be written as a function of any one of the independent variables given in equations (9-54) through (9-115) by substituting the appropriate expressions for v and σ as functions of the single independent variable selected. As an example, the stagnation point temperature may be written as a function of velocity by substituting σ (v) as follows:

(1) Ballistic Trajectory ($L = 0$; γ = constant = γ_b) :

$$T_S(n) = 1.392 \times 10^4 (HF)_{EO}^{\frac{1}{4}} (VF)^{\frac{1}{4}} \left(\frac{k \sin \gamma_b n^6}{UC_D} \ln \frac{n}{n_i} \right)^{\frac{1}{8}} \quad ^\circ\text{R} \qquad (9\text{-}126)$$

(2) Glide Trajectory:

$$T_S(n_\phi) = 1.392 \times 10^4 (HF)_{EO}^{\frac{1}{4}} (VF)^{\frac{1}{4}} \left\{ \frac{n_\phi^{\frac{1}{2}} (1 - n_\phi^2)^{\frac{1}{8}}}{(UC_L)^{\frac{1}{8}}} \right\} \quad ^\circ\text{R} \qquad (9\text{-}127)$$

(3) Skip Trajectory:

$$T_S(\rho) = 1.392 \times 10^4 (HF)_{EO}^{1/4} (VF)^{1/4} \rho^{3/4} \left[\sigma_i + \frac{k \ln \frac{\rho}{\rho_i}}{2UC_D} \left(2\gamma_i - \frac{L}{D} \ln \frac{\rho}{\rho_i} \right) \right]^{1/8} \quad ^\circ R \qquad (9\text{-}128)$$

The stagnation point temperature for all three trajectory profiles is a function of C_L and/or C_D, vehicle mass to area characteristics, and surface satellite dynamic pressure. It is interesting to note, however, that the stagnation point temperature of the glide vehicle is independent of the exponential decay characteristics of the planetary atmosphere.

9.6.7 Maximum Stagnation Point Temperature

From equation (9-125), stagnation point temperature is a maximum when:

$$\frac{d}{d\tau}(v^6 \sigma) = 0 \qquad (9\text{-}129)$$

This corresponds to:

$$v' = \frac{kv^2 \sin\gamma}{6} \qquad (9\text{-}130)$$

For the ballistic vehicle, stagnation point temperature is a maximum when

$$v = 0.846\, v_i \qquad (9\text{-}131)$$

This result may be used in equation (9-126) to give the maximum temperature that may be expected during the ballistic trajectory. For example:

(1) $v_i = 1.0$

$C_D = 1.0$

$\gamma_b = -6^\circ$

(VF) = 1.0

M/S = 1.0

Planet Earth

$T_{s_{max}}$ for this situation is 4850° Rankine.

(2) If all conditions are identical as in (1) above except $C_D = 10$, then $T_{s_{max}} = 3650°$ Rankine.

By differentiating equation (9-127) with respect to τ and setting the result equal to zero, the velocity at maximum stagnation point temperature of the glide vehicle is determined. This occurs when:

$$v_\phi = 0.815 \tag{9-132}$$

The maximum temperature for the skip vehicle is incurred at the following flight path angle:

$$(\gamma)_{T_{s_{max}}} = \frac{L}{6D}\left[1-\sqrt{1+\left(\frac{6D}{L}\right)^2\left(\gamma_i^2+\frac{2L}{D}\frac{UC_D\sigma_i}{k}\right)}\right] \tag{9-133}$$

$$(\gamma)_{T_{s_{max}}} \cong \frac{L}{6D}\left[1-\sqrt{1+\left(\frac{6D}{L}\gamma_i\right)^2}\right] \tag{9-133a}$$

This corresponds to a velocity of:

$$v_{T_{s_{max}}} = v_i\, e^{\left\{\frac{\gamma_i}{L/D}-\frac{1}{6}\left[1-\sqrt{1+\left(\frac{6D}{L}\gamma_i\right)^2}\right]\right\}} \tag{9-134}$$

Comparing equations (9-133) and (9-123) it is seen that for the skip vehicle:

$$(\gamma)_{T_{s_{max}}} = 3(\gamma)_{f_{max}} \tag{9-135}$$

Equation (9-135) shows that in a typical skip trajectory, the maximum temperature level is incurred before the flight path angle reduces to the

value corresponding to maximum specific force level. Comparison of equations (9-124) and (9-134) shows that:

$$\frac{v_{(T_{s\,max})}}{v_{(f_{max})}} = e^{\left[\frac{-2\,\gamma_{(f_{max})}}{(L/D)}\right]} = e^{\left[-\frac{3}{3}\,\frac{\gamma_{(T_{s\,max})}}{(L/D)}\right]} \qquad (9\text{-}136)$$

Equation (9-136) demonstrates that the velocity at maximum temperature is greater than the velocity at maximum specific force level during the skip.

9.7 Summary

Atmospheric entry trajectories were examined in Chapter 8 from a unique and instructive vantage point, namely by studying the behavior of the Conservation Parameter $\left|\frac{1-\xi}{\xi}\right|$. Examination of the conduct of this parameter with respect to altitude, specific force level, energy, and angular momentum led to the conclusion that the entry trajectory could profitably be analyzed in three distinct operational regimes; these regimes were named the Keplerian, Intermediate, and Gas-Dynamic Phases.

The investigation discussed in Chapter 9 was oriented toward utilizing the Conservation Parameter for determination of guidance quantities. Two dissimilar entry profiles were considered:

(1) The direct entry profile results from perturbation of a stable* satellite orbit by means of retro-rocket thrust. In this profile, the vehicle generally traverses in sequence the Keplerian, Intermediate, and Gas-Dynamic Phases to a landing.

- - - - - - - - - - - - - - - - -

* Or relatively stable.

(2) The degenerate orbital profile consists of a series of braking passes through the outer reaches of the atmosphere in order to reduce the energy level preparatory to final direct entry. In this profile, the vehicle enters the Intermediate Phase in a series of near impulses until the energy level is reduced sufficiently for final transition to the Gas-Dynamic Phase.

The feasibility of using the Conservation Parameter as a switching function for profile (1) and as a prediction function for profile (2) was discussed.

Range capabilities and range accuracy in the Keplerian Phase were discussed in terms of geometric quantities at the trajectory modification point for entry from elliptical satellite orbits, and in terms of velocity impulse and engine gimbal angle for entry from circular satellite orbits. Examples of range sensitivity to errors in operation of the retro-rocket system were computed and presented in both graphical and analytical form.

Approximate solutions of various guidance quantities were derived for ballistic, glide, and skip profiles in the Gas-Dynamic Phase. Limitations on the approximate solutions were established after comparing them to numerical solutions obtained from the non-linear equations of motion. Analytical determination of instantaneous and maximum deceleration loads and temperature levels was discussed.

9.8 Derivation Summaries

All Derivation Summaries referred to in the previous sections of this chapter are appended.

Derivation Summary No.	Title	Page No.
9.1	Solution of Keplerian Phase of Entry Trajectory in Terms of Geometric Quantities at the Trajectory Modification Point.	339
9.2	Solution of the Ballistic Trajectory	345
9.3	Solution of the Glide Trajectory	347
9.4	Solution of the Skip Trajectory	350

Derivation Summary 9.1

Solution of Keplerian Phase of Entry Trajectory in Terms of Geometric Quantities at the Trajectory Modification Point.

Angular momentum is conserved in a pure Keplerian trajectory; p is a convenient constant of integration to use in solving the equations of motion for the Keplerian Phase of the trajectory.

$$p = rv_{I\phi} \tag{1}$$

Assuming planar motion*, the horizontal component of velocity with respect to inertial coordinates is:

$$v_{I\phi} = r\phi' \tag{2}$$

Therefore, angular momentum is written:

$$p = r^2\phi' \tag{3}$$

Using equations (3) and (9-4), equation (9-5) is written:

$$r'' - \frac{p^2}{r^3} + \frac{1}{r^2} = 0 \tag{4}$$

This equation may be written in a form suitable for integrating by making the following transformation:

$$u \equiv 1/r \tag{5}$$

Therefore:

$$du = -dr/r^2 \tag{6}$$

$$r' = -r^2u' = -r^2\frac{du}{d\phi}\phi' = -p\frac{du}{d\phi} \tag{7}$$

- - - - - - - - - - - - - - - - -

* See Section 6.1 for a quantitative discussion of the effects of non-spherical gravitational components in limiting the assumption of planar motion.

Derivation Summary 9.1 (cont.)

$$r'' = -p^2u^2 \frac{d^2u}{d\phi^2} \tag{8}$$

Equation (4) is written with the aid of equation (8) as:

$$\frac{d^2u}{d\phi^2} + u = \frac{1}{p^2} = \text{constant} \tag{9}$$

The solution of equation (9) is as follows:

$$u(\phi) = C_1 \cos(\phi + C_2) + \frac{1}{p^2} \tag{10}$$

It is convenient to express u in terms of the true anomaly:

$$\phi = \eta + \theta \tag{11}$$

η is the angle measured from the ascending line of nodes to the line of apsides; θ is true anomaly. If the entry transfer ellipse is fixed in inertial space, then η is constant. Therefore:

$$u(\theta) = C_1 \cos(\theta + C_3) + \frac{1}{p^2} \equiv \frac{1}{r} \tag{12}$$

Constant C_3 is determined by noting that the time rate of change of radius (altitude) is zero at perigee and apogee. From equation (7):

$$r' = -r^2u' = r^2 C_1 \sin(\theta + C_3)\theta' \tag{13}$$

Therefore:

$$\theta + C_3 = 0 + \eta\pi \quad (\eta = 0,1,2\ldots) \tag{14}$$

From Fig. 4.1, it may be seen that $\theta = \pi$ at apogee and $\theta = 0$

at perigee. The equation of the ellipse is given in Fig. 4.1 in terms of R, a, θ, and ε. Writing this in dimensionless form:

$$\frac{1}{r} = \frac{1 + \varepsilon \cos\theta}{a_N(1 - \varepsilon^2)} \tag{15}$$

In equation (15), a_N is the semi-major axis non-dimensionalized with respect to $R_{(m)0}$. Equation (15) may be written:

$$\frac{1}{r} = \frac{a_N}{b_N^2}(1 + \varepsilon \cos\theta) \tag{16}$$

where b_N is dimensionless semi-minor axis of the ellipse. With $C_3 = 0$, equation (12) and equation (16) are used to eliminate r:

$$p^2 = \frac{b_N^2}{a_N} \tag{17}$$

$$C_1 = \frac{a_N}{b_N^2}\varepsilon \tag{18}$$

The constant C_1 can be determined by differentiating (12):

$$C_1 \sin\theta = \frac{r'}{r^2\theta'} = \frac{r'}{p} \tag{19}$$

Using equations (9.4-2) and (9.4-3) given in Fig. 9.4, this may be written:

$$C_1 \sin\theta = \frac{\tan\gamma_I}{r} \tag{20}$$

From equation (12):

$$C_1 \cos\theta = \frac{1}{r} - \frac{1}{r^2 v_I^2 \cos^2\gamma_I} \tag{21}$$

Derivation Summary 9.1 (cont.)

Squaring and adding equations (20) and (21) makes it possible to eliminate θ. Using the result in equations (17) and (18) gives:

$$\varepsilon^2 = 1 - v_I^2 r \cos^2\gamma_I (2 - v_I^2 r) \qquad (22)$$

Equation (22) expresses the eccentricity of the entry transfer ellipse in terms of velocity, radius, and flight path angle. The magnitude of these quantities at the trajectory modification point is denoted by the subscript m.

The semi-major axis is determined from equations (17) and (22) and the following relation:

$$\varepsilon^2 = 1 - \frac{b_N^2}{a_N^2} \qquad (23)$$

The resulting equation in terms of quantities at the trajectory modification point is given as equation (9-8). Equations (9-9) through (9-18) are readily determined from the foregoing results and from the equations listed in Fig. 4.1.

Time of flight may be derived in terms of θ by noting from equation (3) and (11), with η = constant:

$$\theta' = p/r^2 \qquad (24)$$

Using equations (16) and (17), this is written:

$$\theta' = \frac{(1 + \varepsilon \cos\theta)^2}{p^3} \qquad (25)$$

Derivation Summary 9.1 (cont.)

Integrating equation (25) gives the time of flight listed as equation (9-19).

The velocity at any instant in terms of quantities at the trajectory modification point is written from equation (9-8) with a_N = constant. Flight path angle may be written in terms of quantities at the trajectory modification point from equation (9.4-3) with angular momentum equal to a constant.

Range is defined by equation (9-23). With the aid of equations (17) and (18), equations (9-24) and (9-25) are written. The true anomaly may be eliminated from the range expression by taking the cosine of equation (9-23) and substituting equations (9-24) and (9-25) into the result. The range expression so derived is given by equations (9-26) and (9-27).

With equations (9.3-1) through (9.3-5) given in Fig. 9.3, the foregoing results are written in terms of velocity impulse δv, and engine gimbal angle A_e for the special case of a circular reconnaissance orbit. The results are summarized as equations (9-29) through (9-35).

Equations (9-36) through (9-42) are derived by writing for equation (9-3):

$$\cos \theta = \cos X_N \cos \theta_m - \sin X_N \sin \theta_m \qquad (26)$$

θ and θ_m are eliminated from equation (26) by using equations (9-24) and (9-25):

Derivation Summary 9.1 (cont.)

$$\frac{r_m}{r}\left[p^2 - r\right] = \cos X_N\,(p^2 - r_m) - \sin X_N\left[\varepsilon^2 r_m^2 - (p^2 - r_m)^2\right]^{\frac{1}{2}} \qquad (27)$$

Substituting for eccentricity from equation (9-7) and for angular momentum from equations (9.4-3) gives equation (9-36). This may be written in the following alternate forms:

$$v_{Im}^2 = \frac{r\,(1 - \cos X_N)}{\cos\gamma_I\left[r_m^2\cos\gamma_{Im} - r r_m \cos\,(X_N + \gamma_{Im})\right.} \qquad (28)$$

$$\frac{r_m}{r}\cos(2\gamma_{Im}) - \cos(2\gamma_{Im} + X_N) = \frac{2(1-\cos X_N)}{v_{Im}^2 r_m} - \left[\frac{r_m}{r} - \cos X_N\right] \qquad (29)$$

Substituting equations (9-29), (9-31) and (9.3-5) into equation (26) gives equation (9-39) or its alternate form (9-40). Equations (9-41) and (9-42) were derived by implicit differentiation of equation (9-39).

Derivation Summary 9.2

Solution of the Ballistic Trajectory

The most convenient set of planar equations for solving the ballistic trajectory are equations (6-40) through (6-44); these were written in terms of components in the $\bar{l}_X$ and $\bar{l}_Z$ directions. Assuming powerless flight ($\Gamma_N = 0$), it may be seen from equation (6-41) that if the centrifugal force and Coreolis force terms in the $\bar{l}_Z$ direction are balanced by gravitational force, then:

$$\gamma' = 0 \tag{1}$$

Therefore:

$$\gamma = \text{constant} = \gamma_b \text{ ("ballistic" flight path angle)} \tag{2}$$

If the gravity force in the $\bar{l}_X$ direction is small in comparison to drag force, equation (6-40) gives:

$$v' = - n_D = - U C_D v^2 \sigma \tag{3}$$

where:

$$U = \frac{\rho_{(\overline{SL})}}{2} \frac{R_{(m)o} S}{M} \tag{4}$$

The time rate of change of density ratio is:

$$\sigma' = - k v_o \sin\gamma \tag{5}$$

Therefore, from equations (3) and (5):

$$\frac{dv}{d\sigma} = \frac{U C_D}{k \sin\gamma} v \tag{6}$$

Derivation Summary 9.2 (cont.)

Integrating equation (6) gives:

$$\ln \frac{v}{v_i} = \frac{UC_D}{k \sin \gamma_b} (\sigma - \sigma_i) \qquad (7)$$

The solution for range is readily determined from equations (6-43) and (6-44) with $\gamma = \gamma_b$:

$$X_N - X_{Ni} = \cot \gamma_b \ln \frac{r}{r_i} \cong \cot \gamma_b (h - h_i) \qquad (8)$$

Atmospheric density ratio may be solved as a function of time by using equation (5) and (7):

$$\frac{\sigma'}{\sigma e^{\frac{UC_D\sigma}{k \sin \gamma_b}}} = -k v_i \sin \gamma_b \, e^{\frac{-UC_D\sigma_i}{k \sin \gamma_b}} \qquad (9)$$

Integrating equation (9) gives:

$$-(\tau - \tau_i) k v_i \sin \gamma_b \, e^{\frac{-UC_D\sigma_i}{k \sin \gamma_b}} = \ln \left| \frac{\sigma}{\sigma_i} \right| - \frac{UC_D}{k \sin \gamma_b} (\sigma - \sigma_i)$$

$$+ \left(\frac{UC_D}{k \sin \gamma_b} \right)^2 \frac{(\sigma^2 - \sigma_i^2)}{4} + \cdots \left(\frac{-UC_D}{k \sin \gamma_b} \right)^n \frac{(\sigma^n - \sigma_i^n)}{n \cdot n!}$$

(10)

Equations (7), (8), and (10) are three fundamental equations from which all of the equations (9-54) through (9-70) are derived.

Derivation Summary 9.3

Solution of the Glide Trajectory

If the flight path angle, γ , at the onset of the Gas-Dynamic Phase is zero, then the vertical velocity at this point is zero. Basic assumptions required for equilibrium gliding flight to exist throughout the trajectory are:

(a) Vertical accelerations are small, i.e., $v_r' \rightarrow 0$.

(b) Vertical component of drag force is small;

i.e. $UC_D v\, v_r \sigma \rightarrow 0$

With the above assumptions and the following approximations:

$$|\xi| \ll 1.0 \tag{1}$$

$$(1 + (L/D)\frac{v_r}{v_\phi}) \cong 1.0 \tag{2}$$

$$v_{I\phi} \cong v_\phi \tag{3}$$

$$r = (1 + h) \cong 1.0 \tag{4}$$

equation (9-45) is written as follows:

$$(\frac{1 - v_\phi^2}{v_\phi}) = \frac{L}{D} C_D\, v \sigma U \tag{5}$$

Substituting equation (5) into equation (9-46) gives:

$$v_\phi' = \frac{(v_\phi^2 - 1)}{(L/D)} \tag{6}$$

Derivation Summary 9.3 (cont.)

For L/D equal to a constant, equation (6) may be integrated to give:

$$\frac{(v_\phi - 1)\,(v_{\phi_i} + 1)}{(v_\phi + 1)\,(v_{\phi_i} - 1)} = e^{\frac{2(\tau - \tau_i)}{L/D}} \qquad (7)$$

Equation (7) holds only when $v_{\phi_i} < 1.0$. Solving this explicitly for v_ϕ gives equation (9-87).

Flight path angle may be computed by differentiating equation (5) with respect to v_ϕ :

$$\frac{L}{D} U C_D \sigma v \left(\frac{1}{v} \frac{dv}{dv_\phi} + \frac{1}{\sigma} \frac{d\sigma}{dv_\phi} \right) = -\left(\frac{v_\phi^2 + 1}{v_\phi^2} \right) \qquad (8)$$

Using equation (6) above and equation (5) of Derivation Summary 9.2:

$$\frac{1}{\sigma} \frac{d\sigma}{dv_\phi} = \frac{k\left(\frac{L}{D}\right) v_\phi \tan\gamma}{(1 - v_\phi^2)} \qquad (9)$$

Also, the following may be written:

$$\frac{1}{v} \frac{dv}{dv_\phi} = \frac{1}{v_\phi} \left(1 + v_r \frac{d\gamma}{dv_\phi} \right) \qquad (10)$$

The second term in the parenthesis of equation (10) is the product of two small quantities and can be neglected in comparison to 1. Using equation (9) and (10) in equation (8) gives:

$$\tan\gamma \cong \gamma = \frac{-2}{k(L/D) v_\phi^2} \qquad (11)$$

Range is determined as a function of altitude from equations (9-43) and (9-44):

Derivation Summary 9.3 (cont.)

$$\frac{dX_N}{dh} = \frac{1}{r \tan\gamma} \cong \frac{1}{\tan\gamma} \qquad (12)$$

Using equation (11) for $\tan\gamma$ and equation (5) for $v_\phi(h)$ gives:

$$\frac{dX_N}{dh} = \frac{-k\ L/D}{2} \quad \frac{1}{(1+vC_D(L/D)e^{-kh})} \qquad (13)$$

Integrating equation (13) gives equation (9-76).

Range as a function of velocity is determined from equation (9-43) and (6):

$$\frac{dX_N}{dv_\phi} = \frac{v_\phi}{r} \left(\frac{L/D}{v_\phi^2 - 1}\right) \cong \frac{(L/D)v_\phi}{(v_\phi^2 - 1)} \qquad (14)$$

Integrating equation (14) gives equation (9-84). Velocity as a function of range may be written by solving equation (9-84) explicitly for v_ϕ .

Equations (5), (7), (11), (9-76), and (9-84) are fundamental equations from which equations (9-71) through (9-93) were derived by algebraic operations.

Derivation Summary 9.4

Solution of the Skip Trajectory

The glide solution discussed in Derivation Summary 9.3 is valid only when a lifting vehicle enters the planetary atmosphere under very special initial conditions, viz. zero initial flight path angle at velocities equal to or less than orbital velocity. The glide solution does not apply to trajectories with non-zero flight path angles because a finite initial vertical velocity induces a trajectory in which the vertical acceleration term in the equation of motion is not small compared to lift force.

The following basic assumptions are made in deriving the solutions for the skipping trajectory; i.e., the trajectory of a lifting vehicle entering the planetary atmosphere with a finite initial flight path angle:

(1) The difference between the components of gravity and centrifugal force in the lift direction is negligible when compared to lift force.

(2) Coreolis force is negligible when compared to lift force.

(3) The difference between the components of gravity and centrifugal forces in the drag direction is negligible when compared to drag force.

Using assumptions (1) and (2) in equation (6-41), and assuming powerless flight ($\Gamma_N = 0$), gives:

$$v\gamma' = n_L \qquad (1)$$

Derivation Summary 9.4 (cont.)

Using assumption (3) in equation (6-40) gives:

$$v' = -n_D \tag{2}$$

Dividing equation (2) by equation (1) gives:

$$\frac{1}{v}\frac{dv}{d\gamma} = -D/L \tag{3}$$

Assuming (L/D) = constant and integrating gives:

$$v = v_i\, e^{\frac{-(\gamma-\gamma_i)}{L/D}} \tag{4}$$

Equation (4) gives velocity as a function of flight path angle.

Dividing equation (1) by σ' given by equation (5) of Derivation Summary 9.2 gives:

$$\frac{d\gamma}{d\sigma} = -\frac{\cup C_D (L/D)}{k \sin\gamma} \tag{5}$$

Integrating equation (5) for a constant lift-drag ratio gives:

$$\cos\gamma - \cos\gamma_i = \frac{\cup C_D}{k}(L/D)(\sigma - \sigma_i) \tag{6}$$

For small flight path angles:

$$\cos\gamma \cong 1 - \frac{\gamma^2}{2} \tag{7}$$

With equation (7), equation (6) is written:

$$\sigma = \sigma_i + \frac{k}{2 \cup C_D L/D}(\gamma_i^2 - \gamma^2) \tag{8}$$

Derivation Summary 9.4 (cont.)

Equation (8) relates density ratio (altitude) and flight path angle. The rate of change of range with respect to density ratio is determined by dividing equation (6-44) by density ratio given by equation (5) of Derivation Summary 9.2:

$$\frac{dX_N}{d\sigma} = -\frac{\cot\gamma}{\sigma\, k\, r} \qquad (9)$$

At altitudes where skipping may occur, the distance from the center of the planet to the vehicle differs little from the mean planetary radius, hence $r \cong 1.0$. With this assumption and the small angle assumption on $\cot\gamma$, equation (9) is written:

$$\frac{dX_N}{d\sigma} \cong -\frac{1}{\sigma\, k\gamma} \qquad (10)$$

Equation (8) is used to eliminate γ from equation (10). Integrating the resulting equation gives range as a function of density ratio. This integrated expression is listed as equations (9-96) and (9-97).

Flight path angle as a function of time can be determined by writing equation (1) as:

$$\gamma' = \cup v C_L \sigma \qquad (11)$$

Assuming that the velocity change during a single skip is small and substituting $\sigma(\gamma)$ from equation (8) into equation (11) gives an expression for γ' which may be integrated. The resulting solution

Derivation Summary 9.4 (cont.)

for $\gamma(\tau)$ is listed as equation (9-107).

Equations (4), (8), (9-96), and (9-107) are fundamental equations from which equations (9-94) through (9-115) were determined.

The flight path angle at maximum specific force level is determined by substituting equation (2) into equation (9-121):

$$2\sigma U C_D = - k \sin\gamma \quad \text{at } f_{max} \tag{12}$$

Thus, at maximum specific force level:

$$\gamma \cong \frac{-2 U C_D}{k} \sigma \tag{13}$$

Substituting equation (8) for $\sigma(\gamma)$ into equation (13) and solving explicitly for γ gives equation (9-123). The velocity at maximum specific force level is determined by substituting equation (9-123) into equation (4).

The flight path angle at maximum stagnation temperature level is determined by substituting equation (2) into equation (9-130). The velocity at maximum stagnation temperature level is determined by substituting the resulting solution for γ into equation (4).

Chapter 10

APPROXIMATE ANALYTICAL SOLUTION OF GUIDANCE PARAMETERS AND CONSTRAINTS FOR THE DEGENERATE ORBITAL ENTRY PROFILE

10.1 Introduction

The investigation described in Chapter 9 was devoted largely to derivation of guidance parameters and constraints for the direct entry profile. This atmospheric entry trajectory is characterized by sequential transition from Keplerian flight through the Intermediate Phase into the Gas-Dynamic flight. The Conservation Parameter $\left|\frac{1-\xi}{\xi}\right|$ was convenient for defining the boundaries existing at transition points between the three separate operational regimes encountered during the course of entry.

The degenerate orbital profile is examined in Chapter 10 from an entirely different standpoint. This entry profile has a time history far removed from that of the direct entry profile. A series of braking passes through the outer reaches of the atmosphere are employed in this concept of entry for purposes of reducing the energy level of the vehicle until final direct entry is assured. The Intermediate Phase is entered in a series of near impulses in the vicinity of perigee; during each of these pulses, energy is transferred to the planetary atmosphere until ultimately the energy level is low enough that final transition to flight in the Gas-Dynamic Phase evolves.

The characteristics of powerless flight in the outer reaches of the atmosphere are examined in Chapter 10 for vehicles initially in circular and elliptical reconnaissance orbits. For this analysis, the entry mission was assumed to start at the first perigee. Analytical techniques are presented for predicting the range and time of flight of the craft, the rate of circularization of elliptical orbits, the rate of decay of circular orbits, the number of orbits remaining under specified initial conditions, perigeal and apogeal decay rates, and the effect of the vehicle's aerodynamic and mass characteristics on these quantities.

It is shown in this chapter that a true circular orbit or a linear decaying circular orbit cannot exist, even under idealized conditions of injecting a vehicle exactly at circular orbital velocity in the vicinity of a spherical planet. Because of the influence of the planetary atmosphere on the dynamics of energy transfer, the altitude and flight path angle in the high altitude circular orbit oscillate at orbital frequency with such small damping as to be essentially undamped.

The analysis of the circularization phase of elliptical reconnaissance orbits described in this chapter shows that the drag characteristics of the vehicle are important in specifying the resulting trajectory and that the lift characteristics of the vehicle are relatively unimportant. The altitude at apogee decays in proportion to the sum of two large constants which are almost equal in magnitude* while the altitude at perigee decays in proportion to the difference of these two

- - - - - - - - - - - - - - - -

* The constants are described by modified Bessel Functions of the first kind; i.e., Bessel Functions of the first kind with pure imaginary arguments.

near-equal constants. To a first order, therefore, perigeal altitude remains constant during the circularization process.

Guidance parameters important in the conceptual phases of entry systems are derived in closed form in this chapter. The solutions obtained are compared with more exact machine-computed numerical solutions. As a result of this comparison, accuracy and limitations of the analytical solutions of this thesis are determined.

10.2 The Altitude Differential Equation

The planar equations of motion in the $\bar{1}_r$ and $\bar{1}_\phi$ directions were written as equations (6-47) and (6-48) in Chapter 6 of this thesis. In powerless flight ($\Gamma_N = 0$) and assuming ($1 + L/D \tan\gamma$) = 1.0, these equations reduce to:

$$r'' = \frac{v_{I\phi}^2}{r} - \frac{1}{r^2} - n_D \sin\gamma + n_L \cos\gamma \qquad (10\text{-}1)$$

$$v_{I\phi}' = -\frac{v_{I\phi}}{r} r' - n_D \cos\gamma \qquad (10\text{-}2)$$

$$X_N' = \frac{v_\phi}{r} \qquad (10\text{-}3)$$

Equation (10-1) shows that the acceleration in the $\bar{1}_r$ direction is equal to the centrifugal specific force minus gravitational acceleration plus lift and drag specific force components in this direction. For small flight path angles, the drag specific force in the radial direction may be neglected and $\cos\gamma \cong 1.0$. Substituting for n_D and n_L from equation (6-36) and (6-37) and assuming $v \cong v_{I\phi}$, these equations are written:

$$r'' = \frac{v^2}{r} - \frac{1}{r^2} + (L/D)C \frac{v^2}{2} \frac{\rho}{\rho_i} \qquad (10\text{-}4)$$

$$v' = -\frac{v}{r} r' - C \frac{v^2}{2} \frac{\rho}{\rho_i} \qquad (10\text{-}5)$$

$$X_N' = v/r \qquad (10\text{-}6)$$

In equations (10-4) and (10-5), C is a dimensionless constant for a particular vehicle at a given initial altitude above a particular planet:

$$C \equiv R_{(m)o} \frac{C_D S}{M} \rho_i \qquad (10\text{-}7)$$

ρ_i is the atmospheric density in slugs per cubic foot corresponding to the initial flight altitude.

It is convenient to write equations (10-4) and (10-5) in terms of Δr and Δv, which are defined as changes in radius and velocity from given initial values r_i and v_i:

$$\Delta r = r - r_i \qquad (10\text{-}8)$$

$$\Delta v = v - v_i \qquad (10\text{-}9)$$

Since r_i and v_i are constants in equations (10-8) and (10-9), the rate of change of Δr is equal to the rate of change of r and the rate of change of Δv is equal to the rate of change of v, i.e.:

$$\Delta r' = r' \qquad (10\text{-}10)$$

$$\Delta v' = v' \qquad (10\text{-}11)$$

With equations (10-8) through (10-11), equation (10-4) is written:

$$\Delta r'' = \frac{v_i^2}{r_i} \frac{\left[1 + \frac{2\Delta v}{v_i} + \left(\frac{\Delta v}{v_i}\right)^2\right]}{\left(1 + \frac{\Delta r}{r_i}\right)} - \frac{1}{r_i^2 \left[1 + \frac{2\Delta r}{r_i} + \left(\frac{\Delta r}{r_i}\right)^2\right]} + \frac{L}{D} C \frac{v_i^2}{2} \frac{\rho}{\rho_i} \left[1 + \frac{2\Delta v}{v_i} + \left(\frac{\Delta v}{v_i}\right)^2\right] \qquad (10\text{-}12)$$

In the Keplerian and Intermediate Phases of the trajectory and through much of the Gas-Dynamic Phase of flight, $(\frac{\Delta v}{v_i})^2$ and $(\frac{\Delta r}{r_i})^2$ and all higher order terms can be neglected; therefore equation (10-12) is written:

$$\Delta r'' = \frac{v_i^2}{r_i}\left[1-\left(\frac{v_{ci}}{v_i}\right)^2\right] - \Delta r\left(\frac{v_i}{r_i}\right)^2\left[1-2\left(\frac{v_{ci}}{v_i}\right)^2\right] + \Delta v\left[\frac{2v_i}{r_i} + \frac{L}{D}C v_i \frac{\rho}{\rho_i}\right]$$

$$+ \frac{L}{D}C\frac{v_i^2}{2}\frac{\rho}{\rho_i} \qquad (10\text{-}13)$$

v_{ci} in equation (10-13) represents the dimensionless circular orbital velocity at the initial altitude:

$$v_{ci}^2 = \frac{1}{r_i} \qquad (10\text{-}14)$$

There are three time varying quantities in equation (10-13): Δv, Δr, and ρ. Equation (10-5) may be used to give an expression for Δv:

$$\frac{(rv)'}{(rv)^2} = -\frac{C}{2r}\frac{\rho}{\rho_i} \qquad (10\text{-}15)$$

Integrating equation (10-15) with $\tau_i = 0$ gives:

$$\Delta v = -\Delta r\frac{v_i}{r_i} - C\frac{v_i^2}{2}\int_0^{\tau}\left(1-\frac{\Delta r}{r_i}\right)\frac{\rho}{\rho_i}\,d\tau \qquad (10\text{-}16)$$

The first term on the right hand side of equation (10-16) represents the change in velocity resulting from kinetic-potential energy trade-off; the second term represents velocity loss due to drag.

Substituting equation (10-16) into equation (10-13) gives:

$$\Delta r'' = \frac{v_i^2}{r_i}\left[1-\left(\frac{v_{c_i}}{v_i}\right)^2\right] - \Delta r\left\{\left(\frac{v_i}{r_i}\right)^2\left[3-2\left(\frac{v_{c_i}}{v_i}\right)^2+\frac{L}{D}C r_i\frac{\rho}{\rho_i}\right]\right\}+\frac{L}{D}C\frac{v_i^2}{2}\frac{\rho}{\rho_i}$$
$$-Cv_i^3\left(\frac{1}{r_i}+\frac{C}{2}\frac{L}{D}\frac{\rho}{\rho_i}\right)\int_0^\tau\left(1-\frac{\Delta r}{r_i}\right)\frac{\rho}{\rho_i}\,d\tau \qquad (10\text{-}17)$$

Equation (10-17) is the basic equation which must be solved in order to determine the behavior of Δr with time. It is non-linear because of the dependence of ρ on r. If the exponential model of the planetary atmosphere is assumed, then:

$$\frac{\rho}{\rho_i} = e^{-k\Delta r} \qquad (10\text{-}18)$$

Solutions to the non-linear equation (10-17) with the atmospheric model (10-18) are difficult to obtain by conventional techniques. It is shown subsequently in this chapter that a surprisingly accurate analytical solution may be obtained which is valid over reasonably large time intervals by a sequence of approximations. This method may be described as follows:

(1) Assume a reasonable approximation for $\Delta r(\tau)$ based on the initial conditions established for the trajectory.

(2) With this approximation of $\Delta r(\tau)$ the atmospheric density behavior is specified as a function of time for the particular atmospheric model chosen.

(3) Substitute $\rho(\tau)$ from step (2) into equation (10-17) and solve for $\Delta r\,(\tau)$. This gives a refined approximation for $\Delta r(\tau)$ which should be more accurate than the assumed solution of step (1).

(4) Repeat steps (2) and (3) as necessary. Provided the solution converges, the degree of accuracy at any stage may be estimated by comparing successive approximations.

This method for obtaining analytical solutions is carried out in subsequent sections of this chapter for both circular and elliptical reconnaissance orbits. Accuracy of the analytical solutions obtained by this procedure is confirmed by comparing them with machine-computed numerical solutions for various vehicles and initial conditions.

10.3 Circular Orbital Entry

If the vehicle is in a circular reconnaissance orbit at zero time, then certain simplifications may be made in equation (10-17). Specifically:

$$v_i = v_{ci} \tag{10-19}$$

Equation (10-17) therefore reduces to:

$$\Delta r'' = -\Delta r\left\{\left(\frac{v_i}{r_i}\right)^2\left[1+\frac{L}{D}C r_i\frac{\rho}{\rho_i}\right]\right\} + \frac{L}{D}\frac{v_i^2}{2}C\frac{\rho}{\rho_i} - C v_i^3\left(\frac{1}{r_i}+\frac{C}{2}\frac{L}{D}\frac{\rho}{\rho_i}\right)\int_0^\tau\left(1-\frac{\Delta r}{r_i}\right)\frac{\rho}{\rho_i}\,d\tau \tag{10-20}$$

Since the vehicle is initially in a circular orbit, a reasonable approximation to $\Delta r(\tau)$ required in the first step of the method of solution outlined in section 10.2 is:

$$\Delta r = 0 \tag{10-21}$$

Equation (10-21) is the equation of a circle. If Δr does not change,

then regardless of the atmospheric model*:

$$\rho / \rho_i = 1 \tag{10-22}$$

Substituting equation (10-22) into equation (10-20) gives:

$$\Delta r'' + \Delta r\left[\left(\frac{v_i}{r_i}\right)^2\left(1+\frac{L}{D}Cr_i\right)\right] + Cv_i^3\left(\frac{1}{r_i}+\frac{C}{2}\frac{L}{D}\right)\left(\tau - \int_0^\tau \frac{\Delta r}{r_i} d\tau\right) = \frac{L}{D}\frac{C}{2}v_i^2 \tag{10-23}$$

The following constants are defined:

$$\omega_c^2 \equiv \left(\frac{v_i}{r_i}\right)^2 (1 + (L/D)Cr_i) \tag{10-24}$$

$$A_c \equiv (L/D)\frac{Cv_i^2}{2} \tag{10-25}$$

$$B_c \equiv Cv_i^3\left[1/r_i + (L/D)\frac{C}{2}\right] \tag{10-26}$$

$$C_c \equiv \frac{B_c}{r_i} \tag{10-27}$$

The subscript "c" in definitions (10-24) through (10-27) is used for purposes of identifying the constants as applying to the circular orbital case only. In terms of these constants, equation (10-23) is written:

$$\Delta r'' + \omega_c^2 \Delta r - C_c \int_0^\tau \Delta r d\tau = A_c - B_c\tau \tag{10-28}$$

It is noted that at the initial point ($\tau = 0$):

- - - - - - - - - - - - - - - - -

* Equation (10-22) assumes a homogeneous atmosphere around the planet; i.e., the density at a specific altitude is constant. This, of course, neglects diurnal and latitude density variations.

$$\Delta r''(0) = A_c$$

$$\Delta r'(0) = 0 \qquad (10\text{-}29)$$

$$\Delta r\,(0) = 0$$

Equation (10-28) is solved by means of the Laplace transform:

$$\mathcal{L}\{\Delta r(\tau)\} = R(s) = \int_0^\infty e^{-s\tau}\,\Delta r(\tau)\,d\tau \qquad (10\text{-}30)$$

The transform of the first and second derivatives is given by:

$$\mathcal{L}\{\Delta r'(\tau)\} = s\,R(s) - \Delta r(0) \qquad (10\text{-}31)$$

$$\mathcal{L}\{\Delta r''(\tau)\} = s^2 R(s) - s\Delta r(0) - \Delta r'(0) \qquad (10\text{-}32)$$

Applying the transformation to equation (10-28) gives:

$$R(s) = \frac{A_c - B_c/s}{s^3 + \omega_c^2 s - C_c} \qquad (10\text{-}33)$$

Equation (10-33) may be solved by setting:

$$s^3 + \omega_c^2 s - C_c = (s + b_1)(s + b_2)(s + b_3) \qquad (10\text{-}34)$$

where:

$$b_1 = -2x_1 \qquad (10\text{-}35)$$

$$b_2 = x_1 - iy_1 \qquad (10\text{-}36)$$

$$b_3 = x_1 + iy_1 \qquad (10\text{-}37)$$

The following constants are defined:

$$x_1 \equiv \frac{\omega_c}{\sqrt{3}} \sinh\left[\frac{1}{3}\sinh^{-1}\left(\frac{C_c\, 3\sqrt{3}}{2\,\omega_c^3}\right)\right] \tag{10-38}$$

$$y_1 \equiv \omega_c \cosh\left[\frac{1}{3}\sinh^{-1}\left(\frac{C_c\, 3\sqrt{3}}{2\,\omega_c^3}\right)\right] \tag{10-39}$$

$$i^2 = -1 \tag{10-40}$$

Substituting equations (10-34) through (10-40) into equation (10-33), expanding by partial fractions, and taking the inverse transform of the result gives:

$$\begin{aligned}\Delta r(\tau) = {} & \frac{A_c}{(9x_1^2+y_1^2)}\left[e^{2x_1\tau} - e^{-x_1\tau}\left(\cos y_1\tau + \frac{3x_1}{y_1}\sin y_1\tau\right)\right] \\ & + \frac{B_c}{2x_1(x_1^2+y_1^2)(9x_1^2+y_1^2)}\left\{(9x_1^2+y_1^2) - e^{2x_1\tau}(x_1^2+y_1^2)\right. \\ & \left. -2e^{-x_1\tau}\left[4x_1^2\cos y_1\tau + \frac{x_1}{y_1}(3x_1^2-y_1^2)\sin y_1\tau\right]\right\}\end{aligned} \tag{10-41}$$

Equation (10-41) is the solution of equation (10-17) for circular orbital motion. Considerable simplifications may be made in this equation by examining the magnitudes of the quantities involved for reasonable initial reconnaissance orbital conditions:

$$x_1 \cong \frac{3}{2}\,\frac{B_c}{r_i\omega_c^2} \ll 1.0 \tag{10-42}$$

$$y_1 \cong \omega_c \tag{10-43}$$

$$x_1 \ll y_1 \tag{10-44}$$

$$e^{2x_i\tau} \cong 1 + 2x_1\tau \cong 1 + \frac{3}{r_i}\frac{B_c\tau}{\omega_c^2} \tag{10-45}$$

$$e^{-x_i\tau} \cong 1 - \frac{3}{2}\frac{B_c\tau}{r_i\omega_c^2} \tag{10-46}$$

Substituting approximations (10-42) through (10-46) into equation (10-41), and noting that $3x_1 \ll \omega_c$ and $4x_1 \ll \omega_c$ gives:

$$\Delta r(\tau) = \frac{A_c}{\omega_c^2}\left[(1+2x_1\tau) - (1-x_1\tau)\cos\omega_c\tau\right] - \frac{B_c}{\omega_c^2}\left[\tau - (1-x_1\tau)\frac{\sin\omega_c\tau}{\omega_c}\right] \tag{10-47}$$

Equation (10-41) and its simplified version, equation (10-47), correspond to oscillatory motion of Δr; the frequency of the oscillations is equal to orbital frequency. These oscillations are damped at such a small rate* that, from the engineering standpoint in guidance system design, the damping terms can be ignored. Therefore, equation (10-47) reduces to:

$$\Delta r(\tau) = \frac{A_c}{\omega_c^2}\left(1 - \cos\omega_c\tau\right) - \frac{B_c}{\omega_c^2}\left(\tau - \frac{\sin\omega_c\tau}{\omega_c}\right) \tag{10-48}$$

Equation (10-48) is the fundamental solution for the circular orbital trajectory. It may be observed that equation (10-48) is obtained directly by assuming for the integrand of equation (10-20) that:

- - - - - - - - - - - - - - - -

* x_1 is generally an extremely small number.

$$\left(1 - \frac{\Delta r}{r_i}\right) \cong 1.0 \qquad (10\text{-}49)$$

Therefore, equation (10-48) is an accurate solution to equation (10-23) for changes in altitude which are small in comparison to the initial distance of the vehicle from the center of the planet. This does not necessarily mean, of course, that it is an accurate solution of the true trajectory because of the approximations made in arriving at equation (23). Proof of the accuracy and limitations of equation (10-48) is carried out in Figs. 10.1 through 10.7. Before discussing these results, it is desirable to examine equation (10-48) in greater detail.

It is noted that both A_c and B_c in equation (10-48) contain lift terms. For the zero-lift vehicle, $A_c = 0$ and $B_c = \frac{C\, v_i^3}{r_i}$. The altitude of the zero lift vehicle is characterized by a linear decay on which is superimposed a sinusoidal oscillation at orbital frequency. In the case of a lifting vehicle, $A_c > 0$, the trajectory also has a cosine term. Lift, from equation (10-48), has no effect on Δr at the termination of each complete orbit (i.e., at $\omega_c \tau = n2\pi$). It may be seen from equation (10-47), however, that if $2x_1\tau$ becomes significant in comparison to 1.0, lift causes successive perigees to be higher than in the zero-lift case.

Equation (10-48) is plotted on Fig. 10.1 for one complete orbit of a zero lift vehicle with $C_D S/M = 1$ ft.^{2}-slug^{-1}. Superimposed on this plot is Nielsen's[21] numerical solution for the same vehicle. It may be observed that the solution of this thesis and Nielsen's numerical solution are practically identical throughout the orbit. The total

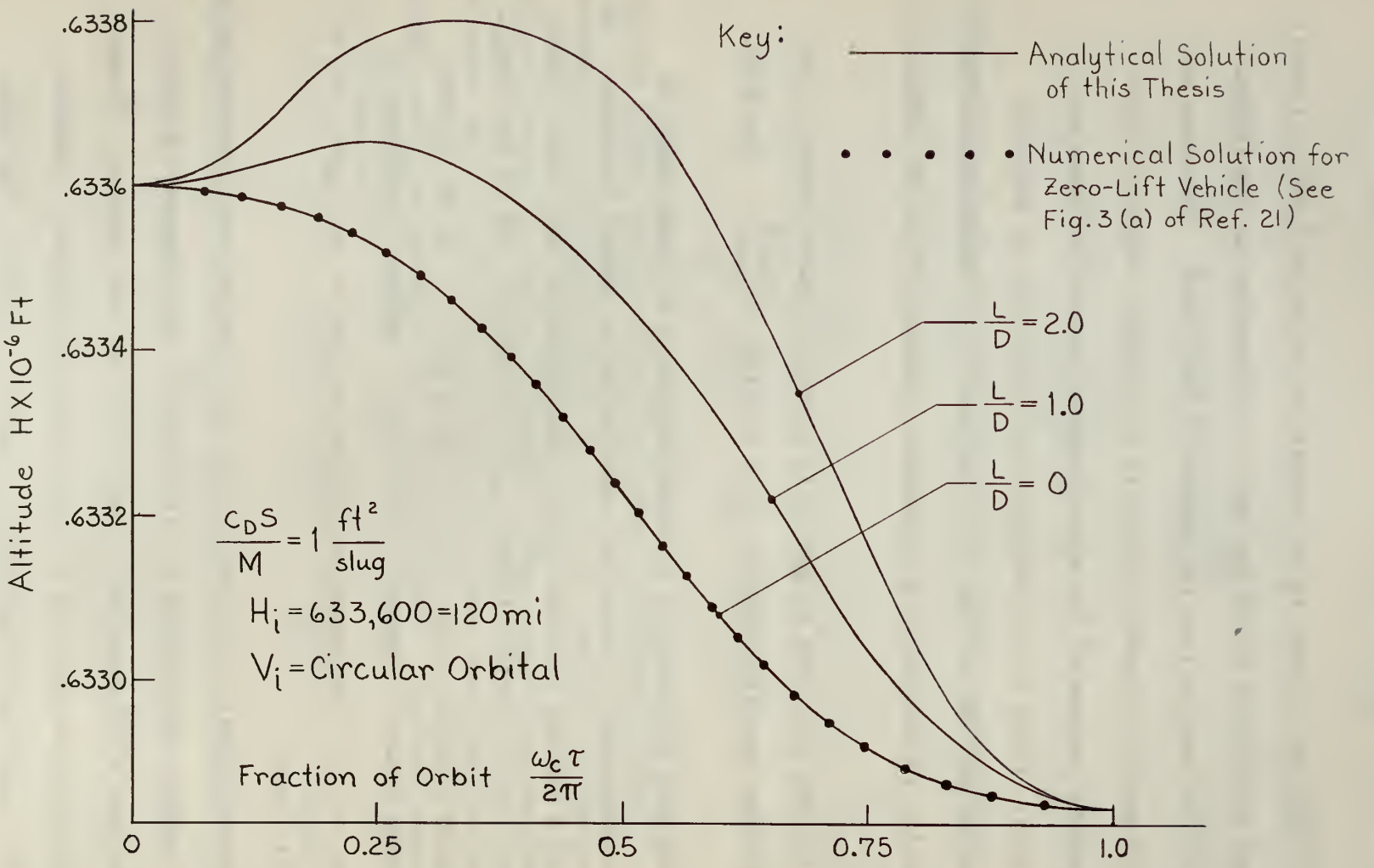

Fig. 10.1: Comparison of Analytical Solution to Machine Computed Numerical Solution for Zero-Lift Vehicle Initially in Circular Orbit at 120 Miles Altitude Above Earth.

altitude loss during the orbit is approximately 760ft. Also shown in Fig. 10.1 are solutions to equation (10-48) for lifting vehicles with L/D = 1.0 and L/D = 2.0 having the same drag parameter ($\frac{C_D S}{M} = 1.0 \frac{ft.^2}{slug}$). It is seen that the L/D = 1.0 vehicle climbs about 50 ft. before descending while the L/D = 2.0 climbs about 200 ft. prior to descending. In any case, Fig. 10.1 and equation (10-48) show that a true circular orbit or a linear decaying circular orbit cannot exist because of the dynamics of energy transfer even if the problem starts under precise circular orbital conditions.

Fig. 10.2 compares the solution given by equation (10-48) with the machine computed numerical solution for the first ten orbits under the identical initial conditions used for Fig. 10.1. It should be noted that the altitude at the completion of each orbit alone is plotted in Fig. 10.2; the sinusoidal oscillations during each orbit have been omitted. It may be observed that the analytical solution and the numerical solution are remarkably close; at the completion of 10 orbits the analytical solution shows an altitude loss of 7,600 ft., while the numerical solution shows about 7,800 ft. altitude loss.

Fig. 10.3 compares the analytical solution of this thesis with numerical solutions for one orbit of a zero-lift vehicle with $\frac{C_D S}{M} = 10 \frac{ft.^2}{slug}$ launched in a circular orbit at 120 miles above the Earth. The trajectory has the same general shape as that of Fig. 10.1 except the total altitude loss is considerably greater here because of the ten to one drag increase of the vehicle. The analytic solution derived a total altitude loss during the first orbit of approximately 7,600 ft. while the numerical solution computed the altitude loss to be

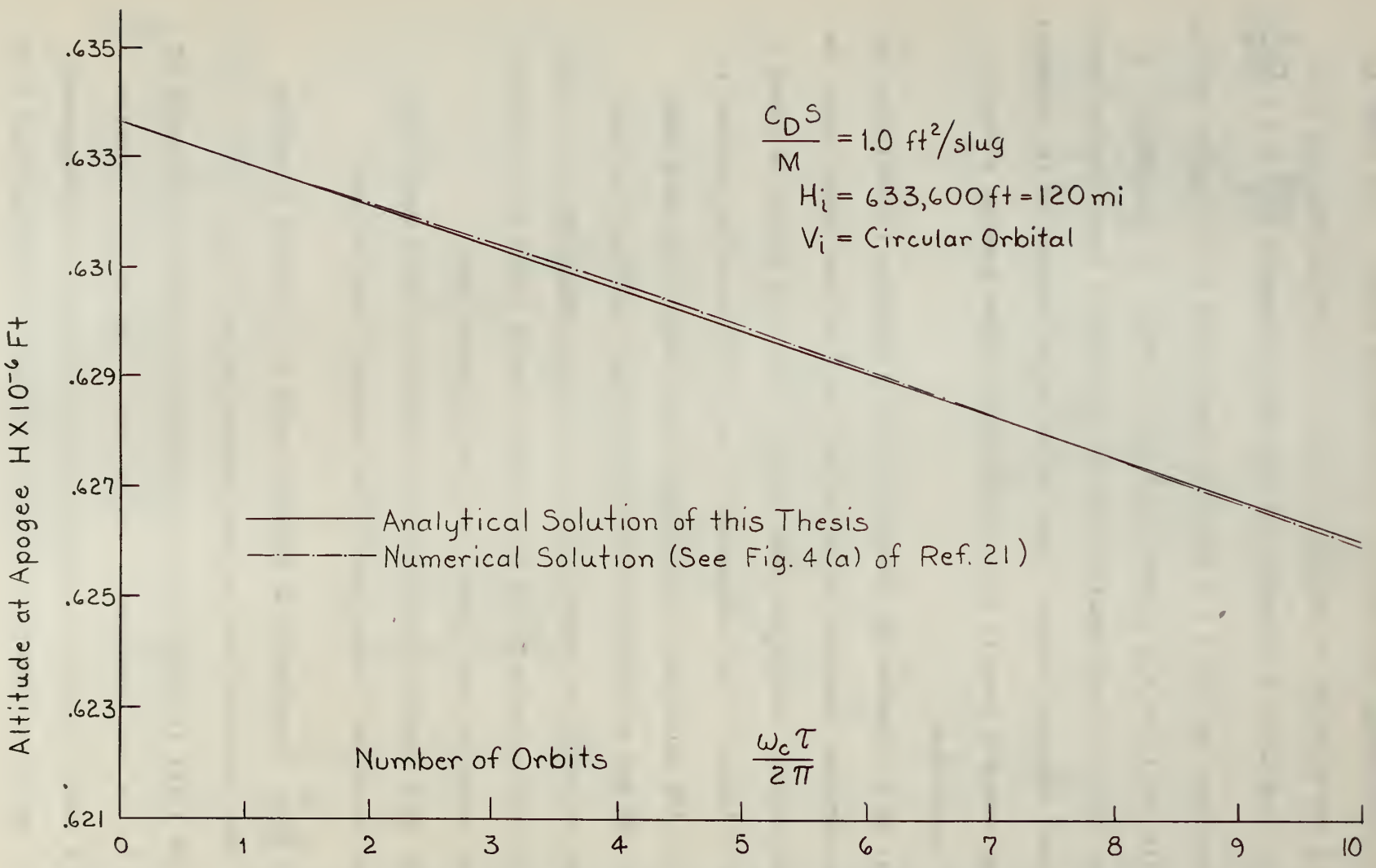

Fig. 10.2: Comparison of Analytical Solution to Machine Computed Numerical Solution for 10 Orbits of Low-Drag Zero-Lift Vehicle Initially in Circular Orbit at 120 Miles Altitude above Earth.

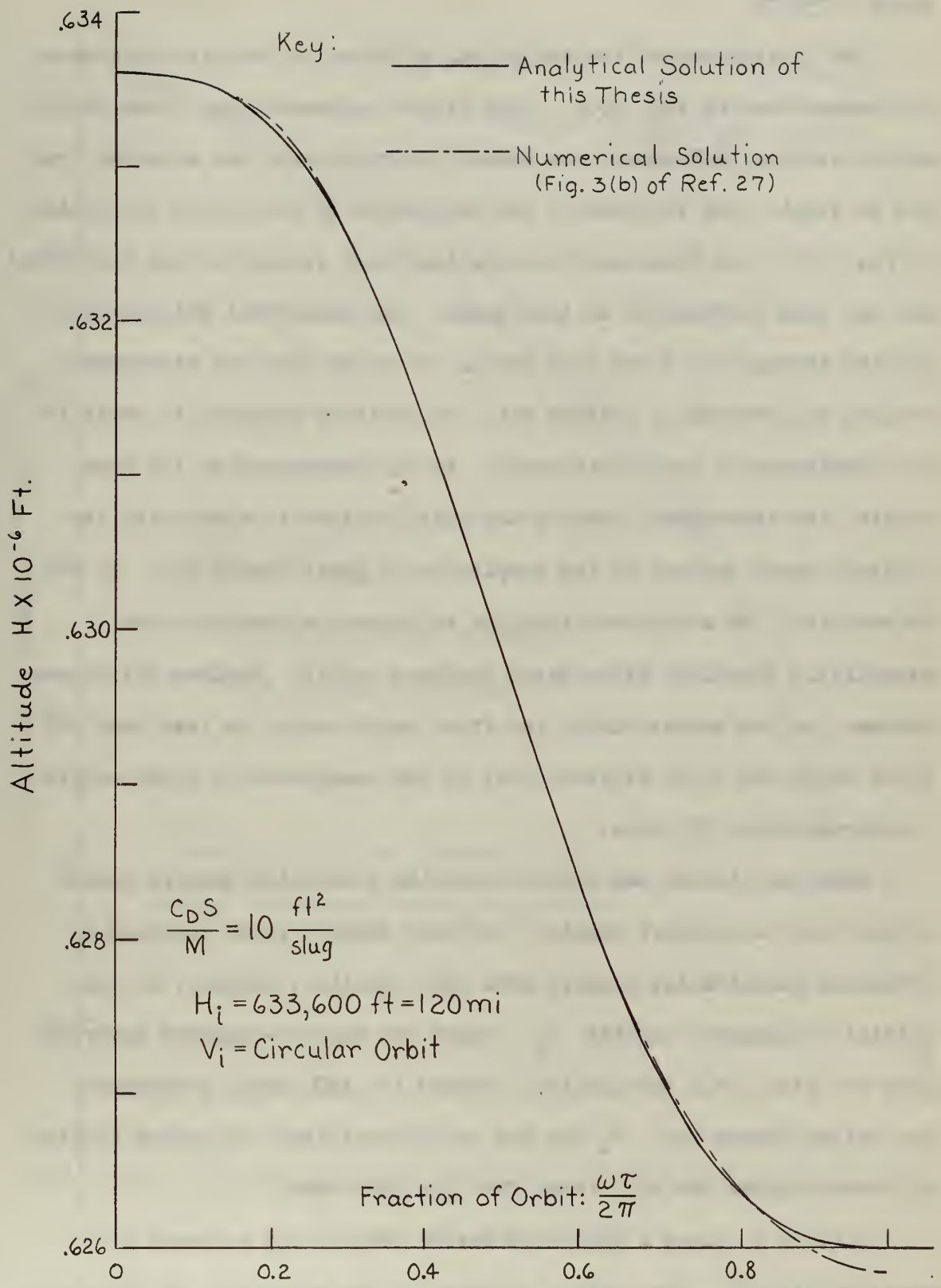

Fig. 10.3 : Comparison of Analytical Solution to Machine Computed Numerical Solution for High-Drag Zero-Lift Vehicle Initially in Circular Orbit at 120 Miles Altitude above the Earth.

about 7,750 ft.

The limitations of the analytical solution in the high drag case is demonstrated by Fig. 10.4. This figure represents the same information as Fig. 10.3 except the number of orbits has been extended from one to eight. The altitude at the completion of each orbit is plotted in Fig. 10.4; the sinusoidal oscillation which is seen during each orbit has not been represented in this graph. The analytical solution was carried through the first four orbits, at which time the atmospheric density was revised to conform with the altitude computed to exist at the completion of the fourth orbit. At the completion of two more orbits, the atmospheric density was again revised to agree with the altitude level derived at the completion of orbit number six. It may be seen that the analytical solution and numerical solution are essentially identical after eight complete orbits. Maximum difference between the two curves during the first eight orbits is less than two miles while the total altitude lost at the completion of eight orbits is approximately 27 miles.

Equation (10-48) was derived with the assumption that an exponential model atmosphere exists. The only density value required in obtaining quantitative answers from this equation, however, is the initial atmospheric density ρ_i. Since the machine-computed numerical data for Figs. 10.1 through 10.7 assumed the ARDC model atmosphere, the values chosen for ρ_i for use in the analytical solutions plotted in these figures was also taken from the ARDC model.

Fig. 10.5 shows a much more severe test of the accuracy of equation (10-48). The initial altitude of the vehicle is 80 miles above the Earth and drag parameter is $\frac{C_D S}{M} = 1.0 \frac{\text{ft.}^2}{\text{slug}}$. Fig. 10.5 shows that

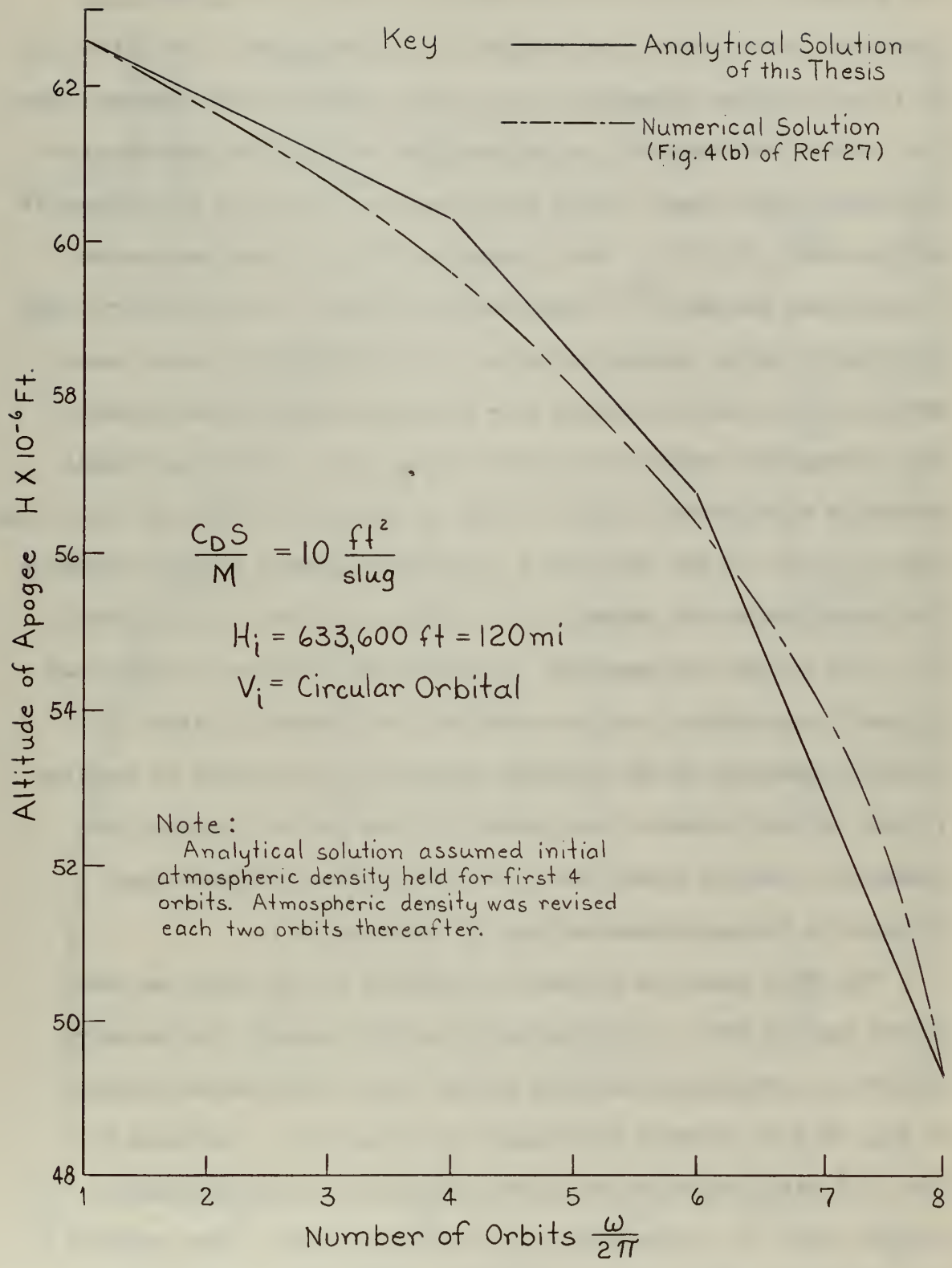

Fig. 10.4 : Comparison of Analytical Solution to Machine Computed Numerical Solutions for 8 Orbits of High-Drag Zero-Lift Vehicle Initially in Circular Orbit at 120 Miles Altitude above Earth.

the analytical solution and the numerical solution are essentially identical for the first 2200 seconds of the trajectory. The total time of flight computed numerically is in the vicinity of 6000 seconds; hence the analytic and numerical solutions agree for more than one-third of the total flight time. During this time, the total loss in altitude is approximately 30,000 ft. Also plotted in Fig. 10.5 are two curves representing Nielsen's[21] approximate solution of the trajectory. His approximate method involves solution of the differential equations of motions over suitably selected time intervals based on predictions of mean atmospheric density during this time interval. His approximate method is represented in Fig. 10.5 in two separate curves, one for a long time interval and the other for a short time interval between piecewise continuous trajectory segments. The solution of this thesis shown in Fig. 10.5 follows the numerical trajectory solution more closely than Nielsen's approximate solution over the time interval plotted. A distinct advantage of the solution advanced in this thesis by equation (10-48) is the piecewise continuous solutions are not required for reasonable accuracy except after much larger time intervals than required by the approximate methods of reference (21).

Fig. 10.6 shows the accuracy of equation (10-48) when the atmospheric density ratio ρ_i is revised after 2000 seconds for the entry trajectory previously considered in Fig. 10.4. The one-step solution of Fig. 10.5 is shown in this figure for comparison. The curve of Fig. 10.6 was plotted for the first 2000 seconds by using equation (10-48) with ρ_i corresponding to 80 miles altitude. This solution was extended to 3000 seconds in order to predict the mean altitude during the interval 2000 sec. $\leq$ t $\leq$ 3000 sec. With the mean altitude

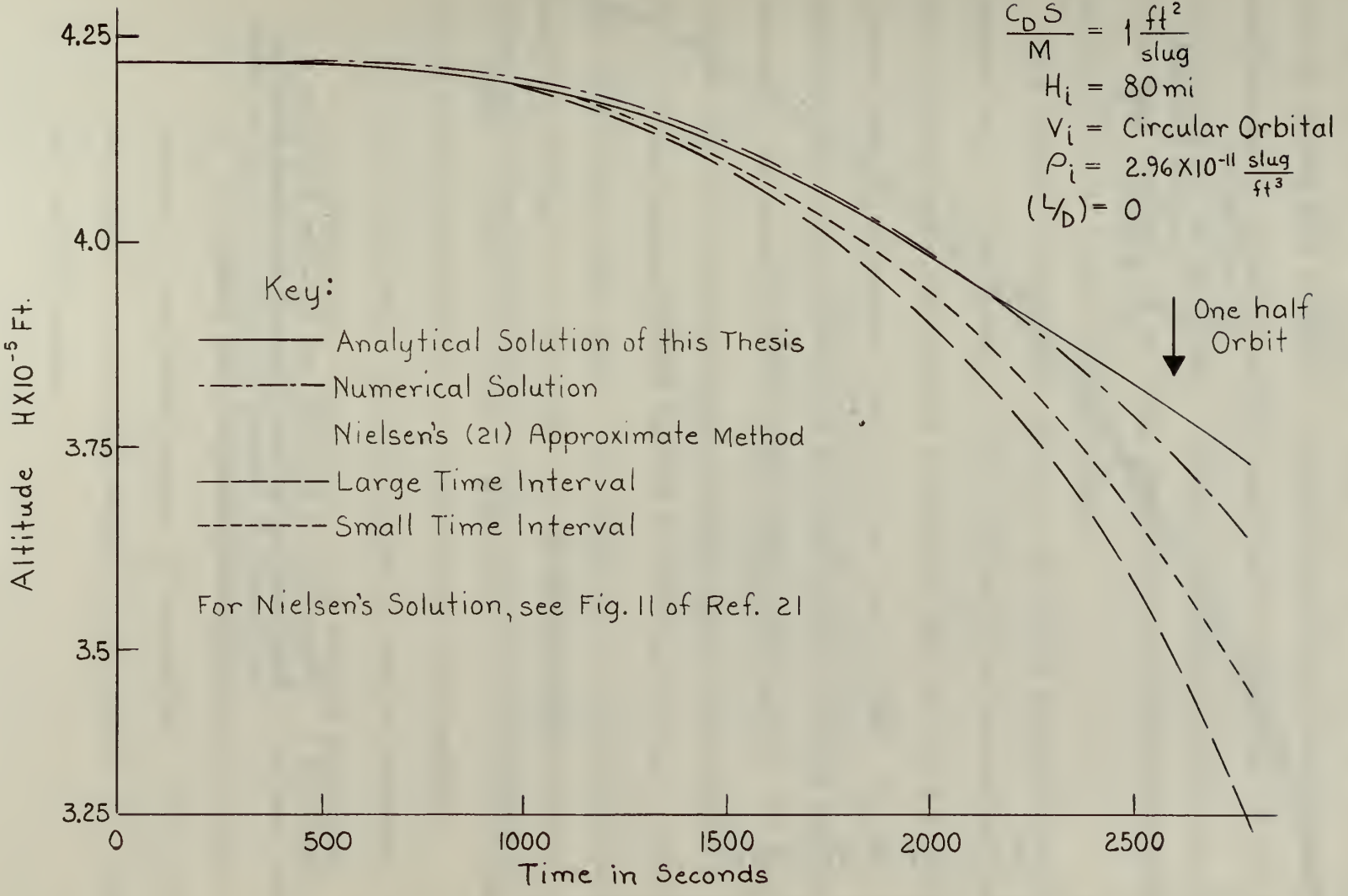

Fig. 10.5: Comparison of Analytical Solution to Machine Computed Numerical Solution for Zero-Lift Vehicle Initially in Circular Orbit at 80 Miles Altitude above Earth.

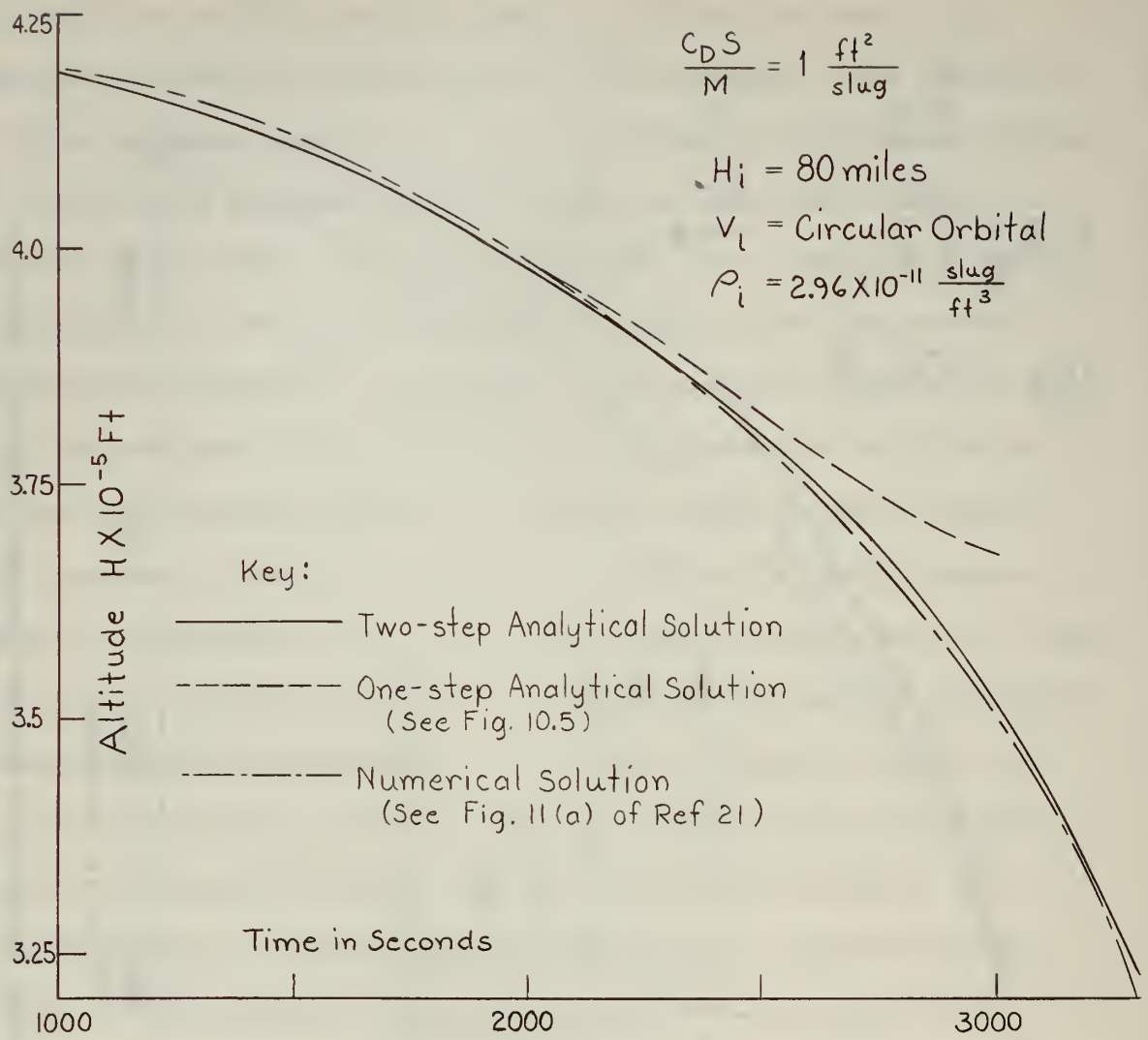

Fig. 10.6 : Comparison of One-Step and Two-Step Analytical Solutions to Machine Computed Numerical Solution for Zero-Lift Vehicle Initially in Circular Orbit at 80 Miles Altitude above Earth.

thus predicted from the initial solution, the second step was plotted over the second time interval. The simple analytical solution and the machine-computed numerical solution are clearly very close for the first 3200 seconds of the trajectory. During this time the vehicle has completed more than half of its total flight time and lost approximately one-fourth of its total initial altitude.

The method of determining values of Δr during the time interval greater than t = 2000 seconds in Fig. 10.6 requires some explanation. After carrying forth the original solution to 3000 sec., the average altitude during the interval 2000-3000 sec. was derived. ρ_i was determined for this altitude from the ARDC model atmosphere and the constant B_c in equation (10-48) was adjusted accordingly*. It should be noted that in the derivation of equation (10-48), the initial altitude rate $\Delta r'$ was assumed zero at zero time. At time 2000 sec., which is zero time for the second step, $\Delta r'$ is <u>not</u> zero; on differentiating equation (10-48), it is seen that $\Delta r'$ is in the neighborhood of -30 ft./sec. at time 2000 seconds. This value of $\Delta r'$ must be carried through the second step of the solution. For example:

(1) At t = 2500 sec., equation (10-48) is used to determine Δr by substituting τ equivalent to 500 seconds into this equation (i.e., $t - t_{i_2} = t_2 = 2500 - 2000 = 500$ sec., where t_{i_2} is initial time of the second segment and t_2 is time measured in the second segment of the solution.) This gives the value of Δr at 2500 seconds if and only if $\Delta r'$ were zero at 2000 seconds.

- - - - - - - - - - - - - - - - -

* $A_c = 0$ in equation (10-48) in this case since lift is zero.

(2) Since $\Delta r'(0) \cong -30$ ft./sec. for the second phase of the solution, approximately 30 X 500 = 15,000 ft. must be added in the negative direction to the Δr computed in (1) above in order to determine the total Δr at t = 2500 sec. This may be summarized as:

$$\Delta r(t) = \underbrace{\Delta r(t_2)}_{\substack{\text{Eq. (10-48) with} \\ \tau \text{ corresponding to} \\ t_2 = t - t_{i_2}}} + \Delta r'(t_{i_2}) \text{ X } t_2 \qquad (10\text{-}50)$$

The time variation of $\Delta r'$ is plotted in Fig. 10.7. This is easily determined by differentiating equation (10-48):

$$\Delta r'(\tau) = \frac{Ac}{\omega_c} \sin\omega_c\tau - \frac{Bc}{\omega_c}(1 - \cos\omega_c\tau) \qquad (10\text{-}51)$$

It should be noted that the value of $\Delta r'$ at 2000 seconds was carried through as an initial value for the second step in the two-step solution. It may be seen from this figure that the difference between the computer solution and the analytical two-step solution of this thesis differ by less than 5 ft./sec. over the first 3000 seconds of flight. During the first 1500 seconds of the trajectory, the numerical and analytical solutions agree exactly.

Velocity may be determined from equations (10-16), (10-48), and (10-49) as follows:

$$\Delta v = -\frac{v_i}{r_i}\frac{A_c}{\omega_c^2}\left[1-\cos\omega_c\tau\right] + \frac{v_i B_c}{r_i \omega_c^2}\left[\tau - \frac{\sin\omega_c\tau}{\omega_c}\right] - \frac{C v_i^2}{2}\int_0^\tau \frac{\rho}{\rho_i}\, d\tau \qquad (10\text{-}52)$$

Using equation (10-18) and equation (10-48) without the oscillatory terms, the last quantity in the above equation may be integrated. The

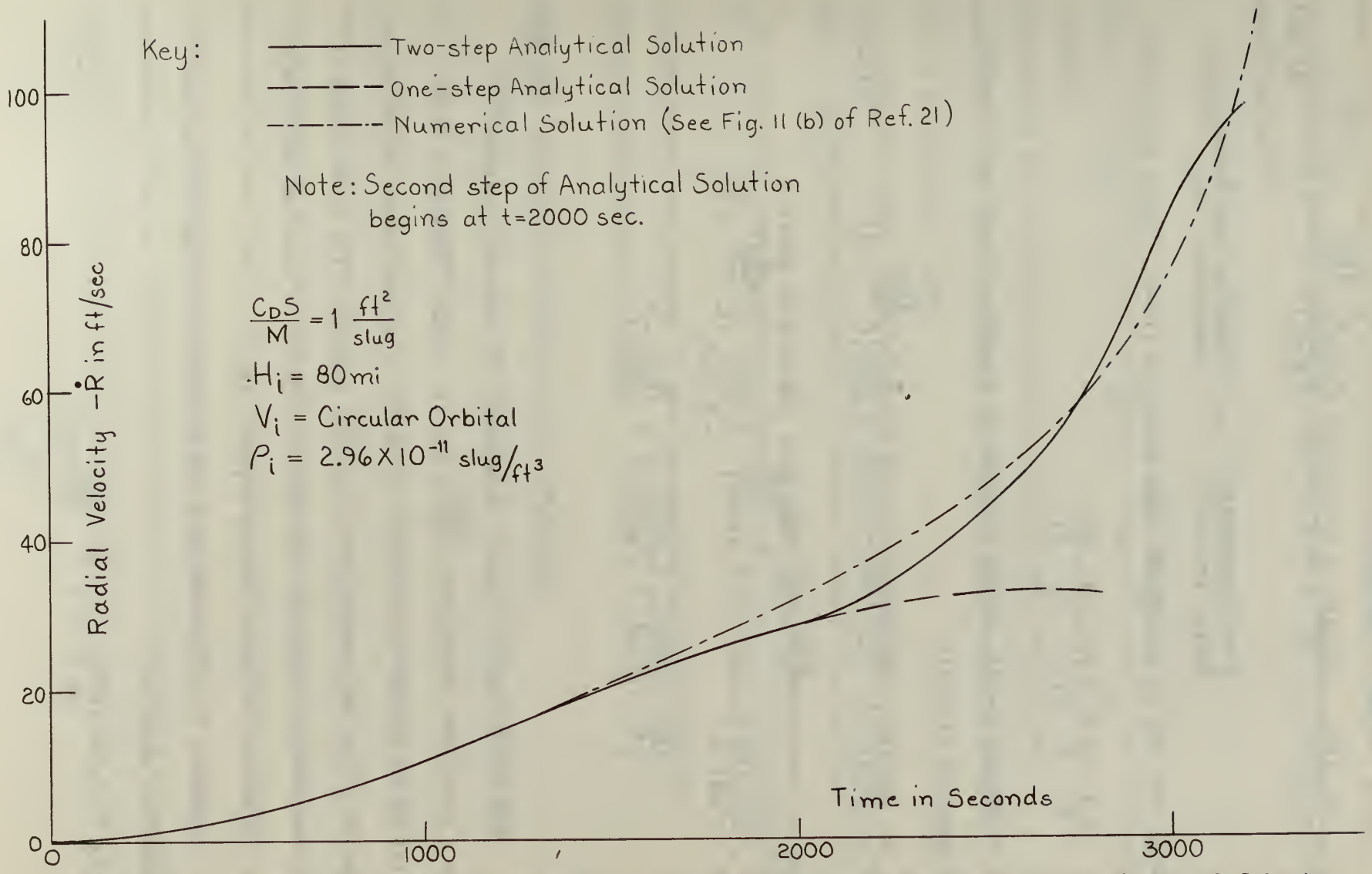

Fig. 10.7: Comparison of Analytical Radial Velocity Solution to Machine Computed Numerical Solution for Zero-Lift Vehicle Initially in Circular Orbit at 80 miles Altitude above Earth.

resulting solution for Δv is:

$$\Delta v = \frac{v_i}{r_i \omega_c^2}\left[B_c\left(\tau - \frac{\sin\omega_c\tau}{\omega_c}\right) - A_c(1-\cos\omega_c\tau)\right] - \frac{C v_i^2 \omega_c^2}{2k B_c}\left[e^{\frac{k B_c \tau}{\omega_c^2}} - 1\right] \qquad (10\text{-}53)$$

Kinetic-potential energy trade-off.

Velocity loss due to atmospheric drag.

Range rate may be determined from equations (10-6), (10-8) and (10-9):

$$X_N' = \frac{v}{r} \cong \frac{v_i}{r_i}\left(1 + \frac{\Delta v}{v_i} - \frac{\Delta r}{r_i}\right) \qquad (10\text{-}54)$$

In equation (10-54), $\Delta r(\tau)$ is given by equation (10-48) and $\Delta v(\tau)$ by equation (10-53):

$$X_N' = \frac{v_i}{r_i} + \frac{2v_i}{r_i^2\omega_c^2}\left[B_c\left(\tau - \frac{\sin\omega_c\tau}{\omega_c}\right) - A_c(1-\cos\omega_c\tau)\right] - \frac{C v_i^2 \omega_c^2}{2k B_c r_i}\left(e^{\frac{k B_c \tau}{\omega_c^2}} - 1\right) \qquad (10\text{-}55)$$

This is integrated to give range as a function of time:

$$X_N = \frac{2v_i}{r_i^2\omega_c^3}\left[\frac{B_c}{\omega_c}(\cos\omega_c\tau - 1) + A_c \sin\omega_c\tau\right] - \frac{C v_i^2 \omega_c^4}{2k^2 B_c^2 r_i}\left(e^{\frac{k B_c \tau}{\omega_c^2}} - 1\right)$$

$$+ \tau\left(\frac{v_i}{r_i} - \frac{2v_i A_c}{r_i^2\omega_c^2} + \frac{C v_i^2 \omega_c^2}{2k B_c r_i}\right) + \frac{B_c v_i}{r_i^2 \omega_c^2}\tau^2 \qquad (10\text{-}56)$$

The total range to impact determined by numerical methods[21] for a zero-lift vehicle with $\frac{C_D S}{M}$ = 1.0 ft.^{2}-slug^{-1} initially at 80 miles in a circular orbit above the Earth is approximately 26,000 miles. Time of flight was determined to be 5991 seconds. The total range of the same vehicle computed from equation (56) in a one-step solution of the trajectory is approximately 28,000 miles.

Equation (7-19) showed that the convective heating rate at the stagnation point is:

$$(\dot{Q}_c)_s = 18{,}000 \frac{(HF)_{EO}}{\sqrt{R}} v^3 e^{\frac{-kh}{2}} \quad \frac{BTU}{ft.^2\text{-sec.}} \qquad (10\text{-}57)$$

where $(HF)_{EO}$ is the heating function ratio tabulated in Table 7.3 for the terrestrial planets and $\mathcal{R}$ is the radius of curvature at the stagnation point.

Equation (10-57) may be written as follows:

$$(\dot{Q}_c)_S \cong \frac{18{,}000(HF)_{EO}}{\sqrt{\mathcal{R}}} v_i^3 \left(1 + \frac{3\Delta v}{v_i}\right) e^{\frac{-kh_i}{2}} e^{\frac{-k\Delta r}{2}} \qquad (10\text{-}58)$$

Substituting for $\Delta v(\tau)$ from equation (10-53) and $\Delta r(\tau)$ from equation (10-48) gives analytical expression for convective heating rate as a function of time.

Stagnation point temperature in degrees Rankine as a function of time is represented analytically in similar fashion from equation (7-21):

$$T_S \cong 1.392 \times 10^4 (HF)_{EO}^{\frac{1}{4}} (VF)^{\frac{1}{4}} v_i^{\frac{3}{4}} \left(1 + \frac{3\Delta v}{v_i}\right)^{\frac{1}{4}} e^{\frac{-kh_i}{8}} e^{\frac{-k\Delta r}{8}} \qquad (10\text{-}59)$$

An approximate time history of vehicle accelerations is given by differentiating equation (10-53).

10.4 The Degenerate Elliptical Entry Trajectory

The initial point for the analysis of the elliptical trajectory is at the first perigee point. An elliptical trajectory results if the velocity of the vehicle at its first perigeal passage is greater than that required to generate a circular orbit; i.e., the first perigee is characterized by an energy excess over circular orbital energy. In the specific case that a vehicle is launched from the planet for the purpose of orbitting the planet a certain desired number of orbits and re-entering, then an elliptical orbit results if the velocity at engine cut-off in the launch phase exceeds circular orbital velocity. In the

case of interplanetary operations in which the high energy level of the vehicle in the interplanetary transfer ellipse is to be reduced by atmospheric braking, the degenerate orbital profile follows the first perigeal passage if the energy transfer is sufficient during this passage for the planet to capture the vehicle.

The basic equation that must be solved in order to determine the time behavior of Δr was given as equation (10-17). It was shown in section 10.3 that the approximation given by equation (10-49) may be made in this equation. Therefore equation (10-17) is written for the exponential atmospheric model as:

$$\Delta r'' + \omega^2 \Delta r = \frac{v_i^2}{r_i}\left[1-\left(\frac{v_{c_i}}{v_i}\right)^2\right] + \frac{L}{D}\frac{C v_i^2}{2} e^{-k\Delta r} - \frac{C v_i^3}{r_i}\left(1+\frac{L}{D}\frac{C}{2} r_i e^{-k\Delta r}\right)\int_0^{\tau} e^{-k\Delta r}\, d\tau \qquad (10\text{-}59)$$

The angular velocity term, ω, in equation (10-59) represents a slowly varying quantity during the circularization phase of the degenerate orbital profile. For the purpose of this analysis, ω is assumed constant; however, by writing it in terms of vehicular velocity and the distance of the vehicle from the planet center, then ω may be changed at each separate initial point chosen for piecewise continuous solution of the trajectory. ω is defined as follows:

$$\omega \equiv \frac{2\pi}{T_N} \qquad (10\text{-}60)$$

where T_N is the dimensionless period of the orbit. Using equations (9-8) and (9-12), the average angular velocity ω is written in terms

of velocity and radius at the initial point as follows:

$$\omega^2 = \left(\frac{2}{r_i} - v_i^2\right)^3 \qquad (10\text{-}61)$$

It is possible to make considerable simplification in equation (10-59) if:

$$\left[1 + (L/D)(C/2)\, r_i e^{-k\Delta r}\right] \cong 1.0 \qquad (10\text{-}62)$$

Equation (10-62) is automatically satisfied for zero-lift vehicles. This approximation is accurate if:

$$N \ll 1.0$$

$$\text{where} \qquad N = (L/D)(C/2)\, r_i e^{-k\Delta r} \qquad (10\text{-}63)$$

The quantity $\frac{N}{\frac{L}{2D}\,\frac{C_D S}{M}}$ is plotted as an approximation parameter in Fig. 10.8 versus the minimum altitude for which the elliptical solution developed herein is accurate in the case of lifting vehicles entering the Earth's atmosphere.

As an example of the use of Fig. 10.8, consider a vehicle with the following characteristics*:

$$L/D = 1.5$$

$$\frac{C_D S}{M} = 0.4625 \text{ ft.}^2/\text{slug}$$

N = 0.1 for this vehicle at an altitude of 54.5 miles above the surface of the Earth. By the time the vehicle has descended to this altitude, orbital flight conditions no longer exist, consequently the limitations on the solution as a result of assuming approximation (10-62) are

- - - - - - - - - - - - - - - - -

* This particular vehicle is used later in this section to compare the analytical solution derived herein to machine-computed numerical solutions.

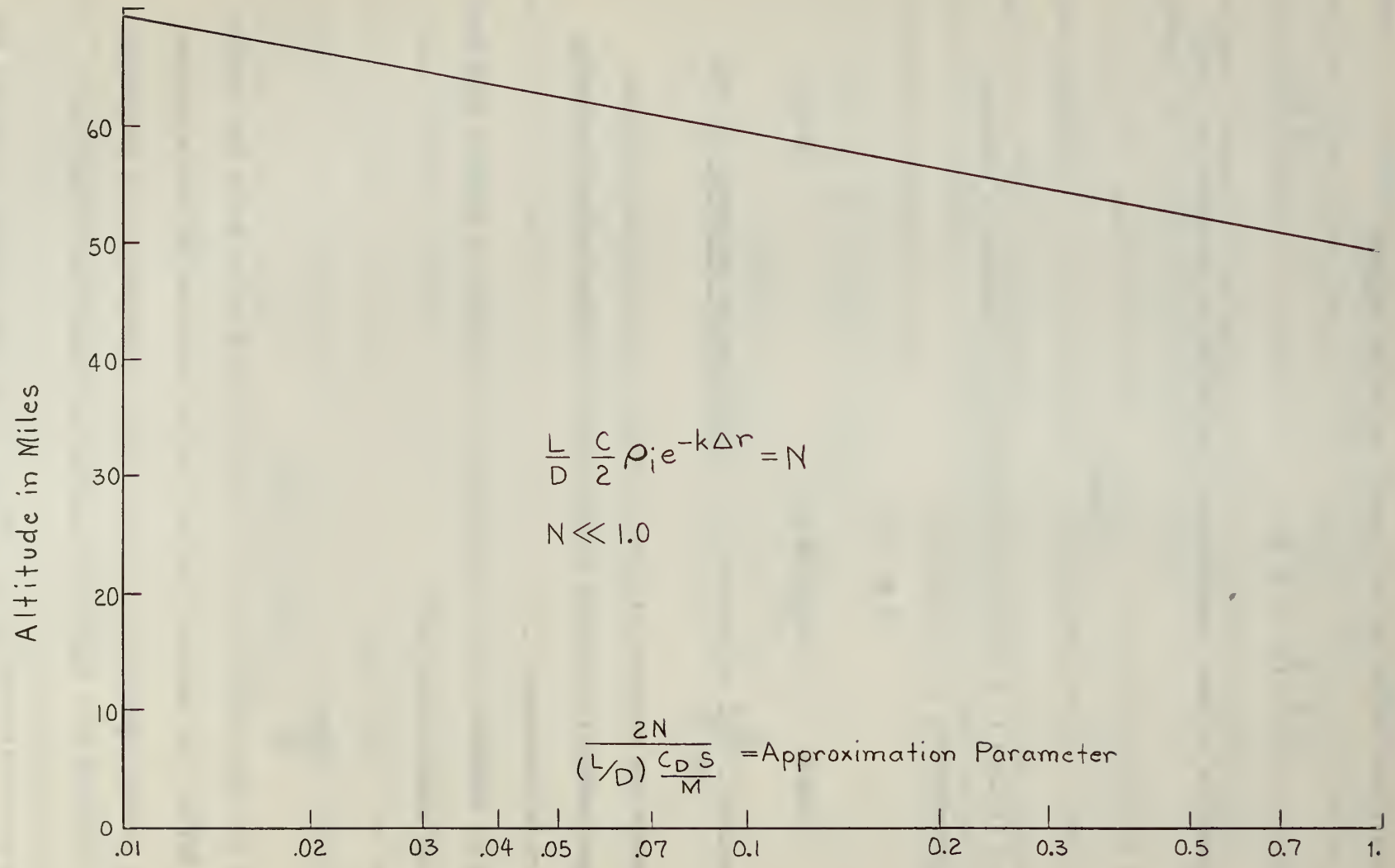

Fig. 10.8: Minimum Earth Altitudes for Which Elliptical Solution is Accurate in the Case of Lifting Vehicles

generally not severe.

With approximation (10-62), equation (10-59) reduces to:

$$\Delta r'' + \omega^2 \Delta r = A_1 e^{-k\Delta r} + A_2 - A_3 \int_0^{\tau} e^{-k\Delta r} d\tau \qquad (10\text{-}64)$$

where the constants are defined as follows:

$$A_1 \equiv (L/D)\, C\frac{v_i^2}{2} \qquad (10\text{-}65)$$

$$A_2 \equiv \frac{v_i^2}{r_i}\left[1 - \left(\frac{v_{ci}}{v_i}\right)^2\right] \qquad (10\text{-}66)$$

$$A_3 \equiv \frac{C v_i^3}{r_i} \qquad (10\text{-}67)$$

In accordance with the method of solution outlined in section 10.2, a first estimate is made for $r(\tau)$ in equation (10-64) by assuming a vacuum trajectory. With $\rho_i = 0$, then $C = 0$ and equation (10-64) reduces to:

$$\Delta r'' + \omega^2 \Delta r = A_2 \qquad (10\text{-}68)$$

The solution to equation (10-68), with $\Delta r(0) = 0$ and $\Delta r'(0) = 0$ is:

$$\Delta r = \frac{A_2}{\omega^2}(1 - \cos \omega\tau) \qquad (10\text{-}69)$$

At apogee of the vacuum trajectory:

$$\Delta r_\alpha = 2\,(a_N - r_i) \qquad (10\text{-}70)$$

where a_N is dimensionless semi-major axis of the ellipse. Comparing equations (10-70) and (10-69) at apogee ($\omega\tau = \pi$) shows that:

$$A_2 = \omega^2 (a_N - r_i) \qquad (10\text{-}71)$$

Therefore, by substituting for a_N from equation (9-8) A_2 may be written in terms of initial velocity, radius, and angular velocity as follows:

$$A_2 = \omega^2 r_i \left[\frac{v_i^2 r_i - 1}{2 - v_i^2 r_i} \right] \tag{10-72}$$

With A_2 defined by equation (10-72) and the first estimate of $\Delta r(\tau)$ given by equation (10-69), equation (10-64) is written:

$$\Delta r'' + \omega^2 \Delta r = A_2 + A_1 e^{-A_4} e^{+A_4 \cos\omega\tau} - A_3 e^{-A_4} \int_0^\tau (e^{A_4 \cos\omega\tau}) d\tau \tag{10-73}$$

where A_4 is defined as follows:

$$A_4 \equiv \frac{kA_2}{\omega^2} = k r_i \left(\frac{v_i^2 r_i - 1}{2 - v_i^2 r_i} \right) \tag{10-74}$$

Equation (10-73) is the fundamental differential equation of the degenerate elliptical entry trajectory.

Taking the Laplace transform of equation (10-73) gives*:

$$R_{(s)} = \frac{1}{s(s^2 + \omega^2)} \left[A_2 + e^{-A_4} (sA_1 - A_3) F_{(s)} \right] \tag{10-75}$$

where R(s) is given by equation (10-30) and F(s) is the Laplace transform of $e^{A_4 \cos \omega\tau}$. Before the inverse transform of this equation can be taken, F(s) must be determined. A search of the mathematical literature failed to disclose a representation of $e^{A_4 \cos \omega\tau}$ suitable for this purpose. Derivation Summary 10.1 analyzes this function in terms of modified Bessel Functions of the first kind. This investigation led to the following representation:

- - - - - - - - - - - - - - - - -

* Note that $\Delta r(0) = 0$ and $\Delta r'(0) = 0$.

$$e^{A_4 \cos\omega\tau} = I_o(A_4) + 2\sum_{n=1}^{\infty} I_n(A_4)\cos n\omega\tau \qquad (10\text{-}76)$$

where I_n is the nth Bessel Function of the first kind with pure imaginary argument.

Fig. 10.9 is a graph of I_n for small values of A_4 taken from reference (80). Engineering analysis of most entry trajectories leads to fairly large values of A_4; for example, A_4 for the vehicle plotted in Fig. 10.10 is in the neighborhood of 58 for the first segment and 19 for the second segment. The following asymptotic series[79] is convenient for large values of A_4:

$$I_n(A_4) \cong \frac{e^{A_4}}{\sqrt{2\pi A_4}}\left[1 - \frac{(4n^2-1^2)}{1!\,8A_4} + \frac{(4n^2-1^2)(4n^2-3^2)}{2!\,(8A_4)^2} - \cdots\right] \qquad (10\text{-}77)$$

The magnitude of I_n for small n is generally extremely large (e.g., of the order of 10^{15} or greater) due to the e^{+A_4} term in equation (10-77).

The Laplace transform of equation (10-76) is:

$$F(s) = \frac{I_o}{s} + 2s\sum_{n=1}^{\infty} \frac{I_n}{s^2 + (n\omega)^2} \qquad (10\text{-}78)$$

Substituting equation (10-77) into equation (10-75), expanding by partial fractions, and taking the inverse transform of the result gives:

$$\Delta r(\tau) = \left(\frac{A_2}{\omega^2} + \frac{A_1 I_o e^{-A_4}}{\omega^2}\right)\left(1 - \cos\omega\tau\right)$$

$$+ \frac{e^{-A_4}}{\omega^2}\left\{-A_3 I_0\left(\tau - \frac{\sin\omega\tau}{\omega}\right) + A_1 I_1 \omega\tau\sin\omega\tau - A_3 I_1\left(\frac{\sin\omega\tau}{\omega} - \tau\cos\omega\tau\right)\right.$$

$$\left. + \sum_{n=2}^{\infty}\left[\frac{2I_n}{(n^2-1)}\left(A_1\left[\cos\omega\tau - \cos n\omega\tau\right] - \frac{A_3}{\omega}\left[\sin\omega\tau - \frac{\sin n\omega\tau}{n}\right]\right)\right]\right\} \qquad (10\text{-}79)$$

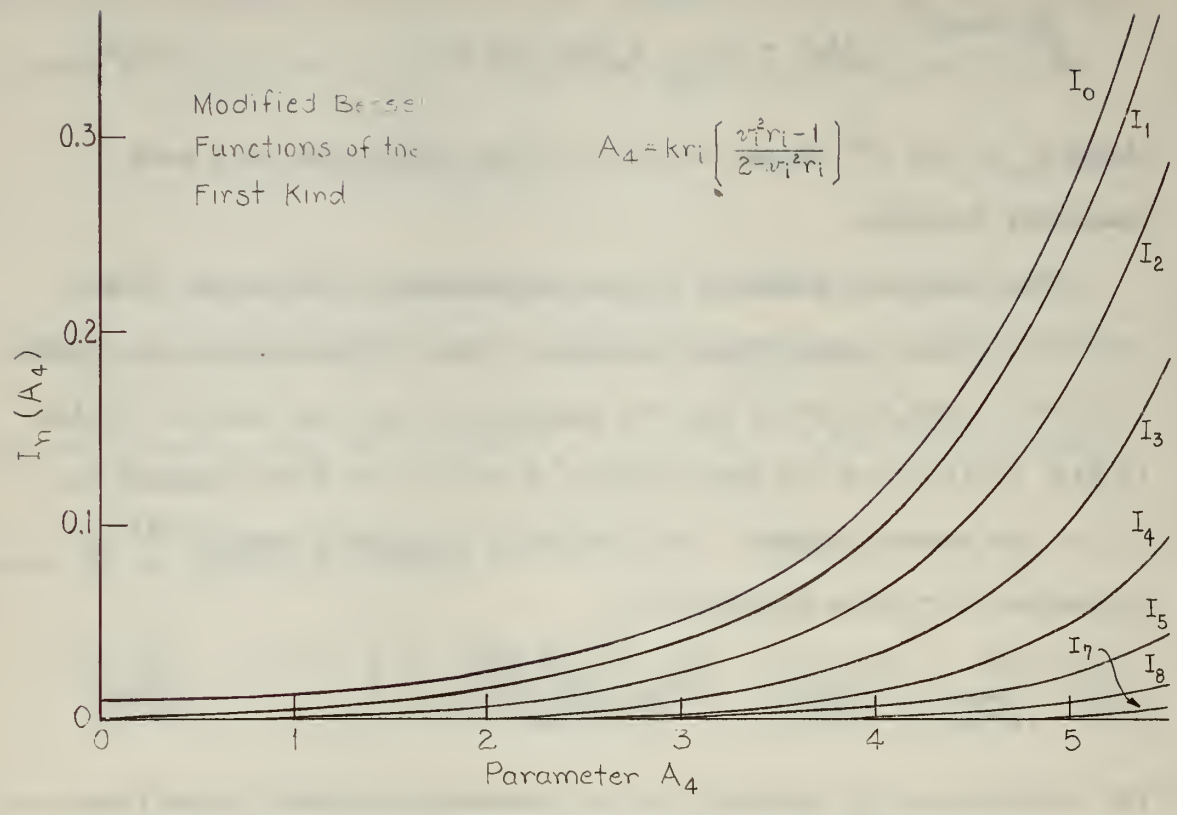

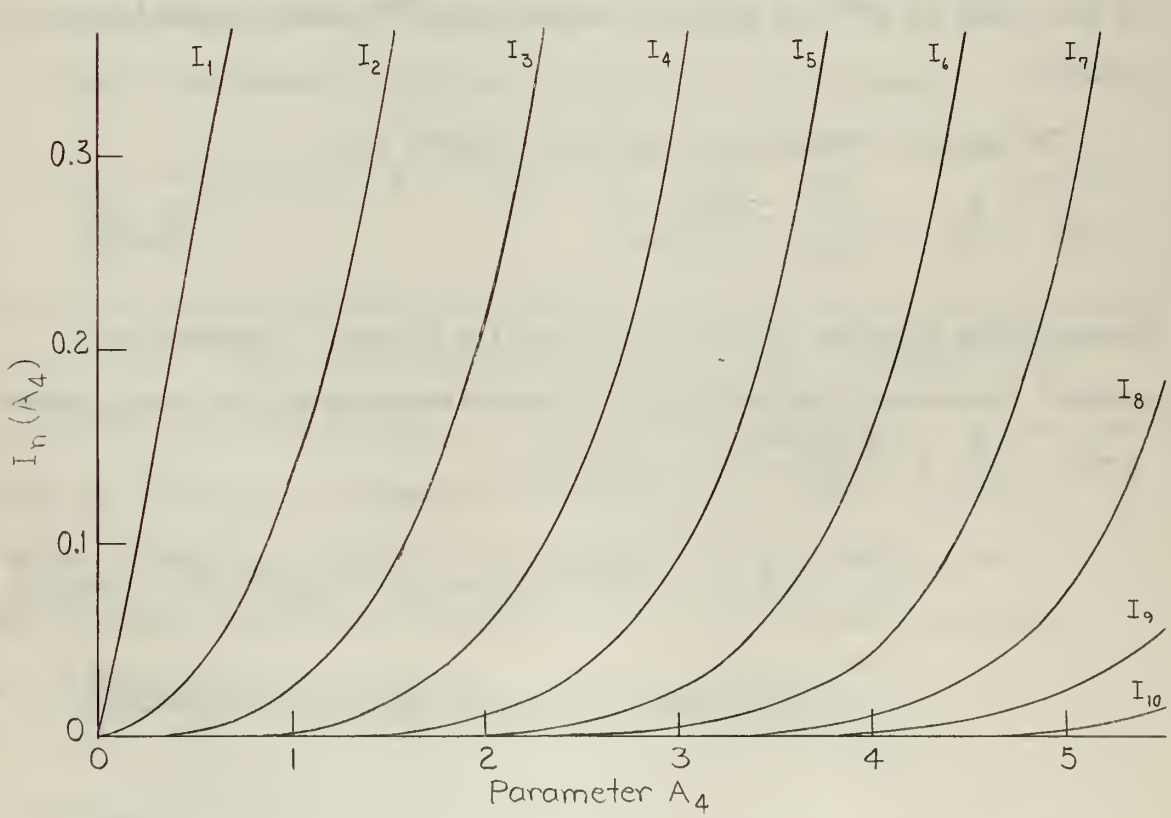

Fig. 10.9 : Values of Coefficients in Elliptical Trajectory Solution for Small A_4

Equation (10-79) is the solution for altitude as a function of time for the degenerate orbital profile. Following is a summary of constants in this equation:

I_n : Fig. 10.9 for small A_4; equation (10-77) for large A_4.

ω : Equation (10-61)

A_1 : Equation (10-65)

A_2 : Equation (10-72)

A_3 : Equation (10-67)

A_4 : Equation (10-74)

The term in curly brackets appears at first glance to be formidable for engineering computations. Fig. 10.9 shows, however, that this solution converges rapidly due to the fact that terms involving $(\frac{2 I_n}{n^2 - 1})$ become relatively unimportant for n greater than 2 or 3. For all reasonable initial problem conditions the asymptotic equation (10-77) is an accurate and easy method for computing I_n. It should be noted that the exponential term in equation (10-77) cancels the exponential term in equation (10-79).

At <u>perigee</u>:

$$\sin n\omega\tau = 0$$
$$\cos n\omega\tau = 1 \qquad (10\text{-}80)$$

Equation (10-79) reduces to the following for the time history of perigeal altitude:

$$\Delta r_\pi(\tau) = -\frac{A_3}{\omega^2} e^{-A_4}(I_0 - I_1)\tau \qquad (10\text{-}81)$$

At <u>apogee</u>:

$$\sin n\omega\tau = 0$$
$$\cos n\omega\tau = -1 \qquad (10\text{-}82)$$

Equation (10-79) reduces to the following for apogeal altitude as a function of time:

$$\Delta r_\alpha(\tau) = \frac{2}{\omega^2}\left(A_2 + A_1 I_0 e^{-A_4}\right) - \frac{A_3}{\omega^2}\tau\left(I_0 + I_1\right)e^{-A_4} \qquad (10\text{-}83)$$

Equations (10-81) and (10-83) were plotted in Fig. 10.10 for a lifting vehicle launched in an elliptical orbit with initial velocity 3% greater than circular orbital velocity. Initial altitude was 350,000 feet above the Earth and the vehicle parameters were arbitrarily selected as follows:

$$L/D = 1.5$$

$$\frac{C_D S}{M} = 0.4625 \text{ ft.}^2/\text{slug.}$$

The analytical solution is represented in two segments with a revised atmospheric density ρ_i chosen for the second segment; the first segment covered $10\frac{1}{2}$ orbits and the second segment used the atmospheric density corresponding to the altitude computed for the 11th perigeal passage. Total flight time during circularization was computed to be 20.3 hours. The perigeal decay rate was computed from equation (10-81) to be approximately 0.14 ft./sec. during the first segment and 0.61 ft./sec. in the second segment. Perigee decayed 8030 ft. over the first 960 minutes and an additional 8780 ft. between 960 and 1200 minutes. Total loss in perigeal altitude during the 20 hour flight was about 3 miles. Apogeal decay rate averaged 31 to 32 ft./sec. during the first segment and increased to 46 ft./sec. during the second segment. Apogee decayed more than 360 miles during the first segment and 170 miles during the second segment.

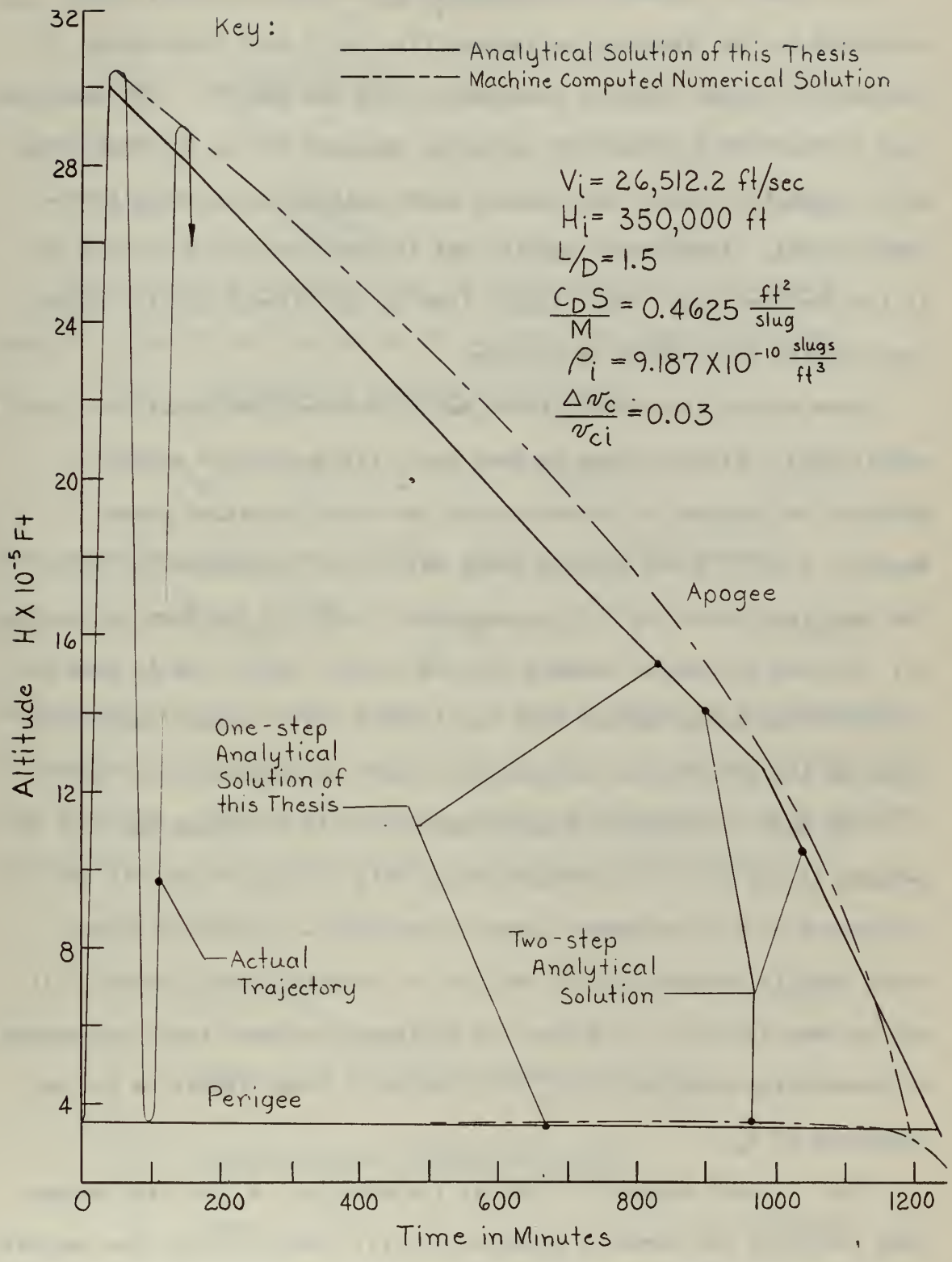

Fig. 10.10 : Comparison of Perigeal and Apogeal Altitudes of Analytical Solution with Those Determined Numerically with IBM-704. Lifting Vehicle Launched with Initial Velocity 3% Greater than Circular Orbital Velocity

In order to estimate the accuracy of the analytical solution discussed in the preceding paragraph, Fig. 10.10 also shows decay of perigee and apogee computed numerically with the IBM-704. The numerical runs represented a trajectory initially inclined 30° to the equatorial plane about the oblate, pear-shaped Earth with an exponential atmospheric model. Atmospheric density was assumed zero above 600,000 ft. in the computer run. Total flight time in the circularization phase was computed to be about 19.9 hours.

Some rather interesting facts may be deduced from equations (10-81) and (10-83). First, it may be seen that lift has little effect on perigeal and apogeal altitudes during the circularization phase. Equation (10-81) shows perigee decay rate to be independent of lift. The only term involving lift in equation (10-83) is the term containing A_1. For the particular example plotted in Fig. 10.10, the A_1 term was orders of magnitude smaller than the A_2 term. The apogeal decay rate given by the second term in equation (10-83) is independent of lift.

The major difference between the decay rate at apogee and that at perigee is the fact that perigeal decay rate is proportional to the difference of two near-equal large numbers $(I_o - I_1)$, while apogeal decay rate is proportional to the sum of these two large numbers. It may be seen from Fig. 10.9 that the <u>difference</u> between these two numbers is essentially constant for $A_4 > 5$; the sum is very sensitive to the magnitude of A_4.

For most degenerate orbital trajectories, A_4 is large enough that the first two terms in equation (10-77) are sufficient for accurate estimation of perigeal and apogeal decay rates. Differentiating equations (10-81) and (10-83), and substituting the first two terms

from equation (10-77) for I_o and I_1 gives:

$$\Delta r_\pi' = - \frac{A_3}{4\sqrt{2\pi}\,\omega^2 A_4^{3/2}} \tag{10-84}$$

$$\Delta r_\alpha' \cong - \frac{2A_3}{\omega^2\sqrt{2\pi A_4}} \tag{10-85}$$

Other guidance parameters may be computed from the foregoing results. Some of the quantities of interest are summarized below:

(1) Dimensionless semi-major axis a_N:

$$a_N = \frac{r_\pi + r_\alpha}{2} = r_i + \frac{\Delta r_\pi + \Delta r_\alpha}{2} \tag{10-86}$$

Using equation (10-81) and (10-83), equation (10-86) becomes:

$$a_N(\Upsilon) = r_i + \frac{(A_2 + A_1 I_o e^{-A_4})}{\omega^2} - \frac{A_3}{\omega^2} e^{-A_4} I_o \Upsilon \tag{10-87}$$

The semi-major axis changes almost as a step function in the vicinity of perigee; hence equation (10-87) should not be viewed as a continuous time solution. Recomputation of a_N should be performed at each perigeal passage with a near constant value during the following orbit.

(2) Period of orbit:

$$T_N = 2\pi a_N^{3/2} \tag{10-88}$$

where $a_N(\Upsilon)$ is given by equation (10-87).

(3) Average angular velocity in orbit:

$$\omega(\Upsilon) = a_N^{-3/2} \tag{10-89}$$

where $a_N(\Upsilon)$ is given by equation (10-87).

(4) Instantaneous velocity:

In a Keplerian elliptical orbit, velocity is given by:

$$v^2 = \frac{2}{r} - \frac{1}{a_N} \qquad (10\text{-}90)$$

Velocity may be approximated during the circularization phase from equation (10-90) as follows:

$$v^2 = \frac{2}{r_i}\left(1 - \frac{\Delta r}{r_i}\right) - \frac{1}{a_N} \qquad (10\text{-}91)$$

$\Delta r(\tau)$ is given by equation (10-79) and $a_N(\tau)$ by equation (10-87). Velocity at perigee is derived from equation (10-91) as follows:

$$v_\pi^2 = \frac{1}{r_i}\left[1 + \frac{1}{2r_i}\left(\Delta r_\alpha - 3\Delta r_\pi\right)\right] \qquad (10\text{-}92)$$

where $\Delta r_\pi(\tau)$ and $\Delta r_\alpha(\tau)$ are given by equations (10-81) and (10-83).

Velocity at apogee is as follows:

$$v_\alpha^2 = \frac{1}{r_i}\left[1 + \frac{1}{2r_i}\left(\Delta r_\pi - 3\Delta r_\alpha\right)\right] \qquad (10\text{-}93)$$

(5) Total energy:

Total energy changes approximately as a step function in the vicinity of each perigeal passage. The time behavior of energy level is given by:

$$E_{(tot)} = -\frac{1}{2a_N} \qquad (10\text{-}94)$$

where $a_N(\tau)$ is given by equation (10-87).

(6) Eccentricity

Eccentricity, like the semi-major axis and energy level,

decreases in a series of near steps in the vicinity of perigee. The value between perigeal steps is reasonably constant. With this step behavior recognized, the time behavior of eccentricity is given by equation (10-94) (which was derived from equations (9-16), (9-18), (10-92) and (10-93)):

$$\varepsilon(\tau) = \frac{1}{2r_i}\left(\Delta r_\alpha - \Delta r_\pi\right) \qquad (10\text{-}95)$$

(7) Heating Rates, Stagnation Temperatures, and Accelerations:

During the circularization phase of the degenerate orbital profile, heating and accelerations are not of major concern in guidance analysis since maximum levels are generally encountered after the trajectory has degenerated to a circle. The methods of Chapter 9 and Section 10.3 may be used to predict these quantities during the Gas-Dynamic Phase of flight.

10.5 Summary

Chapter 10 examines the trajectory of a vehicle in the degenerate orbital profile. Initial conditions assumed in this analysis were that a lifting or non-lifting vehicle was injected in horizontal flight at some initial altitude above an arbitrary planet with $\Delta r(0)$ and $\Delta r'(0)$ equal to zero. The results were described in dimensionless form suitable for analysis of entry into the atmosphere of any planet. The exponential atmospheric density model was assumed.

Two separate trajectory phases were examined:

(1) The circularization phase for the degenerate orbit;

(2) The entry phase which follows the circularization process.

In the special case wherethe vehicle is initially at circular orbital

velocity, the first of these two phases obviously does not exist.

The solution for altitude during the circularization process was derived as equation (10-79). This solution was written in terms of a number of constants which depend on the initial conditions of the problem and on the characteristics of the vehicle. Some of the important constants in this equation were written in terms of Bessel Functions. Since these functions are tabulated, numerical answers to the resulting equations are easily obtained. The time variation of perigeal and apogeal altitudes was given in equations (10-81) and (10-83) and the rate of decay for most practical problems is described by equations (10-84) and (10-85). Analytical representation of other quantities which are important in the conceptual and preliminary design stages of guidance systems are summarized in equations (10-86) through (10-94).

It was shown in the analysis of the circularization phase that the drag characteristics of the vehicle are important in specifying the resulting trajectory and that the lift characteristics of the vehicle are relatively unimportant. It was shown that, within the approximations made in this analysis, lift does not enter in the specification of the decay rates of apogee and perigee. Perigeal altitude, to a first order, remains essentially constant. The major difference between the decay rates of apogee and perigee is that perigeal decay rate is proportional to the difference of two near-equal large numbers* while apogeal decay rate is proportional to the sum of these same numbers.

The solution for altitude in circular orbital entry was given by

- - - - - - - - - - - - - - - - -

* Perigeal decay is proportional to $(I_0 - I_1)$, where I_0 and I_1 are the first two Bessel Functions with an argument that is generally greater than 10.

equation (10-41). This solution was written in simplified forms suited to almost all practical problems as equations (10-47) and (10-48). It was shown in this chapter that a true circular orbit or a linear decaying circular orbit cannot exist even under idealized conditions of injecting a vehicle exactly at circular orbital velocity near a spherical planet. The influence of the atmosphere on the dynamics of energy transfer result in undamped oscillatory motion in altitude and flight path angle.

The analytical solutions derived in this chapter were compared to machine-computed numerical solutions under a variety of initial conditions. It was shown that the analytical solutions presented an accurate picture of the resulting motion except after long periods of time. The analytical solutions depart from more accurate computer solutions only after there is a significant increase in atmospheric density from the assumed initial value as a result of altitude loss during entry. This limitation on the solutions may be greatly alleviated by starting the solution over again under a new set of initial conditions. Examples of this method of solution were given.

Derivation Summary 10.1

Expansion of $e^{a\cos x}$ in Terms of Modified Bessel Functions of the First Kind.

In order to solve equation (10-75), the Laplace transform of $e^{a\cos x}$ is required. An expansion of this function in terms of Bessel Functions of the first kind with pure imaginary arguments was carried out in this thesis. This particular expansion is not given in the mathematical literature that the author has searched.

The following is written:

$$e^{a\cos x} = 1 + a\cos x + \frac{a^2\cos^2 x}{2!} + \frac{a^3\cos^3 x}{3!} + \cdots \tag{1}$$

The following equation defines the nth power of cos x:

$$\cos^n x = \frac{1}{2^{(n-1)}}\left\{\cos nx + n\cos\left[(n-2)x\right] + \frac{n(n-1)}{2!}\cos\left[(n-4)x\right] + \frac{n(n-1)(n-2)}{3!}\cos\left[(n-6)x\right] + \cdots\right\} \tag{2}$$

Substituting equation (2) into equation (1) gives:

$$e^{a\cos x} = 1 + a\cos x + \frac{a^2}{2!}\frac{1}{2}(\cos 2x + 1) + \frac{a^3}{3!}\frac{1}{4}(\cos 3x + 3\cos x) + \frac{a^4}{4!}\frac{1}{8}(\cos 4x + 4\cos 2x + \frac{6}{2}) + \frac{a^5}{5!}\frac{1}{16}(\cos 5x + 5\cos 3x + 10\cos x) + \frac{a^6}{6!}\frac{1}{32}(\cos 6x + 6\cos 4x + 15\cos 2x + \frac{20}{2}) + \frac{a^7}{7!}\frac{1}{64}(\cos 7x + 7\cos 5x + 21\cos 3x + 35\cos x) + \cdots \tag{3}$$

Derivation Summary 10.1 (cont.)

Equation (3) is written:

$$e^{a\cos x} = I_0 + 2I_1\cos x + 2I_2\cos 2x + 2\sum_{n=3}^{\infty} I_n \cos nx \tag{4}$$

After a rather difficult process of mathematical bookkeeping is performed on equation (3), the coefficients in equation (4) are derived as follows:

$$I_n(a) = \sum_{j=0}^{\infty} \frac{a^{(2j+n)}}{2^{(2j+n)}\, j!\,(j+n)!} \tag{5}$$

Equation (5) is the series representation of Bessel Functions of the first kind with pure imaginary argument[79]:

$$I_n(a) = i^{-n} J_n(ia) \tag{6}$$

where J_n are Bessel Functions of the first kind.

$I_n(a)$ are plotted in Fig. 10.9 for small values of a. For large a, the asymptotic series given as equation (10-77) is adequate.

BIOGRAPHICAL SKETCH

Robert Clifton Duncan was born in Jonesville, Virginia, on November 21, 1923. He was educated in the public schools in the state of Ohio and was graduated from the Beavercreek High School, Alpha, Ohio, in 1941.

In the fall of 1941 he entered Ohio State University as an undergraduate student in chemical engineering. In July, 1942, he entered the U.S. Naval Academy and graduated with the degree of Bachelor of Science in June, 1945.

After serving for two years as Combat Information Officer in the heavy cruiser USS BREMERTON (CA-130) engaged in occupational duty in Japan and as flagship of the North China Patrol, he was assigned to Naval flight training. Upon completing flight training in 1948, specializing in fighter type aircraft, he was assigned to duty as a pilot in Fighting Squadron 41 (VF-41), Composite Squadron 5 (VC-5), and Composite Squadron 6 (VC-6). He was a member of the Navy's first carrier based squadrons equipped for delivery of atomic weapons.

He entered the U.S. Naval Postgraduate School in July, 1951, and graduated in June, 1953, with the degree Bachelor of Science in Aeronautical Engineering. In September, 1953, he entered M.I.T. and graduated in June, 1954, with the degree Master of Science in Aeronautical Engineering.

He was assigned in June, 1954, to the Heavy Attack Training Unit as an instructor in atomic weapons delivery for pilots of fighters, light attack, and heavy attack aircraft and for bombardier-navigators of heavy attack aircraft.

In September, 1957, he entered M.I.T. as a doctoral candidate in the Department of Aeronautics and Astronautics. He was elected to Sigma Gamma Tau and is a member of the American Ordnance Association, the U.S. Naval Institute, and the Institute of the Aeronautical Sciences.

Appendix A

COORDINATE FRAMES USED IN ENTRY TRAJECTORY ANALYSIS; GLOSSARY OF SYMBOLS, CONSTANTS, AND DEFINITIONS

A.1 Coordinate Frames

The guidance process consists of measurements of vehicle position and velocity, computation of control actions necessary to properly adjust position and velocity, and delivery of suitable adjustment commands to the vehicle's control system. Guidance of vehicles through or above the atmosphere of a planet involves the twofold functions of indication and control. Navigation is the indication aspect of guidance.

Inherent with an investigation of guidance requirements of vehicles entering planetary atmospheres is the selection of suitable coordinate frames of reference* and trajectory parameters. Many sets of coordinate frames are required to completely specify the three dimensional nature of the entry trajectory under the following general conditions:

(1) The figure of the planet is non-spherical; i.e., it may be an oblate spheroid with local surface irregularities and large scale harmonics leading to a figure resembling that of a pear.

- - - - - - - - - - - - - - - - -

* In this thesis, "frame of reference", "frame", "reference space", etc., are used synonymously.

(2) The planet is rotating about an axis through its center of gravity.

(3) The gravitational mass attraction of the planet is not spherically symmetric.

(4) The atmosphere surrounding the planet is rotating with the planet. Relative motion between the atmosphere and planet may exist; i.e., winds may be present.

(5) The entry vehicle may have the capability of generating variable lift, drag, and thrust forces in order to control the shape of its trajectory.

(6) The vehicle may have the ability to bank; i.e., rotate the direction of the lift vector out of the plane of the trajectory.

(7) The propulsive system may be mounted on gimbals in order to vary the thrust direction as desired.

Seven sets of coordinate systems were chosen in order to analyze the three dimensional dynamical equations important in the study of guidance. One of these coordinate systems is the guidance grid, for which two alternatives are presented herein. The coordinate systems selected were as follows:

(1) Planet centered Inertial Frame: Newton's laws are valid in an inertial frame. The use of a planet centered inertial frame is justified because gravitation and acceleration effects are indistinguishable.

(2) Planet Reference Frame: Establishes the orientation of the planet with respect to the inertial frame.

(3) Instantaneous Trajectory Plane Frame: Establishes the

position and orientation of the instantaneous plane of the trajectory with respect to the inertial frame.

(4) Position Reference Frame (or Guidance Grid): Two alternative methods discussed in subsequent paragraphs of Appendix A are:

(a) The Latitude-Longitude Triad

(b) The Great Circle Triad.

(5) The Wings-Level Triad: This frame is basically orientated by the velocity vector of the vehicle with respect to the atmosphere when the lift vector is in the instantaneous plane of the trajectory.

(6) The Vehicle Coordinate Triad: Required for a vehicle that has the ability to "bank"; i.e., to rotate the lift vector out of the plane of the trajectory in order to generate trajectory curvature as desired.

(7) The Engine Gimbal Triad: Required for a vehicle that has an engine capable of being rotated with respect to the vehicle in order to control the direction in which thrust forces are generated.

Relations among the angles involved are presented for ready reference in converting quantities specified in one frame into components in any of the other frames.

Fig. A.1 shows a vehicle located at the point P entering the atmosphere of a planet. The destination of the vehicle is some landing site on the surface of the planet that was selected prior to initiation of entry. The instantaneous plane of the trajectory is not fixed with respect to an inertial reference. Following is a brief definition of

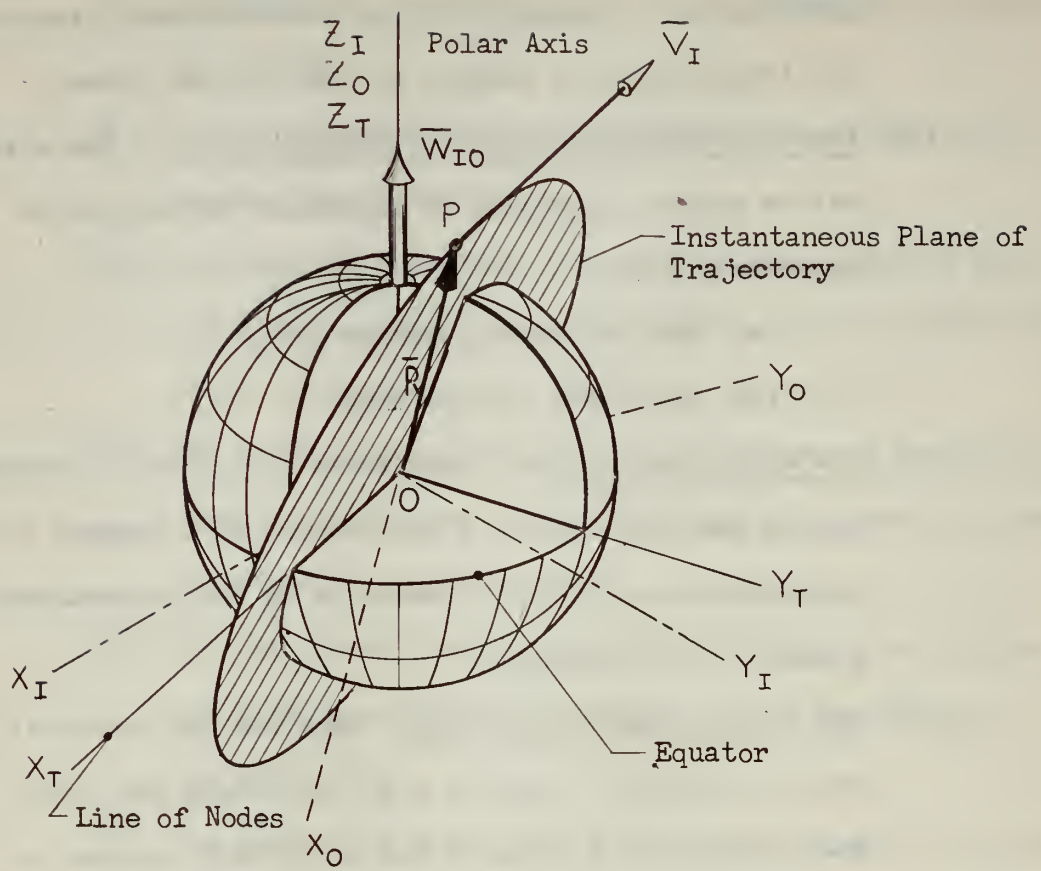

Planet Centered Inertial Frame: Centered at the center of the planet and sidereally nonrotating relative to the "fixed stars". X_I and Y_I are in the equatorial plane and Z_I is directed along the polar axis (North).

Planet Reference Frame: Centered at the center of the planet and nonrotating with respect to the planet. This frame rotates about the planet's polar axis relative to the inertial frame at the planet's daily sidereal rate. X_O and Y_O are in the equatorial plane and fixed with respect to the planet. Z_O is directed along the polar axis.

Instantaneous Trajectory Plane Frame: Centered at the center of the planet. X_T is the line of intersection of equatorial plane with the instantaneous plane of the trajectory; Y_T is in equatorial plane perpendicular to X_T ; Z_T is directed along the polar axis.

Fig. A.1: Definition of the Inertial, Planet, and Instantaneous Trajectory Plane Coordinate Systems.

the coordinate frames shown in Fig. A.1.

X_I, Y_I, Z_I Planet Centered Inertial Frame: Centered at the center of the planet and sidereally nonrotating relative to the "fixed stars". X_I and Y_I are oriented in the equatorial plane and sidereally nonrotating; Z_I is directed along the polar axis (North).

X_O, Y_O, Z_O Planet Reference Frame: Centered at the center of the planet and nonrotating with respect to the planet. This frame rotates about the planet's polar axis relative to the inertial frame at the planet's daily sidereal rate. X_O and Y_O are oriented in the equatorial plane and fixed in the planet; Z_O is directed along the planet's polar axis (North).

X_T, Y_T, Z_T Instantaneous Trajectory Plane Frame: Centered at the center of the planet. X_T is the line of intersection of the planet's equatorial plane with the plane of the trajectory (ascending line of nodes); Y_T axis is in the planet's equatorial plane and is perpendicular to the ascending line of nodes. Z_T axis coincides with the planet's polar axis (North).

In an analysis of the trajectory of entry vehicles, it is convenient to study the motion of the vehicle in spherical polar coordinates. The reference frame is usually selected with one axis along the radius vector from the center of the planet to the point at which the guidance is taking place. This radius vector, for the planet Earth, is the geocentric radius. In this thesis, the term "geocentric" is used in

a more general sense to identify quantities associated with the spherical polar coordinates of any planet*.

The following coordinate axes systems are shown in Fig. A.2:

$\bar{1}_r$, $\bar{1}_\lambda$, $\bar{1}_\Lambda$ Geocentric Latitude-Longitude Triad: Orthogonal set of unit vectors centered at the entry vehicle center of gravity and directed in radial, longitude, and latitude directions respectively.

$\bar{1}_r$, $\bar{1}_\phi$, $\bar{1}_\psi$ Instantaneous Great Circle Triad: Orthogonal set of unit vectors centered at the vehicle center of gravity and directed in radial, along-track, and cross-track directions respectively.

The following quantities are defined in Fig. A.2:

Line of Nodes: The line of intersection of the plane of the instantaneous trajectory with the equatorial plane.

Ascending Node: The point of intersection of the line of nodes and the northerly-directed segment of the instantaneous ellipse describing the trajectory.

Descending Node: The point of intersection of the line of nodes and the southerly-directed segment of the instantaneous ellipse describing the trajectory.

$\bar{R}$: The position vector directed from the center of the planet to the instantaneous position of the vehicle.

- - - - - - - - - - - - - - - - -

* The interpretation of "geocentric" in this thesis may be considered to be a shortening of "geometric-centric" rather than the more precise "geoid-centric".

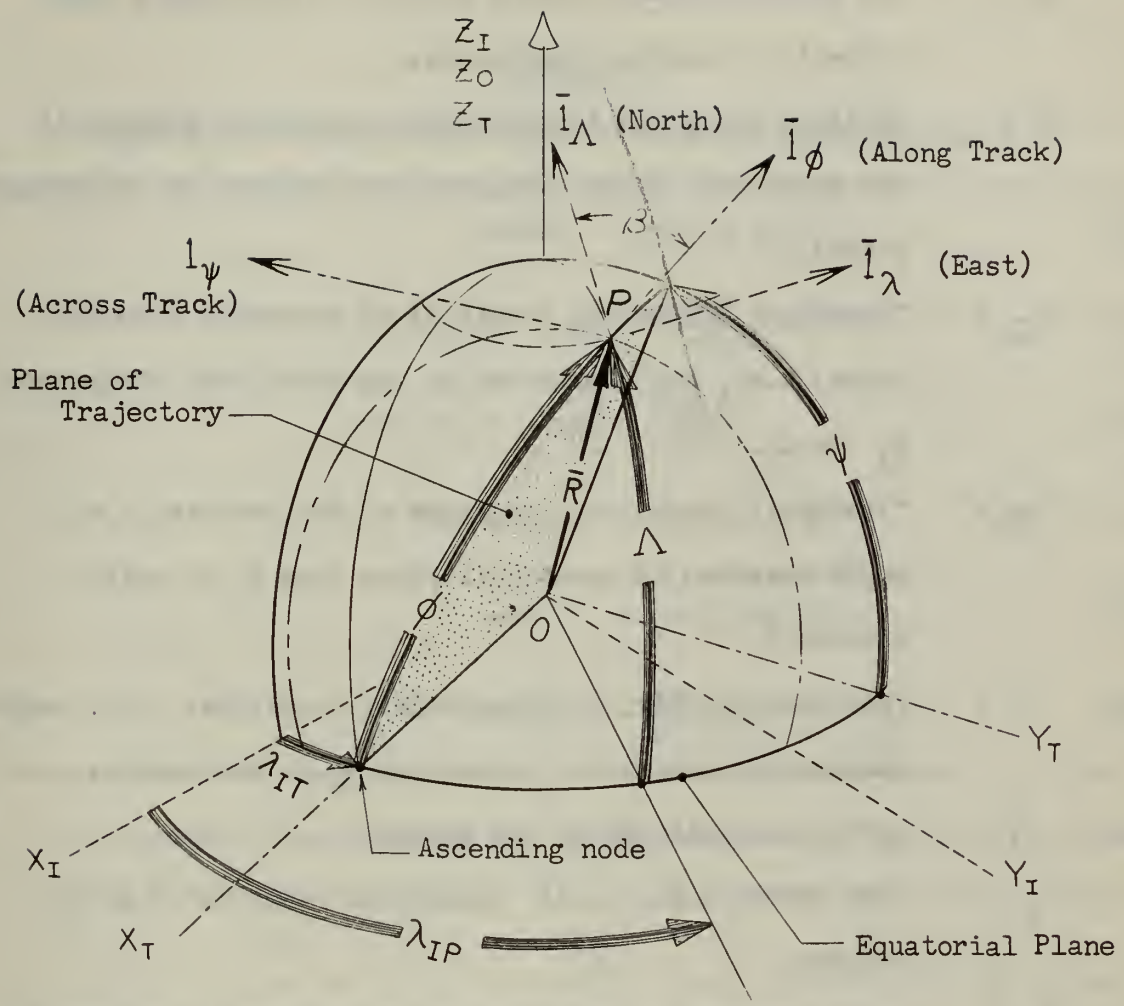

$\bar{1}_r, \bar{1}_\lambda, \bar{1}_\Lambda$ Geocentric Latitude-Longitude Triad: Orthogonal set of unit vectors centered at the entry vehicle center of mass and directed in radial, longitude, and latitude directions respectively.

$\bar{1}_r, \bar{1}_\phi, \bar{1}_\psi$ Instantaneous Great Circle Triad: Orthogonal set of unit vectors centered at the vehicle center of mass and directed in radial, along-track, and across-track directions respectively.

Fig. A.2: Definition of Latitude-Longitude and Great Circle Guidance Grids.

$\bar{V}_I$: The instantaneous velocity vector of the vehicle with respect to inertial coordinates.

ψ : Inclination of the instantaneous trajectory plane with the equatorial plane (measured from equator to trajectory plane).

λ_{IT} : "Inertial" geocentric longitude of ascending line of nodes; i.e., angle measured in the equatorial plane from X_I to X_T.

λ_{IP} : "Inertial" geocentric longitude of the vehicle; i.e., angle measured in equatorial plane from X_I to entry vehicle P.

λ : (not shown in Fig. A.2) geocentric longitude; i.e., angle measured in equatorial plane from X_0 to the vehicle.

Λ : geocentric latitude of the vehicle.

Λ_g : (not shown in Fig. A.2) geographic latitude of entry vehicle.

ϕ : angle measured in the plane of trajectory (in direction of vehicle motion) from ascending line of nodes to the vehicle.

β : bearing angle of entry vehicle as seen by an observer directly under the vehicle on non-rotating planet; angle between North ($\bar{1}_\Lambda$) and the horizontal component of velocity (directed along $\bar{1}_\phi$).

The following angular relations are useful in conversion among the sets of angles defined in Fig. A.2.

Table A-1

Angular relations among coordinate systems given in Fig. A.2.

$$\sin\Lambda = \sin\phi \sin\psi \tag{1}$$

$$\sin(\lambda_{IP} - \lambda_{IT}) = \frac{\sin\phi \cos\psi}{\sin\Lambda} \tag{2}$$

$$\cos(\lambda_{IP} - \lambda_{IT}) = \frac{\cos\phi}{\cos\Lambda} \tag{3}$$

$$\sin\psi \cos\phi = \cos\Lambda \cos\beta \tag{4}$$

$$\cos\psi = \cos\Lambda \sin\beta \tag{5}$$

$$\tan\psi = \frac{\tan\Lambda}{\sin(\lambda_{IP} - \lambda_{IT})} \tag{6}$$

Direction cosines between $\bar{1}_r$, $\bar{1}_\phi$, $\bar{1}_\psi$ system and $\bar{1}_r$, $\bar{1}_\lambda$, $\bar{1}_\Lambda$ system:

	$\bar{1}_r$	$\bar{1}_\phi$	$\bar{1}_\psi$	
$\bar{1}_r$	1	0	0	(7)
$\bar{1}_\lambda$	0	$\sin\beta$	$-\cos\beta$	
$\bar{1}_\Lambda$	0	$\cos\beta$	$\sin\beta$	

Direction cosines between X_T, Y_T, Z_T system and $\bar{1}_r$, $\bar{1}_\phi$, $\bar{1}_\psi$ system:

	$\bar{1}_r$	$\bar{1}_\phi$	$\bar{1}_\psi$	
X_T	$\cos\phi$	$-\sin\phi$	0	(8)
Y_T	$\sin\phi \cos\psi$	$\cos\phi \cos\psi$	$-\sin\psi$	
Z_T	$\sin\phi \sin\psi$	$\cos\phi \sin\psi$	$\cos\psi$	

The drag vector is directed anti-parallel to the velocity vector of the vehicle with respect to the atmosphere. The lift vector is perpendicular to this velocity vector and acts in the plane of symmetry of the vehicle. In the analysis performed herein, it is assumed that the entry vehicle has the capability of rotating the lift vector (i.e., banking) in order to produce curvature of the trajectory in a controlled manner to enable the vehicle to reach landing sites at some distance from the "no-bank" trajectory. For military vehicles, such as a reconnaissance platform, the banking capability may permit adequate military coverage of an entire hositle nation from a single parent satellite.

Two additional vehicle-centered coordinate triads are defined in Fig. A.3; the "Wings Level" triad $\bar{l}_{x_{WL}}$, $\bar{l}_{y_{WL}}$, $\bar{l}_{z_{WL}}$ and the "Vehicle" triad $\bar{l}_x$, $\bar{l}_y$, $\bar{l}_z$. It is noted that both the "Wings Level" triad and the "Vehicle" triad are basically oriented by the velocity vector of the vehicle with respect to the atmosphere. The left wing unit vector in the zero bank condition ($\bar{l}_{y_{WL}}$) always lies in the $\bar{l}_\lambda$ - $\bar{l}_\Lambda$ plane*. Rotation of the vehicle about $\bar{V}_{(AM)}$ (coincident with $\bar{l}_{x_{WL}}$, $\bar{l}_x$) causes the lift vector to move out of the vertical plane, hence causes a side force which tends to curve the trajectory. The amount of rotation of the vehicle from the wings level condition is defined as the bank angle, B.

Following is a brief description of the coordinate systems shown in Fig. A.3:

$\bar{l}_{x_{WL}}$, $\bar{l}_{y_{WL}}$, $\bar{l}_{z_{WL}}$ Wings Level Triad: Orthogonal set of unit vectors centered at entry vehicle center of gravity. $\bar{l}_{x_{WL}}$

- - - - - - - - - - - - - - - - - -

* $\bar{l}_\lambda$ is positive in the geocentric East direction. $\bar{l}_\Lambda$ is positive in the geocentric North direction. The $\bar{l}_\lambda$ - $\bar{l}_\Lambda$ plane is the geocentric horizontal plane, or "level plane" -- hence the term "Wings Level" coordinate system.

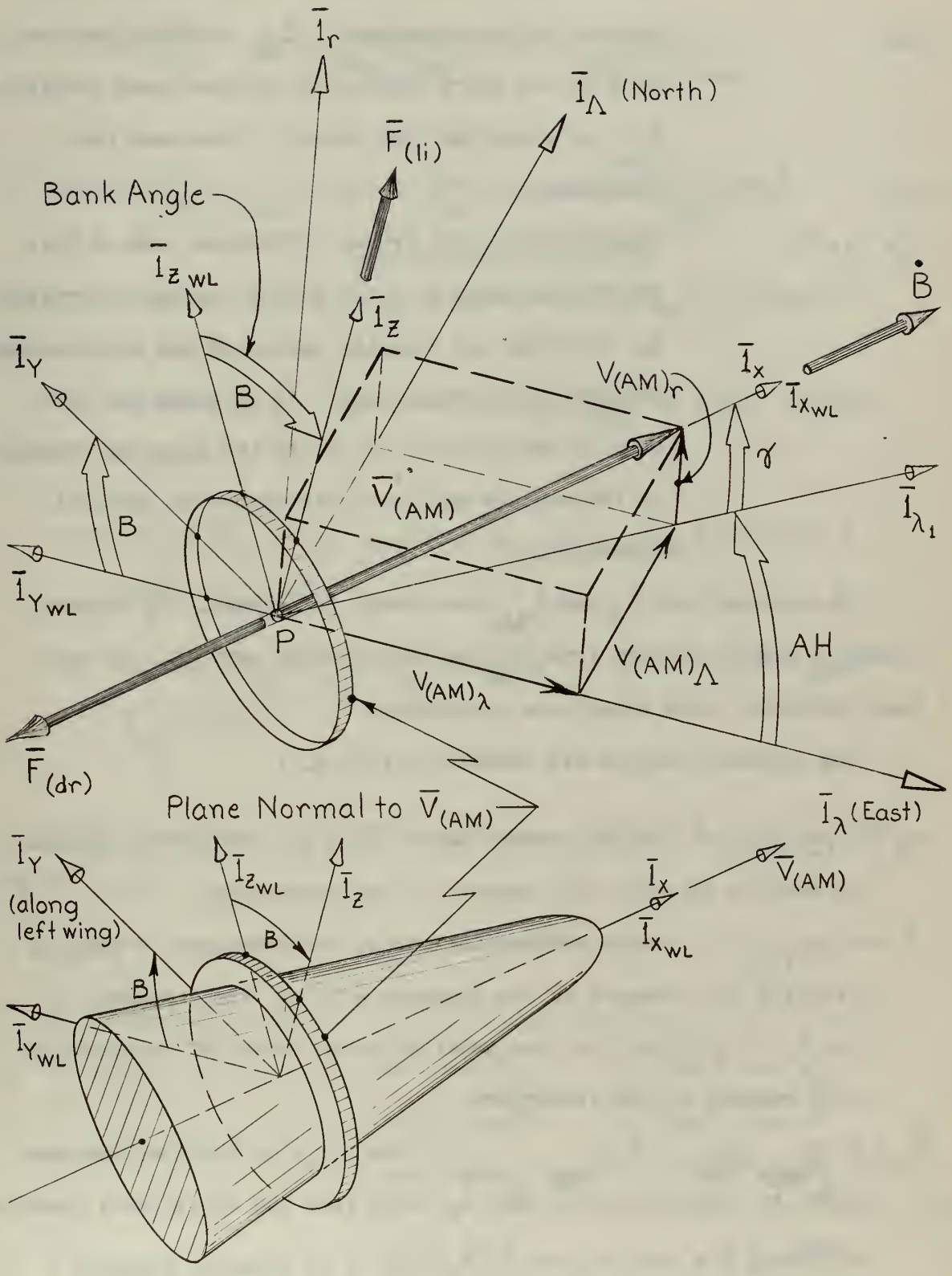

A.3: "Wings Level" and "Vehicle" Coordinate Triads.

is along the velocity vector of the vehicle with respect to the atmosphere. $\bar{l}_{y_{WL}}$ is along the left wing of the entry vehicle in the zero bank condition. $\bar{l}_{z_{WL}}$ is along the lift vector in the zero bank condition.

$\bar{l}_x$, $\bar{l}_y$, $\bar{l}_z$ — Vehicle Coordinate Frame: Orthogonal set of unit vectors centered at entry vehicle center of gravity. $\bar{l}_x$ is along the velocity vector of the vehicle with respect to the atmosphere. $\bar{l}_y$ is along the left wing of the vehicle; $\bar{l}_z$ is in the plane of symmetry of the vehicle and is a unit vector in the lift direction.

It is noted that $\bar{l}_x$ and $\bar{l}_{x_{WL}}$ are always coincident. $\bar{l}_y$ differs from $\bar{l}_{y_{WL}}$ and $\bar{l}_z$ differs from $\bar{l}_{z_{WL}}$ by the angle of bank, B. In zero bank condition, both triads are coincident.

The following angles are defined in Fig. A.3:

$A_H = A\left(\bar{l}_\lambda - \bar{l}_{\lambda_1}\right)$: angle between "East" ($\bar{l}_\lambda$) and horizontal component of vehicle velocity with respect to the atmosphere.

$\gamma = A\left(\bar{l}_{\lambda_1} - \bar{l}_x\right)$: angle between the horizontal component of vehicle velocity with respect to the atmosphere (i.e., the component in the $\bar{l}_\lambda$ - $\bar{l}_\Lambda$ plane) and the total velocity vector of the vehicle with respect to the atmosphere.

$B = A\left(\bar{l}_{y_{WL}} - \bar{l}_y\right) = A\left(\bar{l}_{z_{WL}} - \bar{l}_z\right)$: bank angle of vehicle. Corresponds to rotations about the $\bar{l}_x$ axis from the wings level condition.

Following are definitions of A_H and γ in terms of velocity components:

$$A_H = \arctan \frac{V_{(AM)\Lambda}}{V_{(AM)\lambda}} = \arcsin \frac{V_{(AM)\Lambda}}{\left(V^2_{(AM)\lambda} + V^2_{(AM)\Lambda}\right)^{1/2}} = \arccos \frac{V_{(AM)\lambda}}{\left(V^2_{(AM)\lambda} + V^2_{(AM)\Lambda}\right)^{1/2}} \qquad \text{(A-1)}$$

$$\gamma = \arctan \frac{V_{(AM)r}}{\left(V^2_{(AM)\lambda} + V^2_{(AM)\Lambda}\right)^{1/2}} = \arcsin \frac{V_{(AM)r}}{V_{(AM)}} = \arccos \frac{\left(V^2_{(AM)\lambda} + V^2_{(AM)\Lambda}\right)^{1/2}}{V_{(AM)}} \qquad \text{(A-2)}$$

Rotations from the $\bar{l}_r$, $\bar{l}_\lambda$, $\bar{l}_\Lambda$ triad to the $\bar{l}_z$, $\bar{l}_x$, $\bar{l}_y$ triad are performed in the following order:

(1) Rotate ($\bar{l}_r$, $\bar{l}_\lambda$, $\bar{l}_\Lambda$) to ($\bar{l}_r$, $\bar{l}_{\lambda_1}$, $\bar{l}_{y_{WL}}$) by angle A_H about $\bar{l}_r$ axis.

(2) Rotate ($\bar{l}_r$, $\bar{l}_{\lambda_1}$, $\bar{l}_{yW_L}$) to ($\bar{l}_{z_{WL}}$, $\bar{l}_{x_{WL}}$, $\bar{l}_{y_{WL}}$) by angle γ about $-\bar{l}_{y_{WL}}$ axis.

(3) Rotate ($\bar{l}_{z_{WL}}$, $\bar{l}_{x_{WL}}$, $\bar{l}_{y_{WL}}$) to ($\bar{l}_z$, $\bar{l}_x$, $\bar{l}_y$) by angle B about $\bar{l}_{x_{WL}}$ axis.

Direction cosines between $\bar{l}_r$, $\bar{l}_\lambda$, $\bar{l}_\Lambda$ triad and $\bar{l}_x$, $\bar{l}_y$, $\bar{l}_z$ triad are as follows:

	$\bar{l}_r$	$\bar{l}_\lambda$	$\bar{l}_\Lambda$
$\bar{l}_x$	$\sin\gamma$	$\cos\gamma \cos A_H$	$\cos\gamma \sin A_H$
$\bar{l}_y$	$\cos\gamma \sin B$	$-\sin A_H \cos B$ $-\sin\gamma \cos A_H \sin B$	$\cos A_H \cos B$ $-\sin\gamma \sin A_H \sin B$
$\bar{l}_z$	$\cos\gamma \cos B$	$\sin A_H \sin B$ $-\sin\gamma \cos A_H \cos B$	$-\cos A_H \sin B$ $-\sin\gamma \sin A_H \cos B$

(A-3)

The coordinate systems defined above are not those used in conventional aircraft analysis where it is common to define a set of axes fixed to the airframe. It is necessary to define a set of vehicle-fixed axes if the stability and control characteristics are to be studied -- a subject beyond the scope of this thesis. Lift and drag forces are the primary gas-dynamic forces affecting the shape of the trajectory in the atmospheric phases of flight; secondary forces and moments are of lower order.

Thrust forces generated by the entry vehicle propulsion system will, in general, be applied in such a direction as to slow the vehicle down* (retor-thrust). It was assumed that the thrust vector passes at all times through the vehicle center of gravity in order to avoid excessive moments. The engine gimbal angles shown in Fig. A.4 were selected to describe the thrust direction.

Rotation from the $\bar{l}_x$, $\bar{l}_y$, $\bar{l}_z$ triad to the thrust triad ($\bar{l}_{x_2}$, $\bar{l}_{y_2}$, $\bar{l}_{z_2}$) is performed in the following order:

(1) Rotate ($\bar{l}_x$, $\bar{l}_y$, $\bar{l}_z$) to ($\bar{l}_{x_1}$, $\bar{l}_{y_1}$, $\bar{l}_{z_1}$) by angle A_e about $-\bar{l}_y$ axis.

(2) Rotate ($\bar{l}_{x_1}$, $\bar{l}_{y_1}$, $\bar{l}_{z_1}$) to ($\bar{l}_{x_2}$, $\bar{l}_{y_2}$, $\bar{l}_{z_2}$) by angle A_d about $\bar{l}_{z_1}$ axis.

Direction cosines between $\bar{l}_{x_2}$, $\bar{l}_{y_2}$, $\bar{l}_{z_2}$ triad and $\bar{l}_x$, $\bar{l}_y$, $\bar{l}_z$ triad are as follows:

- - - - - - - - - - - - - - - - -

* Except possibly in the landing phase.

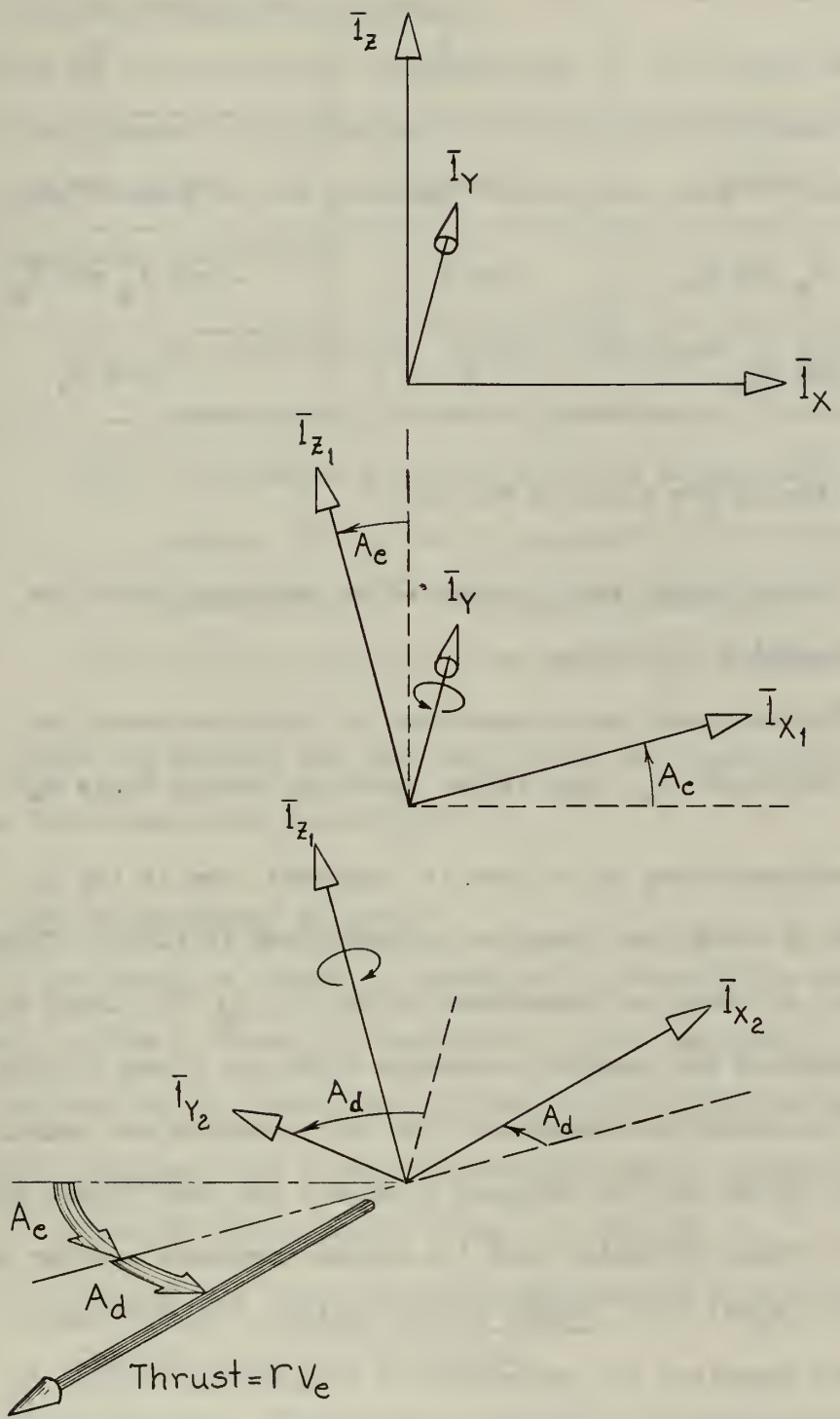

Fig. A.4: Engine Gimbal Angles

	$\bar{l}_x$	$\bar{l}_y$	$\bar{l}_z$
$\bar{l}_{x_2}$	$\cos A_e \cos A_d$	$\sin A_d$	$\sin A_e \cos A_d$
$\bar{l}_{y_2}$	$-\cos A_e \sin A_d$	$\cos A_d$	$-\sin A_e \sin A_d$
$\bar{l}_{z_2}$	$-\sin A_e$	0	$\cos A_e$

(A-4)

The following angles are shown in Fig. A-4:

A_e : Engine gimbal angle generated by rotations about the negative $\bar{l}_y$ axis.

A_d : Engine gimbal angle generated by rotations about the displaced $\bar{l}_z$ axis (after rotating through angle A_e).

Thrust components may be written in component form in the $\bar{l}_r$, $\bar{l}_\lambda$, $\bar{l}_\Lambda$ triad by using the direction cosines given in (A-3). These components may, in turn, be transformed to the $\bar{l}_r$, $\bar{l}_\phi$, $\bar{l}_\psi$ triad by the table of cosines and angular conversion relations given in Table A-1.

Once the velocity requirements of the entry vehicle are established, the propulsion system must be designed in such a way that thrust may be applied in the proper direction with the proper magnitude and for the proper length of time; i.e., thrust vector control. Thrust vector control is also important for generation of orientation torques for attitude stability; problems connected with thrust vector control for attitude orientation and rotational moment stability are not considered in this thesis.

A.2: The Two-Dimensional Trajectory

Most of the analytical study described in this thesis was concerned with a two-dimensional approximation of the entry trajectory. Following is a brief summary of the principal assumptions made in postulating a two-dimensional trajectory:

(1) The gravitational field of the planet is spherically symmetric and is free of anomalies.

(2) The atmosphere rotates with the planet, and no wind exists. The velocity component of the rotating atmosphere in the $\bar{l}_\psi$ direction is negligible.

(3) The vehicle flies in the zero bank condition with $A_d = 0$.

Figure A.5 defines the important forces and geometric quantities of the two-dimensional trajectory.

A.3: The Instantaneous Ellipse

It is common in celestial mechanics to describe the motion of heavenly bodies in terms of parameters of conic sections. There are many definitions of conics; the following definitions are convenient:

(1) Ellipse: The locus of points the sum of whose distances from two fixed points (foci) is constant.

(2) Circle: The locus of points equidistant from a single point (special case of the ellipse).

(3) Hyperbola: The locus of points the difference of whose distances from two fixed points (foci) is constant.

(4) Parabola: The locus of points equally distant from a fixed point (focus) with a fixed straight line (directrix).

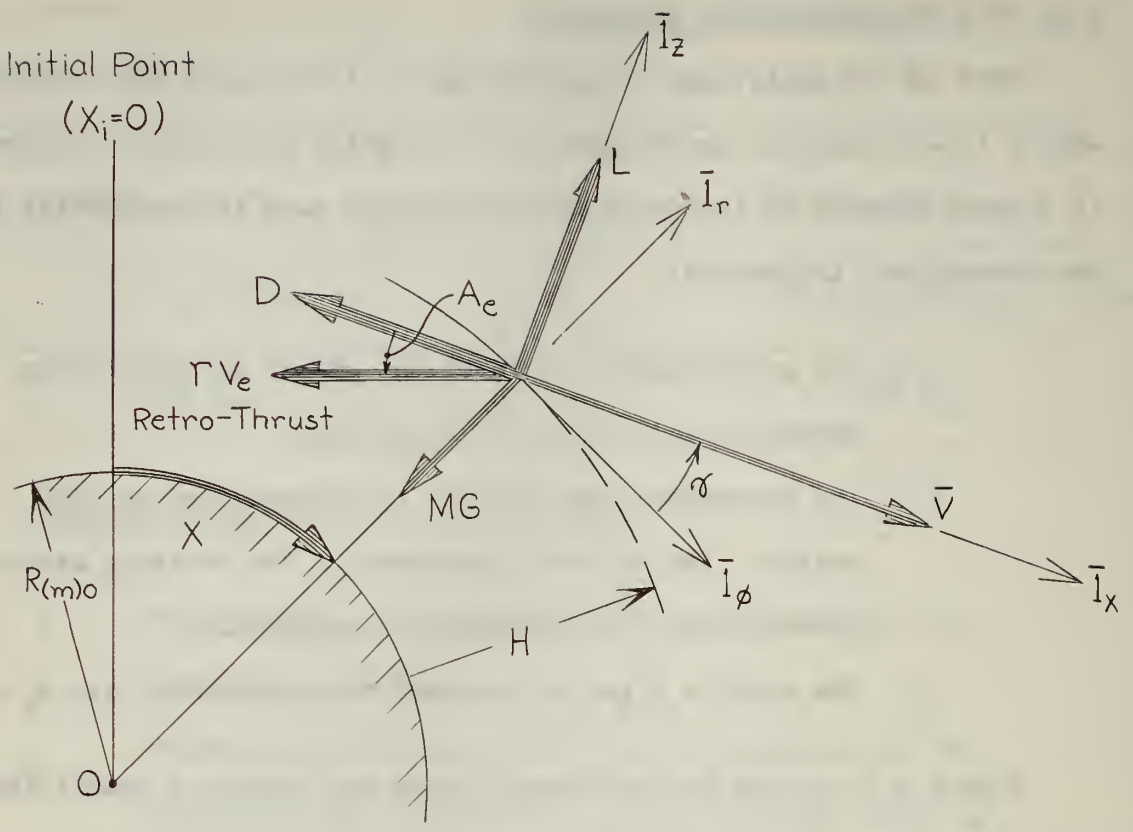

Definitions:

X = distance flown

$\bar{V}$ = velocity of vehicle with respect to coordinates rotating with the planet (same as velocity of vehicle with respect to the planetary atmosphere, $\bar{V}_{(AM)}$, for no-wind condition)

H = altitude of vehicle above planet

γ = flight path angle with respect to local geocentric horizon - positive as shown.

Γ = mass flow rate of propellant

V_e = equivalent exit velocity of rocket propellant (assumed constant)

M = instantaneous mass of vehicle

D = drag

L = lift

A_e = engine gimbal angle of retro-rocket; angle the thrust vector makes with negative $\bar{i}_x$ axis.

Fig. A.5: The Two-Dimensional Trajectory

When a body is in motion under the action of an attractive central force that varies as the inverse square of the distance, and if no external forces act on the body, the path described will be a conic whose focus is at the center of attraction. A particle moving according to such a force obeys Kepler's laws. Kepler's three laws of planetary motion, published around 1610, were the result of his pioneering analysis of planetary observations, and laid the ground work for many of the important contributions of Sir Isaac Newton. Kepler's laws may be summarized as follows:

> A particle moving under the action of an attractive central force that varies as the inverse square of the distance
> (1) travels in an ellipse or a hyperbola (or their special cases, a circle or parabola) with the attracting center at one of the foci;
> (2) the radius vector from the center to the particle sweeps out equal areas in equal time*;
> (3) for the elliptic orbit, which results in periodic motions, the squares of the periods of rotation are proportional to the cubes of the major axis of the orbits.

Elliptical parameters are useful for analyzing the motion of the entry vehicle during the orbital phase and in the early phases of entry where gas-dynamic forces are negligible**. The use of elliptical parameters may be extended to the study of the entire trajectory by using the "instantaneous ellipse" technique; i.e., by describing the trajectory as a time-varying ellipse which matches the position and velocity vectors of the vehicle at each instant.

- - - - - - - - - - - - - - - -

* Kepler's second law, the conservation of areal velocity, is a general theorem for central force motion[19] since angular momentum is always conserved. The first and third laws are restricted specifically to the inverse square law of force.

** This segment of the trajectory is called the "Keplerian Phase" in this thesis.

Frequent reference is made in this thesis to elliptical parameters, particularly in the study of retro-rocket system requirements described in Chapter 9. A description of the parameters of the ellipse are given in Fig. A.6.

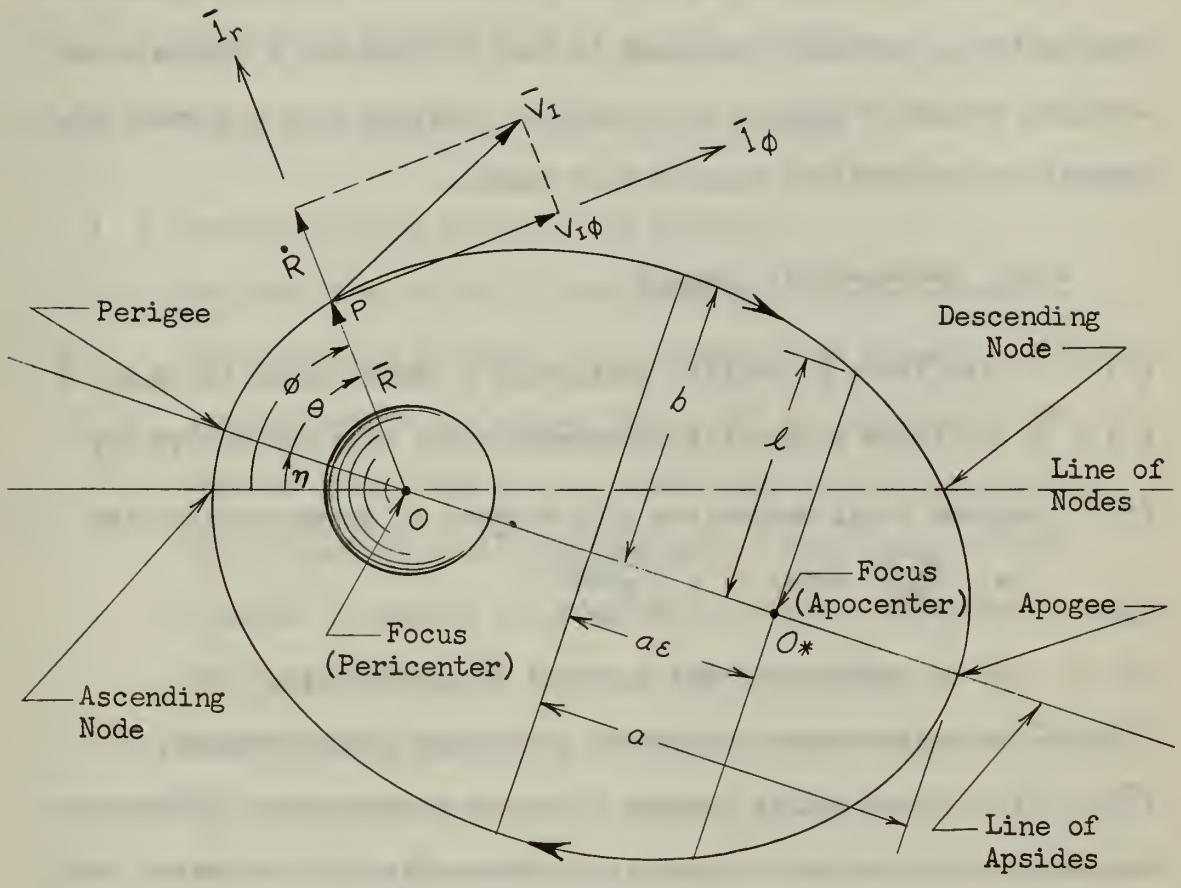

Line of apsides: The major axis of the ellipse, connecting the apsides (apocenter and pericenter).

Major axis = 2a
Minor axis = 2b
Latus rectum = 2l $\quad l = a(1-\varepsilon^2)$

Eccentricity = ε (Always less than 1.0 for ellipse)

$$\varepsilon = \sqrt{1 - (b/a)^2}$$

True anomaly = θ
Area of ellipse = πab

$$\eta = \phi - \theta$$

Equation of ellipse: $\quad R = \dfrac{a(1-\varepsilon^2)}{1+\varepsilon\cos\theta}$

T = period of orbit: $\quad T = \dfrac{2\pi a^{3/2}}{\sqrt{\gamma_g M_o}}$

Fig. A.6: The Instantaneous Ellipse.

A.4 Glossary of Symbols

A fundamental difficulty in the presentation of any mathematical description of physical phenomena is that of choosing a complete and workable system of symbols and notation. Following is a summary of symbols and definitions used in this thesis.

A.4.1 Mathematical Symbols

$(\bar{\ })$: a line above a quantity designates a vector quantity; e.g., $\bar{R}$

$(\dot{\ })$: a dot above a quantity represents total time derivative $\frac{d(\ )}{dt}$

$(')$: denotes total derivative with respect to dimensionless time τ, i.e., $\frac{d(\ )}{d\tau}$ Note: $\tau = \sqrt{\frac{G_{(m)O}}{R_{(m)O}}}\, t$

$\nabla(\ )$: del or gradient of the quantity in parenthesis.

$(\bar{\ }) \times (\bar{\ })$: vector cross product of quantities in parenthesis.

$(\bar{\ }) \cdot (\bar{\ })$: dot or scalar product of vector quentities in parenthesis.

The magnitude of a vector quentity is represented by the letter designation of the quantity with the vector symbol removed. Thus, the magnitude of $\bar{R}$ is R.

$\frac{\partial(\ )}{\partial \bar{x}}$: partial derivative of quantity in parenthesis with respect to x.

$\delta(\ )$: variation of the quantity in parenthesis.

$\Delta(\ )$: incremental change of the quantity in the parenthesis from its initial value; e.g., $\Delta r = r - r_i$

$\sum_{n=1}^{\infty} (\ )_n$: summation of the quantity in parenthesis.

$\log(\ ) = \log_{10}(\ )$

$\ln(\ ) = \log_e(\ )$

A.4.2 Subscripts

r, λ, Λ : Components along the $\bar{1}_r$, $\bar{1}_\lambda$, $\bar{1}_\Lambda$ axes.

r, ϕ, ψ : Components along the $\bar{1}_r$, $\bar{1}_\phi$, $\bar{1}_\psi$ axes.

i : Denotes initial value of the quantity.

f : Denotes final value of the quantity.

0 : The subscript 0 refers to the generalized planet 0. When specialized to the planet Earth, "0" is replaced by "E".

m : Denotes quantities at the "trajectory modification point". The trajectory modification point is that point in the original satellite orbit at which entry is initiated through generation of thrust forces. (See Fig. 9.3)

I : Measured with respect to inertial coordinates. For example, $\bar{V}_I$ is the velocity of the vehicle with respect to inertial space, while $\bar{V}$ denotes velocity of the vehicle with respect to coordinates rotating with the planet.

α : Value of the quantity at apogee; e.g., R_α is the radius at apogee of an elliptical trajectory.

π : Value of the quantity at perigee; e.g., R_π is the radius at perigee of an elliptical orbit.

A.4.3 Symbols

The author has endeavored to be consistent in the use of notation and symbols in this thesis. For example, the symbol $\bar{V}_I$ represents the same quantity regardless of where it may appear in the text.

As is well known, certain particular symbols are used within each scientific field to represent quantities frequently encountered. Examples

of this are ρ for atmospheric density and C_D for drag coefficient of aerodynamics, θ for "true anomaly" of celestial mechanics, "p" or "h" for angular momentum in mechanics or physics, etc. Where possible, such conventions are followed in this thesis. Unfortunately in an analysis that spans many fields, one finds a conflict between the common symbols of one branch of science or engineering with those of another field. In such instances, the author had no alternative except to invent a symbol which he considered convenient: the choice may often be unsuited to the taste of the reader who is conversant with the more conventional representation.

A.4.3-1 English Letters

$\bar{A}$: acceleration vector of entry vehicle, ft./sec.^{2}

A_e : Engine gimbal angle in $\bar{l}_x - \bar{l}_z$ plane (Figs. A.4 and A.5)

$(A_e)_{opt}$: Optimum engine gimbal angle (i.e., that angle for which range errors are minimized with respect to errors in operation of retro-rocket system).

A_d : Engine gimbal angle; consists of rotations out of the $\bar{l}_x - \bar{l}_z$ plane (Fig. A-4).

A_H : Heading angle. Angle between "East" ($\bar{l}_\lambda$) and horizontal component of vehicle velocity with respect to the atmosphere (Fig. A.3).

A_c : Constant defined in circular trajectory study of section 10.3 as follows:

$$A_c \equiv \left(\frac{L}{D}\right) C \frac{v_i^2}{2}$$

A_1 : Constant defined for degenerate elliptical orbital profile

in section 10.4 as follows:

$$A_1 \equiv \left(\frac{L}{D}\right) C\frac{v_i^2}{2} = A_c$$

A_2 : Constant defined in section 10.4 as follows:

$$A_2 \equiv \omega^2 r_i \left(\frac{v_i^2 r_i - 1}{2 - v_i^2 r_i}\right)$$

A_3 : Constant defined in section 10.4 as follows:

$$A_3 \equiv \frac{C v_i^3}{r_i}$$

A_4 : Constant defined in section 10.4 as follows:

$$A_4 \equiv \frac{k A_2}{\omega^2}$$

a : One-half the major axis of the elliptical trajectory

a_N : Dimensionless semi-major axis of the ellipse:

$$a_N = \frac{a}{R_{(m)o}}$$

B : Angle of bank of the entry vehicle; angular rotation about the velocity vector of the vehicle with respect to the atmosphere (Fig. A.3)

B_c : Constant defined in section 10.3 as follows:

$$B_c = C v_i^3 \left(\frac{1}{r_i} + \frac{L}{D}\frac{C}{2}\right)$$

b : One-half the minor axis of the ellipse.

b_N : Dimensionless semi-minor axis of the ellipse

$$b_N = b/R_{(m)o}$$

b_1 : Constant defined in section 10.3 as follows:

$$b_1 = -\,2x_1$$

b_2 : Constant defined in section 10.3 as follows:

$$b_2 = x_1 - i\,y_1$$

b_3 : Constant defined in section 10.3 as follows:

$$b_3 = x_1 + i\,y_1$$

C : Trajectory constant. Defined as follows:

$$C = R_{(m)o}\,\rho_i\,\frac{C_D S}{M}$$

C_c : Constant defined in section 10.3 as follows:

$$C_c = \frac{B_c}{r_i}$$

$C_{(atm)}$: Dimensional constant for the planetary atmosphere (BTU ft.$^{-3/2}$ sec.$^{-1}$)

C_D : Drag coefficient

C_{Do} : Zero-lift drag coefficient.

C_L : Lift coefficient.

C_a : An acceleration constant defined as follows:

$$C_a \equiv -\frac{\log (AC)_{EO}}{k_E \log e}$$

C_e : Auxiliary quantity defined as follows in Eq. (8-24)

$$C_e \equiv -\frac{1}{k_E \log e}\,\log\left(\frac{\rho_{(\bar{s}L)}}{\rho_{(\bar{s}L)E}}\,\frac{R_{(m)o}}{R_{(m)E}}\right)$$

C_g : Auxiliary quantity defined as follows in Eq. (8-28):

$$C_g \equiv \frac{1}{k_E \log e} \log\left(\frac{G_{(m)o}}{G_{(m)E}}\right)$$

C_p : Heat capacity at constant pressure.

C_t : A temperature constant defined as follows:

$$C_t \equiv -\frac{18.44}{4 k_E} \log (HF)_{EO}$$

C_v : Heat capacity at constant volume.

c : Maximum allowable specific force level in Earth g's

C_{th} : Threshold value of accelerations detectable by specific force measuring subsystem in Earth g's.

D : Drag force (lb.)

$\mathcal{E}_{(kin)}$: Kinetic Energy (ft.-lb.) : $\mathcal{E}_{(kin)} = \frac{M}{2}(\overline{V}_I \cdot \overline{V}_I)$

$\mathcal{E}_{(pot)}$: Potential Energy (ft.-lb.) : $\mathcal{E}_{(pot)} = -\frac{\gamma_g M_o M}{R}$

$\mathcal{E}_{(tot)}$: Total Energy (ft.-lb.) : $\mathcal{E}_{(tot)} = \mathcal{E}_{(kin)} + \mathcal{E}_{(pot)}$

$E_{(kin)}$: Dimensionless kinetic energy per unit mass.

$$E_{(kin)} = \frac{\mathcal{E}_{(kin)}}{M V_s^2}$$

$E_{(pot)}$: Dimensionless potential energy per unit mass.

$$E_{(pot)} = \frac{\mathcal{E}_{(pot)}}{M V_s^2}$$

$E_{(tot)}$: Dimensionless total energy per unit mass:

$$E_{(tot)} = \frac{\mathcal{E}_{(tot)}}{M V_s^2}$$

$\overline{F}$: Specific force; i.e., force per unit mass. ft./sec.^{2}

$\overline{F}_{(dr)}$: Drag specific force vector. ft./sec.^{2}

$\overline{F}_{(li)}$: Lift specific force vector. ft./sec.^{2}

$\overline{F}_{(th)}$: Thrust specific force vector. ft./sec.^{2}

$\overline{f}$: Dimensionless specific force (in surface g's of the planet).

$$\overline{f} = \frac{\overline{F}}{G_{(m)O}}$$

$\overline{f}_E$: Dimensionless specific force in surface Earth g's.

$$\overline{f}_E = \frac{\overline{F}}{G_{(m)E}}$$

$\overline{G}$: Gravitational field intensity. (ft./sec.^{2})

$G_{(m)O}$: Mean value of gravitational field intensity at surface of planet O. (ft./sec.^{2})

$G_{(m)E}$: Mean value of gravitational field intensity at surface of Earth. $G_{(m)E} = 32.22848$ ft./sec.^{2}

G_{sp} : Spherical component of gravitational mass attraction.

$$G_{sp} = \frac{\gamma_g M_o}{R^2}$$

$\overline{g}$: Planet's gravity field. (ft./sec.^{2})

$$\overline{g} = \overline{G} - \overline{W}_{IO} \times (\overline{W}_{IO} \times \overline{R})$$

$g_{(m)E}$: Mean value of gravity field at surface of Earth.

$$g_{(m)E} = 32.17405 \text{ ft./sec.}^2$$

H : Altitude of vehicle above planetary surface. (ft.)

h : Dimensionless altitude of vehicle above planetary surface:

$$h = \frac{H}{R_{(m)O}}$$

$I_n(x)$: n^{th} modified Bessel function of the first kind with argument x.

I_{sp} : Specific impulse of the rocket propellant (sec.)

I_t : Total impulse of rocket thrust (lb.-sec.)

i : Symbol used in complex numbers; defined as follows:

$$i^2 = -1$$

K : Exponential decay parameter of planetary atmosphere ($ft.^{-1}$)

$$\rho = \rho_{(SL)} e^{-KH}$$

K_{boltz} : Stefan-Boltzman constant = 4.81×10^{-13} BTU $ft.^{-2}$ $sec.^{-1}$ $^{\circ}R^{-4}$ where $^{\circ}R$ represents degrees Rankine.

K_{rad} : Vehicle surface radiation emissivity.

K_g : Radiation emissivity of atmospheric gas.

k : Dimensionless decay parameter of planetary atmosphere

$$k = KR_{(m)o}$$

$$\rho = \rho_{(SL)} e^{-kh}$$

k_1 : Ratio of rate of total heat input at any point on the surface of the entry vehicle with respect to the rate of total heat input at the stagnation point.

$$k_1 = \dot{Q}/\dot{Q}_s$$

L : Lift force (lb.)

l : One-half the latus rectum of the ellipse: $l = a(1 - \epsilon^2)$

l_N : Dimensionless semi-latus rectum of the ellipse.

$$l_N = \frac{l}{R_{(m)0}}$$

l_g : Unit path length of atmospheric gas.

$\mathcal{L}\{f(\tau)\}$: Laplace transform of $f(\tau)$

M_a : Mach number.

M : Instantaneous mass of vehicle (slugs)

m : Dimensionless instantaneous mass of vehicle: $m = \frac{M}{M_{initial}}$

M_0 : Mass of planet.

M_E : Mass of Earth.

N : Constant defined as follows in section 10.4:

$$N = \frac{L}{D} \frac{C}{2} r_i \, e^{-k \Delta r}$$

This number must be less than about 0.3 for degenerate orbital solution of 10.4 to be accurate.

n_L : Dimensionless lift load factor: $n_L = \frac{L}{MG_{(m)0}}$

n_D : Dimensionless drag load factor: $n_D = \frac{D}{MG_{(m)0}}$

P : Angular momentum per unit mass of the vehicle; twice the areal velocity of the instantaneous ellipse.

$$P = RV_{I\phi} = \frac{\pi ab}{T} \text{ ft.}^2/\text{sec.}$$

p : Dimensionless angular momentum.

$$p = \frac{P}{R_{(m)0}^{3/2} G_{(m)0}^{1/2}}$$

P_r : Prandtl number.

Q : Total heat input per unit surface area of entry vehicle (BTU/ft.^{2})

$$Q = Q_c + Q_r$$

Q_c : Total convective heat absorbed per unit area (BTU/ft.^{2})

Q_r : Total heat entering unit area by gaseous radiation (BTU/ft.^{2})

Q_{rad} : Total heat reradiated from unit surface area of vehicle (BTU/ft.^{2}).

$\mathcal{R}$: Radius of curvature of vehicle in vicinity of stagnation point (ft.)

R_h : Universal Gas Constant = 8.31 X 10^7 ergs/°Kelvin (i.e., work per degree Absolute temperature).

$\overline{R}$: Radius vector from center of planet to vehicle.

$\overline{r}$: Dimensionless radius vector from center of planet to vehicle.

$$\overline{r} = \frac{\overline{R}}{R_{(m)0}}$$

Δr : Incremental change in dimensionless radius from initial value. $\Delta r = r - r_i$

R_e : Reynolds number. $R_e = \rho \frac{V \times \text{length}}{\mu}$

$R_{(eq)0}$: Equatorial radius of planet 0.

$R_{(m)0}$: Mean radius of planet 0.

$R_{(p)0}$: Polar radius of planet 0.

S : Reference area of entry vehicle used in drag and lift computations (ft.^{2})

S_w : Wetted area of entry vehicle ($ft.^2$)

s : Complex variable used in the Laplace transform.

T : Period of elliptical orbit:

$$T = \frac{2\pi a^{3/2}}{\sqrt{\gamma_g M_0}}$$

T_N : Dimensionless period of elliptical orbit:

$$T_N = T\, V_S / R_{(m)0}$$

t : time (sec.)

t_b : Burning time of rocket (sec.)

T_S : Stagnation point temperature (degrees Rankine)

$(T_S)_{max}$: Maximum stagnation point temperature.

$T_{(m)0}$: Mean temperature of planet's atmosphere (degrees Kelvin)

T_t : Stagnation temperature of atmospheric gas (degrees Rankine)

U : Auxiliary quantity defined as follows:

$$U \equiv \frac{\rho_{(SL)}}{2} \frac{R_{(m)0}\, S}{M}$$

u : Independent parameter having no physical meaning introduced to describe propellant mass flow.

$\overline{V}$: Velocity vector of vehicle with respect to coordinates rotating with the planet.

v : Dimensionless velocity with respect to coordinates rotating with the planet.

$$v = \frac{V}{V_S}$$

$\overline{V}_I$: Velocity vector of entry vehicle with respect to inertial coordinates.

v_I : Dimensionless velocity of vehicle with respect to inertial coordinates. $v_I = V_I/V_S$

Δv : Incremental change in dimensionless velocity from initial value. $\Delta v = v - v_i$

$$\Delta v_I = v_I - v_{I_i}$$

$\overline{V}_{(AM)}$: Velocity vector of vehicle with respect to the planetary atmosphere (Note: $\overline{V} = \overline{V}_{(AM)}$ for no-wind condition).

$\overline{V}_{I(AM)}$: Velocity vector of planetary atmosphere with respect to inertial coordinates.

$\overline{V}_{O(AM)}$: Velocity vector of atmosphere with respect to coordinates totating with the planet (i.e., wind).

V_e : Equivalent exit velocity of rocket propellant (assumed constant)

v_e : Dimensionless equivalent exit velocity of rocket propellant.

$$v_e = \frac{V_e}{V_S}$$

V_C : Circular orbital velocity: $V_C = (GR)^{\frac{1}{2}}$

v_c : Dimensionless circular orbital velocity: $v_c = V_C/V_S$

V_S : Circular orbital velocity at surface of planet:

$$V_S = (G_{(m)O}R_{(m)O})^{\frac{1}{2}}$$

δV : Velocity impulse imparted at trajectory modification point by retrorocket system.

δv : Dimensionless velocity impulse imparted at trajectory modification point by retrorocket system:

$$\delta v = \frac{\delta V}{V_S}$$

δv_c : Dimensionless velocity impulse imparted at trajectory modification point by retrorocket system; non-dimensionalized with respect to circular satellite velocity <u>at the trajectory modification point</u>:

$$\delta v_c = \frac{\delta V}{V_C}$$

$\bar{W}_{IO}$: Daily sidereal angular velocity of the planet; a vector quantity directed along the polar axis (North) of the planet.

$\bar{W}_{IP}$: Vector angular velocity of the center of gravity of the entry vehicle with respect to inertial coordinates.

X : Distance flown - measured at surface of planet.

X_N : Dimensionless distance flown:

$$X_N = \frac{X}{R_{(m)O}}$$

x_1 : Constant defined in section 10.3 as follows:

$$x_1 \equiv \frac{\omega_c}{\sqrt{3}} \sinh\left[\frac{1}{3}\sinh^{-1}\left(\frac{C_c 3\sqrt{3}}{2\omega_c^3}\right)\right]$$

Y : A function of angle of attack, angle of sweep, and Mach number in convective heat transfer equation (7-1).

y_1 : A constant defined in section 10.3 as follows:

$$y_1 \equiv \omega_c \cosh\left[\frac{1}{3}\sinh^{-1}\left(\frac{C_c 3\sqrt{3}}{2\omega_c^3}\right)\right]$$

Z : Chapman's transformation variable. Equivalent to:

$$Z = \frac{v \cos\gamma \sin\gamma}{\xi\sqrt{k}}$$

A.4.3-2 Multiple Letter Symbols

(AC) : Dimensional acceleration constant for entry into the planetary atmosphere:

$$(AC) = \frac{\rho_{(SL)}\, G_{(m)O}\, R_{(m)O}}{2\, G_{(m)E}} \qquad \frac{slugs}{ft^2}$$

$(AC)_{EO}$: Ratio of acceleration constant of the planet to that of the Earth:

$$(AC)_{EO} = \frac{(AC)}{(AC)_E}$$

$(HR)_{EO}$: "Heating Ratio" of the atmosphere of planet with respect to Earth:

$$(HR)_{EO} = \left[\left(\frac{\mu_{(SL)}}{\mu_{(SL)E}}\right)^{\frac{1}{2}}\left(\frac{G_{(m)O}}{G_{(m)E}}\right)^{\frac{3}{2}}\left(\frac{R_{(m)O}}{R_{(m)E}}\right)^{\frac{5}{4}}\left(\frac{K}{K_E}\right)^{\frac{1}{4}}\left(\frac{Pr}{Pr_E}\right)^{-\frac{2}{3}}\left(\frac{\left(\frac{\gamma_O - 1}{\gamma_O}\right)}{\left(\frac{\gamma_E - 1}{\gamma_E}\right)}\right)^{\frac{1}{4}}\right]$$

$(HF)_O$: "Heating Function" of the planetary atmosphere.

$$(HF)_O = \rho_{(SL)}^{\frac{1}{2}}\left(\frac{R_{(m)O}}{K}\right)^{\frac{1}{4}}(HR)_{EO} \qquad (slug/ft^2)^{\frac{1}{2}}$$

$(HF)_{EO}$: Ratio of the heating function of the planetary atmosphere to the heating function of the Earth's atmosphere.

$$(HF)_{EO} = \frac{(HF)_O}{(HF)_E}$$

(TC) : "Temperature Constraint Constant" -- a constant for a particular vehicle entering the atmosphere of a particular planet:

$$(TC) \cong \frac{1.392 \times 10^4}{(T_S)_{max}}\,(HF)_{EO}^{\frac{1}{4}}\,(VF)^{\frac{1}{4}}$$

(VF) : Vehicle function.

$$(VF) = \frac{1}{K_{rad} R^{\frac{1}{2}}}$$

Values of the above quantities which are constant for the planet are listed in Table A-2 for the terrestrial planets.

Table A-2: Approximate values of Heating and Acceleration Constants for the Terrestrial Planets

	Venus	Earth	Mars
(AC)	$2.86 \times 10^5 \frac{slug}{ft.^2}$	$2.49 \times 10^4 \frac{slug}{ft.^2}$	$3.44 \times 10^2 \frac{slug}{ft.^2}$
$(AC)_{EO}$	11.5	1.0	0.0138
$(HR)_{EO}$	0.7	1.0	0.09
$(HF)_O$	$104.8 \frac{slug^{\frac{1}{2}}}{ft.}$	$43.5 \frac{slug^{\frac{1}{2}}}{ft.}$	$1.1 \frac{slug^{\frac{1}{2}}}{ft.}$
$(HF)_{EO}$	2.41	1.0	0.0253
$(HF)^{\frac{1}{4}}_{EO}$	1.25	1.0	0.4

A.4.3-3: Greek Symbols

α : angle of attack

β : Bearing angle of entry vehicle as seen by an inertial

observer in the vehicle; angle between North (1_Λ) and tangential velocity vector of vehicle (directed along 1_ϕ).

β_1 : An auxiliary real variable (Eq. 7-26).

γ_I, γ : Flight path angle in inertial framework and planetary axes, respectively.

γ_O : Ratio of heat capacity of the atmosphere of planet O.

$$\gamma_O = \frac{C_P}{C_v}$$

γ_E : Ratio of heat capacity of the Earth's atmosphere.

γ_g : Universal Gravitational Constant = $6.658 \times 10^{-11} \frac{m^3}{KG\text{-}sec.^2}$

Γ : Propellant mass flow rate (slugs per sec.)

Γ_N : Dimensionless propellant mass flow rate:

$$\Gamma_N = \frac{\Gamma}{M_i} \sqrt{\frac{R_{(m)o}}{G_{(m)o}}}$$

$\delta( )$: Variation of the quantity in parenthesis.

$\delta( )$: Incremental change of quantity in parenthesis from initial value; e.g., $\Delta r = r - r_i$

ε : Eccentricity of ellipse $\varepsilon = \sqrt{1 - (b/a)^2}$

ε_1 : Component of eccentricity along major axis: $\varepsilon_1 = \varepsilon \cos \theta$

ε_2 : Component of eccentricity along minor axis: $\varepsilon_2 = \varepsilon \sin \theta$

ε_E : Eccentricity of the Earth: $\varepsilon_E = \sqrt{0.0067226700}$

ζ_1 : An auxiliary real variable (Eq. (7-26))

ζ_2 : An auxiliary real variable (Eq. (7-32))

η : angle measured in the plane of an elliptical trajectory from the ascending line of nodes to the line of apsides.

η_1 : An auxiliary variable (Eq. (7-27))

θ : True anomaly; angle measured from line of apsides in the ellipse to the position of the vehicle.

Θ : Angle defined as follows in equation (9-97):

$$\Theta \equiv \left(\gamma_i^2 + \frac{2UC_D\left(\frac{L}{D}\right)\sigma_i}{k}\right)^{\frac{1}{2}}$$

λ : Geocentric longitude of the vehicle; i.e., equatorial angle measured from planet's X_0 axis to the vehicle.

λ_{IP} : Inertial geocentric longitude of the vehicle; i.e., equatorial angle measured from planet's X_I axis to the vehicle.

λ_{IT} : Inertial geocentric longitude of ascending line of nodes; i.e., angle measured in equatorial plane between X_I and X_T.

$\lambda_1 \cdots \lambda_n$: Lagrange Multipliers

Λ : Geocentric latitude; angle measured between the radius vector from the planet center to the vehicle and the projection of this vector on the planet's equatorial plane.

Λ_g : Geographic latitude; angle measured between the normal to the reference ellipsoid of the planet and the projection of this normal on the equatorial plane.

μ : Coefficient of viscosity of the planet's atmosphere (slug/ft-sec)

μ_E : Coefficient of viscosity of the Earth's atmosphere.

ν : Dimensionless constant describing non-spherical component of planet's gravitational potential.

ξ : The negative of the ratio of percentage change in radial distance of the entry vehicle from the planet center to the percentage change in horizontal component of the vehicle's velocity with respect to inertial coordinates.

$$\xi = -\frac{\dot{R}/R}{\dot{V}_{I\phi}/V_{I\phi}}$$

ξ is used in the definition of the "Conservation Parameter". Conservation Parameter = $\left|\frac{1-\xi}{\xi}\right|$

π : Pi (3.1416)

ρ : Free stream atmospheric density (slug/ft.^{3})

$\rho_{(SL)}$: Sea Level or surface value of atmospheric density (slug/ft.^{3})

$\rho_{(\overline{SL})}$: The intercept of the straight line which best fits a curve of log ρ vs altitude (not the same as true sea level density).

σ : Atmospheric density ratio: $\sigma = \frac{\rho}{\rho_{(\overline{SL})}} \cong e^{-\beta h}$

$\sum_{n=1}^{\infty}(\ )_n$: Summation of quantities in parenthesis

τ : Dimensionless time $\tau = \frac{V_S}{R_{(m)O}} t = \sqrt{\frac{G_{(m)O}}{R_{(m)O}}}\, t$

ϕ : angle measured in plane of trajectory in direction of motion from line of nodes to the vehicle.

$\overline{\Phi}$: Gravitational potential (potential energy per unit mass). In this thesis, the gravitational potential of the Earth is assumed to be:

$$\overline{\Phi} = \frac{-\gamma_g M_E}{R}\left[1 - \frac{\nu R^2_{(eq)E}}{R^2}(1 - 3\cos 2\Lambda)\right]$$

Ψ : Angle of inclination of the trajectory; angle measured from equatorial plane to the trajectory plane (Fig. A-2).

Θ : A constant for the skipping trajectory solution:

$$\Theta = \left(\gamma_i^2 + \frac{2UC_D\left(\frac{L}{D}\right)\sigma_i}{\beta}\right)^{1/2}$$

Ω : Dimensionless angular velocity of the planet about its polar axis:

$$\Omega = W_{IO}\sqrt{\frac{R_{(m)O}}{G_{(m)O}}}$$

ω : Average angular velocity in the degenerate elliptical trajectory:

$$\omega^2 = \left(\frac{2}{r_i} - v_i^2\right)^3$$

ω_t : Angular velocity in the decaying circular orbital trajectory:

$$\omega_t^2 = \left(\frac{v_i}{r_i}\right)^2\left(1 + Cr_i\frac{L}{D}\right)$$

A.5 Summary of Physical Constants of the Planets and Atmospheres

Table A.3 summarizes values of various physical characteristics of the planets and their atmospheres used in the numerical calculations in this thesis. New observations and calculations revise existing data frequently; hence complete agreement is seldom found between any two tables of this type. Much of the physical data concerning many of the planets is fragmentary; large scale revisions may be expected when additional data is obtained from artificial satellites and planetary probes.

Table A.3: Summary of Planetary Atmospheric and Physical Data		
	(a) Data on the planet Earth:	
$R_{(eq)E}$	= 6,378,388 ± 18 meters = 3963.3386 statute miles = 20,926,428 ft.	Ref. (55)
$R_{(p)E}$	= 6,356,911.946 meters = 3949.9941 statute miles = 20,855,969 ft.	Ref. (55)
$R_{(m)E}$	= 20,888,104 ft.	Ref. (55)
Ellipticity	$= \frac{R_{(eq)E} - R_{(p)E}}{R_{(eq)E}} = 1/297 = .0033670034$	Ref. (55)
ε_E^2	= 0.0067226700	Ref. (55)
W_{IE}	= 7.2921159 X 10^{-5} rad/sec.	Ref. (55)
$\gamma_g M_E$	= $(1 \pm 8 \times 10^{-5})(3.986329 \times 10^{20}$ cm.^{3}/sec.^{2}) $0.14077500 \times 10^{17}$ ft.^{3}/sec.^{2}	Ref. (56)
$G_{(m)E}$	= 32.22848 ft./sec.^{2}	
$g_{(m)E}$	= 32.17405 ft./sec.^{2}	
6ν	= 1.638 X 10^{-3}	Ref. (56)

Table A.3 (cont.)

(b) Data on other planets

	Venus	Earth	Mars	Jupiter
$R_{(m)O}$	20.27×10^6 ft.	20.89×10^6 ft.	11.08×10^6 ft.	230×10^6 ft.
$R_{(m)O}/R_{(m)E}$	0.97	1.0	0.5313	11.0
$G_{(m)O}/G_{(m)E}$	0.91	1.0	0.38	2.64
Atmospheric Gases	CO_2, N_2	N_2, O_2	N_2, CO_2	He, H_2, CH_4
μ_O/μ_E	0.8	1.0	1.0	0.5
Mean molecular wgt. (gm/mole)	40	29	30	3
$T_{(m)O}$ (°K)	270	240	220	170
1/K ft.	2.0×10^4	2.35×10^4	6×10^4	6×10^4
k/k_E	1.14	1.0	0.207	4.32
k	1013	889	184.6	3840
Ω	2.69×10^{-4}	.0587	.0675	
$\rho_{(SL)}$ $\frac{\text{slug}}{\text{ft.}^3}$	.0326	.002378	.000193	
$\rho_{(\overline{SL})}$ $\frac{\text{slug}}{\text{ft.}^3}$		.0027		
$\frac{\rho_{(SL)}}{\rho_{(\overline{SL})E}}$	12.1	0.88	.0604	

APPENDIX B

PHYSICAL CHARACTERISTICS OF MAJOR BODIES OF THE SOLAR SYSTEM

The solar system is the collection of bodies, of which the Earth is one, that are distinguished from all other bodies in the universe by having the Sun as the center of motion. The bodies of this system may be classified under the following headings:

(1) Sun

(2) Planets

(a) The four inner planets -- Mercury, Venus, Earth, and Mars -- are relatively small, dense bodies and are known as the "terrestrial" planets.

(b) The next four in distance from the Sun -- Jupiter, Saturn, Uranus, and Neptune -- are often called the "major" or "giant" planets. These are relatively large bodies composed principally of gases with solid ice and rock cores at unknown depths below the visible upper surfaces of their atmospheres.

(c) Pluto, recently discovered (1930), has relatively unknown physical characteristics.

(3) Natural Satellites of the Planets

Thirty-one moons have been discovered to date (1959). The system formed by a planet and its satellites is distinguished by the name of the planet, such as the Martian system, the Jovian system, the Saturnian system.

(4) Asteroids

Some 2000 minor planets have been discovered; others are being discovered each year. The largest, Ceres, has a diameter of 480 miles. Most of the rest are less than 50 miles wide. The

majority move between the orbits of Mars and Jupiter. Most families of asteroids seem strongly influenced by Jupiter, and move in orbits determined by the gravitational attraction of Jupiter and Sun.

(5) Comets

About 5-10 new comets are discovered yearly. Comets are very loose collections of orbital material that sweep into the inner regions of the solar system from space far beyond the orbit of Pluto. Some return periodically; some never do. The body of the comet probably consists of rarified gases and and dust; the heads are thought to be frozen gases or "ices".

(6) Meteors

Meteors exist in untold millions. Meteor fragments that reach the ground are known as meteorites. The average meteor weights 0.0005 ounce[57] and over 100 million strike the Earth's atmosphere daily. F.C. Leonard (1952) [58] estimated the amount of meteoric material falling upon the earth, including the ashes of burned out meteors and unburned micro-meteorites, to be 6000 metric tons daily. This estimate was much larger than former ones, but is confirmed by the work of Hans Pettersson and Henri Rotschi in Sweden. A more recent estimate made by Harvard Observatory favors a value of 2,000 tons per day[59]. Soviet scientists announced in August 1958 that their satellite data indicated an estimate of 8 to 10 x 10^5 tons per day[60].

(7) Micrometeorites and Dust

The smallest dust particles (micrometeorites) are concentrated primarily either in the ecliptic plane* or along the orbits of comets[61]. Evidence that cosmic dust is concentrated in the plane of the ecliptic consists of observations of a faint tapered band of light centered along the ecliptic, called the zodiacal light.

A brief summary of physical data on principal bodies of the solar system is given in Table B-1. New discoveries together with more complete observations and calculations revise existing data frequently.

Table B-2 summarizes physical and astronomical data collected concerning the principal natural satellites of planets in the Solar System.

- - - - - - - - - - - - - - - - -

* Plane of the Earth's orbit about the Sun.

Table B.1: Summary of Physical Data on Principal Bodies of Solar System

Note: Superscript numerals refer to notes at end of table.

	Mass M_o (Earth = 1.0)	Volume (Earth = 1.0)	Density (Earth = 1.0)	Density (Water = 1.0)
☉ Sun	332,500	1,306,000	0.255	1.41
☿ Mercury	0.0543	0.06	0.76	4.0
♀ Venus	0.8136	0.92	0.89	4.9
⊕ Earth	(4.09×10^{23} slugs)*	1.0	1.00	5.52
♂ Mars	0.1069-.1076	0.15	0.69	3.9
♃ Jupiter	318.35	1,318	0.241	1.32
♄ Saturn	93.3	736	0.13	0.72
♅ Uranus	14.54	64	0.23	1.25
♆ Neptune	17.2	60	0.29	1.6
Pluto	0.8	0.07	> 0.9	?
☾ Moon	0.0123	0.02	0.607	-

	$\gamma_g M_o$ ($ft.^3/sec.^2$)	Equatorial Radius $R_{(eq)o}$ (naut. mi.)	Gravitational Accel. at Surface $G_{(m)o}$ ft./sec.^{2}	(Earth 1.0)
Sun	4.679×10^{21}	375,600	900(2)	27.9
Mercury	7.645×10^{14}	1,350	11.4	0.25
Venus	1.145×10^{16}	3,348	27.7	0.91
Earth	1.406×10^{16}	3,440	32.2	1.00
Mars	1.515×10^{15}	1,787	13.2	0.38
Jupiter	4.467×10^{18}	37,700	90.8(3)	2.64
Saturn	1.338×10^{18}	31,100	41.8(3)	1.17
Uranus	2.046×10^{17}	13,800(1)	31.4(3)	0.92
Neptune	2.423×10^{17}	13,500(1)	36.8(3)	1.12
Pluto	1.123×10^{16}	1,575	25.7(?)	0.8
Moon	1.73×10^{14}	938	5.32	0.17

	Circular Satellite Velocity at Surface $V_s = \sqrt{G_{(M)_o} R_{(M)_o}}$ ft/sec	Surface Escape Velocity (ft/sec)	Surface Escape Velocity (km/sec)	Minimum launch Velocity to reach Earth (ft./sec.)	Transit Time
Sun	1.43×10^6				
Mercury	9,655	13,600	4.3	44,000	110 days
Venus	23,730	33,600	10.4	38,000	150 d
Earth	25,950	36,700	11.3	-	-
Mars	11,810	16,700	5.1	38,000	260 d
Jupiter	139,600	197,000	61.0	46,000	2.7 years
Saturn	84,170		36.7	49,000	6 years
Uranus	51,420		22.4	51,000	16 years
Neptune	54,350		25.5	52,000	31 years
Pluto	15,650		3 ?	53,000	46 years
Moon	5,500				

* $5.966 \pm .001 \times 10^{27}$ gms.

Table B-1 (cont.)

	Mean Distance from Sun		Orbital Distance	
	Astronomical Units[4]	Millions of miles	Perihelion ($\times 10^9$ ft.)	Aphelion ($\times 10^9$ ft.)
Sun				
Mercury	0.387	36	151	229
Venus	0.723	67	353	357
Earth	1.00	92.9	483	499
Mars	1.524	142	679	817
Jupiter	5.203	483	2430	2680
Saturn	9.539	886	4520	4940
Uranus	19.19	1,782	8960	9860
Neptune	30.07	2,793	14610	14870
Pluto	39.46	3,670	14510	24100
Moon	1.00	92.9	1.170	1.334

	Orbital Speed (ft./sec.)		Eccentricity of Orbit	Orbital Period
	Perihelion	Aphelion		
Sun				
Mercury	176,000	143,000	.206	88 days
Venus	115,000	114,500	.007	224 d 17 hrs.
Earth	98,500	96,800	.017	365 d 6 hr. 9 min.
Mars	83,000	75,700	.093	687 days
Jupiter	43,900	41,800	.048	4328 days
Saturn	32,200	30,800	.056	29 years 167 days
Uranus	22,800	21,800	.047	84.01 yrs.
Neptune	17,900	17,700	.0086	164.8 yrs.
Pluto				248 yrs.
Moon	3,480	3,260	.055	27 d 7 h 43 m

	Orbital Inclination to Ecliptic Plane	Length of Day	Inclination of Equator	Number of Moons
Sun		24.65^d (5)	7° 10'	
Mercury	7° 1'	88.0 ^{d} (6)	?	0
Venus	3° 24'	224.7 ^{d}	?	0
Earth	0° 0'	24 ^{h}	23° 27'	1
Mars	1° 51'	24.6^h	25° 10'	2(7)
Jupiter	1° 18'	9^h 50^m	3° 7'	12(8)
Saturn	2° 29'	10^h	26° 45'	9(9)
Uranus	0° 46'	10.7^h	98°	5(10)
Neptune	1° 45'	15.7^h	29°	2(11)
Pluto	17° 9'	(?)		0 (?)
Moon	18° 19' to 28° 35' from Earth's equator	27^d		0

Table B-1 (cont.)

	Distance from Earth (millions of miles)		Intensity of Sunlight at mean distance Earth = 1.0	Total Radiation Flux	
	Greatest	Least		watts/ft.^{2}	kw/meter^2
Sun	94.6	91.5			
Mercury	138	48(12)	6.7	835	8.95
Venus	162	26	1.9	238.6	2.55
Earth	-	-	1.0	125	1.34
Mars	234	35	0.43	54.1	0.58
Jupiter	602	367	0.37	4.62	0.0496
Saturn	1031	745	0.11	1.37	0.0147
Uranus	1964	1606	0.0027	0.339	0.00364
Neptune	2915	2678	0.0011	0.139	0.00149
Pluto	4680	2650	0.0006	0.080	0.000859
Moon					

	Ellipticity $\frac{R_{(eq)0} - R_{(p)0}}{R_{(eq)0}}$	Theoretical Radiation Temperature	
		Maximum °K	Average °K
Sun			
Mercury	0	625	-
Venus	0	324	229
Earth	.0033670034	349	246
Mars	.005215	307	217
Jupiter	.0649	145	102
Saturn	.1053	107	76
Uranus	.0714	69	49
Neptune	.0254	56	40
Pluto		60	42
Moon		387	274

Table B-1 (cont.)

Superscript numerical notes of Table B-1.

(1) These values are based on 1950 observations of Kuiper. This diameter of Neptune is 3,300 miles less than usually given. The diameter and volume of Pluto by these observations is considerably less than earlier values.

(2) Has no solid surface.

(3) Location of solid surface (below thousands of miles of dense atmospheric gases covering these planets) is not known; hence gravitational figures at surface are not reliable for the four giant planets.

(4) The "astronomical unit", a fundamental unit of astronomy, is the mean distance of the Sun from the Earth. "Solar parallax" is defined as an arc whose tangent is the radius of the Earth divided by the mean distance of the Earth from the Sun.

For over 2000 years, increasingly accurate determinations of the solar parallax have been made. From about 1900-1940, astronomers were confident that the value of solar parallax was 8.80", with the error in its determination not greater than 0.01". The asteroid Eros, roughly a cylindrical body 5 miles in diameter and 20 miles long, provided a means for recent readjustment in the value of solar parallax. The nearest approach of Eros to the Earth is approximately 10 million miles; its last opposition (1930) was about 16 million miles. Approximately 2500 photographs of Eros, taken in 1930-31, were analyzed in great detail by Sir Harold Spenser Jones over a 10-year period; his determination of solar parallax gave the unexpectedly low value of 8.790" with an estimated accuracy of 1 part in 10,000. Considering the scope of Jones' work, his figure hardly seemed open to question.

Recently, however, a new determination of solar parallax, along with other fundamental data, was published by Eugene Rabe. He made a full rediscussion of all the observations of Eros from 1926 to 1945 and secured a solar parallax value of 8.79835" ± 0.00039", which is much closer to the old value of 8.80" than that of Jones. As a byproduct, the ratio of the masses of the Earth to Moon is 81.375 and of Sun to Earth plus Moon is 328,452. He also secured improved values for the masses of Mercury, Venus, and Mars. There are indeed several very small asteroids which approach the Earth closer than does Eros, and hence might be expected to give better results. Thus far, however, they have proved unavailable because of their extreme faintness and the uncertainty of their orbits.

(5) Period of rotation on axis.

Table B-1 (cont.)

(6) Mercury's rotation period equals its period of revolution about the sun; hence one side always faces the sun. Temperatures here are as high as 750° F. above zero; on the other side, perhaps hundreds of degrees below zero.

(7) Mars' moons, Deimos and Phobos, are about 10 miles in diameter. The inner one (Phobos) revolves so fast that it rises and sets three times in a Martian day.

(8) Four of the moons have diameters of 2,300 to 3,200 miles and revolve about Jupiter in 2-17 days. The other 8 moons are less than 100 miles in diameter. One, very close to Jupiter, revolves at over 1,000 miles per minute. The 12th moon was discovered by S.B. Nicholson of Mt. Wilson and Palomar Observatories in 1951. It is only 14 miles in circumference, 2×10^6 miles from the planet, and circles Jupiter in 700 days retrograde motion (east-to-west). Four of Jupiter's moons are characterized by retrograde motion.

(9) One of Saturn's moons is larger than the Earth's moon and is believed to have an atmosphere. All nine moons are outside the rings characteristic of this planet.

(10) The fifth satellite of Uranus, Miranda, was discovered in February 1948 by Kuiper.

(11) The second satellite of Neptune (Nereid) was discovered on 1 May 1949 by Kuiper. It has a period of 359 days and ranges from 830,000 to 6,100,000 miles with major orbit axis of 0.074 a.u., eccentricity of 0.76 (greater than for any other satellite), and inclination of 5° to ecliptic plane. The first satellite of Neptune is called Triton.

(12) The closest approach of any planet to Earth.

Table B-2: Summary of Physical Data on Principle Natural Satellites of Planets**

Body Name	Parent Planet	Distance from Planet (KM)	Period of Revolution	Orbital Eccentricity
Moon	Earth	384,400	$27^d\ 7^h\ 43.2^m$	0.0549
Phobos	Mars	9.35×10^3	$7^h\ 39.2^m$	0.021
Deimos	Mars	2.35×10^4	$1^d\ 6^h\ 17.9^m$	0.003
J I	Jupiter	4.22×10^5	$1^d\ 18^h\ 27.6^m$	0.0
J II	"	6.714×10^5	$3^d\ 13^h\ 13.7^m$	0.0003
J III	"	1.071×10^6	$7^d\ 3^h\ 42.6^m$	0.0015
J IV	"	1.884×10^6	$16^d\ 16^h\ 32.2^m$	0.0075
J V	"	1.815×10^5	$11^h\ 57.4^m$	0.0028
J VI	"	1.15×10^7	$250^d\ 16^h\ 48^m$	0.155
J VII	"	1.175×10^7	260^d	0.207
J VIII*	"	2.35×10^7	739^d	0.29-0.45
J IX*	"	2.37×10^7	758^d	0.1 -0.4
J X	"	1.175×10^7	260^d	0.08
J XI*	"	2.25×10^7	692^d	0.21
J XII*	"	3.2×10^6	700^d	
Mimas	Saturn	1.857×10^5	$22^h\ 37.1^m$	0.019
Enceladus	"	2.382×10^5	$1^d\ 8^h\ 53.1^m$	0.0001
Tethys	"	2.948×10^5	$1^d\ 21^h\ 18.4^m$	0.0
Dione	"	3.377×10^5	$2^d\ 17^h\ 41.2^m$	0.002
Rhea	"	5.275×10^5	$4^d\ 12^h\ 25.2^m$	0.0009
Titan	"	1.223×10^6	$15^d\ 22^h\ 41.4^m$	0.0289
Hyperion	"	1.484×10^6	$21^d\ 6^h\ 38.4^m$	0.1043
Japetus	"	3.563×10^6	$79^d\ 7^h\ 55.5^m$	0.0284
Phoebe*	"	1.295×10^7	$550^d\ 10.1^m$	0.1659
Ariel*	Uranus	1.918×10^5	$2^d\ 12^h\ 20.4^m$	0.007
Umbriel*	"	2.673×10^5	$4^d\ 3^h\ 27.6^m$	0.008
Titania*	"	4.387×10^5	$8^d\ 16^h\ 56.5^m$	0.023
Oberon*	"	5.866×10^5	$13^d\ 11^h\ 7.1^m$	0.01
Miranda	"			
Triton*	Neptune	3.54×10^5	$5^d\ 21^h\ 2.7^m$	0.0
Nereid	"	1.34 to 9.72×10^6	359^d	0.76

* Satellites indicated by asterisk are characterized by retrograde motion. Motion of Miranda and Nereid is not known.

** Most of this data was taken from reference (62).

Table B-2 (cont.)

Body	Diameter KM	Mass Earth=1.0***	Mean Density Water=1.0	Surface Gravity ft/sec^2	Escape Velocity ft/sec	Theoretical Radiation Temp. °Kelvin Max.	Ave.
Moon	3476	0.0123	3.35	5.31	7873	387	274
Phobos	15						
Deimos	8						
J I	3730	0.0121	4.03	4.3	7476	140	99
J II	3150	0.0079	3.78	4.13	6541	137	97
J III	5150	0.0260	2.35	5.1	9288	156	110
J IV	5180	0.0162	2.06	3.16	7325	166	117
J V	75-150						
J VI	120						
J VII	50						
J VIII	50						
J IX	22						
J X	20						
J XI	25						
J XII	7.2						
Mimas	450	6×10^{-6}	0.5	.1635	491	85	60
Enceladus	500	14×10^{-6}	0.7	.3	702	85	60
Tethys	1100	1.09×10^{-4}	1.2	.467	1298	85	60
Dione	1100	1.76×10^{-4}	2.8	.745	1637	85	60
Rhea	1600	3.8×10^{-4}	2.0	.752	1987	85	60
Titan	4200	2.35×10^{-2}	2.42	7.0	9811	118	83
Hyperion	400	$<7. \times 10^{-6}$		.24	560		
Japetus	1300	2.4×10^{-4}		.715	1747		
Phoebe	300						
Ariel	500						
Umbriel	400						
Titania	1000						
Oberon	900						
Miranda							
Triton	4500	.022	2 ?	5.71	9177	68	48
Nereid							

*** Mass of Earth = $5.966 \pm .001 \times 10^{27}$ gms $= 4.09 \times 10^{23}$ slugs

APPENDIX C

GRAVITATIONAL MASS ATTRACTION AND THE ACCELERATION OF GRAVITY

C.1: Gravitation

According to Newton's law of gravitation, every particle in the universe attracts every other particle with a force varying directly as the product of the two masses and inversely as the square of the distance between them.

$$\text{Force} = \frac{\gamma_g M M_1}{R^2} \qquad \text{(C-1)}$$

γ_g is a universal constant whose numerical value is approximately:

$$\gamma_g = 6.658 \times 10^{-11} \frac{m^3}{KG - sec.^2} \qquad \text{(C-2)}$$

A single fixed mass point of mass M will exert a force on any other particle according to equation (C-1). All space is affected by the mass M; a field of force is set up around the mass. The same general statement is true for any system of bodies; at each point in space a force vector can be drawn which is the vector sum of the forces acting on the mass M by the system of bodies M_1, M_2, ...M_n. The tangents to the force vectors at each point in space give the direction of the force exerted on the mass at every point. The curves map out the field

and are called lines of force.

For the case of a single particle, the lines of force consist of straight lines radiating in all directions from the particle as a center. The lines of force give information as to the direction but not as to the magnitude of the gravitational forces. The latter is specified by introducing the intensity of the force field: the force per unit mass exerted on a particle at any given point. The intensity of the gravitational field is denoted by G; for a single particle of mass M:

$$G = \frac{\text{Force}}{M_1} = F = \frac{\gamma_g M}{R^2} \qquad \text{(C-3)}$$

G is a vector whose magnitude is given by (C-3) and whose direction is inward along the line connecting the masses. For a system of particles the intensity of the field is calculated by vector addition, the resultant intensity being the vector sum of the intensities due to the individual particles.

Gravitational forces are conservative[19], and it is normal to call the fields conservative*. It is convenient to introduce the gravitational potential $\overline{\phi}$, defined as the potential energy per unit mass. For the case of the field of a single particle, the gravitational potential is

$$\overline{\phi} = -\frac{\gamma_g M}{R^2} \qquad \text{(C-4)}$$

and the gravitational intensity vector $\overline{G}$ is the negative gradient of

- - - - - - - - - - - - - - - - -

* A conservative field is defined as one in which the total work done is zero in moving a particle around any closed contour in the field. In moving a particle between any two points in a conservative field, the work done is independent of the path chosen between the points.

the potential $\overline{\Phi}$.

$$\overline{G} = - \nabla \overline{\Phi} \qquad \text{(C-5)}$$

The gravitational field intensity $\overline{G}$ at a point outside a spherical planet is determined by considering the planet to be composed of thin spherical shells, each of constant density. Each spherical shell acts as if its mass were concentrated at the center. Therefore, at any point outside the planet, the gravitational field intensity vector is directed toward the center of the planet with a magnitude directly proportional to the product of the gravitational constant times the mass of the planet and inversely proportional to the square of the distance from the center of the planet to the point.

$$\overline{G} = - \frac{\gamma_g M_O}{R^2} \frac{\overline{R}}{R} \qquad \text{(C-6)}$$

where M_O is total mass of the planet. This result is identical with that for a single particle given in equation (C-3).

C.2 Gravitational Field of Oblate Spheroidal Planets

If the planet were a nonrotating fluid mass, it would form a sphere under the influence of its own gravitational field. Because of rotation about an axis through the planet, the associated centrifugal force field causes the planet to bulge at the equator. In the case of Mercury, the axial rate of rotation is extremely small*, hence the planet must be very nearly a perfect sphere (except for surface anomalies --

- - - - - - - - - - - - - - - - -

* Mercury's day and year are both equal to approximately 88 Earth days.

mountains and valleys). Little is known about the rotational rate of Venus since the surface is not visible through the opaque atmosphere. The best guess is that Venus, too, has equal days and years (224.7 Earth days). Consequently, Venus should be almost a perfect sphere (except for mountains, etc.)

Earth, Mars, and the giant planets have relatively high rotational velocities*. Mars rotates at almost Earth's rate, hence should have nearly the same equatorial bulge as Earth. Jupiter, Saturn, and Uranus have days that range from 9.8 to 10.7 hours, and Neptune's day is slightly under 16 hours. Consequently, the equatorial bulge of these giants is much more pronounced than Earth -- a fact verified by astronomic photographs.

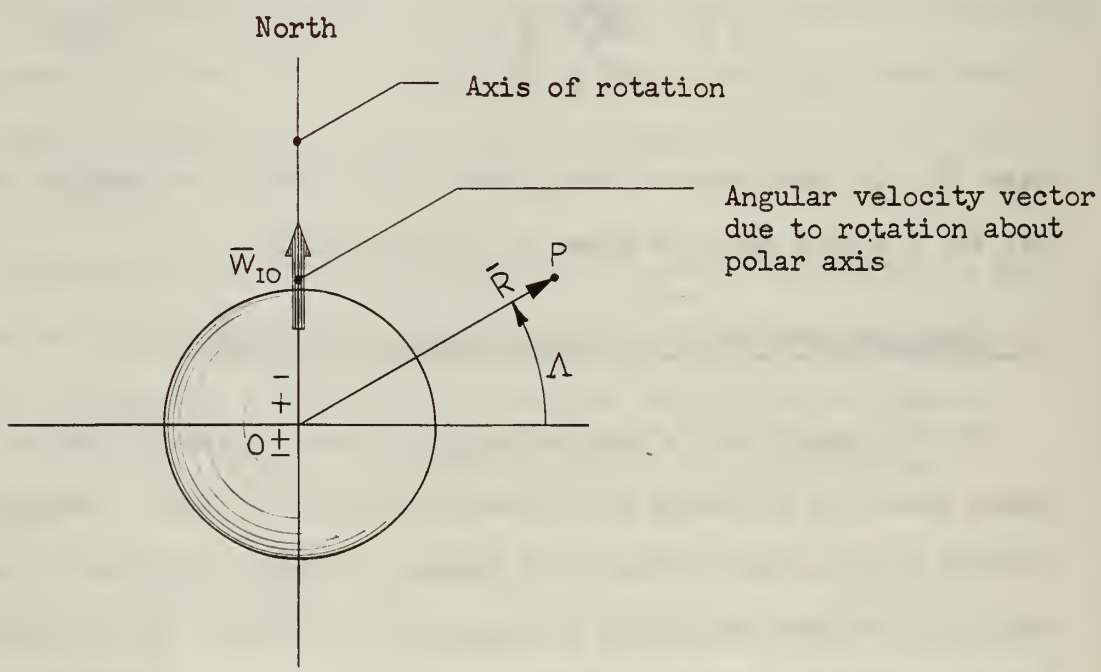

Fig. C.1: Gravitational Field of Oblate Spheroidal Planet

- - - - - - - - - - - - - - - - - -

* See Table B.1.

Due to the interaction of gravitational mass attraction and the centrifugal force due to axial rotation, the actual shape of rotating planets is nearly ellipsoidal, or oblate spheroidal. Because of the non-spherical mass distribution of the planet, its gravitational field is not spherically symmetric. A first order approximation of the non-spherical component of gravitational field intensity may be made by considering it as a quadrupole moment. Fig. C.1 shows two sources and two sinks of equal strength located on the polar axis of the planet near its center to represent the non-spherical mass component. The two sources are located at the center and the two sinks are symmetrically spaced on the polar axis above and below the center. The positions of the sinks approach the center, while the product of strength and spacing remains constant. The quadrupole thus is similar to a pair of dipoles that have mirror symmetry. The gravitational potential including this oblateness quadrupole may be considered to be [63]:

$$\overline{\Phi} = - \frac{\gamma_g M_0}{R} \left[1 - \frac{\nu R^2_{(eq)0}}{R^2} (1 - 3\cos 2\Lambda) \right] \qquad \text{(C-7)}$$

$$\overline{G} = - \nabla \overline{\Phi} \qquad \text{(C-8)}$$

In equation (C-7), ν is a dimensionless constant for the planet, Λ is geocentric latitude, and $R_{(eq)0}$ is equatorial radius of the planet. For the planet Earth, reference (63) lists the value of ν as follows:

$$6\ \nu_E = (1.637 \pm .004) \times 10^{-3} \qquad \text{(C-9)}$$

Ref. (56) gives a value of ν for the international ellipsoid* of Earth as follows:

$$6\ \nu_E = 1.638 \times 10^{-3} \qquad \text{(C-10)}$$

and the value of $\gamma_g M_0$ for Earth as follows:

$$\gamma_g M_E = (1 \pm 8 \times 10^{-5})\ (3.986329 \times 10^{20}\ \text{cm.}^3/\text{sec.}^2)$$

$$= 0.14077500 \times 10^{17}\ \text{ft.}^3/\text{sec.}^2 \qquad \text{(C-11)}$$

C.3 Gravity

The surfaces for which $\overline{\Phi}$ is constant are <u>not</u> oblate spheroids, nor does one surface coincide with the assumed geometric figure of the planet. The surface $\overline{\Phi}$ equal to a constant are everywhere normal to the gravitational field intensity vector of the planet. The vector sum of the planet's gravitational specific force** and centrifugal force

- - - - - - - - - - - - - - - - -

* The Hayford Spheroid of 1909 is the international reference ellipsoid of the Earth. At the Internationale Geodetic and Geophysical Union of 1924, the dimensions of the Earth summarized in Table A.3 were adopted (see Table 716, page 570 of ref. 55).

** Gravitational specific force $\overline{G}$ is identical with gravitational field intensity. Centrifugal specific force, a reaction force, is equal in magnitude but opposite in direction to the associated centripetal acceleration. <u>Specific force</u> is expressed in force-per-mass dimensions.

per unit mass is defined as the planet's gravity field intensity.*

$$\bar{g} = - \nabla\bar{\Phi} - \bar{W}_{IO} \times (\bar{W}_{IO} \times \bar{R}) \qquad (C\text{-}12)$$

where

$\bar{\Phi}$ is given by equation (C-7)

$\bar{R}$ is the vector from the center of the planet to a point on or external to the surface of the planet

W_{IO} is the angular velocity of the planet about its polar axis.

The tangential component of the first term in Equation (C-12) prevents the oceans of the Earth from flowing toward the equator. The direction of gravity is normal to the surface of the planet; if gravity anomalies are neglected, this direction is unique at each point on the surface. The time variation of the direction of gravity on the Earth is less than 0.05 microradians[64] and is mainly due to tidal effects. Fig. C.2 shows the relation of Earth's gravitational specific force and gravity specific force. The angles are exaggerated in this figure for clarity.

- - - - - - - - - - - - - - - - - -

* The specific force of gravity (the force of gravity acting on a unit mass) is identical with the gravity field intensity.

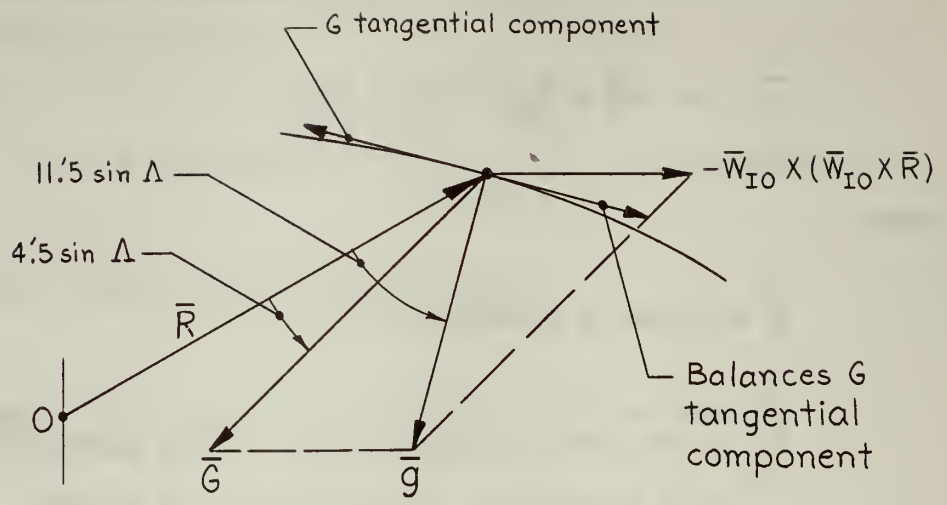

Note:
Angles are exaggerated for clarity in presentation. Numerical values are approximate values for Earth.

Fig. C.2: Relation of Gravitation and Gravity.

The angular velocity of the Earth about its polar axis is[19]

$$W_{IO} = 7.2921159 \times 10^{-5} \text{ rad./sec.} \qquad \text{(C-13)}$$

The international standard gravitational conversion factor is the apparent acceleration of gravity at latitude 45° 32' 40" :

$$g_{(m)E} = 32.17405 \text{ ft./sec.}^2 \qquad \text{(C-14)}$$

Since

$$g_{(m)E} = G_{(m)E} - W_{IE}^2 R_{(m)E} \cos \Lambda \qquad \text{(C-15)}$$

the following is determined for $G_{(m)E}$:

$$G_{(m)E} = 32.17405 + 0.05443 = 32.22848 \text{ ft./sec.}^2 \qquad \text{(C-16)}$$

Appendix D

FIGURE OF THE PLANET AND DEFINITION OF NAVIGATIONAL PARAMETERS

D.1 Figure of the Planet

The figure that would be taken by a fluid body with the mass distribution and axial rotation of the planet is defined as the figure of the planet. The figure of the planet is an equipotential surface of the planet's gravity field.

In connection with the actual configuration of the Earth, study of the motion of Vanguard I has shown the Earth to be slightly pear-shaped, with the more narrow half above the equator and the sag below. There is an approximate 50 ft. rise in mean sea level at the South pole[65]. This deformation is interpreted to mean that the crystal layers of the Earth have more strength and less elasticity than previously assumed.

The figure of other planets in the solar system is not nearly as well known as that of the Earth. Unmanned planetary probes, which are planned for launch in the 1960's should provide the first quantitative information obtained from data sources near the planet to augment astronomical observations and calculations accumulated over many years. The oblateness of the planets is generally estimated from astronomical photographs and from calculations based on observed rotational rates. In general, the terrestrial planets are believed to be more spherical

than the giant planets because of the higher rotational rates and smaller densities of the latter.

The figure of the planet may be approximated by a reference ellipsoid, an analytical figure closely approximating the planet. The Clark Spheroid (1866) is the reference ellipsoid of the Earth used for North American triangulations. The Hayford Spheroid (1909) is the international reference ellipsoid of the Earth adopted by the Internationale Geodetic and Geophysical Union of 1924. This is called the geoid, a "square shouldered" ellipsoid with a slightly undulated surface[11]. The surface of the geoid is represented by mean sea level. Variations in the elevation of the geoid relative to the closest reference ellipsoid are approximately one percent of the topographic variations in elevation[11].

D.2 Navigation Parameters

A manned vehicle entering the atmosphere of a planet must have some means of identifying its present position and the location of its destination. Three coordinates are required in order to uniquely specify position in three-dimensional space. Of the infinite number of possible sets of coordinates that may be used to identify position near a planet, three are most common: altitude, latitude, and longitude.

Three navigational reference frames are discussed in this section and a comparison made between navigational parameters expressed in each of these frames:

(1) Astronomic Frame

Recognizes the actual planet configuration. The coordinate frame is centered at the guidance point and has one axis along the true vertical (gravity vector).

The other two axes depend on the guidance grid desired (e.g., astronomic latitude and longitude).

(2) Geographic Frame

Recognizes the ellipticity of the planet. The coordinate frame is centered at the guidance point and has one axis along the geographic vertical (normal to the surface of the reference ellipsoid). The other two axes depend on the choice of guidance grid (e.g., geographic latitude and longitude).

(3) Geocentric Frame

Utilizes spherical polar coordinates. The coordinate frame is centered at the guidance point and has one axis along the geocentric radius. The other two axes depend on the choice of guidance grid (e.g., $\bar{l}_r$, $\bar{l}_\lambda$, $\bar{l}_\Lambda$ triad or $\bar{l}_r$, $\bar{l}_\phi$, $\bar{l}_\psi$ triad discussed in Appendix A).

It was pointed out in Appendix C that, neglecting anomalies, the direction of the gravity vector $\bar{g}$ is unique at each point on the surface of the planet. The direction of the gravity vector is defined as the true vertical. The uniqueness of the true vertical is the basis for astronomical position. Two angles are sufficient to identify the position of any point on the surface of the planet:

(1) Astronomical latitude:

The complement of the angle between a line parallel to the polar axis of the planet and the local gravity vector.

(2) Astronomical longitude:

The angle about the polar axis of the planet between an arbitrarily chosen reference vertical and the local vertical. Due to the arbitrary choice of reference vertical, longitude is not inertially unique, although change of longitude is.(11)

The geographic vertical* is defined as the normal to the surface

- - - - - - - - - - - - - - - - -

* In the strictest sense, the term "geographic" refers to the Earth (geoid) only. In this thesis, "geographic" is used in a more general sense to refer to quantities associated with the reference ellipsoid of any planet.

of the reference ellipsoid. Because the figure of the planet does not have a smooth surface, the true vertical is not, in general, parallel to the normal to the reference ellipsoid at the same position. The angle measured from the normal of the reference ellipsoid to the true vertical is called the deflection of the vertical, or station error. For the Earth, station error is generally less than 0.3 milliradians; over continental land masses, it rarely exceeds 0.1 milliradians.(11)

Identification of position on the surface of the reference ellipsoid is accomplished with the following two angles:

(1) Geographic Latitude (Λ_9) :

Angle between the normal to the reference ellipsoid and its projection on the equatorial plane.

(2) Geographic Longitude:

Angle between the projection of the normal to the reference ellipsoid on the equatorial plane of the planet and an arbitrarily chosen reference meridian.

The geocentric vertical is defined as a unit vector directed from the point at which the guidance is taking place toward the center of the planet. The angle measured from the geocentric vertical to the normal of the reference ellipsoid is called the deviation of the normal. The maximum deviation of the normal for Earth is approximately 11.5 minutes of arc.

Identification of position by means of spherical polar coordinates may be accomplished through specifying radius from planet center (or altitude above the surface of the planet) and by two independent angles.

One set of independent angles that may be used to specify position are great circle parameters, i.e., angular position along and across the great circle track. Even though the term great circle has no meaning

on any surface other than that of a sphere, it is a useful concept in navigation over non-spherical bodies. An astronomic great circle course is defined by the property that the normals to the planet's surface along such a course are parallel to a single, fixed plane. A geographic great circle course is defined as a course for which the normals to the reference ellipsoid of the planet are parallel to a single, fixed plane. The astronomic and geographic great circle courses are not geodesics, therefore a point on the planet's surface following such a course would experience a geodesic acceleration.*

Another set of spherical angles used to specify position are:

(1) Geocentric Latitude (Λ):

Angle measured between the geocentric radius and its projection on the equatorial plane of the planet.

(2) Geocentric Longitude (λ):

Angle in the equatorial plane of the planet between the projection of the geocentric radius on the equatorial plane and the longitudinal reference meridian.

When the equatorial plane is taken as the true equatorial plane, geocentric and geographic longitudes are identical and astronomic longitude differs by a component of station error. A comparison of geocentric and geographic latitude is made in the next section.

- - - - - - - - - - - - - - - - -

* A horizontal component of acceleration arising from the curvature of the course in the horizontal plane.

D.3 Comparison of Geocentric Latitude and Geographic Latitude

Most of the analysis of this thesis is based on geocentric angles as prime dependent variables in the statement of the guidance problem of vehicles entering planetary atmospheres. Since position on maps and charts is conventionally specified in terms of geographic latitude, it is instructive to compare geocentric and geographic latitudes.

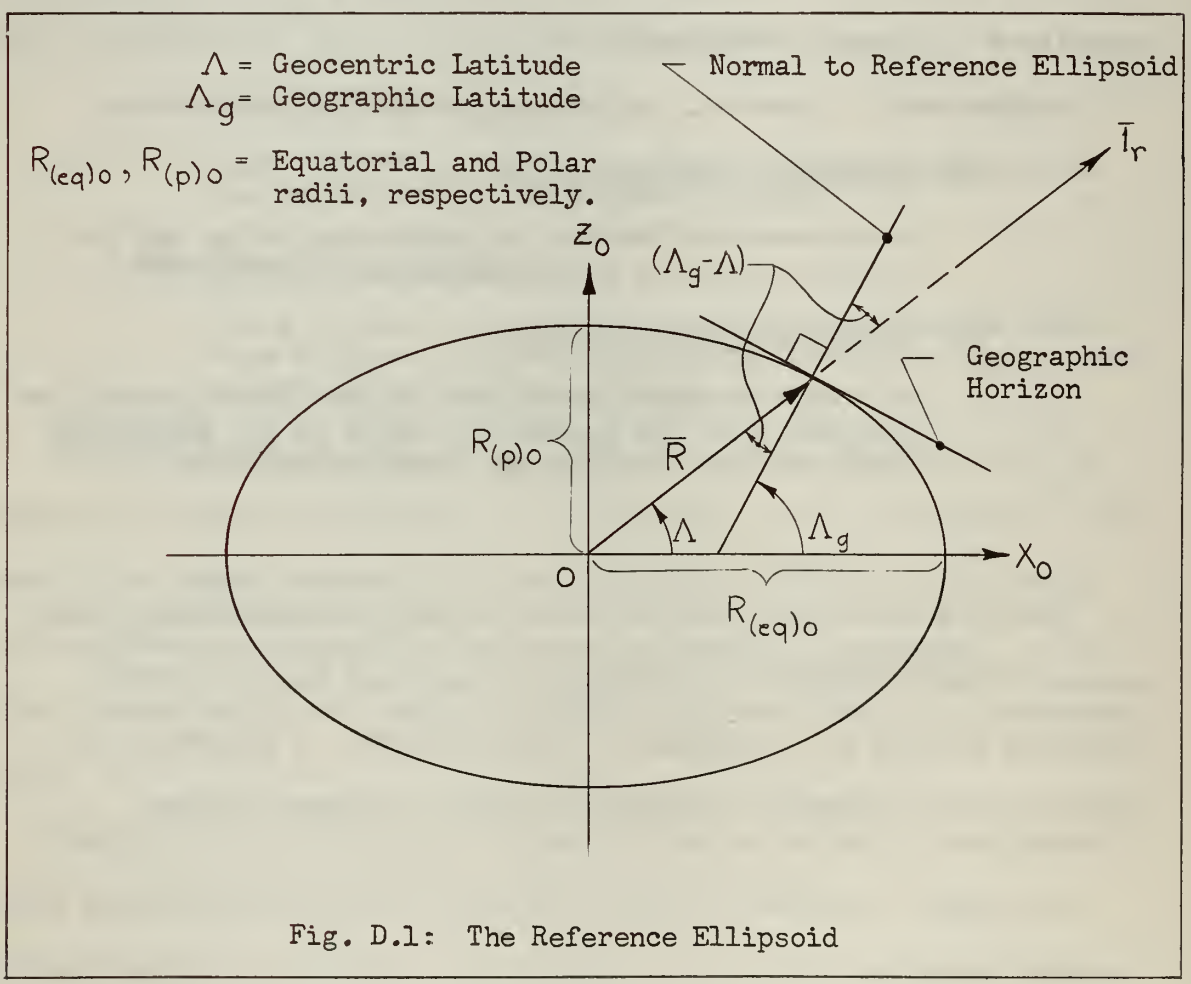

Fig. D.1: The Reference Ellipsoid

It is shown in reference (66) that:

$$\tan(90^\circ + \Lambda_g - \Lambda) = R \frac{d\Lambda}{dR} \qquad \text{(D.1)}$$

Therefore: $$\tan(\Lambda_g - \Lambda) = -\frac{1}{R}\frac{dR}{d\Lambda} \qquad (D.2)$$

The equation of the ellipse in polar coordinates is:

$$\left(\frac{R_x}{R_{(eq)0}}\right)^2 + \left(\frac{R_z}{R_{(p)0}}\right)^2 = 1 \qquad (D.3)$$

where:

$$R_x = R\cos\Lambda$$

$$R_z = R\sin\Lambda$$

Therefore:

$$R^2\left[\left(\frac{\cos\Lambda}{R_{(eq)0}}\right)^2 + \left(\frac{\sin\Lambda}{R_{(p)0}}\right)^2\right] = 1 \qquad (D.4)$$

Solving for R:

$$R = \frac{R_{(eq)0}}{\left[\cos^2\Lambda + \left(\frac{R_{(eq)0}}{R_{(p)0}}\right)^2 \sin^2\Lambda\right]^{\frac{1}{2}}} \qquad (D.5)$$

The eccentricity of the planet, ε , is defined* by (see Fig. A.6):

$$\varepsilon^2 = 1 - \left(\frac{R_{(p)0}}{R_{(eq)0}}\right)^2$$

Equation D.5 thus becomes:

$$R = \frac{R_{(eq)0}}{\left(1 + \frac{\varepsilon^2 \sin^2\Lambda}{1-\varepsilon^2}\right)^{\frac{1}{2}}} \qquad (D.6)$$

- - - - - - - - - - - - - - - - -

* The ellipticity of the Hayford ellipsoid is given as:

$$\text{Ellipticity} = \frac{R_{(eq)E} - R_{(p)E}}{R_{(eq)E}} = 1/297$$

Thus: $\varepsilon_E = \sqrt{593} \times (\text{Ellipticity})$

$\varepsilon_E^2 = 0.0067226700$

Using Eq. (D.6) to eliminate R from Eq. (D.2) gives:

$$\tan(\Lambda_g - \Lambda) = \frac{\varepsilon^2 \sin\Lambda\cos\Lambda}{(1-\varepsilon^2)\left(1+\frac{\varepsilon^2\sin^2\Lambda}{1-\varepsilon^2}\right)} = \frac{\varepsilon^2 \sin\Lambda\cos\Lambda}{(1-\varepsilon^2\cos^2\Lambda)} \qquad \text{(D.7)}$$

Equation (D.7) may be written:

$$\tan(\Lambda_g - \Lambda) = \varepsilon^2 \sin\Lambda\cos\Lambda + \frac{\varepsilon^4 \sin\Lambda\cos^3\Lambda}{1-\varepsilon^2\cos^2\Lambda} \qquad \left\{\begin{matrix}\text{All}\\ \text{Planets}\end{matrix}\right. \text{(D.8)}$$

This expression is an exact* relation between geocentric latitude Λ and geographic latitude Λ_g. Examination of this equation shows that $(\Lambda_g - \Lambda) < 12$ minutes of arc over the Earth's surface. It is probably less than 12' for Mercury, Venus, and Mars; but $(\Lambda_g - \Lambda)$ is probably somewhat greater than 12' for the giant planets (high rotational speeds -- small density). Using the small angle approximation of $(\Lambda_g - \Lambda)$ for terrestrial planets give :

$$\Lambda_g \cong \Lambda + \varepsilon^2 \sin\Lambda\cos\Lambda \qquad \left\{\begin{matrix}\text{Mercury}\\ \text{Venus}\\ \text{Earth}\\ \text{Mars}\end{matrix}\right. \text{only} \qquad \text{(D.9)}$$

D.4 Radius of Spheroidal Planets as Function of Latitude

Equation (D.6) gives an expression for the radius vector to a point on the surface of the ellipsoidal planet in terms of geocentric latitude, eccentricity, and equatorial radius. This may be expanded by the binomial theorem to give:

$$R_{surface} = R_{(eq)o}\left[1 - \frac{1}{2}\frac{(\varepsilon\sin\Lambda)^2}{(1-\varepsilon^2)} + \frac{3}{8}\frac{(\varepsilon\sin\Lambda)^4}{(1-\varepsilon^2)^2} - \cdots\right] \qquad \left\{\begin{matrix}\text{All}\\ \text{Planets}\end{matrix}\right. \text{(D.10)}$$

- - - - - - - - - - - - - - - - -

* "Exact" to the extent that the reference ellipsoid approximates the figure of the planet.

For the terrestrial planets where $R_{(p)0}$ and $R_{(eq)0}$ do not differ greatly, Equation (D.10) may be reduced to a first order in ϵ^2:

$$R_{surface} \cong R_{(eq)0}\left(1 - \frac{\epsilon^2}{2}\sin^2\Lambda\right) \qquad \begin{cases} \text{Mercury} \\ \text{Venus} \\ \text{Earth} \\ \text{Mars} \end{cases} \text{ only} \qquad \text{(D.11)}$$

D.5 Position Reference for First-Time Entry into the Atmospheres of Strange Planets*

First-time entry into the atmospheres of strange planets presents special problems in specifying position when compared to navigation over a well-mapped planet such as the Earth. The choice of a suitable landing site must necessarily be based on reconnaissance of the planetary surface while in orbit around the planet. The orbital altitude for the reconnaissance phase must be high enough such that a prolonged orbit may persist, yet low enough that fairly accurate mapping of the terrain is feasible.

The navigation of a vehicle flying from one point to another point on the surface of a planet is generally based on navigational parameters measured with respect to the planet, i.e., latitude, longitude, and altitude. It is less common to use parameters identified with the particular mission, such as angular displacements measured with respect to the great circle course along-track and across-track.

The entry mission to the surface of a strange planet, on the other hand, does not originate from a point on the planet's surface. The entry mission originates from the reconnaissance orbit, which, if the perigeal altitude is sufficiently great, is very slowly changing with time. The

- - - - - - - - - - - - - - - - -

* "Strange planets", as used in this thesis, signifies any planet on which a vehicle with human occupants has not landed.

non-spherical component of the planet's gravitational field causes the line of nodes to rotate slowly with respect to the inertial framework. Drag forces result in energy transfer from the vehicle to the planetary atmosphere, but for sufficiently high orbits, this transfer causes negligible change in the satellite orbit over periods of time comparable to that required for entry once retro-rocket thrust is generated.

A basic position reference available during the course of entry is the original reconnaissance orbit. If the entry vehicle is launched from a mother satellite, then the mother satellite, which remains in the reconnaissance orbit, may track both the entry vehicle and the pre-selected landing site and transmit this tracking information to the navigational computer of the entry vehicle. In this way, the parent satellite replaces ground tracking stations which are used as an external source of tracking information for Earth satellites and entry vehicles.

In the event that no parent satellite exists, then a navigational satellite to serve the same purpose may be deposited in the reconnaissance orbit by the entry vehicle prior to initiating the entry phase.

Since a navigational scheme such as outlined briefly above uses the reconnaissance orbit as the basic reference from which to measure positions, it may be found convenient to express position and to carry out the guidance computations in terms of elliptical parameters such as those presented in Chapter 4. The landing site may be considered to be a target moving in three dimensional space with respect to the near-stable reconnaissance trajectory represented by the mother or navigational satellite. The entry vehicle is also moving with respect to the reconnaissance trajectory. The entry problem is therefore similar to the Fire Control problem with the entry vehicle (projectile) fired from the

parent satellite (gun)to hit the moving landing site (target). The problem is much more severe than the conventional fire control problem, however, because the projectile must be constrained to paths for which it will not burn up or encounter accelerations beyond tolerable levels.

The nominal or programmed path of the entry vehicle may be computed in advance as one which the vehicle would fly under standard atmospheric conditions starting from the particular initial point and ending at the landing site selected in advance. This trajectory must be consistent with tolerable accelerations and heating rates (Chapter 7).

It was shown in Chapter 4 that there are six elliptical elements required to specify the position and path of the vehicle. One set of six such elements are:

(1) ψ, λ_{IT}, (to specify the instantaneous orientation of the plane of the trajectory).

(2) P, ϵ_1, ϵ_2 (to specify the ellipse which matches instantaneously the dynamical state of the vehicle)

(3) ϕ (to specify the position of the vehicle in this ellipse).

P, ψ , and λ_{IT} are constant or very slowly varying with time in the reconnaissance orbit. ϵ_1 and ϵ_2 are sinusoidal with a very slowly changing magnitude of oscillation. ϕ increases monotonically. The instantaneous state of the entry vehicle, with respect to the navigational satellite in the reconnaissance orbit, may conveniently be specified in terms of the six elliptical quantities. The orbit of the navigation satellite should be predictable to a fairly high degree of accuracy. The predicted values of six elliptical elements for this orbit are part of the data stored for use during the entry mission.

APPENDIX E

THE ATMOSPHERE OF THE PLANETS AND THEIR NATURAL SATELLITES

E.1 Composition of Atmosphere of the Planets and Their Natural Satellites

The presence and stability of planetary atmospheres can be predicted from the kinetic theory of gases[67]. For a stable atmosphere to exist, the root-mean-square molecular velocity of the atmosphere should be less than 20% of escape velocity. The RMS molecular velocity is a function of temperature (which depends on distance from the Sun), atmospheric composition, planetary rotational rates, etc. The relative likelihood of major bodies of the solar system possessing an atmosphere is given in the following list[67]. The higher a planet or moon is on the list, the higher is the probability that there exists an atmosphere around it.

(1) Jupiter*
(2) Saturn*
(3) Neptune*
(4) Uranus*
(5) Earth*
(6) Venus*
(7) Pluto
(8) Triton
(9) Mars*
(10) Titan*
(11) Jovian III
(12) Jovian I

- - - - - - - - - - - - - - - - -

* Proof of the existence of an atmosphere by spectroscopic or other means has been established for all bodies marked with an asterisk(*). Evidence for all other bodies is inconclusive.

(13) Jovian IV
(14) Jovian II
(15) Mercury
(16) Moon

A brief description of the atmosphere and climate of each of the planets and their natural satellites, adapted primarily from references (7) and (58), is summarized below:

(1) Mercury

Mercury is a small rocky sphere, about half again as large as Moon, that always has the same side exposed to the Sun. Maximum surface temperature on the "hot" side is estimated at 650-750° F. while that on the cold side approaches -400 to -415° F. Mercury is not known to have an atmosphere of any significance, nor would a permanent gaseous envelope be expected to occur under the condition existing on the planet. Its rocky surface is probably somewhat similar to that of Moon.

(2) Venus

A dense, dusty, turbulent atmosphere, containing much carbon dioxide and some nitrogen (but negligible free oxygen and water) conceals the planet's surface. The atmosphere of Venus contains white particles in suspension and is opaque to light of all wave lengths. On the basis of all available evidence, it may be presumed that the surface of Venus is probably hot, dry, dusty, windy, and dark beneath a continuous dust storm; that the atmospheric pressure is probably several times the normal barometric pressure at the surface of the Earth; and that carbon dioxide is probably the major atmospheric gas, with nitrogen and argon also present as minor constituents(68).

(3) Mars

Many questions about surface conditions on Mars are still unanswered. It has an appreciable atmosphere and its surface markings exhibit seasonal changes in coloration. Its white polar caps* are apparently thin layers of frost of the order of inches or fractions of inches thick. The atmosphere is composed primarily of nitrogen, carbon dioxide, traces of water vapor, and is believed to be almost totally absent of free oxygen(67).

- - - - - - - - - - - - - - - - - -

* The polar caps of Mars appear during its winter and disappear in summer.

Topographically, its surface is flat, with no abrupt changes in elevation and no prominent mountains. The climate is imagined to be like that which would be encountered on the Earth in a desert at 11 miles altitude. Noon summer temperatures in the tropics may reach 80° - 90° F. while predawn temperatures may drop to -100° F.

There is evidence that some indigenous life forms may exist on Mars. The seasonal color changes, from green in summer to brown in autumn, suggest vegetation. Recent spectroscopic studies give evidence of organic molecules being responsible for the dark areas [69]. The objections raised concerning differences between the color and infra-red reflectivities of terrestrial organic matter and those of the dark areas on Mars have been explained by Tikhov[70]. He has shown that arctic plants differ in infrared reflection from temperate and tropical plants, and an extrapolation to Martian conditions leads to the conclusion that the dark areas are vegetable lift. Human life could not survive without vast environmental modifications, but a self-sustaining local animal colony is possible.

(4) The Giant Planets

The four giant planets are massive bodies of low density and large diameter. They all rotate rapidly, hence have considerable "flattening" at the poles ("bulges" at the equator). It is shown in Table B-1 that their densities vary from about 0.72 to 1.6 times the density of water. On the basis of this and spectral data, they are considered to be composed of a dense rocky core surrounded by a thick shell of ice and covered by thousands of miles of compressed hydrogen and helium.* Methane and ammonia are known to be present as minor constituents of the atmosphere, but no water has been observed[71].

Jupiter and Saturn show light and dark belts in the atmosphere parallel to the equator. These banded clouds are slowly changing in Jupiter; they are not as clear nor are they changing as rapidly on Saturn. Jupiter's great red spot, 20,000 miles long, seems more permanent than its cloud belts, but it is believed to be fading. Bright spots occasionally appear in the cloud banks of Saturn.

Saturn's rings are its most prominent physical feature. They are probably composed of millions of tiny solid particles. They may be material which never formed into a satellite, or fragments of a close satellite torn asunder by the tidal pull of Saturn, or ice particles.

- - - - - - - - - - - - - - - - -

* A "rock-in-a-snowball" structure -- reference (7).

(5) Pluto

Little is known about Pluto beyond the physical characteristics listed in Table B-1 and the fact that it is extremely cold.

(6) Moon

The Moon has no appreciable atmosphere, and its surface is probably dry, dust-covered rock that is not homogeneous either in chemical composition or topography. The origin of the Moon's craters is still a matter of debate. Lunar mountains are higher than Earth mountains, presumably because of the absence of weathering effects.

(7) Planetary Satellites

A number of the satellites of Jupiter, Saturn, and Neptune are larger than the Earth's Moon; some may be as large as Mercury. At least one of Saturn's moons, Titan, is believed to have an atmosphere. Although reliable physical data on the satellites are lacking, it is possible that some of them may be more hospitable than their parent planets.

There are two principal experimental methods for obtaining data concerning the composition of the planetary atmospheres:

(1) Optical observations of the surface and atmosphere.

(2) Spectroscopic measurements of radiation emitting from the surface.

Both methods suffer severely because of interference with the Earth's atmosphere.

In addition to the above experimental methods, other constituents of the atmospheres of the planets can be inferred by correlating estimates of the composition of the atmosphere at the time of formation of the planet with present measurements of physical characteristics of the planet and its atmosphere. Table E.1 gives estimates of composition of the atmospheres of the planets and their natural satellites from observations and calculations recorded in reference (67). If the amount of the constituent is based on spectroscopic measurements, the amount is

recorded in Column 4 as the height in centimeters of an equivalent column of the gas at 0° C. and Earth standard sea level pressure (760 mm Hg). If the amount of the constituent is based on calculations and estimates, it is recorded in Column 3 as a percent by weight of the total planetary atmosphere.

Table E.1: Composition of the Atmospheres of the Planets and Their Major Natural Satellites.

Notes: (1) If the amount of the constituent is based on spectroscopic measurements, it is recorded in Column 4 as the height in centimeters of an equivalent column of the gas at 0°C. and at a pressure equal to a 760 mm column of Hg.

(2) If the amount of the constituent is based on estimates and calculations, it is recorded in Column 3 as a percent by weight of the total planetary atmosphere.

Column 1 Body	Column 2 Gas	Column 3 Amount (%)	Column 4 Amount (see Note (1) above) cm
Mercury	A^{40}	trace	
	Kr	trace	
	Xe	trace	
Venus	CO_2	89-92%	100,000
	N_2	8-10%	
	A	trace	
	CO		<100
	N_2O		<100
	CH_4		<20
	C_2H_4		< 3
	C_2H_6		< 1
	NH_3		<4
	H_2O	negligible	
	O_2	negligible	
Earth	N_2		625,000
	O_2		168,000
	CO_2		220
	CH_4		1.2
	N_2O		0.4
	O_3		0.3

Table E.1 (Cont.): Composition of the Atmosphere of the Planets and Their Major Natural Satellites.

Column 1	Column 2	Column 3	Column 4
Moon	SO_2		<0.0003
	O_3		<0.005
Mars	N_2	97-98%	
	CO_2	0.25-2.4%	
	H_2O	trace	
	O_2	0.1%	
	SO_2		<0.003
	O_3		<0.05
	N_2O		< 200
	CH_4		< 10
	C_2H_4		< 2
	C_2H_6		<1
	NH_3		<2
	A	1.2%	
Jupiter	He	62.8%	
	H_2	23.2%	
	CH_4		15,000
	NH_3		700
	Ne	trace	
	H_2O	trace	
	A	trace	
	SiH_4	trace	
JI-JIV	CH_4		<200
	NH_3		< 40
Saturn	He	20-80%	
	H_2	20-64%	
	CH_4		35,000
	NH_3		< 250
	O_3		< 0.1
	SO_2		< 0.01
Titan	CH_4	33%	20,000
	NH_3		< 300
	A		*
	Ne		

* The total amount of atmosphere for Titan is estimated to be 60,000 cm.

Table E.1 (Cont.): Composition of the Atmosphere of the Planets and Their Major Natural Satellites.

Column 1	Column 2	Column 3	Column 4
Uranus	He	58-75%	
	H_2	20-22%	
	CH_4	2-21%	220,000
	O_3		< 0.1
	SO_2		< 0.01
Neptune	He	58-75%	
	H_2	20-22%	
	CH_4	2-21%	370,000

E.2 Models of the Atmosphere

In much of the work of this thesis, the following two assumptions are made:

(1) The planet and its atmosphere are spherically symmetric.

(2) The atmospheric density varies exponentially with altitude.

The first assumption is reasonable for the terrestrial planets* because of their slow rotational speeds. The giant planets have high rotational speeds, hence this assumption is not nearly so valid for these planets. The second assumption is based on the simple kinetic theory of an isothermal gas in a uniform gravitational field. This theory yields the well-known exponential approximation for the atmosphere:

$$\rho = \rho_{(\overline{SL})} e^{-KH} \qquad \text{(E-1)}$$

- - - - - - - - - - - - - - - - -

* Mercury has no appreciable atmosphere.

where:

ρ = free stream atmospheric density (slug/ft.^{3})

$\rho_{(\overline{SL})}$ = "assumed" mean sea level atmospheric density*

K = atmospheric density decay parameter, ft.$^{-1}$

H = altitude of vehicle above surface of planet (ft.)

K is equal to the mean molecular weight of the planet's atmosphere times the local acceleration due to gravity divided by the product of mean atmospheric temperature and the universal gas constant:

$$K = \frac{g \text{ (Mean molecular weight of atmospheric gases)}}{R_h \, T_{(m)o}} \qquad \text{(E-2)}$$

where:

R_h = universal gas constant = 8.31 X 10^7 ergs/°Kelvin

g = acceleration due to gravity

$T_{(m)o}$ = the mean temperature of the planetary atmosphere (°K)

Two additional models of the planetary atmosphere are sometimes used:

(1) An emperical matching of <u>measured</u> atmospheric data:

$$\frac{\rho}{\rho_{(SL)}} = \sigma \cong (H)^n \qquad \text{(E-3)}$$

This model is useful for the Earth's atmosphere only, since measurements of the density variation with altitude for other planetary atmospheres have not been obtained to date. The model represented by Eq. (E-3), with $n \cong -5$ to -8, generally matches more closely at high altitudes the data accumulated from Vanguard, Sputnik, and Explorer

- - - - - - - - - - - - - - - - - -

* This is <u>not</u> the true sea level atmospheric density $\rho_{(SL)}$. The "assumed" quantity $\rho_{(\overline{SL})}$ is the intercept of the straight line which best fits the curve of log ρ vs altitude.

Earth satellites than does the exponential atmosphere with K constant. Since Eq. (E-3) is based on an emperical curve fit and not on any known physical law, the value of n for other planets cannot be predicted at this time.

(2) The variation of density with altitude for an atmosphere in which temperature decreases linearly with altitude is:

$$\frac{\rho}{\rho_{(SL)}} = \sigma = \left[\frac{(\text{Local temp.})}{(\text{Surface temp.})}\right]^{\frac{1}{\gamma_0 - 1}} = \left[\frac{(\text{Surface temp.}) - (\text{Lapse Rate})H}{\text{Surface Temperature}}\right]^{\frac{1}{\gamma_0 - 1}} \qquad \text{(E-4)}$$

where:

γ_0 = ratio of specific heat $\frac{C_p}{C_v}$

If it is assumed that γ_0 and gravity are constant, the adiabatic lapse rate* is given by:

$$(\text{Adiabatic Lapse Rate}) = \frac{(\text{Mean Molecular Weight of atm. gases})\, g_{(m)o}(\gamma_0 - 1)}{R_h \gamma_0} \qquad \text{(E-5)}$$

E.3 The Venusian Model Atmosphere

It is generally assumed that the atmosphere of Venus originated from volcanic gases. On Venus, water was converted to molecular oxygen, atomic oxygen, ozone, and hydrogen via photodissociation at high altitudes. This action was speeded up because of the nearness of Venus to the Sun. The ozone layer on Venus was probably formed at greater altitudes than on Earth. The oxygen was probably removed from the atmosphere by chemical combination with surface material. This chemical process

- - - - - - - - - - - - - - - - -

* Lapse rate is the rate at which temperature decreases with increasing altitude.

should react about 30 times as fast on Venus as it does on Earth because of the higher surface temperatures on Venus.

Loss of water via photodissociation to oxygen probably stopped the chemical reaction of carbon dioxide with surface material. Once this situation prevailed, it may be expected that carbon dioxide started to appear in the atmosphere of Venus in ever-increasing quantities.

Venus should have about the same amount of nitrogen as Earth, and much greater quantities of carbon dioxide in the atmosphere. The much larger quantities of carbon dioxide are expected in the atmosphere of Venus when compared to Earth because of the high quantities of carbon dioxide combined with surface material on Earth.*

Because of the above reasoning, Dole[68] proposed on atmospheric model containing 90% carbon dioxide and 10% nitrogen. The values of the constants in Equation (E-1) for Venus proposed by Dole are:

$$\rho_{(SL)} = 0.0326 \text{ slug/ft.}^3$$
$$K = 4.88 \times 10^{-5} \text{ ft.}^{-1} \qquad \text{(E-6)}$$

Romer[72], using Equation (E-4), determined $\rho_{(SL)} = 0.0348$ slug/ft.^{3}. He used an atmospheric model of 10% nitrogen and 90% carbon dioxide with a mean molecular weight of 42.4 and a specific heat ratio of $\gamma_o = 1.31$ at 400 °K. The lapse rate was computed to be 10.45 °K/KM. Kuiper[8] suggests the lapse rate is 13° K/KM and $\gamma_o = 1.4$, while de Vancouleurs[62] determines a lapse rate of 10.4 °K/KM.

Values given in (E-6) are used in this thesis for Venus.

- - - - - - - - - - - - - - - - -

* Carbon dioxide was able to combine with surface material on Earth because of the presence of water.

E.4 Martian Model Atmosphere

Evidence for the existence of a Martian atmosphere is conclusive. Clouds are frequently observed. Stars passing behind the disc of Mars are seen longer and appear earlier than possible without atmospheric refraction*. A twilight zone on Mars caused by atmospheric refraction has been observed. Mars appears to be larger when photographed by reflected ultraviolet light than by reflected infrared light. (The atmosphere of Mars is included in ultraviolet photographs). A lower limit of 60 miles can be placed on the altitude of the Martian atmosphere from these photographs. This is probably the altitude to which small ice crystals rise, thus creating a "blue haze". The blue haze often clears when Mars passes close to the Sun. On these occasions, damage is seen to occur to the primitive vegetation which is believed to exist on Mars. When present, the blue haze protects the vegetation from destructive ultraviolet radiation originating from the Sun.

Although nitrogen is probably the main constituent of the Martian atmosphere, it has not yet been detected. This is due to the fact that absorption bands for molecular nitrogen are in the low ultraviolet region. These lines are effectively obscured from observation on Earth by ozone in the upper atmosphere of Earth. Atomic nitrogen in the Martian atmosphere could theoretically be detected through the atmosphere

- - - - - - - - - - - - - - - - -

* It is interesting to note that the only time in recorded history that occultation of a first magnitude star (Regulus) by Venus occurred in mid-July, 1959. The total time that Regulus was obscured was 11 minutes 4.8 seconds. This event was observed from a Spanish observatory by a team led by Dr. Allen Hynek from the Smithsonian Astrophysical Observatory of Cambridge, Mass. Revised information on the Venusian atmosphere (its density variation with altitude, temperature, chemical composition, etc.) based on the results of this observation has not been published at this time.

of the Earth. However, there is a larger quantity of atomic nitrogen in the atmosphere of the Earth than in the atmosphere of Mars. Mars probably had less molecular nitrogen to begin with than Earth, and definitely has less solar energy to produce atomic nitrogen from molecular nitrogen. These two factors have combined to provide a weak spectrum against a background that even sensitive Doppler techniques have proven futile for the detection of atomic nitrogen.

It is generally thought that the atmosphere of Mars, like that of Venus and Earth, originated from volcanic gases. These gases consisted of water vapor, carbon dioxide, nitrogen, and other minor constituents in that order. Nitrogen was probably the only major constituent of volcanic gas which was not readily removed from the atmosphere of Mars by chemical reaction with rock formations or by escape since nitrogen is inert and highly resistant to photodissociation.

Water was probably removed first from the Martian atmosphere. Atomic oxygen, ozone, molecular oxygen, and hydrogen are some of the gases produced as a result of photodissociation of water. Most of the hydrogen probably escaped from the Martian atmosphere. Since ozone would be produced at low altitudes on Mars, it could combine rapidly with surface material. Water probably remained close to the surface making the rapid combination of carbon dioxide with surface material possible. With the loss of oxygen via ozone formation and chemical reaction, there would result a shift in the chemical equilibrium to more ozone; this gas, in turn, could continue to combine with surface material until most of the water disappeared.

After the disappearance of most of the water from the Martian atmosphere, carbon dioxide could no longer combine with surface material

at an appreciable rate. Consequently, it may be reasoned that the atmosphere of Mars has more carbon dioxide than the atmosphere of Earth. This has been verified by spectroscopic measurements (see Table E.1). In addition, water and oxygen are known to be absent from the Martian atmosphere in quantities which are significant in gas-dynamic problems (less than a few hundredths of a per cent.) The reasoning outlined in the foregoing paragraphs may account qualitatively for the composition listed in Table E.1.

The Gazley[14] model for the atmosphere of Mars assumes that it consists of 95% nitrogen and 5% carbon dioxide. This model ignores minor constituents, especially argon, and is subject to a large error in the estimation of carbon dioxide content. Nevertheless, it is doubtful that a more accurate model would allow a significant improvement in the accuracy of gas-dynamic calculations.

The average surface temperature of Mars was estimated by Gazley from the Stefan-Boltzman relationship to be minus 40° F.* He made the following assumptions in determining the average surface temperature:

(1) The ratio of the heat flux reaching Mars and Earth is determined by their respective solar constants (3/7 for Mars and 1.0 for Earth).

(2) The emissivities are the same for both planets.

(3) The temperature of the surroundings to which the planet radiates is sufficiently low to be neglected.

It is noted that a value of -40° F. was listed by Wanders[74] as an

- - - - - - - - - - - - - - - - -

* Kuiper[67] and de Vaucouleurs[73] use a surface temperature of 273° K. (0° C.) The maximum diurnal temperature change is about 50° C. This is also approximately the maximum seasonal average temperature variation (occurring in summer and fall).

average experimental value.

The ratio of the absolute mean-sea-level temperature of Earth to the absolute ground-level temperature of Mars is 1.23. The temperature lapse rate of the Martian atmosphere is lower than for the Earth* ; therefore, this temperature ratio decreases with increasing altitude.

Gazley[14] uses a surface density value of 6.2×10^{-3} lbs./ft.^{3} for the Martian atmosphere which is in close agreement with the value of 1.94×10^{-4} slugs/ft.^{3} given by Hess[75]. Gazley uses a value for K (see equations E-1 and E-2) of 1.15×10^{-5} ft.$^{-1}$. Chapman[15] uses a value for K of 1.665×10^{-5} ft.$^{-1}$. In the numerical calculations of this thesis, the following are used for the values of the constants in Eq. (E-1) for the Martian atmosphere:

$$\rho_{(SL)} = 1.93 \times 10^{-4} \text{ slugs/ft.}^3$$
$$K = 1.665 \times 10^{-5} \text{ ft.}^{-1} \qquad \text{(E-7)}$$

The maximum error in decelerations computed in this thesis should be no greater than about 20% for Mars, and the maximum error in heating rates and stagnation point temperatures should not exceed 10%.

E.5 Model Atmosphere for the Giant Planets and Titan

Information on the density characteristics of the atmospheres of Jupiter, Saturn, Titan, Uranus, and Neptune is fragmentary at best. Because of the cloud layer which obscures the surface of the giant planets, extrapolation of density characteristics to the surface is not

- - - - - - - - - - - - - - - - -

* The lapse rate for Earth at sea level is 9.8 °K/KM. The average measured lapse rate at all altitudes is approximately 5 °K/KM, which indicates that the atmosphere is not completely in adiabatic equilibrium. Most authorities[67] [73] have computed a lapse rate of 3.7 - 3.9 °K/KM for Mars.

possible. Table E.2 summarizes briefly Kuiper's model atmospheres for the giant planets and Titan.

Table E.2: Model Atmospheres for Giant Planets and Titan

1. Jupiter

Height of cloud tops from main cloud deck: 20-30 KM.

Exponential decay parameter: $K = 1.65 \times 10^{-5}$ ft.$^{-1}$.

Pressure at main cloud deck: 6-9 atmospheres.

Temperature at top of atmosphere: 80-90°K.

Atmospheric Model I: $\gamma_o = 1.46$
Mean molecular weight 2.47.
Lapse rate 2.64 °K/KM

Atmospheric Model II: $\gamma_o = 1.56$
Mean molecular weight 3.26
Lapse rate 3.96 °K/KM

Temperature at top of clouds: Model I: 165° K
Model II: 170° K

Temperature at main cloud deck: Model I: 215-245°K
Model II: 250-290°K

2. Saturn

Height of cloud tops from main cloud deck: 20-30 KM

Temperature at top of atmosphere: 60-70° K.

Atmospheric Model I: $\gamma_o = 1.46$
Mean molecular weight 2.47
Lapse rate 1.17 °K/KM

Atmospheric Model II: $\gamma_o = 1.56$
Mean molecular weight 3.26
Lapse rate 1.75 °K/KM

Temperature at top of clouds: 155° K.

Temperature at main cloud deck: Model I: 175-190° K.
Model II: 190-210° K.

Table E.2: (Cont.) Model Atmospheres for Giant Planets and Titan.

3. Uranus and Neptune:

Mean molecular weight 3.55.

Mean temperature of atmosphere: 78 °K.

Pressure at main cloud deck: 9 atmospheres

Exponential decay parameter: $K = 1.87 \times 10^{-5}$ ft.$^{-1}$

4. Titan

$\gamma_o = 1.5$

Mean molecular weight: 20

Mean temperature of atmosphere: 70-83° K.

Lapse rate 1.4 °K/KM

Pressure at surface: 8.9×10^{-4} atmospheres

$\rho_{(SL)} = 0.006$ slugs/ft.^{3}

E.6 Model Atmosphere for Earth

The 1956 ARDC model atmosphere is generally accepted as a reasonably good representation of average atmospheric characteristics of the Earth below 100 miles. This profile was constructed with only one point above 100 miles. Data obtained from various sounding rockets and Earth satellites during 1957-1959, however, suggests that substantial revision of this model of the atmosphere is needed. Revised data obtained from satellites indicates that density of the ARDC model may be in error by an order of magnitude at low altitudes, and that densities at altitudes in excess of 100 miles are much higher than predicted

by the ARDC model. Furthermore, satellite data shows that the density at high altitudes is approximately twice as high in summer as in winter, and twice as high in the daytime as at night. Therefore, any model of the atmosphere is at best, a crude representation of conditions that may actually be encountered by a vehicle entering the atmosphere.

Fig. E.1 compares atmospheric density at high altitudes predicted by the ARDC model atmosphere with actual measurements made by recent satellites and sounding rockets[76]. A mean curve is shown on this figure which more closely matches measured densities at high altitudes than does the ARDC model; this mean curve matches the ARDC model at altitudes below 90 KM, and does not depart much from the ARDC model below 120 KM.

The exponential approximation to the Earth's atmosphere was used in most of the numerical computations of this thesis. Values used in Equation (E-1) for Earth are:

$$\rho_{(SL)} = 0.0027 \text{ slug/ft.}^3$$
$$K = 1/23{,}500 \text{ ft.}^{-1} \qquad \text{(E-8)}$$

The measured sea level atmospheric density of the Earth is 2.38×10^{-3} slug/ft.^{3}

The exponential approximation for Earth using the values given in Eq. (E-8) are compared in Fig. E.2 with the 1956 ARDC Model atmosphere. It is clear that a single value of K is a reasonable approximation below 400,000 ft. (approximately 80 miles)*. Numerical comparison of

- - - - - - - - - - - - - - - -

* It is shown in ref. (15) that peak decelerations and maximum aerodynamic heating of an entry vehicle occurs well below this altitude. The region of most important heating and deceleration for a given vehicle occurs over a strip of altitude approximately 70,000 ft. thick across with the density changes by a factor of 20. Once the

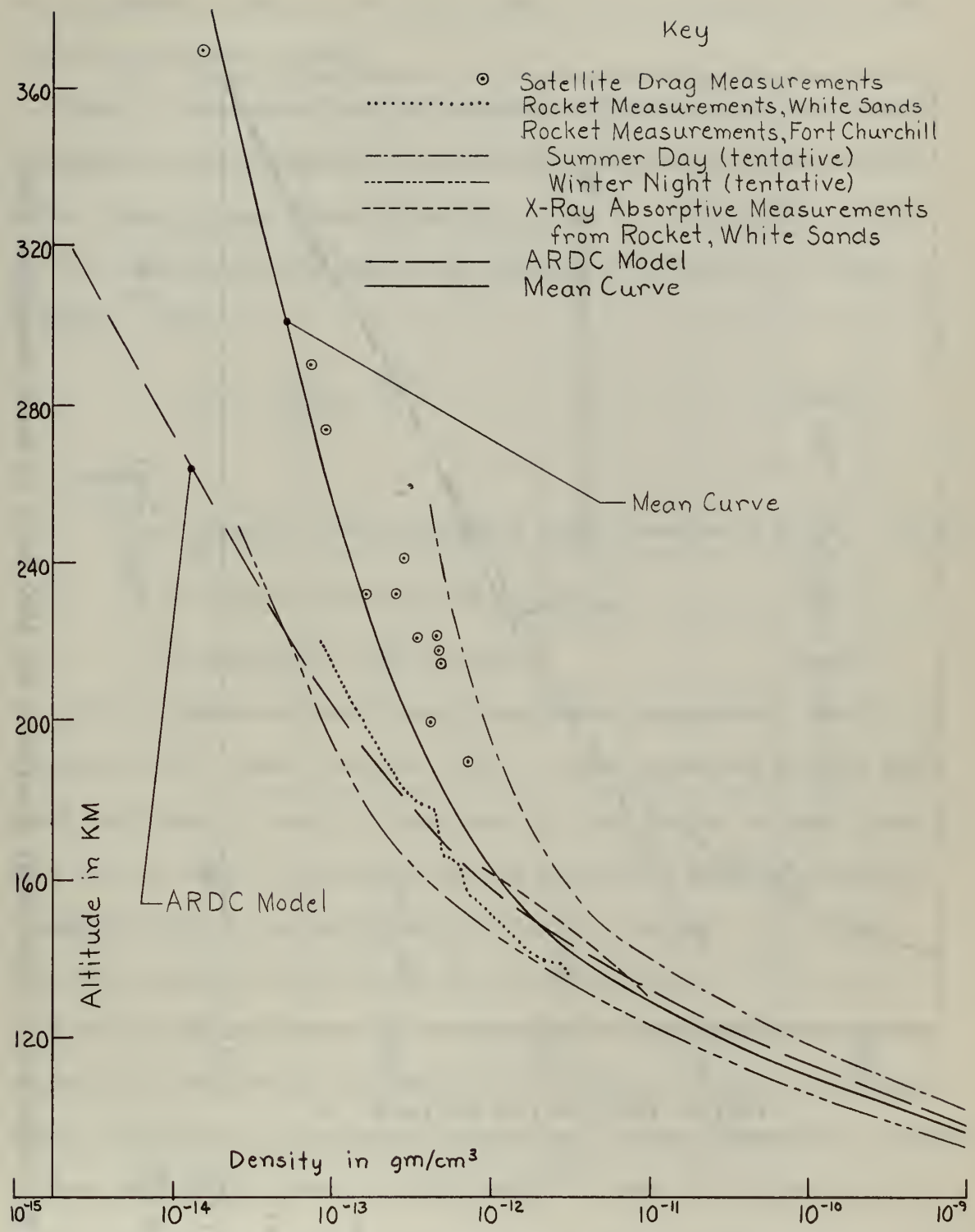

Fig. E.1 : Comparison of Recent Measurements of Atmospheric Density with ARDC Model Atmosphere[76].

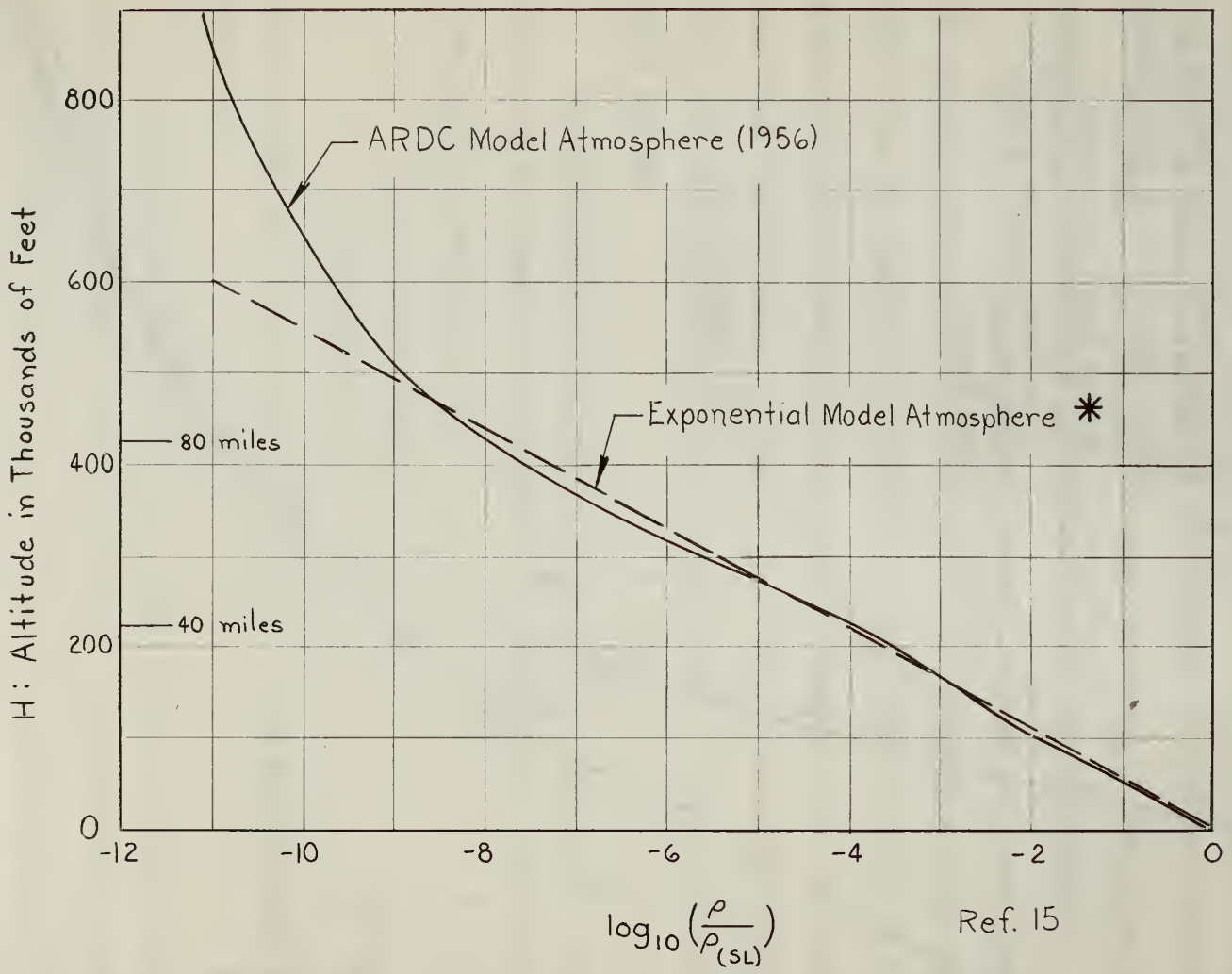

* $\frac{\rho}{\rho_{(SL)}} = e^{-KH}$

$K = \frac{1}{23{,}500}\ ft^{-1}$

$\rho_{(SL)} = 0.0027\ \frac{slug}{ft^3}$

$\rho_{(SL)} = 0.00238\ \frac{slug}{ft^3}$

Fig. E.2: Comparison of Exponential Atmosphere with ARDC Model of Earth Atmosphere (1956)

the exponential model and the ARDC model is given in Table E.3 to four or five significant figures.

Most of the derivations and numerical calculations of this thesis use dimensionless parameters in order that the results may be applied to any planet. Mean planetary radius is used as the reference length for non-dimensionalizing quantities having the dimensions of length or distance. Thus:

$$\sigma = \frac{\rho}{\rho_{(SL)}} = e^{-kh} \qquad \text{(E-9)}$$

where:

k = dimensionless atmospheric decay parameter = $KR_{(m)0}$ (E-10)

h = dimensionless altitude = $H/R_{(m)0}$ (E-11)

σ = atmospheric density ratio (E-12)

Fig. E.3 shows a plot of the dimensionless exponential decay parameter $\sqrt{k}$ taken from ref. (15). k was determined for the ARDC model atmosphere at each altitude point by determining the mean slope of a plot of $\log\rho$ vs altitude for the 70,000 ft. strip of altitude immediately above the particular altitude in question. It is seen from Fig. E.3 that below 400,000 ft. the variation in $\sqrt{k}$ is no more than about 10% from a mean value of 30. These variations are due primarily to temperature changes with altitude (a constant exponential decay rate assumes an isothermal atmosphere). Since temperature changes as much as 15% with season and latitude[77], than $\sqrt{k}$ (which is pro-

- - - - - - - - - - - - - - - - -

altitude of this critical strip is determined for a given vehicle entering a given atmosphere, the exponential decay parameter K can be adjusted to correspond more nearly to that of the critical strip of altitude.

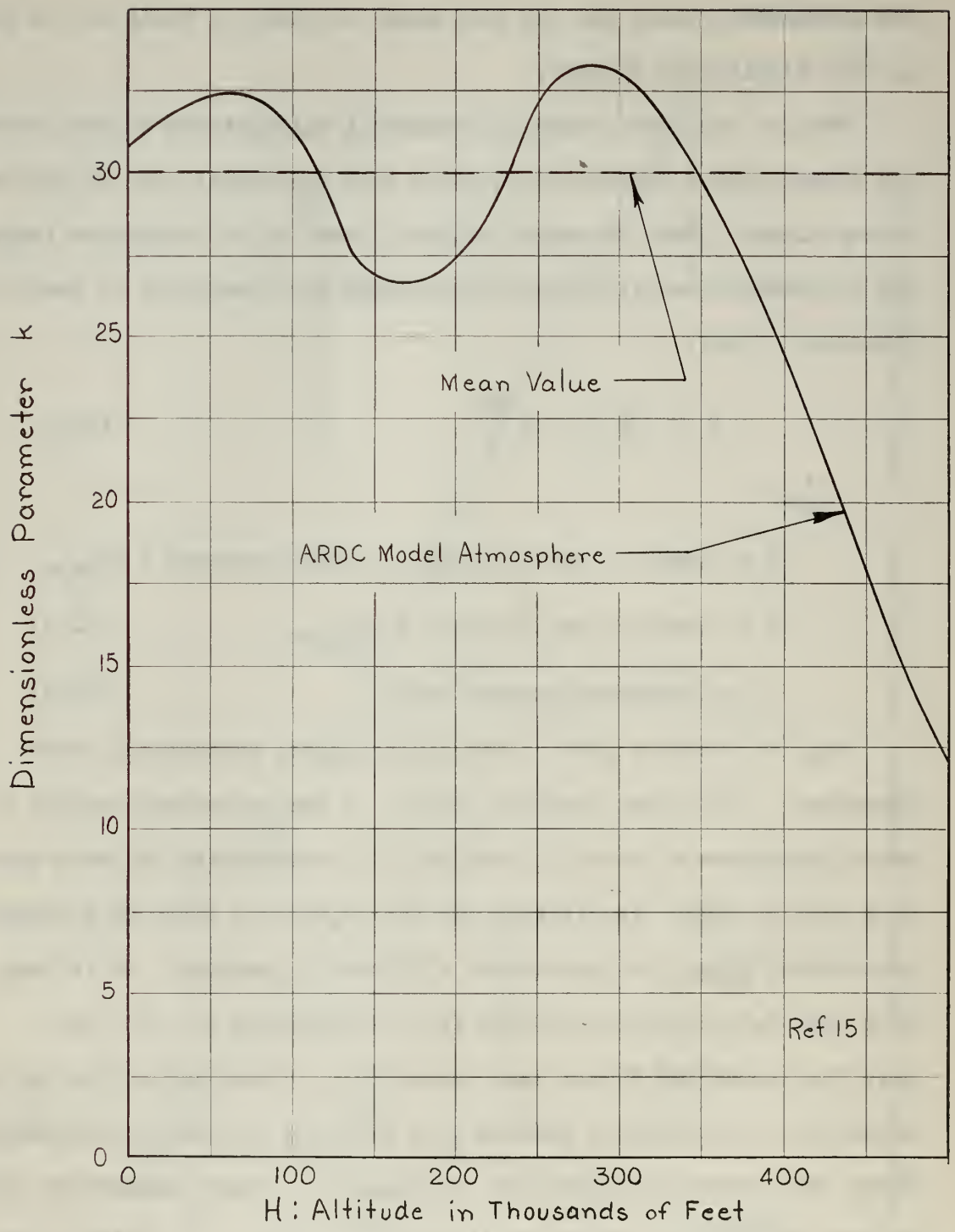

Fig. E.3 : Dimensionless Exponential Parameter k for ARDC Model of Earth Atmosphere.

portional to $T_{(m)o}^{-\frac{1}{2}}$, see equation (E-2)) may fluctuate by 7% due to seasonal changes and latitude changes alone.

For calculations of this thesis where the Earth is considered, k = 889 is used (corresponding to a mean atmospheric temperature of 240° K (432° R)) together with $\rho_{(SL)} = 0.0027$ slug/ft.^{3}.

E.7 Comparison of the Exponential Model Atmospheres of Venus, Earth, and Mars

Fig. E.4 shows the isothermal atmospheric models used in this thesis for the terrestrial planets. It is apparent that the atmospheres of Venus and Earth are distributed in a similar way. Even with large errors in the assumed atmospheric composition of Venus, gas-dynamic heating and deceleration loads would, to a first approximation, be the same as they are on the Earth. A parachute on Venus, however, should be about three times as effective as on Earth.

Maximum deceleration loads will be severe on Earth and Venus for some trajectories as pointed out in this thesis. These problems may be solved by resorting to lifting vehicles, by entering at lower entry angles (requires precision guidance) or coming in at slower velocities (requires large amounts of propellants).

The atmosphere of Mars is characterized by a gradual decrease in density with increasing altitude and low surface density as compared to that of the Earth. The low ground-level density of this atmosphere will reduce the effectiveness of a parachute and will require the use of a high drag (low density) entry vehicle. The gradual change in atmospheric density of the Martian atmosphere will reduce the severity of peak gas-dynamic accelerations and heating loads. For identical size, weight, shape, and velocity, a body entering the Martian atmosphere would be

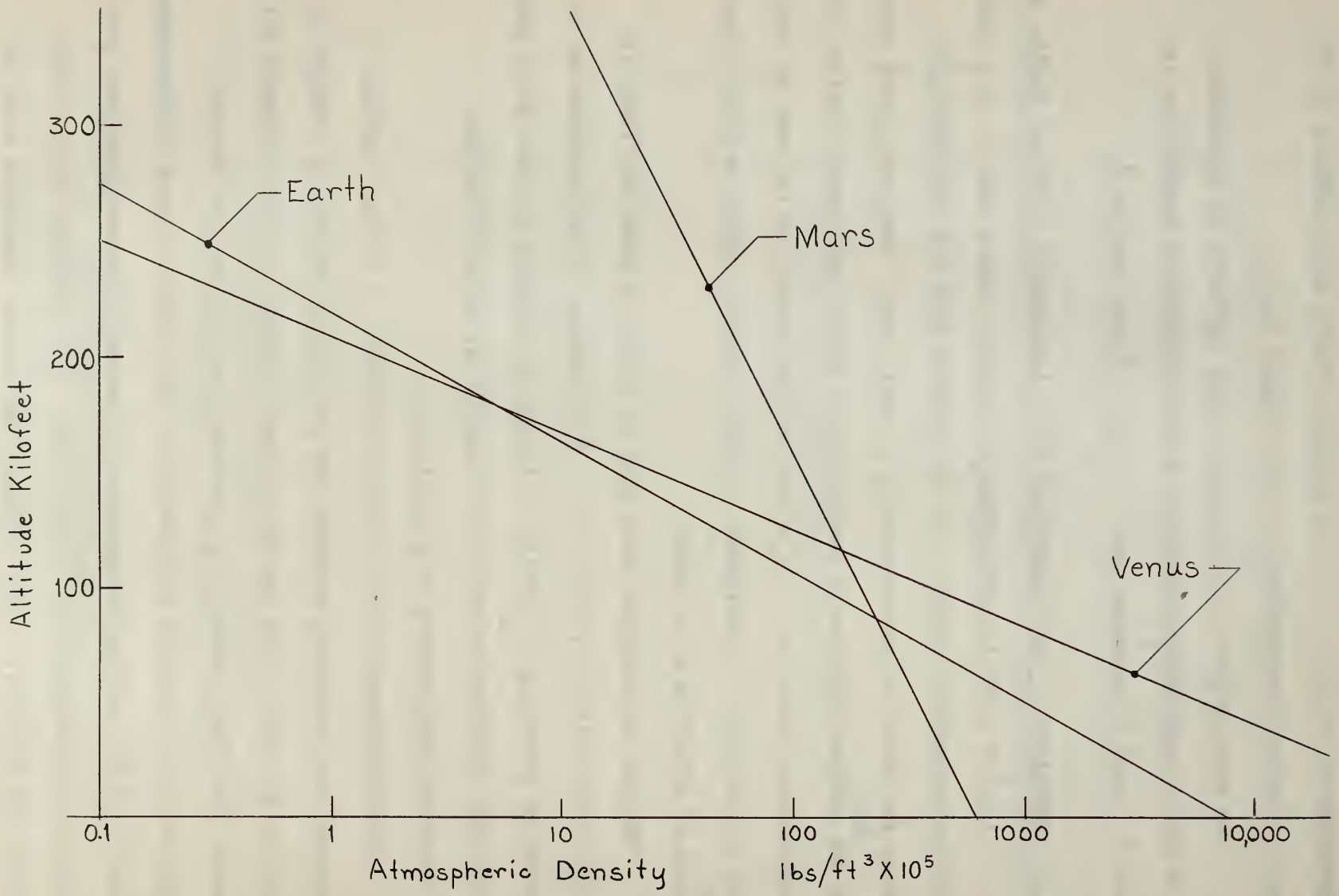

Fig. E4 Isothermal Atmospheric Models for Terrestrial Planets

subjected to about 25% of the peak deceleration load and about 80% of the peak heating load that it would encounter during entry into the Earth's atmosphere.

Table E.3: Comparison of ARDC Model Atmosphere (1956) with Exponential Approximation ($\rho_{(SL)} = 2.7 \times 10^{-3}$) (1/K = 2.35×10^{4})

H (feet)	ARDC (slug/ft.^{3})	$\rho = \rho_{(SL)} e^{-KH}$ (slug/ft.^{3})
0	2.3769×10^{-3}	2.7×10^{-3}
10^4	1.7556×10^{-3}	1.7642×10^{-3}
2×10^4	1.2673×10^{-3}	1.1528×10^{-3}
3×10^4	8.9068×10^{-4}	7.5326×10^{-4}
4×10^4	5.8727×10^{-4}	4.9220×10^{-4}
5×10^4	3.6391×10^{-4}	3.2162×10^{-4}
6×10^4	2.2561×10^{-4}	2.1015×10^{-4}
7×10^4	1.3993×10^{-4}	1.3732×10^{-4}
8×10^4	8.6831×10^{-5}	8.9730×10^{-5}
9×10^4	5.2531×10^{-5}	5.8632×10^{-5}
10×10^4	3.2114×10^{-5}	3.8311×10^{-5}
11×10^4	2.0014×10^{-5}	2.5034×10^{-5}
12×10^4	1.2697×10^{-5}	1.6358×10^{-5}
13×10^4	8.1894×10^{-6}	1.0688×10^{-5}
14×10^4	5.3640×10^{-6}	6.9840×10^{-6}
15×10^4	3.5642×10^{-6}	4.5631×10^{-6}
16×10^4	2.4329×10^{-6}	2.9817×10^{-6}
17×10^4	1.6929×10^{-6}	1.9483×10^{-6}
18×10^4	1.1995×10^{-6}	1.2731×10^{-6}
19×10^4	8.5890×10^{-7}	8.3184×10^{-7}
20×10^4	6.0583×10^{-7}	5.4354×10^{-7}
22×10^4	2.8710×10^{-7}	2.3207×10^{-7}
24×10^4	1.2580×10^{-7}	0.9909×10^{-7}
26×10^4	4.772×10^{-8}	4.231×10^{-8}
28×10^4	1.702×10^{-8}	1.806×10^{-8}
30×10^4	6.065×10^{-9}	7.713×10^{-9}
32.5×10^4	1.610×10^{-9}	2.662×10^{-9}
35.0×10^4	4.957×10^{-10}	9.187×10^{-10}
37.5×10^4	1.718×10^{-10}	3.171×10^{-10}
40.0×10^4	6.565×10^{-11}	10.943×10^{-11}
42.5×10^4	2.672×10^{-11}	3.777×10^{-11}
45.0×10^4	1.111×10^{-11}	1.304×10^{-11}
47.5×10^4	5.348×10^{-12}	4.499×10^{-12}
50.0×10^4	2.862×10^{-12}	1.553×10^{-12}

APPENDIX F

EXTERNALLY-AIDED SELF ADAPTIVE CONTROL OF THE ENTRY VEHICLE

The operational extremes experienced by a vehicle during entry into a planetary atmosphere suggest a control system that adapts itself to the changing environment. The Conservation Parameter, defined in section 1.7, is a measurable function that has sharp behavior at the boundaries between operational phases; behavior of this function is discussed in some detail in Chapters 8 and 9. The conservation parameter may be useful as a switching function and as a variable sensitivity factor to improve control system operation.

The generalized guidance and control system represented functionally in Fig. 1.4 is a three-dimensional system. The command signal to the control system from the guidance computer may be in the form of acceleration components along three axes fixed to the entry vehicle. Fig. F.1 suggests a relatively simple functional instrumentation of the control system for one of these axes, the normal axis, which utilizes the conservation parameter for adapting to the operational environment. Similar adaptive techniques may be applied to other control channels.

The function of the acceleration control system of Fig. F.1 is to produce normal accelerations of the vehicle in response to command inputs, while minimizing changes in flight direction that result from

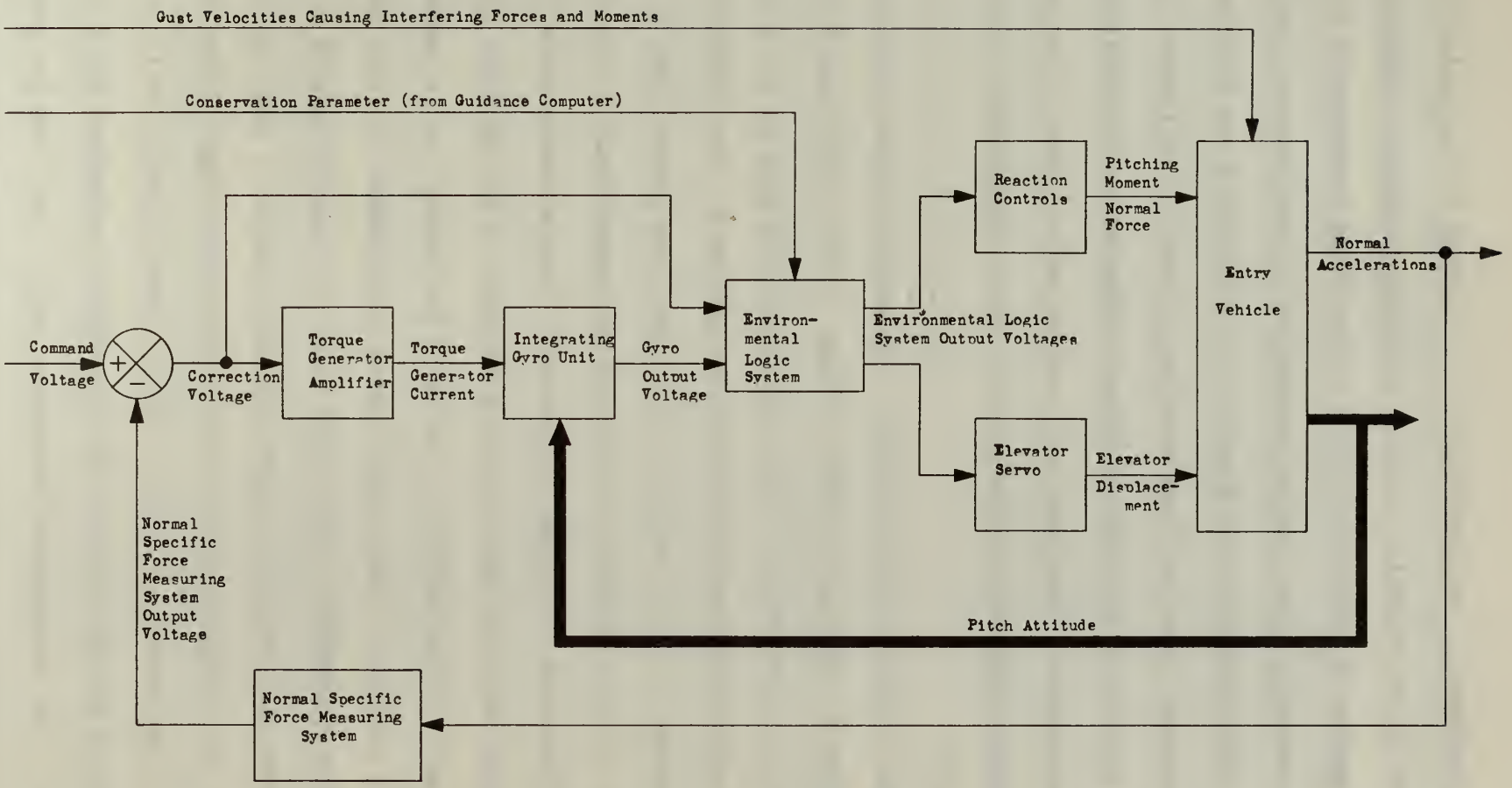

Fig. F.1: Functional Diagram of Normal Acceleration Flight Control System which Adapts to the Operating Environment

gust disturbances. The operation of this system is not unlike that used to control guided missiles and high performance aircraft except for the unique feature of incorporating the conservation parameter as an input. The environmental logic system compensates for environmental influences on the effectiveness of the elevators in controlling the vehicle.

The normal specific force measuring system in the feedback loop detects the sum of all specific force components in the normal direction. With measurements of bank and pitch angles and altitude, it is possible to introduce compensations for gravity. Such compensation is not shown on Fig. F.1.

After compensating for gravity, the measured normal acceleration is compared to the input command voltage. When a difference exists, a correction is introduced. The correction signal goes to the environmental logic system and the integrating gyro unit. The integrating gyro unit produces a signal containing two terms, one proportional to the integral of the correction voltage and one proportional to the integral of the pitch rate. In order to produce a large elevator angle for given pitch deviation such as may be required in the subsonic phase of flight near the termination of the entry trajectory, it is necessary to provide a signal to the elevator servo proportional to pitch rate[78].

The environmental logic system takes the time derivative of the signal from the integrating gyro unit and combines it with the correction voltage. The output voltage of the environmental logic system is sent either to the reaction controls, to the elevator servo, or to both, depending on the magnitude of the conservation parameter and its time behavior. The conservation parameter, which comes from the guidance computer, indicates the phase of flight (see Chapters 8 and 9) and

reflects the degree of effectiveness that can be expected from the elevators due to flight conditions.

The system of Fig. F.1 is not a self-adaptive control system, i.e., it does not monitor its own performance and automatically adjust itself for optimum performance in a changing environment. The system is "adaptive", however, in the sense that it uses environmental data from the guidance computer to adjust its performance characteristics. Augmenting the adaptive features of a system similar to Fig. F.1 with self-adaptive inner loops to optimize control system operation is suggested for future investigations.

BIBLIOGRAPHY

(1) C.L. Taylor and W.V. Blockley; "Crew Performance in a Space Vehicle" Chapter 30, Space Technology, John Wiley and Sons, Inc. N.Y. (1959)

(2) S. Chapman; "The Earth and the Sun's Atmosphere"; Scientific American (Oct. 1959)

(3) R. Jastrow; "Artificial Satellites and the Earth's Atmosphere" Scientific American, Aug. 1959

(4) A.J. Eggers, Jr.; "The Possibility of a Safe Landing"; Chapter 13, Space Technology, John Wiley and Sons, N.Y. (1959)

(5) Time Magazine, July 20, 1959.

(6) Aviation Week, June 22, 1959.

(7) Space Handbook: Astronautics and its Applications; Staff Report of the Select Committee in Congress on Astronautics and Space Exploration. Government Printing Office, Washington, D.C. (1959)

(8) J.M. Eggleston, and D.C. Cheatham; "Piloted Entries into the Earth's Atmosphere"; IAS Paper No. 59-98; N.Y. (June 1959).

(9) R.W. Detra, F.R. Riddell, and P.H. Rose; "Controlled Recovery of Non-Lifting Satellites"; ARS Paper 784-59 (April 1959)

(10) A.L. Webber; "Investigation of the Instrumentation of an Atmospheric Re-Entry"; Massachusetts Institute of Technology Instrumentation Laboratory Report T-218 (Sept. 1959)

(11) W. Wrigley, R.B. Woodbury, and J. Hovorka; "Inertial Guidance"; Sherman M. Fairchild Publication Fund Paper FF-16; Institute of the Aeronautical Sciences; N.Y. (Jan. 1957)

(12) L.R. Young; "Inertial Navigation in an Orbital Vehicle", Massachusetts Institute of Technology Instrumentation Laboratory Report T-219 (Sept. 1959)

(13) B.D. Fried; "Trajectory Optimization for Powered-Flight in Two or Three Dimensions"; Chapter 4, Space Technology, John Wiley and Sons, Inc., N.Y. (1959)

(14) C. Gazley, Jr.; "Deceleration and Heating of a Body Entering a Planetary Atmosphere from Space"; Rand Report P-955 (2-18-57)

(15) D.R. Chapman; "An Approximate Analytical Method for Studying Entry into Planetary Atmospheres", NACA TN 4276; Washington, D.C. (May 1958)

(16) L. Lees, F.W. Hartwig, C.B. Cohen; "The Use of Aerodynamic Lift During Entry into the Earth's Atmosphere". ARS Paper 785-59 (April 1959)

(17) D.I. Kepler; "Concepts Influencing the Selection of a Configuration for Atmospheric Re-entry", ARS Paper 786-59 (April 1959)

(18) T. Alexander, Jr.; "Gravitational Potential and the Gravity Vector"; Report M1137, Massachusetts Institute of Technology Instrumentation Laboratory (April 1959)

(19) H. Goldstein; Classical Mechanics, Addison-Wesley Press, Inc. Cambridge 42, Mass (1951)

(20) G.P. Taratynova: "The Motion of an Artificial Satellite in the Noncentral Gravitational Field of the Earth in the Presence of Atmospheric Resistance". U.S. Joint Pub. Res. Serv. Report 187: Symposium of Sovient Research on Artificial Earth Satellites and Related Subjects, part 1, 25 Jan. 1958, pages 69-81. (Translation of USPEKHI FIZICHESKIKH NAUK, Progress in Physical Sciences, Vol. 63, No. 1a, Sept. 1957, pp. 51-58.)

(21) J.N. Nielsen; F.R. Goodwin; and W.A. Mersman: "Three Dimensional Orbits of Earth Satellites, Including Effects of Earth Oblateness and Atmospheric Rotation", NASA MEMO 12-4-58A, Washington, D.C. (Dec. 1958).

(22) P.E. Sandorff,: Unpublished notes for MIT Course 16.76, "Orbital Vehicles", MIT, Cambridge 39, Mass. (1959).

(23) Roberson, R.E.: "Orbital Behavior of Earth's Satellites," Journal of the Franklin Institute, Vol. 264, Nol 4 (Oct. 1957)

(24) F.B. Hildebrand; Advanced Calculus for Engineers; Prentice-Hall, Inc. N.Y. (1949)

(25) C.A. Whitney: "Atmospheric Conditions at High Altitudes From Satellite Observations"; ARS Paper 779-59, N.Y. (April 1959)

(26) R.A. DiTaranto and J.J. Lamb: "Preliminary Investigation of Hyper Environments and Methods of Simulation -- Part I Natural and Induced Environments above 75,000 ft." WADC Tech Report 57-456 (July 1957).

(27) I.G. Henry: "Lifetimes of Artificial Satellites of the Earth" Jet Propulsion 27, 1 (Jan. 1957).

(28) C.D. Perkins and P.E. Hage: Airplane Performance, Stability, and Control; John Wiley and Sons, N.Y. (1949)

(29) Aviation Week, Oct. 19, 1959.

(30) A. Meile: "General Variational Theory of the Flight Paths of Rocket-Powered Aircraft, Missiles, and Satellite Carriers". Astronautics Acta, Vol. 4, #4 (1958)

(31) A. J. Eggers, Jr.; H.J. Allen; and S.E. Neice: "A Comparative Analysis of the Performance of Long-Range Hypervelocity Vehicles" NACA TN 4046; Washington, D.C. (Oct. 1957)

(32) H.A. Panofsky and R.A. McCormick: "The Spectrum of Vertical Velocity Near the Surface"; IAS Report No. 59-6, N.Y. (Jan. 1959)

(33) R.C. Hakes: "Some Fundamental Problems Associated with Injecting, Orbiting, and Recovering a Man from Orbit"; IAS Report 59-80; N.Y. (Jan. 1959)

(34) G.P. Sutton: "Rocket Propulsion Systems for Interplanetary Flight"; 1959 Minta Martin Lecture at Massachusetts Institute of Technology; Sherman M. Fairchild Publication Fund Paper FF-21, Institute of the Aeronautical Sciences, N.Y. (March 1959)

(35) The Effects of Atomic Weapons; U.S. Government Printing Office (1950)

(36) Lester Lees: "Recovery Dynamics -- Heat Transfer at Hypersonic Speeds in a Planetary Atmosphere"; Chapter 12, Space Technology John Wiley and Sons (1959)

(37) M.W. Rubensin: "The Influence of Aerodynamic Heating on the Structural Design of Aircraft"; VIDYA Associates; Palo Alto, Calif. (Sept. 1958).

(38) Mary F. Romig: "Stagnation Point Heat Transfer for Hypersonic Flow" Jet Propulsion, Vol. 26, No. 12 (Dec. 1956) pp. 1098-1101

(39) R.W. Detra; N.H. Demp; and F.R. Riddell: Addendum to "Heat Transfer to Satellite Vehicles Re-entering the Atmosphere". Jet Propulsion, Vol. 27, No. 12 (Dec. 1957) pp. 1256-1257.

(40) Lester Lees: "Laminar Heat Transfer Over Blunt-Nosed Bodies at Hypersonic Flight Speeds"; Jet Propulsion, Vol. 26, No. 4 (April 1956) pp. 259-269

(41) A. Ferri; L. Feldman; and W. Daskin: "The Use of Lift for Re-Entry From Satellite Trajectories"; Jet Propulsion, Vol. 27, No. 11 (Nov. 1957) pp. 1184-1191.

(42) A. Miele: "Mathematical Theory of the Optimum Trajectories of a Rocket"; AFOSR-TR-58-154; AD-206 361 (Nov. 1958)

(43) G. Leitmann: "On a Class of Variational Problems in Rocket Flight" Lockheed Missiles Systems Division Report No. LSMD-5067 (Sept. 1958)

(44) C.H. Woodling and C.C. Clark: "Studies of Pilot Control During Launching and Reentry of Space Vehicles, Utilizing the Human Centrifuge," IAS Report No. 59-39, N.Y. (Jan. 1959).

(45) C.F. Lombard: "Human Tolerances to Forces Produced by Accelerations" Douglas Aircraft Co. Report ES 21072 (Feb. 1958)

(46) North American Aviation, Inc. "Human Tolerance Accelerations, A Practical Tool for the Engineer"; May 6, 1957.

(47) N.P. Clark and S. Bondourant: "Human Tolerances to Prolonged Forward and Backward Accelerations", WADC Tech Report 58-267 (July 1958)

(48) W. Hohmann: "Die Erreichbarkeit der Himmelskorper"; R. Oldenberg Munich (1925)

(49) D.A. Lawden; "Minimal Rocket Trajectories", ARS Journal, Nov.-Dec. 1953; 23, 360.

(50) R.H. Battin; "The Determination of Round-Trip Planetary Reconnaissance Trajectories", M.I.T. Instrumentation Laboratory Report R-219, Jan. 1959.

(51) H.J. Allen, and A.J. Eggers, Jr.: "A Study of the Motion and Aerodynamic Heating of Missiles Entering the Earth's Atmosphere at High Supersonic Speeds". NACA TN 4047, Washington, D.C. (Oct. 1957).

(52) E. Sanger: "Raketen-Flugtechnik"; R. Oldenbourg (Berlin) 1933

(53) E. Sanger and J. Bredt: "A Rocket Drive for Long Range Bombers"; Deutsche Luftfahrtforschung UM 3538 (1944). Translation CGD-32, Tech Information Branch, BUAER, Navy Department.

(54) H.J. Allen: "Motion of a Ballistic Missile Angularly Misaligned with the Flight Path Upon Entering the Atmosphere and Its Effect Upon Aerodynamic Heating, Aerodynamic Loads, and Miss Distance". NACA TN 4048, Washington, D.C. (Oct. 1957).

(55) F.E. Fowle: Smithsonian Physical Tables; Eighth edition (revised). Smithsonian Institute; Washington, D.C., 1934.

(56) S. Flugge: Handbuch der Physik, Bank XLVII, Geophysik I, Springer-Verlag, 1956, page 636.

(57) H.S. Zim and R.H. Baker: Stars; Simon and Schuster, N.Y. (1956)

(58) The Encyclopedia Americana; The Americana Corporation, N.Y.

(59) F.L. Whipple: "The Meteoric Risk to Space Vehicles", Vistas in Astronautics, Pergamon Press, p. 115.

(60) I.N. Nazarova: "Rocket and Satellite Investigation of Meteors", presented at the fifth meeting of the Comite' Speciale de l'Annee Geophysique Internationale, Moscow, August 1958.

(61) D.B. Beard: "Interplanetary Dust Distribution and Erosion Effects"; American Astronautical Society, Preprint No. 58-23; Aug. 18-29, 1958.

(62) K.A. Ehricke: "Interplanetary Operations", Chapter 8, Space Technology, John Wiley and Sons, N.Y. (1959).

(63) Blitzer, Leon, Weisfeld, Morris, and Wheelon: "Perturbations of a Satellite's Orbit Due to Earth's Oblateness"; Journal Applied Physics, Vol. 27, No. 10, Oct. 1956, pp. 1141-1149.

(64) Bulletin 78: "Physics of the Earth-II, The Figure of the Earth". National Research Council; Washington, D.C. (1931)

(65) "Astronautics" magazine; vol . 4, No. 3; March 1959; page 8.

(66) J.H. Neeley and J.I. Tracey: Differential and Integral Calculus MacMillan Company, N.Y. (1939)

(67) G.P. Kuiper; The Atmospheres of the Earth and Planets; Univ. of Chicago Press (1952)

(68) S.H. Dole; "The Atmosphere of Venus"; The Rand Corp. paper P-978 (Oct. 12, 1956)

(69) W.M. Sinton; "Further Evidence of Vegetation on Mars"; paper presented at American Astronomical Society, Gainesville, Fla. (Dec. 27-30, 1958).

(70) G.A. Tikhov; "Is Life Possible on Other Planets?"; Journal of the British Astronomical Association; Vol. 65, No. 3, pp. 193 (April 1955)

(71) H.C. Urey; The Planets, Their Origin and Development, Yale Univ. Press, New Haven, Conn. (1952)

(72) E.M.Romer; "Planetary Atmospheres and Some Associated Flight Problems"; Unpublished paper presented in Course 16.46, M.I.T. Spring, 1959.

(73) G. de Vancouleurs: Physics of the Planet Mars; Faber and Faber, London (1954)

(74) A.J.M. Wanders: "The Physical Conditions on the Planet Mars;" International Astronautical Federation Congress, The Netherlands, Aug. 1958

(75) S.L. Hess: "Some Aspects of the Meteorology of Mars"; Journal of Meteorology, Vol. 7, 1950, pp. 1-13.

(76) N.P. Carleton; "Bibliography on Upper Atmosphere; Summary of Current Knowledge of Basic Properties of the Upper Atmosphere"; AVCO Research Note 91, Sept. 1958.

(77) Goody, R.M.: The Physics of the Stratosphere; Cambridge Univ. Press (1954)

(78) Seamans, Barnes, Howard, and Garber: "Recent Developments in Aircraft Control"; IAS Preprint 459, N.Y. (Jan. 1954)

(79) H.B. Dwight; Tables of Integrals and Other Mathematical Data MacMillan Company, N.Y. (1957)

(80) E. Jahnke and F. Emde: Funktionentafeln Mit Formeln und Kurven Dover Publications, N.Y. (1945)

thesD789v.2
Guidance parameters and constraints for
3 2768 001 89569 1
DUDLEY KNOX LIBRARY